

Università degli Studi di Trento

Facoltà di Scienze Matematiche Fisiche e Naturali

Tesi di Dottorato di Ricerca in Fisica

**QUANTUM MONTE CARLO  
STUDY  
OF ULTRACOLD GASES**

Relatori:  
Dr. Stefano Giorgini  
Prof. Lev P. Pitaevskii

Candidato:  
G.E. Astrakharchik

Dottorato di Ricerca in Fisica, XVII Ciclo

15 Dicembre 2004



# Contents

<b>Notation and abbreviations</b>	<b>2</b>
<b>Introduction</b>	<b>5</b>
<b>1 Tools</b>	<b>9</b>
1.1 Introduction . . . . .	9
1.2 Correlation functions and related quantities . . . . .	11
1.2.1 Correlation functions: second quantization form . . . . .	11
1.2.2 Correlation functions: first quantization form . . . . .	12
1.2.3 Homogeneous system . . . . .	13
1.2.4 Momentum distribution and static structure factor . . . . .	14
1.2.5 Trapped system . . . . .	15
1.3 The scattering problem . . . . .	15
1.3.1 Introduction . . . . .	15
1.3.2 Three-dimensional scattering problem . . . . .	16
1.3.2.1 General approach . . . . .	16
1.3.2.2 Scattering on a hard sphere potential . . . . .	17
1.3.2.3 Scattering on a soft sphere potential . . . . .	18
1.3.3 One-dimensional scattering problem . . . . .	19
1.3.3.1 General approach . . . . .	19
1.3.3.2 Scattering on a pseudopotential . . . . .	20
1.3.3.3 Scattering on a 1D square well potential . . . . .	22
1.3.3.4 Scattering on a hard-rod potential . . . . .	22
1.3.4 Pseudopotential . . . . .	23
1.3.4.1 The pseudopotential method . . . . .	23
1.3.5 Resonance scattering . . . . .	24
1.3.5.1 Scattering on a square-well potential . . . . .	24
1.3.5.2 Scattering on a modified Pöschl-Teller potential . . . . .	25
1.4 Energy of the TG and HR gas . . . . .	26
1.4.1 Energy of the Tonks-Girardeau gas . . . . .	26
1.4.2 Hard-rod gas . . . . .	26
1.5 Gross Pitaevskii Equation . . . . .	27
1.5.1 Variational derivation of the GPE . . . . .	27
1.5.2 Coupling constant in quasi one- and two- dimensional systems . . . . .	29
1.6 Local Density Approximation . . . . .	30
1.6.1 General method . . . . .	30

1.6.2	Exact solution for 1D “perturbative” equation of state . . . . .	32
1.6.3	Exact solution for 3D “perturbative” equation of state . . . . .	33
1.6.4	Static structure factor of a trapped Tonks-Girardeau gas . . . . .	35
1.7	Correlation functions in a Luttinger liquid . . . . .	36
1.7.1	Stationary density-density correlation function . . . . .	36
1.7.2	Time-dependent density-density correlation function . . . . .	38
1.7.3	Calculation with non-logarithmic accuracy . . . . .	39
1.7.4	Dynamic form factor . . . . .	40
1.7.5	Popov’s coefficient . . . . .	41
<b>2</b>	<b>Quantum Monte Carlo technique</b> . . . . .	<b>45</b>
2.1	Introduction . . . . .	45
2.2	Variational Monte Carlo . . . . .	46
2.2.1	Variational principle . . . . .	46
2.2.2	Applications . . . . .	46
2.2.3	Implementation . . . . .	46
2.3	Diffusion Monte Carlo . . . . .	47
2.3.1	Schrödinger equation . . . . .	47
2.3.2	Green’s function . . . . .	49
2.3.3	Primitive algorithm . . . . .	51
2.3.4	Higher-order algorithm . . . . .	52
2.4	Fixed-node Diffusion Monte Carlo method . . . . .	52
2.5	Construction of trial wave functions: system of Bosons . . . . .	53
2.5.1	Introduction . . . . .	53
2.5.2	Bijl-Jastrow wave function . . . . .	53
2.5.3	One-body Bijl-Jastrow term in an anisotropic trap . . . . .	54
2.5.4	One-dimensional wave functions . . . . .	54
2.5.4.1	Tonks-Girardeau wave function . . . . .	55
2.5.4.2	Hard-rod wave function (exact) . . . . .	55
2.5.4.3	Hard-rod wave function (approximate) . . . . .	55
2.5.4.4	Wave function of the Lieb Liniger gas . . . . .	56
2.5.4.5	Phonon trial wave function ( $\delta$ -potential) . . . . .	57
2.5.4.6	Super-Tonks trial wave function (attractive $\delta$ -potential) . . . . .	58
2.5.4.7	Scattering on the resonance state of a Bose gas . . . . .	58
2.5.5	Three-dimensional wave functions . . . . .	58
2.5.5.1	Hard sphere trial wave function . . . . .	58
2.5.5.2	Soft sphere trial wave function . . . . .	60
2.5.5.3	Trial wave function of 3D zero range potential . . . . .	61
2.5.5.4	Scattering on the resonance state of a Bose gas . . . . .	62
2.6	Construction of trial wave functions: system of Fermions . . . . .	63
2.6.1	Trial wave function in the BCS limit . . . . .	63
2.6.2	Kinetic energy . . . . .	64
2.6.3	Calculation of the tail energy . . . . .	65
2.6.4	Bijl-Jastrow term (square well trial wave function) . . . . .	65
2.6.5	Trial wave function: zero energy scattering state . . . . .	66
2.6.5.1	Matching to a constant . . . . .	67

2.7	Measured quantities . . . . .	67
2.7.1	Local energy . . . . .	67
2.7.1.1	Local kinetic energy and the drift force . . . . .	67
2.7.1.2	Exponentiation . . . . .	68
2.7.2	Static structure factor . . . . .	69
2.7.3	One body density matrix in a homogeneous system . . . . .	69
2.7.4	One body density matrix in a harmonic trap . . . . .	70
2.7.5	Pair distribution . . . . .	71
2.7.6	Pure estimators and extrapolation technique . . . . .	72
<b>3</b>	<b>3D-1D crossover of a trapped Bose gas</b>	<b>75</b>
3.1	Introduction . . . . .	75
3.2	Theory . . . . .	76
3.2.1	Model Hamiltonian . . . . .	76
3.2.2	Relevant parameters and DMC approach . . . . .	76
3.2.3	Mean-field approach . . . . .	77
3.2.4	1D system: local density approximation . . . . .	77
3.2.5	1D system: beyond local density approximation . . . . .	78
3.3	Results . . . . .	79
3.3.1	Small system, medium scattering length . . . . .	79
3.3.2	Small system, small scattering length . . . . .	80
3.3.3	Small system, large scattering length . . . . .	80
3.3.4	Large system . . . . .	80
3.3.5	Radial size of the system . . . . .	82
3.4	Conclusions . . . . .	83
<b>4</b>	<b>Quasi 1D Bose gases with large scattering length</b>	<b>85</b>
4.1	Introduction . . . . .	85
4.2	Two Bosons under quasi-one-dimensional confinement . . . . .	86
4.3	$N$ bosons under quasi-one-dimensional confinement . . . . .	92
4.4	Energetics of quasi-one-dimensional Bose gases . . . . .	95
4.4.1	Two-body system . . . . .	95
4.4.2	$N$ -body system . . . . .	98
4.5	Stability of quasi-one-dimensional Bose gases . . . . .	101
4.6	Conclusions . . . . .	103
<b>5</b>	<b>Ground state properties of a one-dimensional Bose gas</b>	<b>107</b>
5.1	Introduction . . . . .	107
5.2	Lieb-Liniger Hamiltonian . . . . .	108
5.3	Quantum Monte Carlo Method . . . . .	111
5.4	Homogeneous system . . . . .	112
5.5	Trapped system . . . . .	116
5.6	Conclusions . . . . .	120

<b>6</b>	<b>Beyond Tonks-Girardeau: super-Tonks gas</b>	<b>123</b>
6.1	Introduction . . . . .	123
6.2	The model and method . . . . .	124
6.3	Energy . . . . .	125
6.4	One-body density matrix and static structure factor . . . . .	126
6.5	Collective modes . . . . .	127
6.6	Conclusions . . . . .	128
<b>7</b>	<b>Motion of a heavy impurity through a Bose-Einstein condensate</b>	<b>131</b>
7.1	Introduction . . . . .	131
7.2	Three-dimensional system . . . . .	132
7.2.1	Perturbed solution . . . . .	132
7.2.2	Total energy . . . . .	133
7.2.3	Effective mass and normal fraction . . . . .	135
7.2.4	Drag force and energy dissipation . . . . .	135
7.3	Low dimensional systems . . . . .	137
7.3.1	Two-dimensional system . . . . .	137
7.3.1.1	Drag force . . . . .	137
7.3.1.2	Effective mass . . . . .	138
7.3.2	One-dimensional system. Mean-field theory . . . . .	138
7.3.2.1	Drag force . . . . .	138
7.3.2.2	Effective mass . . . . .	139
7.3.2.3	Density profile . . . . .	139
7.3.3	One-dimensional system. Bethe-ansatz theory . . . . .	141
7.4	Conclusions . . . . .	142
<b>8</b>	<b>Interacting fermions in highly elongated harmonic traps</b>	<b>143</b>
8.1	Introduction . . . . .	143
8.2	Model . . . . .	144
8.3	Homogeneous system . . . . .	145
8.4	Trapped system . . . . .	147
8.5	Conclusions . . . . .	148
<b>9</b>	<b>BEC-BCS crossover</b>	<b>151</b>
9.1	Introduction . . . . .	151
9.2	Model . . . . .	152
9.3	Results . . . . .	154
9.4	Conclusions . . . . .	156
	<b>Conclusions</b>	<b>159</b>
	<b>References</b>	<b>161</b>
	<b>Appendix:</b>	<b>171</b>

<b>A</b>	<b>Bethe <i>ansatz</i> solutions</b>	<b>173</b>
A.1	Lieb-Liniger equations . . . . .	173
A.2	Attractive Fermi gas . . . . .	174
A.3	Repulsive Fermi gas . . . . .	174
A.4	Numerical solution . . . . .	176
A.5	Expansions . . . . .	177
<b>B</b>	<b>Obtaining the momentum distribution from <math>g_1(r)</math></b>	<b>179</b>
	<b>Acknowledgements</b>	<b>183</b>

## Notation and abbreviations

For the notation of other quantities either an unambiguous standard notation is used, or the notation is given explicitly in the text. List of the special notation used throughout the Dissertation:

<i>SYMBOL</i>	<i>MEANING</i>	<i>DEFINITION</i>
$a_{1D}$	one-dimensional $s$ -wave scattering length	(1.63)
$a_{3D}$	three-dimensional $s$ -wave scattering length	(1.44)
$a_{\perp}$	oscillator length of the transverse confinement	$a_{\perp} = \sqrt{\hbar/m\omega_{\perp}}$
$a_z$	oscillator length of the longitudinal confinement	$a_z = \sqrt{\hbar/m\omega_z}$
$D$ [dimensionless]	number of dimensions	
$D$	diffusion constant	$D = \hbar^2/2m$
$E$	total energy of the system	
$E^{loc}(\mathbf{R})$	local energy of a walker $\mathbf{R}$	(2.14)
$\mathcal{E}^{loc}(r)$	Bijl-Jastrow component of a local energy	(2.40)
$\mathbf{F}(\mathbf{R})$	drift force	(2.15)
$\mathcal{F}_2(r)$	Bijl-Jastrow component of the drift force	(2.39)
$f_1(\vec{r})$	one-body Bijl-Jastrow term	see (2.37)
$f_2(r)$	two-body Bijl-Jastrow term	see (2.37)
$g_1(r)$	non-diagonal element of the OBDM	(1.18)
$g_2(r)$	pair-distribution function	(1.19)
$g_3(0)$	value at zero of the three-body correlation function	(1.22)
$g_{1D}$	one-dimensional coupling constant	(1.69)
$g_{3D}$	three-dimensional coupling constant	(1.86)
$L$	size of the system or side of the simulation box	
$m$	particle mass	
$n_{1D}$	linear density	$n_{1D} = N/L$
$n_{3D}$	(total) particle density	$n_{3D} = N/V$
$N$	number of particles	
$\vec{r}_i$	coordinate of $i$ -th particle	$\vec{r}_i = (x_i, y_i, z_i)$
$\mathbf{R}$	a point in $DN$ -dimensional phase space (a <i>walker</i> )	$\mathbf{R} = \{\vec{r}_1, \dots, \vec{r}_N\}$
$R$	range of the potential	(1.47)
$R_m$	(variational) matching distance	
$R_z$	size of the cloud in $z$ -direction	
$R_{\perp}$	size of the cloud in the transverse direction	
$u(r)$	exponentiation of the Bijl-Jastrow term	(2.38)
$V_{ext}(\vec{r})$	external potential	
$V_{int}( \vec{r}_i - \vec{r}_j )$	pair-interaction potential	
$\lambda$	anisotropy parameter ( <i>aspect ratio</i> )	$\lambda = \omega_z/\omega_{\perp}$
$\mu$ [units of energy]	chemical potential	
$\mu$ [units of mass]	reduced mass	$\mu = m/2$
$\tau$	imaginary time	$\tau = it$
$\phi_0(\mathbf{R})$	ground state many body wave function	
$\psi_T(\mathbf{R})$	trial many body wave function	
$\omega_{\perp}$	frequency of the transverse harmonic confinement	
$\omega_z$	frequency of the longitudinal harmonic confinement	



## List of used abbreviations:

BCS	Bardeen Cooper Schriffer
BEC	Bose-Einstein condensation
BJ	Bijl-Jastrow
DMC	Diffusion Monte Carlo
FN-MC	Fixed Node Monte Carlo
JS	Jastrow-Slater
GP	Gross-Pitaevskii
HR	hard rod
HS	hard sphere
LDA	local density approximation
LL	Lieb-Liniger
OBDM	one-body density matrix
TG	Tonks-Girardeau
SR	short range
SS	soft sphere
SW	square well
QMC	Quantum Monte Carlo
VMC	Variational Monte Carlo



# Introduction

Although proposed by Einstein [Ein24, Ein25] for an ideal quantum gas a long time ago Bose-Einstein condensation (BEC) almost remained only a mathematical artifact. After many years of intense experimental activity in 1995 BEC was observed in alkali vapours in a remarkable series of experiments [AEM<sup>+</sup>95, DMA<sup>+</sup>95]. Since that time there has been an explosion of experimental and theoretical interest worldwide in the study of dilute Bose gases. The Bose condensate, a macroscopically occupied quantum wave, exhibits peculiar properties and often is referred to as a new state of matter.

One of the directions where very important achievements were made in the years passed from the first realization of the BEC in gases, is the the development techniques of cooling quantum gases to extremely low temperatures and of trapping methods allowing for the realization of low-dimensional geometries (for example, [GVL<sup>+</sup>01, SKC<sup>+</sup>01, GBM<sup>+</sup>01, MSKE03, TOH<sup>+</sup>04, SMS<sup>+</sup>04]). This combination leads to highly non-trivial effects, like the *fermionization* of bosons which may happen in one-dimensional quantum system. The progress in cooling methods has led to the possibility of observing both Bose and Fermi systems at temperatures much smaller than the degeneration temperature. The development of the techniques of diagnostics allows to get a quantitative description of the system under investigation: the size of the cloud, release energy, the momentum distribution, structure factor and frequencies of collective excitations are available in many experiments.

The most widely used approach for the description of quantum degenerate bosonic system is the mean-field Gross-Pitaevskii (GP) theory[Gro61, Pit61]. In this approach all particles are considered to be in the same quantum state described by the condensate wave function, which evolves in time according to the Gross-Pitaevskii equation. The mean-field approach has proven very useful as it is mathematically much easier to solve the equation for one particle in an effective field of other particles, than to solve the full many body problem. The GP approach holds when the depletion of the condensate is negligible or, more generally, when the correlation length is much larger than the interparticle distance. One-dimensional gases in a regime of strong quantum correlations where the above condition fails, have already been realized.

The problem of solving the many-body Schrödinger equation and finding multidimensional averages integrating out  $3N$  degrees of freedom is very complicated. The Monte Carlo methods are indispensable tools in the calculation of multidimensional integrals (see, for example[Cep95, CB95, MFS95]) and have been shown to be highly useful in the investigation of quantum systems (see, for example, [ABCG02, GGMB04]). We are most of all interested in the quantum properties of the system at zero temperature. The diffusion Monte Carlo method is the best suited for this type of study.

The confining potentials (magnetic trapping, optical trapping, etc.) can be well described by harmonic potentials. If the frequencies of the confinement are equal in all three directions (*i.e.* the trap is spherical) the sample of the gas inside is three-dimensional. If, instead, the trap is made tighter in two directions, the shape of the gas cloud becomes elongated, and in the limit  $\omega_{\perp} \gg \omega_z$  the system becomes effectively one-dimensional (see Fig. 1). The crossover of a trapped gas from

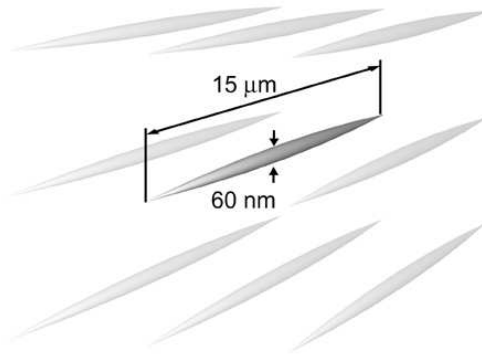


Figure 1: An example of realization of a quasi one dimensional bosonic system (taken from [MSKE03]). Two counterpropagating laser beams create a tight two dimensional optical lattice. In the transversal direction the gas is in the ground state of the confining potential. Excitation of the next levels is highly suppressed due to the low temperature  $k_B T / \hbar \omega_{\perp} < 6 \cdot 10^{-3}$  and low value of the available one-dimensional energy  $\mu / \hbar \omega_{\perp} - 1 < 0.1$ .

three- to one- dimensional behaviour is highly interesting and we have studied it using a Quantum Monte Carlo method[AG02].

The reduced dimensionality enhances the effect of interactions and the properties of a one-dimensional system can be very different from the ones of a three-dimensional gas. The phenomenon of Bose condensation is absent in a one-dimensional homogeneous system. Furthermore, the behavior of repulsive bosons is very peculiar in one dimensional system: in the limit of low density the particles get completely reflected in the process of two-body collisions (limit of impenetrable particles) and the interaction between particles plays a role of an effective Pauli principle. In this Tonks-Girardeu limit fermionization of bose particles happens. The wave function of strongly interacting bosons can be mapped onto a wave function of ideal spinless fermions[Gir60]. The system of bosons acquires many fermionic properties: the energy, pair distribution function, static structure factor, etc. are the same. In the low-density regime beyond mean-field effects are important and they can not be accounted for by the Gross-Pitaevskii approach, which is valid instead in the opposite regime of large densities. In the regime of intermediate densities (recently realized in experiments[TOH<sup>+</sup>04]) both methods are not applicable. The system with contact repulsive interaction (Lieb-Liniger gas) is exactly solvable. Many of its properties are known exactly: the ground-state energy [LL63], value of the pair distribution function at zero distance[GS03b], long- and short-range expansions of the OBDM[OD03]. Still the complete description of correlation functions in the Lieb-Liniger gas (also value at zero of the three-body correlation function which was measured in the experiment[TOH<sup>+</sup>04]) is unknown. The DMC is well suited to study this problem[AG03].

In a one-dimensional system with attractive contact interactions a two-body bound state appears for any strength of the  $\delta$ -potential While the Pauli exclusion principle prohibits fermions from occupying a state with the same quantum numbers, bosons are free to populate the lowest state. An exact result for a system of bosons[McG64] shows that the ground state is a soliton-like state with large negative energy. In a system of two-component fermions two particles with different spin can form a bound state (particles with parallel spins can not interact with contact potential), but other particles (or pairs) have to stay apart. The exact solution[Gau67, KO75] shows formation of dimers

which form a gas-like state. In the dilute regime the internal structure of the composite dimer can be neglected and the system behaves as a Tonks-Girardeau gas of bosons with twice the mass of the atoms[ABGP04].

For a gas of 1D bosons we propose to obtain a large attractive interaction in this special way: start with a gas of repulsive bosons, increase the strength of the interactions using the Feshbach resonance up to Tonks-Girardeau regime ( $a_{1D} \rightarrow -0$ ) and then change the sign of the interaction ( $a_{1D} \rightarrow +0$ ). The new state (“super-Tonks”) will have correlations which are even stronger than in the Tonks-Girardeau gas. The super-Tonks gas is a metastable state which has analogies with a gas of hard-rods of size  $a_{1D}$ . The super-Tonks is a metastable state. A very important question is to find out if the super-Tonks gas is stable and, thus, can be realized in an experiment. We use the variational Monte Carlo method to investigate this problem[ABCG04a]. Interaction effects in quasi-one-dimensional systems can be studied in experiments by exciting “breathing” mode oscillations. The local density approximation can be used to obtain the density profile of a trapped system of bosons or fermions. We solve the local density approximation for a quite general class of equations of state analytically. Using the sum rule approach we extract the oscillation frequencies numerically for all densities and analytically in the limits where the expansion of the equation of state is known.

A peculiar property of a low temperature system is the possibility of being superfluid. One of the most important predictions of Landau theory of superfluidity is the existence of a finite critical velocity. If a body moves in a superfluid at  $T = 0$  with velocity  $V$  less than  $v_c$ , the motion is dissipationless. At  $V > v_c$  a drag force arises because elementary excitations are created. Recently, existence of a critical velocity for the superfluid motion in a Bose-Einstein condensed gas was confirmed in various experiments. For example, at MIT a trapped condensate was stirred by a laser beam and the dissipated energy was measured[RKO<sup>+</sup>99, ORV<sup>+</sup>00]. According to Landau if one imagines to move a small body through the system and there is no normal part, no dissipation will happen if the speed is smaller than the speed of sound. We calculate the effect of a small impurity moving through a condensate which is described by the Gross-Pitaevskii equation[AP02]. We want to find an answer to a question which is rather complicated. We know that in the large density mean-field regime that the system should be superfluid. On the other side, in the Tonks-Girardeau regime the system is mapped to the fermions, which are not superfluid.

An important question concerns effective interactions in 1D, *i.e.* how the one-dimensional effective coupling constant is related to the three dimensional  $s$ -wave scattering length. A solution for the problem of two-body scattering on a pseudopotential in a waveguide was found by Olshanii[Ols98] and shows a resonant behavior in the regime  $a_{3D} \sim a_{\perp}$  due to virtual excitations of transverse modes confinement levels. Since in normal experimental conditions  $a_{3D} \ll a_{\perp}$ , a resonant scattering in the vicinity of a Feshbach resonance should be used in order to enter this regime. In experiments a possible way to fulfill this condition is to make use of the Feshbach resonance. An important question is to prove the existence of the confinement induced resonance in a many body system. We consider a resonant scattering on a smooth attractive potential of very small range and use Fixed-Node Monte Carlo to study the problem of quasi-one-dimensional Bose gases with large scattering length[ABGG04b, ABGG04a].

The use of Feshbach resonance allows one to vary the interaction strength in a controlled way and tune the scattering length essentially to any arbitrary value. Recent experiments on two-component ultracold atomic Fermi gases near a Feshbach resonance have opened the possibility of investigating the crossover from a Bose-Einstein condensate (BEC) to a Bardeen-Cooper-Schrieffer (BCS) superfluid. For positive values of the  $s$ -wave scattering length  $a_{3D}$ , atoms with different spins are observed to pair into bound molecules which, at low enough temperature, form a Bose conden-

sate [JBA<sup>+</sup>03, GRJ03, ZSS<sup>+</sup>03]. The molecular BEC state is adiabatically converted into an ultracold Fermi gas with  $a < 0$  and  $k_F|a| \ll 1$  [BAR<sup>+</sup>04a, BKC<sup>+</sup>04], where standard BCS theory is expected to apply. In the crossover region the value of  $|a_{3D}|$  can be orders of magnitude larger than the inverse Fermi wave vector  $k_F^{-1}$  and one enters a new strongly-correlated regime known as unitary limit [OHG<sup>+</sup>02, BAR<sup>+</sup>04b, BKC<sup>+</sup>04]. In dilute systems, for which the effective range of the interaction  $R_0$  is much smaller than the mean interparticle distance,  $k_FR_0 \ll 1$ , the unitary regime is believed to be universal. In this regime, the only relevant energy scale should be given by the energy of the noninteracting Fermi gas. The unitary regime presents a challenge for many-body theoretical approaches because there is not any obvious small parameter to construct a well-posed theory. Quantum Monte Carlo techniques are the best suited tools for treating strongly-correlated systems. We use Fixed-Node Monte Carlo method to obtain for the first time the equation of state covering all regimes (BEC, unitary, BCS)[ABCG04b]. The equation of state can be tested in experiments by measuring the frequencies of collective oscillations. We also investigate the behavior of correlation functions.

The structure of the Dissertation is as follows.

In the Chapter 1 we introduce the analytical approaches and approximations used in the subsequent Chapters. Chapter 2 explains in details the Quantum Monte Carlo methods used in the study. In Chapter 3 we consider a system of bosons in an anisotropic trap and study the transition from a three dimensional behaviour to a quasi one dimensional one as the trap is made very elongated. We study the properties of a quasi-one-dimensional Bose gas with resonant scattering in Chapter 4. The system of  $\delta$ -interacting bosons in the case of repulsive interactions (Lieb-Liniger gas) is investigated in Chapter 5 and in the case of attractive interactions in Chapter 6. The motion of an impurity as a test for superfluidity is considered in Chapter 7. In the next two chapters we consider systems of two component fermions in a quasi one dimensional system (Chapter 8) and in a three-dimensional uniform system (Chapter 9). Conclusions are drawn in the last Chapter (Chapter 9.4).

# Chapter 1

## Tools

### 1.1 Introduction

This Chapter is intended to introduce tools for the subsequent Chapters. Here we define the quantities (correlation functions, static structure factor, etc.) that later are used to describe the properties of quantum systems. We explain the analytical methods (Gross-Pitaevskii approach) and approximations (local density approximation, pseudopotential approximation) used in our study. We review the 2-body scattering problem in three- and one-dimensional systems as it gives insight into the many-body physics and is relevant for the implementation of the Monte Carlo techniques. Most of the content of the Chapter is standart and is presented for the completeness of the discussion. Only in several sections some new results are obtained (Secs. 1.6,1.7).

The structure of the Chapter is as follows.

In Section 1.2 we introduce quantities which characterize a quantum system and can be accessed in experiments. We start by considering the representations of the first and second quantization (Secs. 1.2.1, 1.2.2). A special attention is paid to the relation between mean averages and correlation functions. The calculation of the correlation functions can be largely simplified in a homogeneous system (Sec. 1.2.3), although the case of trapped systems is also considered (Sec. 1.2.5). The momentum distribution and static structure factor are introduced in Sec. 1.2.4.

The scattering theory is addressed in Section 1.3. The scope of our study is general and we consider the theory in a three-dimensional system (Sec. 1.3.2), as well as in a one-dimensional system (Sec. 1.3.3). The scattering problem is solved for a number of potentials that appear in different models. The scattering solutions are used to construct the trial wave function (see Chapter 2) and make comparison of  $N$ -body and 2-body physics (see Chapter 5). We discuss scattering on a  $\delta$ -potential (*pseudopotential*) in a one dimensional system (Sec. 1.3.3.2), where the problem is well posed, and also in a three dimensional system (Sec. 1.3.4.1), where instead a regularization procedure is needed. We relate the coupling constant to the  $s$ -wave scattering length (in 1D and 3D) for the scattering on the pseudopotential, which is a highly important theoretical tool widely used throughout this dissertation. In the conclusion of Section 1.3 we consider the case of resonant scattering, when the scattering length can be much larger than the range of the potential.

A dilute quantum system of repulsive bosons shows very peculiar properties in 1D. Fermionization of the bosonic system takes place (Tonks-Girardeau gas[Gir60]), and the particles behave as if they were ideal fermions. We address some of the properties of an ideal Fermi gas in Section. 1.4. The Fermi momentum and Fermi energy of an ideal 1D Fermi gas (Sec. 1.4.1) provide an important physical scale not only in the TG regime but in the whole range of densities. The ground-state

energy of a gas of impenetrable particles (hard-rod gas) is calculated in Sec. 1.4.2. The properties of a gas of hard-rods are important in the proposed relation of such a system to a short-range attractive potential (super-Tonks) gas (see Chapter 6). Also the HR gas equation of state is related to the expansion of the energy of a Lieb-Liniger gas in the regime of strong correlations and this expansion is relevant for the estimation of the properties of correlation functions in this regime.

In this dissertation the Monte Carlo results are systematically compared to the predictions of the mean-field Gross-Pitaevskii approach (when GP equation is applicable). In Section 1.5.1 the GP equation is derived from a energy functional, which later is used to study the properties of a condensate disturbed by an impurity (see Chapter 7). In a similar way the GP equations in restricted geometries (cigar- and disk- shaped condensates) are derived in Sec. 1.5.2. In this approach virtual excitations in the tight direction are neglected and the resulting expression of the coupling constants is to be compared with the one of an exact solution of a two-body scattering problem in 1D obtained by Olshanii [Ols98].

If the equation of state of the homogeneous system is known, the local density approximation allows one to estimate the properties of a system in the presence of an external confinement. The general idea of this method is explained in Sec. 1.6.1 and the characteristic parameters in three- and one-dimensional systems are discussed. We propose an exact solutions of the LDA problem for a “perturbative” equation of state both in one dimension (Sec. 1.6.2) and in three dimensions (Sec. 1.6.3). The obtained formulas are applied to bosonic systems (see Chapter 6) as well as fermionic systems (see Chapter 8). In particular the LDA method together with the sum rule approach (in 1D) and scaling approach (in 1D) can be used to estimate the frequencies of collective excitations. Expansions for those frequencies are obtained and later are compared to the result of the numerical results obtained using LDA (see Figs. 6.4, 8.4). Finally in Section 1.6.4 we consider the LDA applied to the Tonks-Girardeau gas and calculate the static structure factor in a trapped system.

This introductory Chapter is concluded with a newly proposed derivation of the dynamic form factor, pair distribution function and the one-body density matrix of a weakly interacting bosonic gas in 1D. The Haldane description [Hal81] of this system is corrected in order to replace the phononic excitation spectrum with the more precise Bogoliubov spectrum. In this way we eliminate logarithmic divergences present in the problem and estimate the prefactors of the long-range asymptotics. In particular the coefficient of the decay of the OBDM (Sec. 1.7.5) is compared to the exact DMC result (see Sec. 5) and is found to be extremely accurate (less than 0.3% error).



## 1.2 Correlation functions and related quantities

### 1.2.1 Correlation functions: second quantization form

Quantum description of identical particles can be conveniently done in terms of the creation and annihilation field operators. The operator  $\hat{\Psi}^\dagger(\vec{r})$  puts a particle into a point  $\vec{r}$ , while  $\hat{\Psi}(\vec{r})$  destroys a particle at the same point. Field operators can be conveniently presented in terms of creation  $\hat{a}_k$  (annihilation  $\hat{a}^\dagger$ ) operator that puts (destroys) a particle in a single particle orbital  $\varphi_{\vec{k}}(\vec{r})$ :

$$\begin{cases} \hat{\Psi}^\dagger(\vec{r}) &= \sum_{\vec{k}} \varphi_{\vec{k}}^*(\vec{r}) \hat{a}_{\vec{k}}^\dagger \\ \hat{\Psi}(\vec{r}) &= \sum_{\vec{k}} \varphi_{\vec{k}}(\vec{r}) \hat{a}_{\vec{k}} \end{cases}, \quad (1.1)$$

In a uniform gas occupying a volume  $V$  single particle orbitals  $\varphi_{\vec{k}}(\vec{r})$  are plain waves  $\varphi_{\vec{k}}(\vec{r}) = \frac{1}{\sqrt{V}} e^{i\vec{k}\vec{r}}$ . In a system of bosons operators (1.1) commute  $[\hat{\Psi}(\vec{r}), \hat{\Psi}^\dagger(\vec{r}')] = \delta(\vec{r} - \vec{r}')$ ,  $[\hat{\Psi}(\vec{r}), \hat{\Psi}(\vec{r}')] = 0$  and anticommute in a system of fermions.

Before giving the definition of the correlation functions in terms of the field operators (1.1), let us discuss how the correlation functions come naturally from the calculation of the mean values of operators. We shall start with a very general form of a Hamiltonian consisting of one- and two- body operators

$$\hat{H} = \hat{F}^{(1)} + \hat{F}^{(2)}, \quad (1.2)$$

where the one-body operator  $\hat{F}^{(1)}$  is a sum of operators  $\hat{f}_i^{(1)}$  each acting only on one particle:

$$\hat{F}^{(1)} = \sum_{i=1}^N \hat{f}_i^{(1)}(\vec{r}_i) \quad (1.3)$$

$$\hat{F}^{(2)} = \frac{1}{2} \sum_{i \neq j}^N \hat{f}_i^{(2)}(\vec{r}_i, \vec{r}_j) \quad (1.4)$$

For example, it can be an external potential  $f^{(1)}(\vec{r}) = V_{ext}(\vec{r})$  (and, thus, the operator is diagonal the coordinate representation) or it can be the kinetic energy  $f^{(1)}(p) = p^2/2m$  (the operator is diagonal in the momentum representation). A commonly used two-body operator is a particle-particle interaction is usually defined in the coordinate representation  $f^{(2)}(\vec{r}_1, \vec{r}_2) = V_{int}(\vec{r}_1, \vec{r}_2)$ .

In the second quantization representation the one-body  $\hat{F}^{(1)}$  and two-body  $\hat{F}^{(2)}$  operators are conveniently expressed in terms of the field operators (1.1).

$$\hat{F}^{(1)} = \iint \hat{\Psi}^\dagger(\vec{r}) f^{(1)}(\vec{r}, \vec{r}') \hat{\Psi}(\vec{r}') d\vec{r} d\vec{r}' \quad (1.5)$$

$$\hat{F}^{(2)} = \frac{1}{2} \iint \hat{\Psi}^\dagger(\vec{r}) \hat{\Psi}^\dagger(\vec{r}') f^{(2)}(\vec{r}, \vec{r}') \hat{\Psi}(\vec{r}') \hat{\Psi}(\vec{r}) d\vec{r} d\vec{r}' \quad (1.6)$$

Here we assume that the one-body operator can be either local  $\langle \vec{r} | f^{(1)} | \vec{r}' \rangle = f^{(1)}(\vec{r}) \delta(\vec{r} - \vec{r}')$  (like in the case of an external field), either non local (like in the case of the kinetic energy), so, in general, we have two arguments  $f^{(1)} = f^{(1)}(\vec{r}, \vec{r}')$ . Instead, for the two-body term we always assume that

it is local (*i.e.* it has a form similar to the particle-particle interaction energy)  $\langle \vec{r}_1, \vec{r}_2 | f^{(1)} | \vec{r}'_1, \vec{r}'_2 \rangle = f^{(2)}(\vec{r}_1, \vec{r}_2) \delta(\vec{r}_1 - \vec{r}'_1) \delta(\vec{r}_2 - \vec{r}'_2)$ , so in (1.6) we have only two arguments instead of four.

The quantum averages of  $\hat{F}^{(1)}$  and  $\hat{F}^{(2)}$  can be extracted from  $\hat{f}^{(1)}$  and  $\hat{f}^{(2)}$  if the *correlation functions* are known<sup>1</sup>:

$$\langle \hat{F}^{(1)} \rangle = \iint \hat{f}^{(1)}(\vec{r}, \vec{r}') G_1(\vec{r}, \vec{r}') d\vec{r} d\vec{r}' \quad (1.7)$$

$$\langle \hat{F}^{(2)} \rangle = \frac{1}{2} \iint \hat{f}^{(2)}(\vec{r}, \vec{r}') G_2(\vec{r}, \vec{r}') d\vec{r} d\vec{r}' \quad (1.8)$$

Here  $G_1(\vec{r}, \vec{r}')$  and  $G_2(\vec{r}, \vec{r}')$  are the *non normalized correlation functions* defined as

$$G_1(\vec{r}, \vec{r}') = \langle \hat{\Psi}^\dagger(\vec{r}) \hat{\Psi}(\vec{r}') \rangle \quad (1.9)$$

$$G_2(\vec{r}, \vec{r}') = \langle \hat{\Psi}^\dagger(\vec{r}) \hat{\Psi}^\dagger(\vec{r}') \hat{\Psi}(\vec{r}') \hat{\Psi}(\vec{r}) \rangle \quad (1.10)$$

The function  $G_1(\vec{r}, \vec{r}')$  characterizes correlations existing between values of the field in two different points  $\vec{r}$  and  $\vec{r}'$ . The total phase does not enter in the definition, but instead the relative phase between two points is important. The diagonal term  $\vec{r} = \vec{r}'$  of (1.9) gives the density of the system  $n(\vec{r}) = \langle \hat{\Psi}^\dagger(\vec{r}) \hat{\Psi}(\vec{r}) \rangle = G_1(\vec{r}, \vec{r})$ , so the trace of the matrix  $G_1$  gives the total number of particles  $\text{tr} G_1 = \int G_1(\vec{r}, \vec{r}) d\vec{r} = N$ . The function  $G_2(\vec{r}, \vec{r}')$  characterizes the density correlations between points  $\vec{r}$  and  $\vec{r}'$ .

It is convenient to introduce dimensionless versions of functions (1.9) and (1.10):

$$g_1(\vec{r}, \vec{r}') = \frac{G_1(\vec{r}, \vec{r}')}{\sqrt{G_1(\vec{r}, \vec{r})} \sqrt{G_1(\vec{r}', \vec{r}')}} \quad (1.11)$$

$$g_2(\vec{r}, \vec{r}') = \frac{G_2(\vec{r}, \vec{r}')}{G_1(\vec{r}, \vec{r}) G_1(\vec{r}', \vec{r}')} \quad (1.12)$$

The function (1.11) is limited to the range  $[0, 1]$  and can be understood as the probability to destroy a particle at  $\vec{r}$  and put it at  $\vec{r}'$ . It is always possible to put a particle to the place where it was, so  $g_1(\vec{r}, \vec{r}) = 1$ . The non-diagonal long range asymptotic vanishes in trapped systems and also in homogeneous systems in the absence of Bose-Einstein condensation  $g_1(\vec{r}, \vec{r}') \rightarrow 0, |\vec{r}, \vec{r}'| \rightarrow \infty$ .

A more detailed introduction to the analytic properties of the correlation functions can be found, for example, in [Gla63, NG99, GS03a]

## 1.2.2 Correlation functions: first quantization form

The meaning of the correlation functions (1.11,1.12) is best of all understood in terms of the field operators as discussed in the previous Section. Instead for the implementation of the Monte-Carlo technique it is necessary to express the correlation functions in terms of the wave function  $\psi(\mathbf{R})$  of the system. The easiest way to do SO is to find an expression of the operator average in form similar to (1.7,1.8).

The mean value of a one-body operator in the first quantization Is written as

$$\langle F^{(1)} \rangle = \frac{\int \psi^*(\mathbf{R}) F^{(1)}(\mathbf{R}) \psi(\mathbf{R}) d\mathbf{R}}{\int |\psi(\mathbf{R})|^2 d\mathbf{R}} = \frac{\sum_{i=1}^N \int \psi^*(\vec{r}_1, \dots, \vec{r}_N) f^{(1)}(\vec{r}_i) \psi(\vec{r}_1, \dots, \vec{r}_N) d\mathbf{R}}{|\psi(\mathbf{R})|^2 d\mathbf{R}} =$$

<sup>1</sup>At zero temperature the expectation value  $\langle \dots \rangle$  is taken with respect to the ground state of the system.

$$= \frac{N \iint F^{(1)}(\vec{r}_1, \vec{r}'_1) |\psi(\vec{r}_1, \dots, \vec{r}_N)|^2 d\mathbf{R}}{\int |\psi(\mathbf{R})|^2 d\mathbf{R}} = \iint f^{(1)}(\vec{r}, \vec{r}') G_1(\vec{r}, \vec{r}') d\vec{r} d\vec{r}', \quad (1.13)$$

where  $G_1(\vec{r}, \vec{r}')$  stands for

$$G_1(\vec{r}, \vec{r}') = \frac{N \int \psi^*(\vec{r}, \vec{r}_2, \dots, \vec{r}_N) \psi^*(\vec{r}', \vec{r}_2, \dots, \vec{r}_N) d\vec{r}_2 \dots d\vec{r}_N}{\int \psi^*(\vec{r}_1, \dots, \vec{r}_N) \psi^*(\vec{r}_1, \dots, \vec{r}_N) d\vec{r}_1 \dots d\vec{r}_N} \quad (1.14)$$

The expression for the two-body correlation function (1.10) can be deduced from the average of a two-body operator (1.8):

$$\langle F^{(2)} \rangle = \frac{\int \psi^*(\mathbf{R}) F^{(2)}(\mathbf{R}) \psi(\mathbf{R}) d\mathbf{R}}{\int |\psi(\mathbf{R})|^2 d\mathbf{R}} = \frac{\frac{1}{2} \sum_{i \neq j} \int \psi^*(\vec{r}_1, \dots, \vec{r}_N) f^{(2)}(\vec{r}_i, \vec{r}_j) \psi(\vec{r}_1, \dots, \vec{r}_N) d\mathbf{R}}{|\psi(\mathbf{R})|^2 d\mathbf{R}} = \quad (1.15)$$

$$= \frac{N(N-1) \int f^{(2)}(\vec{r}_1, \vec{r}_2) |\psi(\vec{r}_1, \dots, \vec{r}_N)|^2 d\mathbf{R}}{2 \int |\psi^*(\mathbf{R})|^2 d\mathbf{R}} = \frac{1}{2} \iint f^{(2)}(\vec{r}_1, \vec{r}_2) g_2(\vec{r}_1, \vec{r}_2) d\vec{r}_1 d\vec{r}_2, \quad (1.16)$$

where the first quantization expression for the two body correlation function is

$$G_2(\vec{r}', \vec{r}'') = \frac{N(N-1) \int |\psi(\vec{r}', \vec{r}'', \vec{r}_3, \dots, \vec{r}_N)|^2 d\vec{r}_3 \dots d\vec{r}_N}{\int |\psi(\vec{r}_1, \dots, \vec{r}_N)|^2 d\vec{r}_1 \dots d\vec{r}_N} \quad (1.17)$$

### 1.2.3 Homogeneous system

Many simplifications can be done in a homogeneous system due to the presence of the translational symmetry. The correlation functions discussed above depend only on the relative distance between two coordinates  $|\vec{r} - \vec{r}'|$ . The diagonal element of  $G_1$  is simply a constant  $G_1(\vec{r}, \vec{r}) = n$ . The non-diagonal element of the normalized one-body density matrix (in following we will address it as OBDM) is written as

$$g_1(r) = \frac{N \int \psi^*(\vec{r}, \vec{r}_2, \dots, \vec{r}_N) \psi(0, \vec{r}_2, \dots, \vec{r}_N) d\vec{r}_2 \dots d\vec{r}_N}{n \int |\psi(\vec{r}_1, \dots, \vec{r}_N)|^2 d\vec{r}_1 \dots d\vec{r}_N} \quad (1.18)$$

The normalized two-body density matrix (pair distribution function) is then given by

$$g_2(r) = \frac{N(N-1) \int |\psi(\vec{r}, 0, \vec{r}_3, \dots, \vec{r}_N)|^2 d\vec{r}_3 \dots d\vec{r}_N}{n^2 \int |\psi(\vec{r}_1, \dots, \vec{r}_N)|^2 d\vec{r}_1 \dots d\vec{r}_N} \quad (1.19)$$

At the zero temperature some of the properties of the pair distribution can be easily understood. At large distances the correlation between particles becomes weaker and weaker and we can approximate the field operator  $\hat{\Psi}(r) = \sqrt{\hat{n}(r)} e^{i\hat{\phi}(r)} \approx \sqrt{\hat{n}(r)}, r \rightarrow \infty$  and at zero temperature one has  $g_2(r) \rightarrow 1 - \frac{1}{N}$  and  $g_2(r)$  approaches unity in the thermodynamic limit. On the contrary at short distances particles “feel” each other and the value at zero can be very different from the value in the bulk. In case of impenetrable particles, two particles are not allowed to overlap, thus  $g_2(0) = 0$ . For purely repulsive interaction  $g_2(0) < 1$  and for purely attractive  $g_2(0) > 1$ .

In the average of a two-body operator (1.8) it is possible to integrate out the dummy variable and get a simple expression

$$\langle F^{(2)} \rangle = \frac{n^2}{2} \iint f^{(2)}(\vec{r}_1 - \vec{r}_2) g_2(\vec{r}_1, \vec{r}_2) d\vec{r}_1 d\vec{r}_2 = \frac{Nn}{2} \int f^{(2)}(r) g_2(r) dr \quad (1.20)$$

For a particular case of a contact potential  $V_{int}(r) = g\delta(r)$  the potential energy is directly related to the value of the pair distribution function at zero:

$$\frac{E_{int}}{N} = \frac{1}{2}gn g_2(0) \quad (1.21)$$

We will also give definition of the *three-body density matrix*<sup>2</sup>

$$g_3(0) = \frac{N(N-1)(N-2)}{n^3} \frac{\int |\psi(0, 0, 0, \vec{r}_4, \dots, \vec{r}_N)|^2 d\vec{r}_4 \dots d\vec{r}_N}{\int |\psi(\vec{r}_1, \dots, \vec{r}_N)|^2 d\vec{r}_1 \dots d\vec{r}_N} \quad (1.22)$$

Its value at zero gives the probability of finding three particles in the same point.

### 1.2.4 Momentum distribution and static structure factor

In terms of the field operator (1.1) the momentum distribution  $n_k$  is given as

$$n_{\vec{k}} = \langle \hat{\Psi}_{\vec{k}}^\dagger \hat{\Psi}_{\vec{k}} \rangle, \quad (1.23)$$

The field operator in momentum space  $\hat{\Psi}_{\vec{k}}$  is related to the  $\hat{\Psi}(\vec{r})$  by the Fourier transform

$$\begin{cases} \hat{\Psi}_{\vec{k}} &= \int e^{-i\vec{k}\vec{r}} \hat{\Psi}(\vec{r}) \frac{d\vec{r}}{\sqrt{2\pi}} \\ \hat{\Psi}(\vec{r}) &= \int e^{i\vec{k}\vec{r}} \hat{\Psi}_{\vec{k}} \frac{d\vec{k}}{\sqrt{2\pi}} \end{cases} \quad (1.24)$$

Substitution of (1.24) into (1.23) gives following expression for the momentum distribution

$$n_{\vec{k}} = \frac{1}{2\pi} \iint e^{i\vec{k}\vec{s}} G_1 \left( \vec{R} + \frac{\vec{s}}{2}, \vec{R} - \frac{\vec{s}}{2} \right) d\vec{R} d\vec{s} \quad (1.25)$$

Note, that the dependence on  $\vec{k}$  enters through the relative distance, so the center of the mass motion can be integrated out independently of  $k$ . This procedure is used in the DMC (see Sec.2.7). In the homogeneous system one has

$$n_k = n \int e^{ikr} g_1(r) dr \quad (1.26)$$

At zero temperature the dynamic structure factor  $S(k, \omega)$  is related to the  $k$ -component of the density operator

$$\rho_k = \int e^{-ikr} n(r) dr \quad (1.27)$$

in the following way

$$S(k, \omega) = \sum_n |\langle n | \hat{\rho}_k^\dagger - \langle \hat{\rho}_k^\dagger | 0 \rangle|^2 \delta(\hbar\omega - \hbar\omega_n) \quad (1.28)$$

---

<sup>2</sup>It is interesting to note that the normalization factor  $N!/(N-m)!$  of the  $m$ -body correlation function comes from the number of ways to make groups of  $m$ -particles out of  $N$  particles, but at the same time can be found from the properties of the field operators  $\hat{\Psi}^\dagger|N\rangle = \sqrt{N}|N-1\rangle$ ,  $\hat{\Psi}|N\rangle = \sqrt{N+1}|N+1\rangle$

It characterizes the scattering cross-section of inelastic reactions where the scattering probe transfers momentum  $\hbar k$  and energy  $\hbar\omega$  to the system. By integrating out the  $\omega$  dependence we obtain the static structure factor

$$S(k) = \frac{\hbar}{N} \int_0^\infty S(k, \omega) d\omega = \frac{1}{N} (\langle \rho_k \rho_{-k} \rangle - |\langle \rho_k \rangle|^2) \quad (1.29)$$

This expression is used in QMC calculations (refer to Sec. 2.7.2). Another useful representation can be obtained from Eqs. (1.10,1.27) and commutation relations for the field operator  $\hat{\Psi}(r)$ . It relates the static structure factor to the two-body density matrix

$$S(k) = 1 + \frac{1}{N} \iint e^{ik(r_2-r_1)} (G_2(r_1, r_2) - n(r_1)n(r_2)) dr_1 dr_2 \quad (1.30)$$

In a homogeneous system the two-body density matrix depends only on the relative distance  $r = r_1 - r_2$  and the static structure factor  $S(r)$  is directly related to the pair distribution function (1.12)

$$S(k) = 1 + n \int e^{ikr} (g_2(r) - 1) dr \quad (1.31)$$

### 1.2.5 Trapped system

The presence of an external harmonic confinement removes the translational invariance. We will restrict ourselves to one dimensional case as the relevant to the study presented in Chapter 4. The one-body density matrix (1.11)  $g_1(z_1, z_2)$  depends on both arguments:

$$n \left( \frac{z' + z''}{2} \right) g_1(z', z'') = \frac{N \int \psi^*(z', \dots, z_N) \psi(z'', \dots, z_N) dz_2 \dots dz_N}{\int |\psi(z_1, \dots, z_N)|^2 dz_1 \dots dz_N}, \quad (1.32)$$

where  $n(z)$  is the density profile.

The momentum distribution of a trapped system is obtained from the OBDM by the Fourier transform with the respect to the relative distance

$$n(k) = \iint g_1 \left( Z + \frac{z'}{2}, Z - \frac{z'}{2} \right) n(Z) e^{ikz'} dZ dz', \quad (1.33)$$

## 1.3 The scattering problem

### 1.3.1 Introduction

Apart from the rare cases when the exact wave function of the system is known (like exactly solvable TG (2.5.4.1) and HR (2.48) gases) the construction of the trial wave function is commonly done by matching the solution of a two-body problem with a decay to a constant. We will pay much attention to the problem of a two-body scattering both in three- and in one-dimensional geometries.

## 1.3.2 Three-dimensional scattering problem

### 1.3.2.1 General approach

In this section we will formulate the generic scattering problem in a three-dimensional space. At low density the interaction between particles of a gas is well described by binary collisions.

Consider a collision of two particles having coordinates  $r_1$  and  $r_2$ , masses  $m_1$  and  $m_2$ . The aim is to find the stationary solution  $f_{12}(\vec{r}_1, \vec{r}_2)$  of the Schrödinger equation:

$$\left( -\frac{\hbar^2}{2m_1}\Delta_{\vec{r}_1} - \frac{\hbar^2}{2m_2}\Delta_{\vec{r}_2} + V_{int}(|\vec{r}_1 - \vec{r}_2|) \right) f_{12}(\vec{r}_1, \vec{r}_2) = \mathcal{E}_{12}f_{12}(\vec{r}_1, \vec{r}_2) \quad (1.34)$$

In absence of an external confinement the problem is translational invariant and the center of mass moves with a constant velocity. The solution of problem gets separated in the center of the mass frame. The Schrödinger equation for the movement of the center of mass  $\vec{\mathcal{R}} = (m_1\vec{r}_1 + m_2\vec{r}_2)/M$  is trivial:

$$-\frac{\hbar^2}{2M}\Delta_{\vec{\mathcal{R}}}f_{\vec{\mathcal{R}}}(\vec{\mathcal{R}}) = \mathcal{E}_{\vec{\mathcal{R}}}f_{\vec{\mathcal{R}}}(\vec{\mathcal{R}}), \quad (1.35)$$

here  $M = m_1 + m_2$  is the total mass. The solution of Eq. 1.35 is a free wave<sup>3</sup>  $f_{\vec{\mathcal{R}}}(\vec{\mathcal{R}}) = \exp\{i\vec{k}_{\vec{\mathcal{R}}}\vec{\mathcal{R}}\}$  with  $\vec{k}_{\vec{\mathcal{R}}}$  being the initial wavenumber of the system and  $\mathcal{E}_{\vec{\mathcal{R}}} = \hbar^2k_{\vec{\mathcal{R}}}^2/2M$ .

The equation for the relative coordinate  $\vec{r} = \vec{r}_1 - \vec{r}_2$  involves the interaction potential:

$$\left( -\frac{\hbar^2}{2\mu}\Delta_{\vec{r}} + V_{int}(|\vec{r}|) \right) f(\vec{r}) = \mathcal{E}f(\vec{r}), \quad (1.36)$$

where

$$\mu = \frac{m_1m_2}{m_1 + m_2} \quad (1.37)$$

is the reduced mass. Once solutions of Eqs. 1.35-1.36 are known the solution of the scattering problem (1.34) is given by

$$\begin{cases} f_{12}(\vec{r}_1, \vec{r}_2) &= f_{\vec{\mathcal{R}}}(\vec{\mathcal{R}})f(\vec{r}) \\ \mathcal{E}_{12} &= \mathcal{E}_{\vec{\mathcal{R}}} + \mathcal{E} \end{cases} \quad (1.38)$$

In order to proceed further we will assume that the energy of the incident particle  $E$  is small and the solution has a spherical symmetry  $f(\vec{r}) = f(|\vec{r}|) \equiv f(r)$ . In this case the Laplacian gets simplified  $\Delta = \frac{\partial^2}{\partial r^2} + \frac{2}{r}\frac{\partial}{\partial r}$  and the Eq. 1.36 is conveniently rewritten by introducing function  $g(r)$

$$u(r) = \frac{f(r)}{r} \quad (1.39)$$

$$u(0) = 0 \quad (1.40)$$

in such a way that its form reminds a one-dimensional Schrödinger equation:

$$-\frac{\hbar^2}{2\mu}u''(r) + V_{int}(r)u(r) = \mathcal{E}u(r) \quad (1.41)$$

---

<sup>3</sup>The normalization of the scattering solution is of no interest to us, so in following we will always omit the normalization factor.

The solution of this equation in a general form can be written as

$$u(r) = \sin(kr + \delta(k)), \quad (1.42)$$

where

$$\hbar k = \sqrt{2mE} \quad (1.43)$$

is the momentum of the incident particle and  $\delta(k)$  is the scattering phase.

The scattering at low energy (which describes well a binary collisions in a dilute gas) has a special interest as it becomes universal and can be described in terms of one parameter, the *s-wave scattering length*  $a_{3D}$ :

$$a_{3D} = -\lim_{k \rightarrow 0} \frac{\delta(k)}{k} \quad (1.44)$$

In the asymptotic limit of slow particles  $k \rightarrow 0$  the scattering solution (1.42) can be expanded

$$f(r) \rightarrow \text{const} \left( 1 - \frac{a_{3D}}{r} \right) \quad (1.45)$$

and has the node at a distance equal to  $a_{3D}$ . It gives an equivalent definition of the three-dimensional scattering length as a position of the first node of the positive energy scattered solution in the low-momentum limit.

In the next several sections we will solve the problem of the scattering on a hard-sphere potential (1.3.2.2) and a soft-sphere potential (1.3.2.3). We will find explicit expressions for the scattered functions, which are of a great importance, as in many cases can provide a physical insight into properties of a many body problem. Indeed, at a certain conditions the correlation functions can be related to the scattered function  $f(r)$ . Another point is that the two-body Bijl-Jastrow term  $f_2(r)$  (2.37) in the construction of the trial wave function is very often taken in a form of  $f(r)$ . Thus such calculations are very important for the implementation of the Quantum Monte Carlo methods.

We will also find expressions for the scattering length  $a_{3D}$  in terms of the height (or depth) of the potential  $V_0$ :

$$V_0 = \max_r |V_{int}(r)| \quad (1.46)$$

and the *range of the potential*  $R$ , which in this Dissertation will be understood as a characteristic distance on which the potential acts. In other words the potential can be neglected for distances much larger than  $R$ :

$$R = \min_r \{V(|r|) \approx 0\} \quad (1.47)$$

### 1.3.2.2 Scattering on a hard sphere potential

As pointed out in Sec. 1.3.2.1, in the the limit of low energy collisions the information about the interaction potential enters in the terms of only one parameter, the *s-wave scattering length* and scattering on all potentials having the same scattering length is the same (the scattering becomes *universal*). This allows us to choose as simple potential as one can think of. If we consider the scattering on a repulsive potential, then the easiest choice is the hard sphere (HS) potential:

$$V^{HS}(r) = \begin{cases} +\infty, & r < a_{3D} \\ 0, & r \geq a_{3D} \end{cases} \quad (1.48)$$

This potential has only one parameter, which we name  $a_{3D}$  in the definition (1.48). Obviously it has the meaning of the range of the potential (1.47). At the same time it has meaning of the scattering length, as introduced in (1.44). It will come out naturally from the solution of the scattering problem.

The Schrödinger equation (1.41) becomes ( $\mu = m/2$ )

$$-\frac{\hbar^2}{m}u''(r) + V^{HS}(r)u(r) = \mathcal{E}u(r) \quad (1.49)$$

A particle can not penetrate the hard core of the potential and the solution vanishes for distances smaller than the size of the hard sphere<sup>4</sup>:

$$\begin{cases} u(r) = 0, & |r| < a_{3D} \\ u''(r) - k^2u(r) = 0, & |r| \geq a_{3D} \end{cases} \quad (1.50)$$

The solution of the differential equation (1.50) can be easily found. Together with (1.39) we obtain:

$$f(r) = \begin{cases} 0, & |r| < a_{3D} \\ A \sin(k(r - a_{3D})) / r, & |r| \geq a_{3D} \end{cases}, \quad (1.51)$$

where  $A$  is an arbitrary constant and  $k$  is given by (1.43). The phase shift is linear in the wave vector of the incident particle  $\delta(k) = -ka_{3D}$  and from (1.44) we prove that the range of the potential (1.48) has indeed meaning of the three-dimensional scattering length as stated in the beginning of this section.

### 1.3.2.3 Scattering on a soft sphere potential

In order to test the universality assumption and if the details of the potential are important it is useful to have a potential, where the range of the potential  $R$  can be varied while keeping the  $s$ -wave scattering length constant. In the case of the hard-sphere (Sec. 1.3.2.2) both distances are the same. The easiest way to modify the hard sphere potential (1.48) in such a way that it has desired properties is to make the height of the potential finite. The resulting potential is called the *soft-sphere* (SS) potential:

$$V^{SS}(r) = \begin{cases} V_0, & r < R \\ 0, & r \geq R \end{cases} \quad (1.52)$$

where  $V_0$  is positive.

The Schrödinger equation (1.41) for a pair of particles in the center of mass system is given by

$$\begin{cases} u''(r) + (k^2 - \varkappa^2)u(r) = 0, & r < R \\ u''(r) + k^2u(r) = 0, & r \geq R \end{cases}, \quad (1.53)$$

where we express the energy of the incident particle in terms of the wave number  $k^2 = m\mathcal{E}/\hbar^2$  and introduce a characteristic wave number related to the height of the potential:

$$\varkappa^2 = mV_0/\hbar^2 \quad (1.54)$$

---

<sup>4</sup>Note that therefore the energy is purely kinetic and the interaction potential does not enter in an explicit way, instead it sets the boundary condition on the solution.



We are interested in scattering at small energy, so  $\mathcal{E} < V_0$ . For convenience we introduce  $\mathcal{K}^2 = \varkappa^2 - k^2$ , where  $\mathcal{K}$  is real. The second equation out of the pair (1.53) has a free wave solution which extends with the same amplitude to large distances, although the first equation has a decaying solution expressed in terms of the hyperbolic sinus:

$$u(r) = \begin{cases} A \sinh(\mathcal{K}r + \delta_1), & r < R \\ B \sin(kr + \delta), & r \geq R \end{cases} \quad (1.55)$$

The phase  $\delta_1$  must be equal to zero in order to obtain a solution which is not divergent at  $r = 0$  (see condition 1.40). We impose continuity of solution and its derivative in the point  $R$ :

$$\begin{cases} A \sinh(\mathcal{K}R) & = B \sin(kR + \delta) \\ A\mathcal{K} \cosh(\mathcal{K}R) & = Bk \cos(kR + \delta) \end{cases} \quad (1.56)$$

Condition of the continuity of the logarithmic derivative  $\mathcal{K} \cotanh(\mathcal{K}R) = k \cotan(kR + \delta)$  fixes the phase  $\delta(k)$  of the solution:

$$\delta(k) = \arctan\left(\frac{k}{\mathcal{K}} \tanh \mathcal{K}R\right) - kR \quad (1.57)$$

This defines the relation between constants  $A$  and  $B$ :

$$A^2 = \frac{B^2}{\sinh^2 kR + \left(\frac{\mathcal{K}}{k} \cos kR\right)^2} \quad (1.58)$$

By taking limit of low energy in (1.57) and using the definition (1.44) one obtains the expression for the  $s$ -wave scattering length for the scattering on the SS potential:

$$a_{3D} = R \left[ 1 - \frac{\tanh \varkappa R}{\varkappa R} \right] \quad (1.59)$$

If in the case of the hard core potential (1.48) the potential energy is absent, it is no longer so here. This makes it reasonable to use a pair of potentials SS-HS in order to test the universality of the  $s$ -wave description (see, *e.g.*, study done in Chapter. 3).

### 1.3.3 One-dimensional scattering problem

#### 1.3.3.1 General approach

We already have explored some aspects of the scattering problem in three-dimensions in Sec. 1.3.2. Here we will consider the problem of a one-dimensional scattering.

The scattering solution in a uniform system separates in center of the mass frame, as the property (1.38) is valid also in a 1D case. Thus in the following we will skip the trivial solution for the movement of the center of the mass and we will address the most interesting part due to solution for the relative coordinate  $z = z_1 - z_2$ . The one dimensional Schrödinger equation for the relative motion is written as

$$-\frac{\hbar^2}{2\mu} f''(z) + V_{int}(z)f(z) = \mathcal{E}f(z), \quad (1.60)$$

where the reduced mass  $\mu$  is given by (1.37). We will always consider scattering with a positive energy, even if the interaction potential itself might be attractive. Then the scattering energy can be written as  $\mathcal{E} = \hbar^2 k^2 / 2\mu$ , where  $k$  is real. The equation (1.60) becomes

$$f''(z) + \left( k^2 - \frac{2\mu V_{int}(z)}{\hbar^2} \right) f(z) = 0 \quad (1.61)$$

Its general solution can be written as<sup>5</sup>

$$f(z) = \cos(k|z| + \Delta(k)) \quad (1.62)$$

The one-dimensional scattering length is defined as the derivative of the phase  $\Delta(k)$  in the limit of low-energy scattering<sup>6</sup>

$$a_{1D} = - \lim_{k \rightarrow 0} \frac{\partial \Delta(k)}{\partial k} \quad (1.63)$$

### 1.3.3.2 Scattering on a pseudopotential

In a one-dimensional system the contact  $\delta$ -potential is a “good” potential and the problem of a scattering on it is solved in a standard manner, as described in Sec. 1.3.3.1 without any special tricks. The situation is different in three-dimensions where the  $\delta$ -potential has to be regularized (refer to Sec.1.3.4.1) in order to avoid a possible divergence which can be caused by the behavior of a symmetric solution (1.39).

The  $\delta$ -pseudopotential turns out to be highly useful theoretical tool. Indeed the commonly used Gross-Pitaevskii equation corresponds to pseudopotential interaction  $V_{int}(z) = g_{1D}\delta(z)$ . A system of particles with  $\delta$ -pseudopotential interaction (5.1) is one of few exactly solvable one dimensional quantum systems.

The Schrödinger equation (1.61) of the scattering on a pseudopotential

$$- \frac{\hbar^2}{2\mu} f''(z) + g_{1D}\delta(z)f(z) = \mathcal{E}f(z), \quad (1.64)$$

In the region  $|z| > 0$  it takes form of a free particle propagation  $f''(z) + k^2 f(z) = 0$  with the even solution given by

$$f(z) = \cos(k|z| + \Delta) \quad (1.65)$$

We are left with the only point  $z = 0$ , where the scattering potential is nonzero  $V_{int}(r) \neq 0$ . The infinite strength of the  $\delta$ -potential makes the first derivative of the potential be discontinuous. Indeed, the proper boundary condition can be obtained by integrating the equation (1.64) from

---

<sup>5</sup>In the three-dimensional system we look for solutions with spherical symmetry. In a one-dimensional system it is equivalent to searching even solutions.

<sup>6</sup>The textbook definition for the three-dimensional scattering length (1.44) can be recasted in a similar form  $a_{3D} = \lim_{k \rightarrow 0} \partial \delta / \partial k$ . We prefer to have a definition in terms of a derivative, as it does not cause any ambiguity in the choice a free particle phase. In three dimensions the phase of sinus (1.42) in absence of the scattering potential is fixed to zero due to the condition (1.40), which is no longer so in 1D case, as it should be fixed to  $\pi/2$ . Instead the definition (1.63) takes into account the difference between the phase in presence of scatterer and in its absence. See also footnote on p. 21.

infinitesimally small  $-\varepsilon$  up to  $+\varepsilon$ . The integral of the continuous function  $f_2(z)$  is proportional to  $\varepsilon$  and vanishes in the limit  $\varepsilon \rightarrow 0$ . Instead the  $\delta$ -function extracts the value of the function in zero and one obtains the relation

$$f'(\varepsilon) - f'(-\varepsilon) = \frac{2\mu g_{1D}}{\hbar^2} f(0) \quad (1.66)$$

This boundary condition for the solution (1.65) provides a relation between the scattering phase  $\Delta$  and the momentum  $k$  of an incident particle

$$\Delta(k) = -\operatorname{arccot} \frac{\hbar^2 k}{\mu g_{1D}} \quad (1.67)$$

Taking the limit of the low energy scattering from (1.63) one obtains the value of the scattering length

$$a_{1D} = -\frac{\hbar^2}{\mu g_{1D}} \quad (1.68)$$

This expression can be read the other around: for equal mass particles  $\mu = m/2$  the strength of the potential  $g_{1D}$  in a one-dimensional homogeneous system is related to the value of the one-dimensional coupling constant as

$$g_{1D} = -\frac{2\hbar^2}{ma_{1D}} \quad (1.69)$$

It is interesting to note, that the sign in the relation of the scattering length to the coupling constant is opposite to the one of a three dimensional system. In  $3D$  positive scattering length corresponds to repulsion and negative one to attraction. Another difference is that the  $3D$  coupling constant is directly proportional to the scattering length, although  $g_{1D}$  is inversely proportional to  $a_{1D}$ .

In terms of  $a_{1D}$  the phase (1.67) becomes

$$\Delta(k) = \operatorname{arccot} ka_{1D} \quad (1.70)$$

The scattering solution (1.65) gets written as:

$$f(z) = \cos(k|z| + \operatorname{arccot} ka_{1D}) \quad (1.71)$$

In the low energy limit  $k \rightarrow 0$  the phase (1.70) can be expanded  $\Delta(k) = \pi/2 - ka_{1D} + \mathcal{O}(k^3)$  and the scattering solution becomes simply  $f(z) = k(z - a_{1D})$ . One sees that the one-dimensional scattering length coincides with the position of the first node of the analytic continuation of the low-energy solution<sup>7</sup>.

---

<sup>7</sup>It turns out that this property is general and can be used as an alternative to (1.63) definition of the one-dimensional scattering length.

### 1.3.3.3 Scattering on a 1D square well potential

In this section we will consider scattering on a one-dimensional square well. The potential is similar to the one of the soft sphere with the difference that now the potential is attractive:

$$V^{SW}(z) = -V_0 \Theta(R^2 - z^2), \quad (1.72)$$

where  $R$  is the range of the potential. In the region  $|z| < R$  the kinetic energy of the slow particle can be neglected

$$f''(z) + V_0 f(z) = 0 \quad (1.73)$$

All solutions can be decomposed into a sum of even and odd solutions distinguished by the boundary condition at zero which can be either  $f(0) = 0$  or  $f'(0) = 0$ . We choose the state with the minimal energy, *i.e.*  $f'(0) = 0$ , which leads to the solution of the form

$$f(z) = A \cos(\sqrt{V_0} z), \quad |z| < R \quad (1.74)$$

In the other region  $|z| > R$  the interaction potential is absent and the solution is a plain wave

$$f(z) = B \sin(kz + \delta_0), \quad |z| < R \quad (1.75)$$

The scattering phase can be defined from the continuity condition of the logarithmic derivative at the matching distance  $R$ . This condition reads as

$$\frac{f'(R)}{f(R)} = -\sqrt{V_0} \tan(\sqrt{V_0} R) = k \cotan(kR + \delta_0) \quad (1.76)$$

Eq. (1.76) fixes the dependence of the phase on the wave number of the scattering particle:

$$\Delta(k) = -\operatorname{arccot} \frac{\sqrt{V_0} \tan(\sqrt{V_0} R)}{k} - kR \quad (1.77)$$

Finally, from (1.63) we obtain the expression for the scattering length on the 1D square well potential:

$$a_{1D} = R \left( 1 + \frac{\cotan(\sqrt{V_0} R)}{\sqrt{V_0} R} \right) \quad (1.78)$$

### 1.3.3.4 Scattering on a hard-rod potential

The hard-rod potential is a one-dimension version of the hard core potential, which in 3D correspond to a hard sphere (1.48). The HR potential is defined by its radius  $|a_{1D}|$

$$V^{HR}(z) = \begin{cases} +\infty, & |z| < |a_{1D}| \\ 0, & |z| \geq |a_{1D}| \end{cases} \quad (1.79)$$

The scattering phase in the solution (1.62) is fixed by the condition that the function vanishes at the HR radius  $\Delta = -k|a_{1D}| - \pi/2$ . From (1.63) immediately follows that the radius defined as (1.79) coincides with the value of the one dimensional scattering length. Again, as in Sec. 1.3.2.2 we have a hard core potential, for which its radius, the scattering length and the range of the potential are completely the same.

The scattering solution on a hard rod potential reads as

$$f(z) = \sin(k(|z| - |a_{1D}|)) \quad (1.80)$$

## 1.3.4 Pseudopotential

### 1.3.4.1 The pseudopotential method

As it was discussed above, in Secs. 1.3.2.1-1.3.2.3, scattering on different short-ranged potentials in the low-energy limit is universal, *i.e.* depends essentially on one parameter, the scattering length and the particular shape of the potential is of no large importance. Thus it is very useful to relate scattering on all those potentials to a scattering on a simple  $\delta$ -potential. In other words instead of considering a particular shape of the interaction potential, we give the description in terms of a free scattering solution at  $|\vec{r}'| > 0$  with an appropriate boundary condition at  $r = 0$ , which takes properly into account the scattering length and, thus, the interaction potential.

In one dimensional case the application of this scheme is straight as the Schrödinger equation for two particles can be directly solved, as it is explained in the Sec. 1.3.3.2. In three dimensions the situation is more complicated as the behavior of the solution (1.39) is not compatible with scattering on a  $\delta$ -potential and special adjustments should be made.

Let us revise the solution of the Schrödinger equation in the limit of low energy scattering. From the definition of the three-dimensional scattering length (1.44) it follows that the scattering solution vanishes at the distance  $r = a_{3D}$ . Thus we define the scattering function of the pseudopotential in such a way that it satisfies the free scattering equation in the region  $r > 0$ :

$$(\Delta + k^2)f(r) = 0, \quad r > 0 \quad (1.81)$$

We will use the expression (1.45) to approach the  $r \rightarrow 0$  limit:

$$f(r) \rightarrow \chi \left(1 - \frac{a_{3D}}{r}\right) \quad (1.82)$$

where the constant  $\chi$  can be related to the scattering length by multiplying (1.82) by  $r$  and differentiating

$$\chi = \lim_{r \rightarrow 0} \frac{\partial}{\partial r}(rf(r)) \quad (1.83)$$

We can now modify Eq. 1.81 in such a way that it satisfies the correct boundary condition (1.82). By inserting (1.82) into (1.81) we obtain<sup>8</sup>

$$(\Delta + k^2)\chi \left(1 - \frac{a_{3D}}{r}\right) = -4\pi\delta(r)\frac{\partial}{\partial r}(rf(r)) \quad (1.84)$$

The operator  $\delta(\vec{r})\frac{\partial}{\partial r}(r\cdot)$  is called the *pseudopotential*. Going back to energy units we obtain the relation between the strength of the pseudopotential  $g_{3D}$  (*coupling constant*) and the three-dimensional scattering length

$$V_{int} = g_{3D}\delta(\vec{r})\frac{\partial}{\partial r}(r\cdot) \quad (1.85)$$

$$g_{3D} = \frac{4\pi\hbar^2}{m}a_{3D}, \quad (1.86)$$

---

<sup>8</sup>We used property  $\Delta(1/r) = -4\pi\delta(r)$ , which can be easily obtained from the solution  $f(\vec{r}) = -\frac{1}{4\pi} \int \frac{\rho(\vec{r}')}{|\vec{r}-\vec{r}'|} d\vec{r}'$  to the Poisson equation  $\Delta f(\vec{r}) = \rho(\vec{r})$  substituting the point charge  $\rho(\vec{r}) = \delta(\vec{r})$ .

where we considered the case of equal-mass particles  $\mu = m/2$ .

The pseudopotential (1.85,1.86) was used by Olshanii [Ols98] to solve quasi one dimensional scattering problem in a tight harmonic transverse confinement.

Finally, the wave function  $f(r)$  satisfies the equation<sup>9</sup>:

$$\left( -\frac{\hbar^2}{2m}\Delta_1 - \frac{\hbar^2}{2m}\Delta_2 + \frac{4\pi\hbar^2}{m}\delta(r_{12})\frac{\partial}{\partial r_{12}}(r_{12} \cdot) \right) f(\vec{r}_1, \vec{r}_2) = \mathcal{E}f(\vec{r}_1, \vec{r}_2), \quad (1.87)$$

### 1.3.5 Resonance scattering

In the previous sections we considered situation, when the scattering happens on the lowest energy level. In this case the  $s$ -wave scattering length  $a$  for any finite strength potential is smaller than the range of the potential  $R$  (see, *e.g.* Secs. 1.3.2.3,1.3.3.3) and equals to  $R$  in the case of the infinite strength potential (Secs. 1.3.2.2,1.3.3.4). The pseudopotential description (Secs. 1.3.3.2,1.3.4.1) falls into a different class of problem used at a small density, where the exact type of the potential is not important and it is substituted by the boundary condition at  $r = 0$ . In this sense the range of the pseudopotential is zero  $R = 0$  and we have opposite condition

$$|a| \gg R \quad (1.88)$$

A physical realization of 3D scattering satisfying the condition (1.88) can be achieved in the case of a *resonant scattering*. In this Section we will describe scattering on the first excited state of attractive potentials supporting a bound state in the case when the position of the excited state is close to zero-energy continuum level.

#### 1.3.5.1 Scattering on a square-well potential

Let us consider an attractive version of the soft sphere potential (1.52):

$$V^{SW}(r) = \begin{cases} -V_0, & r < R \\ 0, & r \geq R \end{cases} \quad (1.89)$$

Interaction (1.89) is called a *square-well* potential, with  $V_0$  (positive) being its depth and  $R$  being its range. The Schrödinger equation (1.41) for a pair of particles in the center of mass system is given by

$$\begin{cases} u''(r) + (k^2 + \varkappa^2)u(r) = 0, & r < R \\ u''(r) + k^2u(r) = 0, & r \geq R \end{cases}, \quad (1.90)$$

where, as usual,  $k^2 = m\mathcal{E}/\hbar^2$  and

$$\varkappa^2 = -mV_0/\hbar^2 > 0 \quad (1.91)$$

We are interested in finding solutions with positive energies, as that are the solutions corresponding to a scattered state, instead solutions with negative energy are localized. On the opposite to the situation described in Sec. 1.3.5.1, the interaction potential is always lower than the value of the

---

<sup>9</sup>Additional literature on the topic of pseudopotential description can be found in classical articles [Fer36],[HY57] and in books [BW52],p.74, [Hua87].

scattering energy  $V_{int}(r) < \mathcal{E}$ . For convenience we introduce  $\mathcal{K}^2 = \varkappa^2 + k^2 > 0$ . In both regions the solution is a free-wave like:

$$u(r) = \begin{cases} A \sin(\mathcal{K}r + \delta_1), & r < R \\ B \sin(kr + \delta), & r \geq R \end{cases} \quad (1.92)$$

The condition (1.40) immediately fixes the phase  $\delta_1 = 0$ . The matching equations for the function and its derivative read as

$$\begin{cases} A \sin(\mathcal{K}R) & = B \sin(kR + \delta) \\ A\mathcal{K} \cos(\mathcal{K}R) & = Bk \cos(kR + \delta) \end{cases} \quad (1.93)$$

Condition of the continuity of the logarithmic derivative  $\mathcal{K} \cotan(\mathcal{K}R) = k \cotan(kR + \delta)$  fixes the phase  $\delta(k)$  of the solution

$$\delta(k) = \arctan\left(\frac{k}{\mathcal{K}} \tan \mathcal{K}R\right) - kR \quad (1.94)$$

This builds the relation between constants  $A$  and  $B$ :

$$A^2 = \frac{B^2}{\sin^2 kR + \left(\frac{\mathcal{K}}{k} \cos kR\right)^2} \quad (1.95)$$

By taking limit of low energy in (1.94) and using the definition (1.44) one obtains the expression for the  $s$ -wave scattering length:

$$a_{3D} = R \left[ 1 - \frac{\tan \varkappa R}{\varkappa R} \right] \quad (1.96)$$

The dependence of the scattering length of the scattering on a soft sphere potential (Eq. 1.59) looks similar to (1.96) with the only difference that the trigonometric tangent is substituted with the hyperbolic one. The difference is crucial. Indeed, as  $0 < \tanh(x)/x \leq 1$ , the scattering length on the SS potential is always smaller than the range of the potential. Instead, the term  $\tan(x)/x$  is unbound. When the scattering happens at *resonant* momentum  $\varkappa R = \pi/2 + \Delta(\varkappa)$  with small detuning  $|\Delta(\varkappa)| \ll 1$ , the scattering length becomes extremely large and changes its sign.

The square well potential is attractive and in principle can have the bound state solution with energy  $E_b = -\hbar^2 k_b^2/m < 0$ . In outer region  $r > R$  the solution (1.92) gets modified and decays exponentially fast. The condition of the continuity of the logarithmic derivative in the limit  $k \rightarrow 0$  is  $\varkappa \tan \varkappa R = k_b \tanh k_b R$ . This condition can not be satisfied before crossing the resonance, as inequality  $\tan x > \tanh x$  holds for arguments  $x < 0 < \pi/2$ . Instead immediately after the resonance position  $\Delta(\varkappa) > 0$  a shallow bound state appears in the system.

### 1.3.5.2 Scattering on a modified Pöschl-Teller potential

The potential (1.89) considered in the previous section might be inconvenient in some cases, as it produces large gradients of the solution at its border  $r \approx R$  due to the abrupt change of its value from  $-V_0$  to zero. This can be avoided by using, for example, the modified Pöschl-Teller potential

$$V(r) = -\frac{V_0}{\cosh^2(r/R)} = -\frac{\hbar^2}{2mR^2} \frac{\lambda(\lambda-1)}{\cosh^2(r/R)}, \quad (1.97)$$

where  $V_0$  is the depth of the potential and  $R$  is its range.

The problem of three-dimensional scattering on this potential can be solved analytically (see, *e.g.* [Flu71]) and the dependence of the  $s$ -wave scattering length on the depth of the potential well can be found explicitly:

$$\frac{a_{3D}}{R} = \frac{\pi}{2} \cotan \frac{\pi\lambda}{2} + \gamma + \Psi(\lambda), \quad (1.98)$$

where  $\gamma = 0.5772\dots$  is the Euler's constant and  $\Psi$  is the Digamma function. This dependence is expressed in the Fig. 4.2.

## 1.4 Energy of the TG and HR gas

### 1.4.1 Energy of the Tonks-Girardeau gas

In the very dilute  $1D$  regime, when the one-dimensional gas parameter becomes extremely small  $n_{1D}|a_{1D}| \ll 1$ , the  $1D$  system of bosons can be mapped onto  $1D$  system of fermions [Gir60]. In a fermionic system the number of fermions is given by the volume of the fermi sphere (the bosons are mapped onto spinless fermions). In a one-dimensional system this volume degenerates to  $2k_F$ :

$$N = L \int_{-k_F}^{k_F} \frac{dk}{2\pi} = \frac{1}{\pi} k_F L \quad (1.99)$$

We obtain that the relation of the fermi wave number  $k_F$  to the density  $n_{1D}$  is linear

$$k_F = \pi n_{1D} \quad (1.100)$$

The value of  $k_F$  fixes the scale for the correlation functions. The static structure factor (5.5) completely changes its behavior at  $k = 2k_F$ . The value of  $k_F$  fixes period of oscillations in the pair distribution function (5.4). Being the only spatial length scale in a homogeneous system,  $1/k_F$  fixes at the same time value of the healing length  $\xi$ , and consequently the border at which starts the asymptotic power law decay of the one-body density matrix.

The chemical potential equals to the fermi energy (this is the definition of the fermi energy):

$$\mu_F = \frac{\pi^2 \hbar^2}{2m} n_{1D}^2 \quad (1.101)$$

The energy is obtained by integration of the chemical potential. The energy per particle turns out to be equal to

$$E_F = \frac{\pi^2 \hbar^2}{6m} n_{1D}^2 \quad (1.102)$$

### 1.4.2 Hard-rod gas

Let us consider a gas of  $N$  hard rod bosons of size  $a_{1D}$ <sup>10</sup>. The energy of the hard-rod gas is easily obtained from the expression for the energy of the Tonks-Girardeau gas (1.102) by subtracting the

---

<sup>10</sup>As discussed in Sec. 1.3.3.4, the size of a hard-rod equals to the one-dimensional scattering length on HR potential (1.79).



excluded volume  $n \rightarrow N/(L - Na_{1D})$  [Gir60, KMJ99]

$$\frac{E_{HR}}{N} = \frac{\pi^2 \hbar^2 n_{1D}^2}{6m} \frac{1}{(1 - n_{1D} a_{1D})^2} \quad (1.103)$$

The chemical potential is the derivative of the energy with respect to number of particles

$$\mu_{HR} = \frac{\pi^2 \hbar^2 n_{1D}^2}{2m} \frac{(1 - a_{1D} n_{1D}/3)}{(1 - a_{1D} n_{1D})^3}, \quad (1.104)$$

If the density is small  $n_{1D} a_{1D} \ll 1$ , one is allowed to make an expansion of (1.103) in terms of the small parameter:

$$\frac{E}{N} = \frac{\pi^2 \hbar^2 n_{1D}^2}{6m} + \frac{\pi^2 \hbar^2 n_{1D}^3 a_{1D}}{3m} \quad (1.105)$$

It is interesting to note, while the ‘‘excluded volume’’ term was derived for  $a_{1D} > 0$ , it still provides the leading correction to the TG energy (1.102) in the Lieb-Liniger Hamiltonian (5.1), *i.e.* for  $a_{1D} < 0$ . The point is that it describes the interaction energy, which is absent in a TG gas (see argumentation done on page 124). The equation of state in LL model can be found exactly by solving the integral equations (A.1-A.3). An iterative solution in the considered region  $n_{1D} |a_{1D}| \ll 1$  provides a way for the calculation of the expansion

$$e(n|a_{1D}|) = \frac{\pi^2}{3} - \frac{2}{3} \pi^2 n_{1D} |a_{1D}|, \quad (1.106)$$

where we adopt standard for LL equations notation (5.3). This formula is consistent with (1.105) and can be obtained by solving recursively the Lieb-Liniger integral equations (A.1-A.3).

## 1.5 Gross Pitaevskii Equation

### 1.5.1 Variational derivation of the GPE

Let us consider  $N$  identical bosons in an external potential  $V_{ext}$ . For  $T \ll T_c$  all particle stay in the ground state of the Hamiltonian:

$$\hat{H} = \sum_{i=1}^N \left[ \frac{\hat{p}_i^2}{2m} + V_{ext}(\vec{r}_i) \right] + \frac{1}{2} \sum_{i \neq j}^N V_{int}(\vec{r}_i - \vec{r}_j), \quad (1.107)$$

At low temperatures, namely when the de Broglie wavelength  $\lambda_T$  becomes much larger than the range of  $V_{int}(r_{ij})$ , only s-wave scattering between pairs of bosons remains significant, and we can approximate  $V_{int}(r_{ij})$  by a pseudopotential (1.86).

Generally, the ground state of  $\hat{H}$  cannot be determined exactly. In the absence of interactions however, it is a product state: all the bosons are in the ground state of the single particle Hamiltonian. In the presence of *weak* interactions, one still can approximate the ground state of  $\hat{H}$  by a product state:

$$|\phi_0\rangle = |\psi(1)\rangle \dots |\psi(N)\rangle, \quad (1.108)$$

where all bosons are in the same state  $|\psi\rangle$ <sup>11</sup>.

Obviously,  $|\phi_0\rangle$  is symmetric with the respect to exchange of particles and has the correct symmetry for a system of bosons. Contrary to the non-interacting case,  $|\psi\rangle$  is no longer the ground state of the single particle Hamiltonian, but has to be determined by minimizing the energy:

$$E = \frac{\langle\phi_0|\hat{H}|\phi_0\rangle}{\langle\phi_0|\phi_0\rangle} \quad (1.109)$$

Let us calculate the value of (1.107) averaged over the Fock state (1.108). In the coordinate representation the external potential energy becomes:

$$\langle\phi_0|\sum_{i=1}^N V_{ext}(\vec{r}_i)|\phi_0\rangle = \int \psi^*(\vec{r}_N)\dots\psi^*(\vec{r}_1) \sum_{i=1}^N V_{ext}(\vec{r}_i)\psi(\vec{r}_1)\dots\psi(\vec{r}_N) d\mathbf{R} = N \int \psi^*(\vec{r})V_{ext}(\vec{r})\psi(\vec{r}) d\vec{r}$$

For the interaction between the particles we obtain:

$$\begin{aligned} \langle\phi_0|\sum_{i\neq j}^N \frac{1}{2}V_{int}(r_{ij})|\phi_0\rangle &= \int \psi^*(\vec{r}_N)\dots\psi^*(\vec{r}_1) \frac{1}{2} \sum_{i\neq j}^N V_{int}(r_{ij})\psi(\vec{r}_1)\dots\psi(\vec{r}_N) d\mathbf{R} = \\ &= \frac{1}{2} \sum_{i\neq j}^N \iint \psi^*(\vec{r}_i)\psi^*(\vec{r}_j)V_{int}(r_{ij})\psi(\vec{r}_i)\psi(\vec{r}_j) d\vec{r}_i d\vec{r}_j = \frac{N(N-1)}{2} \iint \psi^*(\vec{r})\psi^*(\vec{r}')V_{int}(|\vec{r}-\vec{r}'|)\psi(\vec{r})\psi(\vec{r}') d\vec{r}d\vec{r}' \end{aligned}$$

Thus we obtain the expression of the total Hamiltonian in the first quantization (see, also, (1.16))

$$\langle\hat{H}\rangle = N \int \psi^*(\vec{r}) \left( -\frac{\hbar^2 \Delta}{2m} + V_{ext} \right) \psi(\vec{r}) d\vec{r} + \frac{N(N-1)}{2} \iint \psi^*(\vec{r})\psi^*(\vec{r}')V_{int}(|\vec{r}-\vec{r}'|)\psi(\vec{r})\psi(\vec{r}') d\vec{r}d\vec{r}' \quad (1.110)$$

We now look for the minimum of the energy  $\langle\phi_0|\hat{H}|\phi_0\rangle$  keeping the normalization fixed  $\langle\phi_0|\phi_0\rangle = 1$ . Because  $\psi$  in general is a complex number, we can consider the variations  $\delta\psi$  and  $\delta\psi^*$  as independent. Using the method of Lagrange multipliers, the approximate ground state  $|\phi_0\rangle$  has to satisfy:

$$\delta \left[ \langle\phi_0|\hat{H}|\phi_0\rangle \right] - \mu \delta \langle\phi_0|\phi_0\rangle = 0, \quad (1.111)$$

where  $\mu$  is the Lagrange multiplier associated with the constraint  $\langle\phi_0|\phi_0\rangle = 1$ .

Inserting the expression (1.110) in equation (1.111) and setting to zero the linear term  $\delta\psi^*$  we yield:

$$\left( -\frac{\hbar^2}{2m}\Delta + V_{ext} \right) \psi(\vec{r}) + (N-1) \left( \int V_{int}(|\vec{r}-\vec{r}'|)|\psi(\vec{r}')|^2 d\vec{r}' \right) \psi(\vec{r}) = \mu\psi(\vec{r}) \quad (1.112)$$

Now we use that the properties of the  $s$ -wave scattering at the discussed conditions can be described by using the pseudopotential (1.86) and, finally, obtain

$$\left( -\frac{\hbar^2}{2m}\Delta + V_{ext} \right) \psi(\vec{r}) + (N-1)g_{3D}|\psi(\vec{r})|^2\psi(\vec{r}) = \mu\psi(\vec{r}) \quad (1.113)$$

---

<sup>11</sup>It is important to note that  $|\psi\rangle$  is not a wave function and in this sense the derived below GPE (1.115) is not a “non linear Schrödinger equation”. In particular its time evolution is driven by the chemical potential  $\mu$  instead of the energy of the system  $E$ , as it happens for the solution of the Schrödinger equation.

This is the Gross-Pitaevskii equation [Gro61, Pit61]. It has a straightforward interpretation: each boson evolves in the external potential  $V_{ext}$  and in the *mean-field* potential produced by the other  $N - 1$  bosons.

Let us clarify the meaning of the parameter  $\mu$ , which was introduced formally as a Lagrange multiplier. Multiplying GP equation (1.113) by  $\psi^*(r)$  and by carrying out an integrating over  $r$  we have:

$$\mu = \int \psi^*(\vec{r}) \left( -\frac{\hbar^2 \Delta}{2m} + V_{ext} \right) \psi(\vec{r}) d\vec{r} + (N - 1) \int \psi^*(\vec{r}) \psi^*(\vec{r}') V_{int}(|\vec{r} - \vec{r}'|) \psi(\vec{r}) \psi(\vec{r}') d\vec{r} d\vec{r}' \quad (1.114)$$

A direct comparison to (1.110) shows that  $\mu = \frac{d}{dN} \langle \phi_0 | \hat{H} | \phi_0 \rangle$  (number of considered particles is large) and thus  $\mu$  has a physical meaning of the chemical potential.

An alternative way is to normalize the wave function to the number of particles in the system  $\langle \phi_0 | \phi_0 \rangle = N$ . In this normalization GPE reads as ( $N \gg 1$ ):

$$\left( -\frac{\hbar^2}{2m} \Delta + V_{ext} \right) \psi(\vec{r}) + g_{3D} |\psi(\vec{r})|^2 \psi(\vec{r}) = \mu \psi(\vec{r}) \quad (1.115)$$

## 1.5.2 Coupling constant in quasi one- and two- dimensional systems

The mean-field relation of the coupling constant in 1D,  $g_{1D}$  and in 2D,  $g_{2D}$ , to the three dimensional scattering length  $a_{3D}$  in restricted geometries can be found by repeating the derivation given in Sec. 1.5.1 while assuming that the order parameter  $\psi$  can be factorized. We start from the energy functional (1.110)

$$E[\psi] = \int \left( \frac{\hbar^2}{2m} |\nabla \psi|^2 + V_{ext} |\psi|^2 + \frac{g_{3D}}{2} |\psi|^4 \right) d\mathbf{r}, \quad (1.116)$$

where, according to (1.86),  $g_{3D} = 4\pi\hbar^2 a/m$  is the three dimensional coupling constant. The variational procedure

$$i\hbar \frac{\partial \psi}{\partial t} = \frac{\delta E}{\delta \psi^*} \quad (1.117)$$

gives time-dependent Gross-Pitaevskii equation

$$i\hbar \frac{\partial \psi(\vec{r}, t)}{\partial t} = \left( -\frac{\hbar^2 \Delta}{2m} + g_{3D} |\psi(\vec{r}, t)|^2 \right) \psi(\vec{r}, t) \quad (1.118)$$

In the presence of an external confinement along one direction (disk-shaped condensate)  $V_{ext}(\vec{r}) = m\omega^2 x^2/2$  we assume a gaussian *ansatz* for the wave function  $\psi(\mathbf{r}, t) = \psi_{osc}(x) \varphi(y, z, t)$  with  $\psi_{osc}(x) = \pi^{-1/4} a_{osc}^{-1/2} \exp(-x^2/2a_{osc}^2)$  being ground state wave function of a harmonic oscillator. The integration over  $x$  in (1.116) can be easily done by using following properties of the gaussian function  $\psi_{osc}$ :

1. Normalization properties

$$\int \psi_{osc}^2(x) dx = 1, \quad \int \psi_{osc}^4(x) dx = \frac{1}{\sqrt{2\pi} a_{osc}} \quad (1.119)$$

2. The function  $\psi_{osc}$  is a stationary solution of a one-dimensional Schrödinger equation in a trap

$$\left(-\frac{\hbar^2}{2m}\frac{\partial^2}{\partial x^2} + \frac{m\omega^2 x^2}{2}\right)\psi_{osc}(x) = \frac{\hbar\omega}{2}\psi_{osc}(x) \quad (1.120)$$

Integrating out  $x$  from the GP energy functional (1.116) and doing the variational procedure (1.117) we obtain the Gross-Pitaevskii equation in a quasi two dimensional system

$$i\hbar\frac{\partial\varphi(y,z,t)}{\partial t} = \left(-\frac{\hbar^2}{2m}\left(\frac{\partial^2}{\partial y^2} + \frac{\partial^2}{\partial z^2}\right) + g_{2D}|\varphi(y,z,t)|^2 + \frac{\hbar\omega}{2}\right)\varphi(y,z,t), \quad (1.121)$$

where the two dimensional coupling constant is given by

$$g_{2D} = \frac{g_{3D}}{\sqrt{2\pi}a_{osc}} = \frac{2\sqrt{2\pi}\hbar^2 a}{ma_{osc}} \quad (1.122)$$

If the external potential restricts the motion in two dimensions (*i.e.* in a cigar-shaped condensate) and the confinement is so strong that no excitations in the radial direction are possible, the wave function gets factorized in the following way:  $\psi(\vec{r}, t) = \psi_{osc}(x)\psi_{osc}(y)\phi(z)$ . The explicit integration in (1.116) over  $x$  and  $y$  leads to one-dimensional Gross-Pitaevskii equation

$$i\hbar\frac{\partial\varphi(z,t)}{\partial t} = \left(-\frac{\hbar^2}{2m}\frac{\partial^2}{\partial z^2} + g_{1D}|\varphi(z,t)|^2 + \hbar\omega\right)\varphi(z,t) \quad (1.123)$$

Here  $g_{1D}$  denotes effective one-dimensional coupling constant

$$g_{1D} = \frac{g_{3D}}{2\pi a_{osc}^2} = \frac{2\hbar^2 a}{ma_{osc}^2} \quad (1.124)$$

Comparing it with the definition of the 1D coupling constant  $g_{1D} = -2\hbar^2/(ma_{1D})$  (1.69) we find the mean-field relation of one-dimensional scattering length  $a_{1D}$  to the three-dimensional scattering length  $a$  and oscillator length  $a_{osc}$ :

$$a_{1D} = -\frac{a_{osc}^2}{a} \quad (1.125)$$

## 1.6 Local Density Approximation

It happens often, that properties of a homogeneous system are well known (*e.g.* the homogeneous model is exactly solvable, or numerical calculation has been done), but the properties of the system in an external field are not known. If number of particles is large enough one can refer to the *local density approximation* in order to obtain the desired properties.

### 1.6.1 General method

In the local density approximation one assumes that the chemical potential  $\mu$  is given by sum of the local chemical potential  $\mu_{loc}$ , which is the chemical potential of the uniform system, and the external field:

$$\mu = \mu_{hom}(n(\vec{r})) + V_{ext}(\vec{r}) \quad (1.126)$$

The local chemical potential  $\mu_{\text{hom}}$  is defined by the equation of state in absence of the external field and accounts for the interaction between particles and partially for the kinetic energy.

The value of the chemical potential  $\mu$  is fixed by the normalization condition

$$N = \int n(\vec{r}) d\vec{r}, \quad (1.127)$$

where the density profile is obtained by inverting the density dependence of the local chemical potential  $n = \mu_{\text{hom}}^{-1}$ .

Once the chemical potential  $\mu$  is known a lot of useful information can be inferred: the density profile, energy, size of the cloud, density moments  $\langle r^2 \rangle$ , etc.

In the following we will always consider a harmonic external confinement:

$$V_{\text{ext}}(\vec{r}) = \frac{1}{2}m\omega_x x^2 + \frac{1}{2}m\omega_y y^2 + \frac{1}{2}m\omega_z z^2 \quad (1.128)$$

The normalization condition (1.127) becomes:

$$N = \iiint \mu_{\text{hom}}^{-1} \left[ \mu - \frac{1}{2}m\omega_x x^2 - \frac{1}{2}m\omega_y y^2 - \frac{1}{2}m\omega_z z^2 \right] dx dy dz \quad (1.129)$$

The sizes of the cloud in three directions  $R_x, R_y, R_z$  is fixed by the value of the chemical potential and corresponding frequencies of the harmonic confinement through relation:

$$\mu = \frac{1}{2}m\omega_x R_x^2 = \frac{1}{2}m\omega_y R_y^2 = \frac{1}{2}m\omega_z R_z^2 \quad (1.130)$$

We express the distances in the trap in units of the size of the cloud:  $\tilde{r} = (x/R_x, y/R_y, z/R_z)$  and in front of the integral (1.129) we have the geometrical average  $R_x R_y R_z = R^3$  appearing. It means that the trap frequencies (even if the trap is not spherical) enter only through combination  $\omega_{ho} = (\omega_x \omega_y \omega_z)^{1/3}$  and the oscillator lengths correspondingly through parameter  $a_{ho} = \sqrt{\hbar/m\omega}$ . Now the integral is to be taken inside a sphere of radius 1 and is symmetric in respect to  $\tilde{r}$ . It follows immediately, that the normalization condition (1.129) in general can be written as

$$\Delta_{3D}^3 = \tilde{\mu}^{3/2} \int_0^1 a^3 \mu_{\text{hom}}^{-1} \left[ \frac{\hbar^2}{ma^2} \tilde{\mu} \Delta_{3D}^2 (1 - \tilde{r}^2) \right] 4\pi \tilde{r}^2 d\tilde{r}, \quad (1.131)$$

here the dimensionless chemical potential  $\tilde{\mu}$  is obtained by choosing  $\frac{N^{1/3}}{2} \hbar \omega_{ho}$  as the unit of energy in the trap, the density in a homogeneous system  $\mu_{\text{hom}}^{-1}$  is measured in units of  $a^{-3}$ , where  $a$  is a length scale convenient for the homogeneous system (for example it can be equal to the  $s$ -wave scattering length  $a_{3D}$ ), chemical potential (*i.e.* the argument of the inverse function  $\mu_{\text{hom}}^{-1}$ ) is measured in units of  $\hbar^2/ma^2$ , and, finally, the characteristic parameter  $\Delta_{3D}$  is defined as

$$\Delta_{3D} = N^{1/6} \frac{a}{a_{ho}} \quad (1.132)$$

From the Eq. 1.131, which is basically a dimensionless version of Eq. 1.129 we discover there is a scaling in terms of the characteristic parameter  $\Delta_{3D}$ . In other words systems having different number of particles and oscillator frequencies will have absolutely the same density profile and other LDA properties (once expressed in the correct units as discussed above) if they have equal values of parameter (1.132).

A similar procedure can be carried in a one-dimensional case (we choose the  $z$  axis), where the normalization condition reads as

$$N = \int \mu_{\text{hom}}^{-1} \left[ \mu - \frac{1}{2} m \omega_z z^2 \right] dz \quad (1.133)$$

Its dimensionless form is obtained by measuring the energies in the trap in units of  $\frac{1}{2} N \hbar \omega_z$

$$\Delta_{1D} = \tilde{\mu}^{1/2} \int_{-1}^1 a \mu_{\text{hom}}^{-1} \left[ \frac{\hbar^2}{m a^2} \tilde{\mu} \Delta_{1D}^2 (1 - \tilde{z}^2) \right] d\tilde{z}, \quad (1.134)$$

and the one-dimensional characteristic parameter is related to the number of particles as

$$\Delta_{1D} = \frac{N^{1/2} a}{a_z} \quad (1.135)$$

### 1.6.2 Exact solution for 1D “perturbative” equation of state

We will start from very general equation of state of a homogeneous system which can be found in any type of first-order perturbation theory. In the zeroth approximation one has<sup>1213</sup>:

$$\mu_{\text{hom}}^{(0)} = C_1 (na)^{\gamma_1} \frac{\hbar^2}{m a^2}, \quad (1.136)$$

here  $a$  is unit of length,  $C_1$  is a numerical coefficient of the leading term in the chemical potential and  $\gamma_1$  is the power of the dependence on the gas parameter  $na$ . The next term of perturbation in general can be written as

$$\mu_{\text{hom}}^{(1)} = C_1 (na)^{\gamma_1} (1 + C_2 (na)^{\gamma_2} + \dots) \frac{\hbar^2}{m a^2}, \quad (1.137)$$

where  $C_2 (na)^{\gamma_2} \ll 1$ . We will use local density approximation (Sec. 1.6) in order to obtain properties of trapped system. The equation (1.126) can be inverted by using (1.137) to obtain the density profile  $n(z)$ :

$$n(z)a = \left( \frac{1}{C_1} \frac{\mu}{\hbar^2/m a^2} \left( 1 - \frac{z^2}{R^2} \right) \right)^{\frac{1}{\gamma_1}} - \frac{C_2}{\gamma_1} \left( \frac{1}{C_1} \frac{\mu}{\hbar^2/m a^2} \left( 1 - \frac{z^2}{R^2} \right) \right)^{\frac{1+\gamma_2}{\gamma_1}}, \quad (1.138)$$

here size of the cloud  $R$  is related to the chemical potential  $\mu = \frac{1}{2} m \omega^2 R^2$  (1.130).

The value of the chemical potential is fixed by the normalization condition (1.127). It is convenient to make use of the integral equality [GR80]

$$\int_{-1}^1 (1 - x^2)^\alpha dx = \frac{\sqrt{\pi} \Gamma(\alpha + 1)}{\Gamma(\alpha + \frac{3}{2})}, \quad \alpha > -1 \quad (1.139)$$

<sup>12</sup>This approximation is called *polytropic*.

<sup>13</sup>Many theories produces results that fall into the class of equations of state described by formula (1.136). For example GP theory, ideal fermi gas, TG gas.

Thus we have restriction on the polytropic indices  $\gamma_1 > -1$ ,  $\frac{\gamma_1+\gamma_2}{\gamma_1} > -1$ . If those conditions are satisfied, then the leading contribution to the chemical potential is given by

$$\frac{\mu^{(0)}}{\hbar^2/ma^2} = \left( \frac{C_1^{1/\gamma_1} \Gamma(\frac{1}{\gamma_1} + \frac{3}{2})}{\sqrt{2\pi}\Gamma(\frac{1}{\gamma_1} + 1)} \Delta_{1D}^2 \right)^{\frac{2\gamma_1}{2+\gamma_1}}, \quad (1.140)$$

where  $\Delta_{1D}$  is the characteristic parameter of a one-dimensional trapped gas defined by (1.135).

In the next order of accuracy the chemical potential is given by

$$\frac{\mu^{(1)}}{\hbar^2/ma^2} = \frac{\mu^{(0)}}{\hbar^2/ma^2} + \frac{\sqrt{8\pi} C_1^{-\frac{1+\gamma_2}{\gamma_1}} C_2}{(2+\gamma_1) \Delta_{1D}^2} \frac{\Gamma(1 + \frac{1+\gamma_2}{\gamma_1})}{\Gamma(\frac{3}{2} + \frac{1+\gamma_2}{\gamma_1})} \left( \frac{\mu^{(0)}}{\hbar^2/ma^2} \right)^{\frac{3}{2} + \frac{1+\gamma_2}{\gamma_1}} \quad (1.141)$$

The mean square displacement  $\langle z^2 \rangle = \frac{1}{N} \int_{-R}^R z^2 n(z) dz$  is directly related to the potential energy of the oscillator confinement and is given by

$$\frac{\langle z^2 \rangle}{R^2} = \frac{\gamma_1}{2+3\gamma_1} \left( 1 + \frac{\sqrt{\pi} C_2 \gamma_2}{2^{1+\frac{2}{\gamma_1}}} \frac{\Gamma(2 + \frac{2}{\gamma_1}) \Gamma(1 + \frac{1+\gamma_2}{\gamma_1})}{\Gamma(\frac{1}{\gamma_1})^2 \Gamma(\frac{5}{2} + \frac{1+\gamma_2}{\gamma_1})} \left( \frac{1}{C_1} \frac{\mu}{\hbar^2/m a^2} \right)^{\frac{\gamma_2}{\gamma_1}} \right) \quad (1.142)$$

The frequencies of the collective oscillations can be predicted within LDA. The frequency of the breathing mode is inferred from the derivative of the mean square displacement  $\Omega_z^2 = -2 \langle z^2 \rangle / \frac{\partial \langle z^2 \rangle}{\partial \omega^2}$  [MS02] and equals to

$$\frac{\Omega_z^2}{\omega_z^2} = (2+\gamma_1) + \frac{\sqrt{\pi} C_2 \gamma_2 (\gamma_1 + \gamma_2) \left( \frac{3}{2} + \frac{1}{\gamma_1} \right) \Gamma(1 + \frac{1+\gamma_2}{\gamma_1}) \Gamma(2 + \frac{2}{\gamma_1})}{2^{1+\frac{2}{\gamma_1}} \Gamma(1 + \frac{1}{\gamma_1}) \Gamma(\frac{1}{\gamma_1}) \Gamma(\frac{5}{2} + \frac{1+\gamma_2}{\gamma_1})} \left( \frac{\Gamma(\frac{3}{2} + \frac{1}{\gamma_1}) \Delta_{1D}^2}{\sqrt{2\pi} C_1 \Gamma(1 + \frac{1}{\gamma_1})} \right)^{\frac{2\gamma_2}{2+\gamma_1}} \quad (1.143)$$

The obtained formula is very general and gives an insight to many interesting cases where the perturbation theory can be developed. In the table (1.1) we summarize some of the examples.

### 1.6.3 Exact solution for 3D “perturbative” equation of state

In this Section we will develop theory in three-dimensions for the “perturbative” equation of state which we define as:

$$\mu_{\text{hom}}^{(0)} = C_1 (na^3)^{\gamma_1} (1 + C_2 (na^3)^{\gamma_2}) \frac{\hbar^2}{ma^2}, \quad (1.144)$$

where the  $|C_2 (na^3)^{\gamma_2}| \ll 1$  is the perturbative term.

Within the local density approximation we obtain the chemical potential in a trapped system. The leading term is given by

$$\frac{\mu^{(0)}}{N^{1/3} \hbar \omega_{ho}} = \frac{1}{\Delta_{3D}^2} \left( \frac{C_1^{1/\gamma_1} \Delta_{3D}^6 \Gamma(\frac{5}{2} + \frac{1}{\gamma_1})}{(2\pi)^{3/2} \Gamma(1 + \frac{1}{\gamma_1})} \right)^{\frac{2\gamma_1}{3\gamma_1+2}}, \quad (1.145)$$

Limit	$C_1$	$\gamma_1$	$C_2$	$\gamma_2$	$\Omega_z^2/\omega_z^2$
Lieb-Liniger: weak interaction	$2\pi^2$	1	$-\sqrt{2}/\pi$	-1/2	$3 + \frac{5(9\pi)^{1/3}}{32\sqrt{2}}/\Delta_{1D}^{2/3}$
Lieb-Liniger: strong interaction	$\pi^2/2$	2	-8/3	1	$4 - \frac{128\sqrt{2}}{15\pi^2}\Delta_{1D}$
Attractive Fermi gas: strong interaction	$\pi^2/32$	2	2/3	1	$4 + \frac{64\sqrt{2}}{15\pi^2}\Delta_{1D}$
Attractive Fermi gas: weak interaction	$\pi^2/8$	2	$-8/\pi^2$	-1	$4 + \frac{32}{3\pi^2}/\Delta_{1D}$
Repulsive Fermi gas: strong interaction	$\pi^2/2$	2	$-8\ln(2)/3$	1	$4 - \frac{128\sqrt{2}\ln 2}{15\pi^2}\Delta_{1D}$
Repulsive Fermi gas: weak interaction	$\pi^2/8$	2	$8/\pi^2$	-1	$4 - \frac{32}{3\pi^2}/\Delta_{1D}$
Gas of Hard-Rods	$\pi^2/2$	2	8/3	1	$4 + \frac{128\sqrt{2}}{15\pi^2}\Delta_{1D}$

Table 1.1: Summary for some of one-dimensional models where the expansion of the equation of state is known. The first column labels the considered model. The coefficients of the expansion are given in columns 2-5. The last column gives the predictions for the oscillation frequencies calculated as (1.143). The parameter  $\Delta_{1D}$  is defined by (1.132). Note that the presence of a term in the chemical potential independent of the density (for example, binding energy of a molecule) does not modify the frequencies of oscillations and is ignored.

where  $\Delta_{3D}$  is the characteristic combination (1.132). The next correction to (1.145) is given by

$$\frac{\mu^{(1)}}{\mu^{(0)}} = 1 + \frac{2C_2}{2 + 3\gamma_1} \frac{\Gamma(\frac{5}{2} + \frac{1}{\gamma_1})\Gamma(1 + \frac{1+\gamma_2}{\gamma_1})}{\Gamma(1 + \frac{1}{\gamma_1})\Gamma(\frac{5}{2} + \frac{1+\gamma_2}{\gamma_1})} \left( \frac{\Delta_{3D}^6 \Gamma(\frac{5}{2} + \frac{1}{\gamma_1})}{(2\pi C_1)^{3/2} \Gamma(1 + \frac{1}{\gamma_1})} \right)^{\frac{2\gamma_2}{3\gamma_1+2}} \quad (1.146)$$

The density profile is given by

$$n(r)a^3 = \left( \frac{1}{C_1} \frac{\mu}{\hbar^2/ma^2} \left( 1 - \frac{r^2}{R^2} \right) \right)^{\frac{1}{\gamma_1}} - \frac{C_2}{\gamma_1} \left( \frac{1}{C_1} \frac{\mu}{\hbar^2/ma^2} \left( 1 - \frac{r^2}{R^2} \right) \right)^{\frac{1+\gamma_2}{\gamma_1}}, \quad (1.147)$$

where the chemical potential is given by (1.145-1.146), the size of the condensate  $R$  is defined in (1.130) while the relation between different units of energy is provided by  $N^{1/3}\hbar\omega_{ho} = \Delta_{3D}^2\hbar^2/ma^2$ .

We give an explicit expression for the density in the center of the trap. The leading term is:

$$n^{(0)}(0)a^3 = \left( \frac{\Gamma(\frac{5}{2} + \frac{1}{\gamma_1})}{(2\pi C_1)^{\frac{3}{2}} \Gamma(1 + \frac{1}{\gamma_1}) \Delta_{3D}^{\frac{4}{\gamma_1}}} \right)^{\frac{2}{2+3\gamma_1}} \Delta_{3D}^{\frac{4}{\gamma_1}} \quad (1.148)$$

The next term is:

$$n^{(1)}(0) = n^{(0)}(0) - \frac{C_2}{\gamma_1} \left( 1 - \frac{2}{(2 + 3\gamma_1)} \frac{\Gamma(1 + \frac{1+\gamma_2}{\gamma_1})\Gamma(\frac{5}{2} + \frac{1}{\gamma_1})}{\Gamma(1 + \frac{1}{\gamma_1})\Gamma(\frac{5}{2} + \frac{1+\gamma_2}{\gamma_1})} \right) \left( \frac{\Delta_{3D}^6 \Gamma(\frac{2+5\gamma_1}{2\gamma_1})}{(2\pi C_1)^{\frac{3}{2}} \Gamma(\frac{1+\gamma_1}{\gamma_1})} \right)^{\frac{2(1+\gamma_2)}{2+3\gamma_1}} \quad (1.149)$$



The scaling approach allows calculation of the frequencies of the collective oscillations. The frequency of the breathing mode is<sup>14</sup>  $\Omega^2/\omega_{ho}^2 = 3/2 \Xi - 1$  in a spherical trap,  $\Omega_z^2/\omega_z^2 = 3 - 2/\Xi$  and  $\Omega_\perp^2/\omega_\perp^2 = \Xi$  in a very elongated trap  $\omega_z \ll \omega_\perp$ . The parameter  $\Xi$  defining oscillation frequencies is given by

$$\Xi = 2(1 + \gamma_1) + \frac{4C_2(\gamma_1 + \gamma_2)\gamma_2}{1 + \gamma_1 + \gamma_2} \frac{\Gamma(\frac{7}{2} + \frac{1}{\gamma_1})\Gamma(1 + \frac{1+\gamma_2}{\gamma_1})}{\Gamma(1 + \frac{1}{\gamma_1})\Gamma(\frac{7}{2} + \frac{1+\gamma_2}{\gamma_1})} \left( \frac{\Delta_{3D}^6}{(2\pi C_1)^{\frac{3}{2}}} \frac{\Gamma(\frac{5}{2} + \frac{1}{\gamma_1})}{\Gamma(1 + \frac{1}{\gamma_1})} \right)^{\frac{2\gamma_2}{2+3\gamma_1}} \quad (1.150)$$

The ‘‘expansion’’ equation of states (1.137,1.144) can be naturally applied to the problems, where it is possible to construct a perturbation theory. Another possible application of the discussed above method is to consider the parameters  $C_1, C_2, \gamma_1, \gamma_2$  as variational and fix them by fitting to an equation of state, where an exact solution to the LDA problem is not known. An arbitrary equation of state can be expanded as (1.137,1.144) in any point, for example, by demanding that the first three derivatives of the function and the function itself coincide with the ones calculated from the (1.137,1.144). The four conditions of the continuity fixes four parameters.

#### 1.6.4 Static structure factor of a trapped Tonks-Girardeau gas

The chemical potential of the Tonks-Girardeu gas is known due to fermion-bosonic mapping [Gir60]. It equals to the fermi energy of a one-dimensional spinless fermi gas and is given by the formula (1.101). The dependency on the density is simple and lies within class of functions (1.136) for which the LDA problem was solved in Sec. 1.6.2. The TG gas is described by the subsequent set of parameters:  $C_1 = \pi^2/2, \gamma_1 = 2, C_2 = 0$ .

The value of the chemical potential of the TG gas in a trap is immediately found from Eq. 1.140 and equals to  $\mu = N\hbar\omega_z$ . Its integration with the respect of the number of particles gives the total energy in the LDA<sup>15</sup>:

$$\frac{E}{N} = N \frac{\hbar\omega_z}{2} \quad (1.151)$$

The density profile is a semicircle

$$n(z) = n_0 \left( 1 - \frac{z^2}{R_z^2} \right)^{1/2}, \quad (1.152)$$

with system size given by (1.130)  $R_z = \sqrt{2N}a_z$  and the density in the center equal to  $n_0 a_z = \sqrt{2N}/\pi$ . The mean square radius of the trapped system is given then by

$$\sqrt{\langle z^2 \rangle} = \sqrt{\frac{N}{2}} a_z \quad (1.153)$$

<sup>14</sup>S. Stringari, unpublished.

<sup>15</sup>It is interesting to note that the result (1.151) of an *approximate* solution for particles of infinite repulsion coincides with an *exact* result for particles interacting with  $g/r^2$  interaction (Calogero-Sutherland model [Cal69, Sut71]) in the limit  $g \rightarrow 0$ . Indeed, as shown in [Sut71] the energy of such a gas equals  $E/N = \frac{1}{2}\hbar\omega_z(1 + \lambda(N - 1))$ , where  $\lambda$  is related to the strength of interaction  $g = 2\lambda(\lambda - 1)$ . There are two different ways of taking the limit  $g \rightarrow 0$ : 1)  $\lambda \rightarrow 0, E/N \rightarrow \frac{1}{2}\hbar\omega_z$  *i.e.* this limit corresponds to non-interacting bosons all staying in the lowest state of a harmonic oscillator 2)  $\lambda \rightarrow 0, E/N \rightarrow \frac{1}{2}N\hbar\omega_z$ , *i.e.* this limit preserves the singularity of the interaction while makes the potential energy vanishing.

The static structure factor of a uniform system depends on value of momentum  $k$  and on the density (*i.e.* on the value of the fermi momentum  $k_f$ ) as given by formula (5.5). We approximate the static structure factor in a trap by averaging it over the density profile (1.152):

$$S^{LDA}(k) = \frac{1}{2R_z} \int_{-R}^R S(k, n(z)) dz = \frac{ka_z}{\sqrt{8N}} \arcsin \sqrt{1 - \frac{(ka_z)^2}{8N}} + 1 - \sqrt{1 - \frac{(ka_z)^2}{8N}} \quad (1.154)$$

It is easy to check that it vanishes for small momenta  $S^{LDA}(k) \rightarrow 0, k \rightarrow 0$ , while it saturates to unity at large values of momenta  $S^{LDA}(k) = 1, |k| > \sqrt{8N}/a_z$ .

## 1.7 Correlation functions in a Luttinger liquid

### 1.7.1 Stationary density-density correlation function

The long-range properties of a weakly interacting one-dimensional bosonic gas can be calculated using the macroscopic representation of the field operator (1.1):  $\hat{\Psi}(x) = \sqrt{\rho_0 + \hat{\rho}'(x)} e^{i\hat{\varphi}(x)}$ , where  $\rho_0$  is the mean density<sup>16</sup> and  $\hat{\varphi}(x)$  is the phase operator. Those operators can be expressed in terms of quasiparticle creation and annihilation operators (see., for example, [PS03] Eqs.(6.65-6.66), and consider a one-dimensional system):

$$\hat{\varphi} = -i \sum_k \sqrt{\frac{\pi}{\eta|k|L}} (\hat{b}_k e^{ikx} - \hat{b}_k^\dagger e^{-ikx}) \quad (1.155)$$

$$\hat{\rho}' = \sum_k \sqrt{\frac{\eta|k|}{4\pi L}} (\hat{b}_k e^{ikx} + \hat{b}_k^\dagger e^{-ikx}), \quad (1.156)$$

where we introduced an important parameter describing the interactions between particles:

$$\eta = \frac{2\pi\hbar\rho_0}{Mc} \quad (1.157)$$

The operators (1.155,1.156) satisfy the commutation rule  $[\hat{\varphi}(x), \hat{\rho}'(x')] = -i\delta(x - x')$ .

Our approach is applicable in a weakly interacting gas  $\rho_0 \rightarrow \infty$ . Deep in this regime the speed of sound has a square root dependence on the density  $c = \sqrt{g\rho_0/M}$  and the coefficient  $\eta$  is large  $\eta = 2\pi\hbar\sqrt{\rho_0/Mg}$ . In the opposite regime of strong correlations  $\rho \rightarrow 0$  (TG limit) the bosonic system of impenetrable particles is mapped onto a system of non-interacting fermions [Gir60] with the speed of sound given by the fermi velocity  $c_F = \pi\hbar\rho_0/M$  (1.100) and is proportional to the density. In this regime  $\eta = 2$ . By generalizing the definition of the fermi velocity from the TG regime, where the fermionization of a bosonic system happens, to an arbitrary density we obtain a simple interpretation of the parameter (1.157):  $\eta = 2c_F/c$ . The speed of sound in a system with a repulsive contact potential is not larger than the fermi velocity, thus in LL system (5.1)  $\eta \geq 2$ . The situation becomes different in a gas of hard-rods of size  $a_{1D}$ . Presence of an excluded volume makes the available phase space be effectively smaller  $L \rightarrow L - Na_{1D}$ , which in turn renormalizes the speed of sound (see 1.103) and makes it be larger. In this special case of the super-Tonks gas (Sec. 6) the parameter  $\eta$  (1.157) can be smaller than 2.

<sup>16</sup>In this section we keep a different notation for the linear density  $\rho \equiv n_{1D} = N/L$

Following Haldane [Hal81] we introduce a new field  $\hat{\vartheta}(x)$  such that  $\nabla\hat{\vartheta}(x) = \pi[\rho_0 + \hat{\rho}'(x)]$ . The operator  $\hat{\vartheta}$  satisfy boundary conditions  $\hat{\vartheta}(x+L) = \hat{\vartheta}(x) + \pi N$  and increases monotonically by  $\pi$  each time  $x$  passes the location of a particle. Particles are thus taken to be located at the points where  $\hat{\vartheta}(x)$  is a multiple of  $\pi$ , allowing the density operator to be expressed as  $\hat{\rho}(x) = \nabla\hat{\vartheta}(x)\{\sum_n \delta[\hat{\vartheta}(x) - \pi\rho]\}$ , or, equivalently,

$$\hat{\rho}(x) = [\rho_0 + \hat{\rho}'(x)] \sum_{m=-\infty}^{\infty} \exp[i2m\hat{\vartheta}(x)] \quad (1.158)$$

Integrating (1.156) we obtain an expression of this field in terms of creation and annihilation operators:

$$\hat{\vartheta}(x) = \vartheta_0 + \pi\rho_0 x - i \sum_k \sqrt{\frac{\pi\eta}{4|k|L}} \text{sign } k (\hat{b}_k e^{ikx} - \hat{b}_k^\dagger e^{-ikx}) \quad (1.159)$$

We will start with calculation of asymptotics of the density-density correlation function:

$$\langle \hat{\rho}(x)\hat{\rho}(0) \rangle \approx (\rho_0^2 + \langle \hat{\rho}'(x)\hat{\rho}'(0) \rangle) \langle \sum_{m,m'} \exp[i2(m\hat{\vartheta}(x) + m'\hat{\vartheta}(0))] \rangle \quad (1.160)$$

First of all we calculate the contribution coming from density fluctuations  $\hat{\rho}'(x)$ :

$$\langle \hat{\rho}'(x)\hat{\rho}'(0) \rangle = \langle \sum_{k,k'} \frac{\eta\sqrt{|kk'|}}{4\pi L} (\hat{b}_k e^{ikx} + \hat{b}_k^\dagger e^{-ikx})(\hat{b}_{k'} + \hat{b}_{k'}^\dagger) \rangle \quad (1.161)$$

The creation and annihilation operators satisfy bosonic commutation relations  $[\hat{b}_k, \hat{b}_{k'}^\dagger] = \delta_{k,k'}$  and at zero temperature excitations are absent  $\langle \hat{b}_k^\dagger \hat{b}_k \rangle = 0$ , so in the averaging in Eq. 1.161 we get non zero result only for  $\langle \hat{b}_k \hat{b}_k^\dagger \rangle = 1$ , *i.e.*

$$\langle \hat{\rho}'(x)\hat{\rho}'(0) \rangle = \sum_k \frac{\eta|k|e^{ikx}}{4\pi L} = \int_{-\infty}^{\infty} \frac{\eta|k|}{4\pi M c} e^{ikx} \frac{dk}{2\pi} = \frac{\eta}{4\pi^2} \left( \frac{1}{x^2} - \frac{ik}{x} \right) e^{ikx} \Big|_0^{\infty} \quad (1.162)$$

We consider contribution only from the lower limit of the integration  $k = 0$  and, thus, obtain

$$\langle \hat{\rho}'(x)\hat{\rho}'(0) \rangle = -\frac{\eta}{4\pi^2} x^{-2} \quad (1.163)$$

Now let us calculate the contribution of the phase fluctuations in (1.160):

$$\begin{aligned} & \langle \sum_{m,m'} \exp[i2(m\hat{\vartheta}(x) + m'\hat{\vartheta}(0))] \rangle = \\ & = \left\langle \sum_{m,m'} \exp \left\{ i2(m+m')\vartheta_0 + i2\pi m\rho_0 x + \sum_k \sqrt{\frac{\pi\eta}{|k|L}} \text{sign } k \left( \hat{b}_k (m e^{ikx} + m') - \hat{b}_k^\dagger (m e^{-ikx} + m') \right) \right\} \right\rangle \quad (1.164) \end{aligned}$$

An average of a phonon operator  $\hat{A}$  is gaussian and satisfies an equality  $\langle \exp\{\hat{A}\} \rangle = \exp\{\langle \hat{A}^2 \rangle / 2\}$ . In this way we can pass from an average of an exponent to an exponent of averaged quantities:

$$\begin{aligned} & \langle \sum_{m,m'} \exp[i2(m\hat{\vartheta}(x) + m'\hat{\vartheta}(0))] \rangle = \sum_{m,m'} \exp \{ i2(m+m')\vartheta_0 + i2\pi m\rho_0 x \} \\ & \exp \left\{ \sum_k \frac{\pi\eta}{2|k|L} \langle (\hat{b}_k (m e^{ikx} + m') - \hat{b}_k^\dagger (m e^{-ikx} + m')) (\hat{b}_k (m e^{ikx} + m') - \hat{b}_k^\dagger (m e^{-ikx} + m')) \rangle \right\} \quad (1.165) \end{aligned}$$

At the zero temperature excitations are absent. This simplifies the calculation as the averaging in (1.165) gives simply  $\langle \dots \rangle = -(me^{-ikx} + m')(me^{ikx} + m') = -(m^2 + m'^2 + 2mm' \cos kx)$ . We substitute the summation in the exponent of (1.165) with integration over  $k$ :

$$- \sum_k \frac{\pi\eta}{2|k|L} (m^2 + m'^2 + 2mm' \cos kx) = -2 \int_0^\infty \frac{\pi\eta}{2k} (m^2 + m'^2 + 2mm' \cos kx) \frac{dk}{2\pi} \quad (1.166)$$

This integral has an infrared divergence unless  $m' = -m$ , so we consider only these terms. Now the integral converges at small  $k$  and takes the leading contribution in the interval  $1/x < k < 1/\xi$  where  $\xi$  is minimal length at which the hydrodynamic theory can be applied. In this region one can neglect the contribution coming from the oscillating cosine term and one has

$$- 4m^2 \int_{1/x}^{1/\xi} \frac{\pi\eta}{2k} \frac{dk}{2\pi} = -m^2\eta(\ln(1/\xi) - \ln(1/x)) = -\eta m^2 \ln(x/\xi) \quad (1.167)$$

Finally, collecting together (1.163,1.164,1.167) we obtain an expression for the stationary density-density correlation function

$$\frac{\langle \hat{\rho}(x)\hat{\rho}(0) \rangle}{\rho_0^2} = \left(1 - \frac{\eta}{4\pi^2}(\rho_0 x)^{-2}\right) \left(1 + 2 \sum_{m=1}^{\infty} C_m \cos(2\pi m \rho_0 x) \left(\frac{x}{\xi}\right)^{-\eta m^2}\right) \quad (1.168)$$

## 1.7.2 Time-dependent density-density correlation function

In this Section we develop an approach which allows an estimation of correlations between different moments of time. We substitute the stationary hydrodynamic expressions of phase and density operators (1.155,1.156) on time-dependent hydrodynamic expressions (see, for example, [LP80], Eqs.(24.10)):

$$\hat{\varphi}(x, t) = -i \sum_k \sqrt{\frac{\pi}{\eta|k|L}} (\hat{b}_k e^{i(kx - |k|ct)} - \hat{b}_k^\dagger e^{-i(kx - |k|ct)}), \quad (1.169)$$

$$\hat{\rho}'(x, t) = \sum_k \sqrt{\frac{\eta|k|}{4\pi L}} (\hat{b}_k e^{i(kx - |k|ct)} + \hat{b}_k^\dagger e^{-i(kx - |k|ct)}) \quad (1.170)$$

It is easy to note (see Eqs. 1.155,1.156) that the time  $t$  enters always in the combination  $(kx - |k|ct)$ , which means that time-dependent solution can be obtained from stationary solution by changing  $kx \rightarrow kx - |k|ct$  in integrands and carrying out integration again. Density fluctuations (1.161) are than given by

$$\langle \hat{\rho}'(x, t)\hat{\rho}'(0, 0) \rangle = \int_0^\infty \frac{\eta k}{4\pi} (e^{ik(x-ct)} + e^{ik(x+ct)}) \frac{dk}{2\pi} = -\frac{\eta}{8\pi^2} \left( \frac{1}{(x+ct)^2} + \frac{1}{(x-ct)^2} \right) \quad (1.171)$$

Here again we considered the contribution from the lower limit  $k = 0$ .

The contribution from the phase fluctuations (1.164) is calculated analogously to (1.166):

$$- \eta m^2 \left[ \int_0^\infty \frac{[1 - \cos k(x+ct)]}{k} dk + \int_0^\infty \frac{[1 - \cos k(x-ct)]}{k} dk \right] \quad (1.172)$$

The main contribution to integrals comes from momenta  $1/(x+ct) < k < 1/\xi$  in the first integral and  $1/(x-ct) < k < 1/\xi$  in the second one. As we are interested in description of asymptotically large distances condition  $x > ct$  is always fulfilled. In this conditions the integration gives

$$-\frac{1}{2}\eta m^2 \left[ \ln \frac{x+ct}{\xi} + \ln \frac{x-ct}{\xi} \right] = -\frac{1}{2}\eta m^2 \ln \frac{x^2 - c^2 t^2}{\xi^2} \quad (1.173)$$

Thus we find that the asymptotic behavior of the time-dependent density-density correlation function is given by

$$\frac{\langle \hat{\rho}(x, t) \hat{\rho}(0, 0) \rangle}{\rho_0^2} = 1 - \frac{\eta}{8\pi^2 \rho_0^2} \left( \frac{1}{(x+ct)^2} + \frac{1}{(x-ct)^2} \right) + 2 \sum_{m=1}^{\infty} C_i \cos(2\pi m \rho_0 x) \left( \frac{x^2 - c^2 t^2}{\xi^2} \right)^{-\frac{1}{2}\eta m^2} \quad (1.174)$$

### 1.7.3 Calculation with non-logarithmic accuracy

The phonon dispersion  $\omega = c|k|$  relation which was used in the derivation above leads to infrared divergence in some of the integrals (1.166) and was resolved by truncation of the integral. This problem can be cured using a more precise Bogoliubov dispersion law:

$$\omega(k) = \sqrt{(kc)^2 + \left( \frac{\hbar k^2}{2M} \right)^2} \quad (1.175)$$

It is easy to see that results for the new dispersion can be obtained by changing formally the speed of sound  $c|k| \rightarrow c|k|\sqrt{1 + (\hbar k/2Mc)^2}$  in definitions of hydrodynamic operators (1.169-1.170). This will lead to a converging value of the integral (1.166):

$$-2 \int_0^{\infty} \frac{\eta \pi 2m^2 (1 - \cos kx) dk}{2k \sqrt{1 + (\hbar k/2Mc)^2} 2\pi} = -\eta m^2 \int_0^{\infty} \frac{1 - \cos z}{\sqrt{1 + \varepsilon^2 z^2}} \frac{dz}{z}, \quad (1.176)$$

Here we introduced the notation  $z = xk$  and  $\varepsilon = \hbar/2Mcx$ . Let us split the integral (1.176) in two parts:

$$\int_0^{\infty} \frac{1 - \cos z}{\sqrt{1 + \varepsilon^2 z^2}} \frac{dz}{z} \approx \int_0^N (1 - \cos z) \frac{dz}{z} + \int_N^{\infty} \frac{dz}{z \sqrt{1 + \varepsilon^2 z^2}}, \quad (1.177)$$

in such a way that  $1 \ll N \ll 1/\varepsilon$ . The term  $(1 + \varepsilon^2 z^2)$  can be neglected in the integration up to  $N$  and oscillating term can be neglected at larger distances. In order to proceed further we shift the lower integration limit by short distance  $\varepsilon \rightarrow 0$ . Then the first integral becomes equal to  $\ln N/\varepsilon - \text{Ci } N + \text{Ci } \varepsilon$ . The second integral can be easily calculated by using substitution  $y^2 = 1 + \varepsilon^2 z^2$  and equals  $\frac{1}{2} \ln \frac{\sqrt{1 + \varepsilon^2 N^2} + 1}{\sqrt{1 + \varepsilon^2 N^2} - 1}$ . Collecting everything together we obtain

$$\int_0^{\infty} \frac{1 - \cos z}{\sqrt{1 + \varepsilon^2 z^2}} \frac{dz}{z} \approx \gamma + \ln \frac{4Mcx}{\hbar} = \gamma + \ln \frac{8\pi \rho_0 x}{\eta}, \quad (1.178)$$

where  $\gamma \approx 0.577$  is Euler's constant.

The static density-density correlation function (1.168) (more precisely its  $m \neq 0$  part) is equal to

$$\frac{\langle \hat{\rho}(x) \hat{\rho}(0) \rangle}{\rho_0^2} = 1 + 2 \sum_{m=1}^{\infty} \left( \frac{\eta}{8\pi C} \right)^{\eta m^2} \frac{\cos(2\pi m \rho_0 x)}{(\rho_0 x)^{\eta m^2}}, \quad (1.179)$$

where  $C = e^\gamma \approx 1.781$ .

The time-dependent result differ from the stationary case (1.179) only by substitution  $x \rightarrow \sqrt{x^2 - c^2 t^2}$  in the denominator, as it was already shown in the calculation with logarithmic accuracy (compare 1.168 and 1.174):

$$\frac{\langle \hat{\rho}(x, t) \hat{\rho}(0, 0) \rangle}{\rho_0^2} = 1 + 2 \sum_{m=1}^{\infty} \left( \frac{\eta}{8\pi C} \right)^{\eta m^2} \frac{\cos(2\pi m \rho_0 x)}{(\rho_0 \sqrt{x^2 - c^2 t^2})^{\eta m^2}}, \quad (1.180)$$

### 1.7.4 Dynamic form factor

The dynamic form factor is related to the time-dependent density-density correlation function by the means of the Fourier transform:

$$S(k, \omega) = \frac{\rho_0}{\hbar} \iint e^{i(\omega t - kx)} \left[ \frac{\langle \hat{\rho}(x, t) \hat{\rho}(0, 0) \rangle}{\rho_0^2} - 1 \right] dx dt \quad (1.181)$$

The correlation function was calculated with non-logarithmic accuracy and is given by formula (1.180). The evaluation of direct Fourier transform (1.181) would give us the expression for the dynamic form factor. It turns out that it is easier to go other way around, *i.e.* guess the form of the  $m$ -th component of  $S(k, \omega)$

$$S(k, \omega) = A(\omega^2 - c^2(k - 2mk_F)^2)^{\frac{m^2\eta}{2}-1}, \quad (1.182)$$

make the inverse Fourier transform to go back from  $(k, \omega)$  to  $(x, t)$  and comparing obtain result to (1.180) fix the value of the constant  $A$ . Here we use notation  $k_F = \pi\rho_0$ . We start by doing the integration over momentum.  $S(x, \omega) = \int_{-\infty}^{\infty} e^{ikx} S(k, \omega) \frac{dk}{2\pi}$ . We introduce notation  $\Delta k = k + 2mk_F$  the integral is limited to the region  $(-\omega/c, \omega/c)$ :

$$S(x, \omega) = A c^{m^2\eta-2} e^{i2mk_F x} \int_{-\omega/c}^{\omega/c} \cos(\Delta k x) \left[ \left( \frac{\omega}{c} \right)^2 - (\Delta k)^2 \right]^{\frac{m^2\eta}{2}-1} \frac{d(\Delta k)}{2\pi} \quad (1.183)$$

As a reference we use formula 3.771(464/465) from Gradstein-Ryzhik book [GR80]:

$$\int_0^u (u^2 - x^2)^{\nu-\frac{1}{2}} \cos(ax) dx = \frac{\sqrt{\pi}}{2} \left( \frac{2u}{a} \right)^\nu \Gamma\left(\nu + \frac{1}{2}\right) J_\nu(au), \quad \left[ a > 0, u > 0, \text{Re}\nu > -\frac{1}{2} \right]$$

The substitution  $u = \omega/c$ ,  $a = x$ ,  $\nu = (m^2\eta - 1)/2$  gives an expression in terms of  $(x, \omega)$

$$S(x, \omega) = \frac{A e^{i2mk_F x}}{2\sqrt{\pi}c} \left( \frac{2\omega c}{x} \right)^{\frac{m^2\eta-1}{2}} \Gamma\left(\frac{m^2\eta}{2}\right) J_{\frac{m^2\eta-1}{2}}\left(\frac{\omega x}{c}\right), \quad (1.184)$$

where  $J_n(x)$  is the Bessel function of the first kind. The integration over the frequencies  $S(x, t) = \int_0^\infty e^{-i\omega t} S(x, \omega) \frac{d\omega}{2\pi}$  can be done easily by using the formula (6.699.5) from [GR80]

$$\int_0^\infty x^\nu \cos(ax) J_\nu(bx) dx = 2^\nu \frac{b^\nu}{\sqrt{\pi}} \Gamma\left(\frac{1}{2} + \nu\right) (b^2 - a^2)^{-\nu - \frac{1}{2}} \left[ 0 < a < b, \quad |\operatorname{Re} \nu| < \frac{1}{2} \right]$$

and gives

$$S(x, t) = A \frac{(2c)^{m^2\eta-1}}{2\pi^2} \Gamma^2\left(\frac{m^2\eta}{2}\right) \frac{\cos(2mk_F)}{(x^2 - c^2t^2)^{\frac{m^2\eta}{2}}} \quad (1.185)$$

Comparing this result with (1.180) we fix so far unknown coefficient of the proportionality to the value  $A = \frac{8\pi^2 c \rho_0}{\hbar \Gamma^2(m^2\eta/2)} \left(\frac{\hbar}{8Mc^2}\right)^{m^2\eta}$  and, finally, obtain

$$S(k, \omega) = \sum_{m=1}^\infty \frac{8\pi^2 \rho_0 c}{\Gamma^2\left(\frac{m^2\eta}{2}\right) \hbar} \left(\frac{\hbar}{8Mc^2}\right)^{m^2\eta} \left[ \frac{(\omega^2 - c^2(k-2mk_F)^2)^{\frac{m^2\eta}{2}-1} + (\omega^2 - c^2(k+2mk_F)^2)^{\frac{m^2\eta}{2}-1}}{2} \right] \quad (1.186)$$

### 1.7.5 Popov's coefficient

The introduced above approach allows us to find the asymptotic behavior of the one-body density matrix and estimate the coefficient of its decay. Within the first order of accuracy we split the average as

$$g_1(x) = \langle \sqrt{\hat{\rho}(x)\hat{\rho}(0)} e^{i(\hat{\varphi}(x) - \hat{\varphi}(0))} \rangle \approx \langle \sqrt{\hat{\rho}(x)\hat{\rho}(0)} \rangle \langle e^{i(\hat{\varphi}(x) - \hat{\varphi}(0))} \rangle \quad (1.187)$$

We first calculate the contribution coming from the phase fluctuations

$$g_1^{phase}(x) = \langle e^{i(\hat{\varphi}(x) - \hat{\varphi}(0))} \rangle = \left\langle \exp \left\{ \sum_k \sqrt{\frac{\pi}{\eta|k|L}} (\hat{b}_k(e^{ikx} - 1) - \hat{b}_k^\dagger(e^{-ikx} - 1)) \right\} \right\rangle \quad (1.188)$$

The average of the exponent can be further developed by using the relation for the gaussian average  $\langle \exp A \rangle = \exp \langle \frac{1}{2} A^2 \rangle$ . At zero temperature excitations are absent and the only nonzero average is  $\langle \hat{b}_k \hat{b}_k^\dagger \rangle = 1$ . Thus we obtain

$$g_1^{phase}(x) = \exp \left\{ -\frac{1}{2} \sum_k \frac{\pi}{\eta|k|L} (e^{ikx} - 1)(e^{-ikx} - 1) \right\} = \exp \left\{ -\int_{-\infty}^\infty \frac{\pi(1 - \cos kx)}{\eta|k|} \frac{dk}{2\pi} \right\} \quad (1.189)$$

At this point we substitute the phononic excitation spectrum with the proper Bogoliubov dispersion. This can be done by changing  $\eta \rightarrow \eta/\sqrt{1 + (\hbar k/2Mc)^2}$ .

$$g_1^{phase}(x) = \exp \left\{ -\frac{1}{\eta} \int_0^\infty \frac{\sqrt{1 + (\hbar k/2Mc)^2} (1 - \cos kx) dk}{k} \right\} \quad (1.190)$$

Formally this integral is diverging. However, we will take use of the properties of the  $\delta$ -function

$$\int_{-\infty}^{\infty} \cos \frac{kx}{2\pi} = \delta(x) \quad (1.191)$$

As we are interested in long range asymptotical behavior we subtract (1.191) from the exponent of (1.190) and consider a well-convergent expression

$$g_1^{phase}(x) = \exp \left\{ -\frac{1}{\eta} \int_0^{\infty} \left( \frac{\sqrt{1 + (\hbar k/2Mc)^2}}{k} - 1 \right) (1 - \cos kx) \right\} dk \quad (1.192)$$

Partial integration together with the notation  $\varepsilon = \hbar/(2xMc) \ll 1$  and  $z = kx$  gives

$$g_1^{phase}(x) = \exp \left\{ -\frac{1}{\eta} \int_0^{\infty} \frac{z - \sin z}{z^2 \sqrt{1 + \varepsilon^2 z^2}} \right\} dz \quad (1.193)$$

This equation can be calculated with non-logarithmic accuracy at  $x \gg \xi$  by splitting the integral in three parts  $1 \ll N \ll 1/\varepsilon$

$$\int_0^{\infty} \frac{z - \sin z}{z^2 \sqrt{1 + \varepsilon^2 z^2}} dz = \int_{\lambda}^N \frac{1}{z} dz - \int_{\lambda}^N \frac{\sin z}{z^2} dz + \int_N^{\infty} \frac{1}{z \sqrt{1 + \varepsilon^2 z^2}} dz = \gamma - 1 - \ln \frac{\hbar}{4xMc} \quad (1.194)$$

The calculation gives the result

$$g_1^{phase}(x) = \left( \frac{e^{1-\gamma}\eta}{8\pi\rho_0 x} \right)^{\frac{1}{\eta}} \quad (1.195)$$

In order to take into account the density fluctuations we develop (1.187) using Taylor expansion  $\sqrt{1+x} = 1 + x/2 - x^2/8 + \mathcal{O}(x^3)$ , so  $g_1^{\rho}(x) = \langle \sqrt{\hat{\rho}(x)\hat{\rho}(0)} \rangle \approx \rho_0 + \frac{1}{4\rho_0} \langle [\hat{\rho}'(x) - \hat{\rho}'(0)]\hat{\rho}'(0) \rangle$ . Writing the density operator in terms of creation and annihilation operators (eq. 1.156) we obtain

$$g_1^{\rho}(x) = \rho_0 + \frac{1}{4} \sum_k \frac{\rho_0 \hbar |k|}{2LMc(k)} \langle (\hat{b}_k(e^{ikx} - 1) + \hat{b}_k^{\dagger}(e^{-ikx} - 1))(\hat{b}_k + \hat{b}_k^{\dagger}) \rangle = \rho_0 + \frac{1}{4} \int_0^{\infty} \frac{\rho_0 \hbar k}{Mc(k)} (\cos kx - 1) \frac{dk}{2\pi}$$

We substitute the speed of sound for the Bogoliubov dispersion relation  $c(k) = c\sqrt{1 + (\hbar k/2Mc)^2}$  and express the integral in dimensionless units  $\varepsilon = \hbar/(2Mcx)$ ,  $z = kx$

$$\langle \sqrt{\hat{\rho}(x)\hat{\rho}(0)} \rangle = \rho_0 + \frac{\rho_0 \hbar}{8\pi Mcx^2} \int_0^{\infty} \frac{(\cos z - 1)z dz}{\sqrt{1 + \varepsilon^2 z^2}} \quad (1.196)$$

The integral can be evaluated and expanded for small  $\varepsilon$

$$\int_0^{\infty} \frac{(\cos z - 1)z dz}{\sqrt{1 + \varepsilon^2 z^2}} = \frac{1}{\varepsilon^2} + \frac{\pi}{2\varepsilon^2} \left( I_1 \left( \frac{1}{\varepsilon} \right) - L_{-1} \left( \frac{1}{\varepsilon} \right) \right) \approx \frac{1}{\varepsilon^2} + (-1 - 3\varepsilon^2 + \mathcal{O}(\varepsilon^4)), \quad (1.197)$$



where  $I_1(z)$  is modified Bessel function of first kind and  $L_{-1}(z)$  is modified Struve function.

In terms of the parameter  $\eta$  we have

$$\langle \sqrt{\hat{\rho}(x)\hat{\rho}(0)} \rangle = \rho_0 \left( 1 + \frac{1}{\eta} - \frac{\eta}{16\pi\rho_0^2 x^2} \right) \quad (1.198)$$

Combining together (1.195) and (1.198) we obtain finally the expression for the coefficient of the long-range asymptotics

$$g_1(x) = \rho_0 \left( \frac{e^{1-\gamma}\eta}{8\pi} \right)^{\frac{1}{\eta}} \left( 1 + \frac{1}{\eta} - \frac{\eta}{16\pi\rho_0^2 x^2} \right) (\rho_0 x)^{-\frac{1}{\eta}} \quad (1.199)$$

In order to get an expression for the one-body density matrix at a finite temperature, one should account for thermal quasi-particle excitations. The long-range excitations are phonons and obey Bose-Einstein statistics  $\langle \hat{b}_k^\dagger \hat{b} \rangle = (\exp(\hbar k c / k_B T) - 1)^{-1}$ . We are interested at the long-range behavior of the one-body density matrix, which corresponds to the limit  $k \rightarrow 0$ . In this conditions one can do a Taylor expansion and get  $\langle \hat{b}_k^\dagger \hat{b} \rangle = k_B T / \hbar |k| c$ . The calculation of the average (1.188) leads to appearance of an additional term, which depends on the temperature (compare with (1.189)):

$$g_1^{phase}(x) = \exp \left\{ - \int_{-\infty}^{\infty} \frac{\pi(1 - \cos kx)(1 + 2k_B T / \hbar |k| c) dk}{\eta |k|} \frac{dk}{2\pi} \right\} \quad (1.200)$$

As we will show, the additional thermal suppression becomes dominating and will change the asymptotic behaviour of  $g_1(x)$  significantly. The effect of the thermal phase fluctuations can be separated:

$$g_1^{phase}(x) = g_{1,T=0}^{phase}(x) \exp \left\{ - \int_{-\infty}^{\infty} \frac{\pi(1 - \cos kx) 2k_B T / \hbar |k| c dk}{\eta |k|} \frac{dk}{2\pi} \right\} \quad (1.201)$$

where the zero temperature part  $g_{1,T=0}^{phase}(x)$  is readily given by the formula (1.195). The integral in (1.201) is well behaved and can be easily calculated. It turns out to be proportional to  $-|x|$  leading to exponential decay of the thermal fluctuation part at large distances:

$$g_1^{phase}(x) = \left( \frac{e^{1-\gamma}\eta}{8\pi\rho_0 x} \right)^{\frac{1}{\eta}} \exp \left( - \frac{|x|}{\xi_T} \right) \quad (1.202)$$

The characteristic thermal decay length  $\xi_T$  is inversely proportional to the temperature:

$$\xi_T = \frac{2\hbar^2 \rho_0}{m k_B T} = 4\pi \rho_0 \lambda^2, \quad (1.203)$$

where the de Broglie thermal length is defined in the usual way  $\lambda = \hbar / \sqrt{2\pi m k_B T}$ .



# Chapter 2

## Quantum Monte Carlo technique

### 2.1 Introduction

Quantum Monte Carlo methods (QMC) are very powerful tools for the investigation of quantum many body systems (for a review see, for example, [Cep95],[Gua98]). The usage of QMC techniques provides deep insight into understanding of the physical problem. It allows one to accomplish the *ab initio* calculation and, starting from a microscopic model (commonly a model Hamiltonian), earn knowledge of the macroscopic behavior of the system. Often it turns out that this approach is the only accessible tool for studying sophisticated problems, as in order to have a model, which can be solved analytically in exact way, one usually has to make severe assumptions, which can be relaxed in QMC. In many cases it is possible to construct analytically a perturbation theory, then its applicability is restricted by smallness of the perturbation parameter and also in cases like that QMC methods can be used to avoid the restrictions. The QMC techniques solve the many-body Schrödinger equation for the ground state and for excited states at zero temperature. Similar to other MC approaches, these techniques are based on stochastic numerical algorithms, which are powerful when one is treating systems with many degrees of freedom.

We are interested in exploring the quantum properties of systems. The quantum effects manifest the most at the lowest temperatures, when the system stays in the ground state. Thus we choose the Diffusion Monte Carlo method to address the problem. This method is *exact*<sup>1</sup> for calculation a ground state energy of a bosonic system

In order to study a fermionic system we use Fixed-Node Monte Carlo technique (FN-MC), which is a modification of the DMC method. In general this approach gives an upper bound to the ground state energy, but with a good choice of the trial wave function the difference can be significantly minimized.

In this chapter we will start from the Variational Monte Carlo method which is applicable both for bosons and fermions. Then we will discuss bosonic Diffusion Monte Carlo method and fermionic Fixed-Node Monte Carlo method. We will address in details construction of the trial wave functions and, next, will discuss the implementation of the measurements of the quantities of interest.

---

<sup>1</sup>Of course, as this method is a statistical one and all outputs are obtained within statistical errors which can be decreased by making a longer series of measurements.

## 2.2 Variational Monte Carlo

### 2.2.1 Variational principle

The simplest of the Quantum Monte Carlo methods is the *variational* method (VMC). The idea of this method is to use an approximate wave function  $\psi_T$  (*variational* or *trial wave function*) and then by sampling the probability distribution

$$p(\mathbf{R}) = |\psi_T(\mathbf{R})|^2 \quad (2.1)$$

calculate averages of physical quantities. It is easy to show that the average

$$E_T = \frac{\langle \psi_T | \hat{H} | \psi_T \rangle}{\langle \psi_T | \psi_T \rangle} \geq E_0 \quad (2.2)$$

gives an upper bound to the ground-state energy. By minimizing the variational energy with respect to the external parameters one can optimize the wave function within the given class of wave functions considered.

Importantly, the variational principle also applies to excited states. For a trial wave function  $\psi_T$  with a given symmetry, the variational estimate provides an upper bound to the energy of the lowest excited state of the Hamiltonian  $\hat{H}$  with that symmetry.

### 2.2.2 Applications

If the wave function of the ground state is known exactly, then the VMC sampling will provide *exact* ground state properties. For example, in a system of hard-rods one has a knowledge of the ground state wave function and energy, but the correlation functions are not known. In this case the VMC calculation allows to complete the description of the system. In a similar manner if one knows exactly an eigenstate wave function, then the properties of the system can be obtained by the VMC sampling in an exact way.

The VMC can be effectively used for studying the metastable states. In particular one can make estimations of the critical parameters leading to the system collapse (see Sec. 6).

The VMC is used to optimize the variational parameters before doing DMC or FN-MC calculations, as the efficiency of the latter depends significantly on the quality of the trial wave function.

### 2.2.3 Implementation

It is convenient to work in the coordinate representation, as this representation is the most natural for writing the interaction potential and external potential. In a system of  $N$  particles in  $D$  dimensions the distribution function depends on  $DN$  variables  $p(\mathbf{R}) = p(\vec{r}_1, \dots, \vec{r}_N)$ . An average value of an operator  $\hat{A}$  is then given by a  $DN$ -multidimensional integral

$$\langle A \rangle = \frac{\int \dots \int A(\vec{r}_1, \dots, \vec{r}_N) p(\vec{r}_1, \dots, \vec{r}_N) d\vec{r}_1 \dots d\vec{r}_N}{\int \dots \int p(\vec{r}_1, \dots, \vec{r}_N) d\vec{r}_1 \dots d\vec{r}_N} \quad (2.3)$$

Even for a few particles  $N \approx 10$  the structure of the integral becomes too difficult for implementation usual discretization methods of integration and instead one can use stochastic Monte Carlo

methods. The idea of the method is to generate a set of states (*chain*)  $\mathbf{R}_1, \dots, \mathbf{R}_M$  with the probability distribution  $p(\mathbf{R})$  and approximate the  $\langle A \rangle$  as the average

$$\langle A \rangle \approx \frac{1}{M} \sum_{i=1}^M A(\mathbf{R}_i) \quad (2.4)$$

Such a chain where the next configuration  $\mathbf{R}'$  depends only on the previous configuration  $\mathbf{R}$  (Markov chain) can be generated by the Metropolis algorithm [MRR<sup>+</sup>53]: the new configuration is accepted with the probability  $P(\mathbf{R} \rightarrow \mathbf{R}')$  given by the rule

$$P(\mathbf{R} \rightarrow \mathbf{R}') = \begin{cases} 1, & \text{if } p(\mathbf{R}') \geq p(\mathbf{R}) \\ p(\mathbf{R}')/p(\mathbf{R}), & \text{if } p(\mathbf{R}') < p(\mathbf{R}) \end{cases} \quad (2.5)$$

In a quantum system the probability distribution is given by the square of the wave function module as Eq. 2.1. The specific construction of wave functions will be discussed in Sec. 2.5.

The efficiency significantly depends on the type of the trial moves. A natural way to generate a new configuration is to move all particles  $\vec{r}_i' = \vec{r}_i + \vec{\xi}_i, i = \overline{1, N}$ , here  $\vec{\xi}_i$  is a random shift delimited to range  $|\vec{\xi}_i| < \Xi$ . If the amplitude of the shift  $\Xi$  is too large the acceptance rate becomes too small, if instead  $\Xi$  is very small, almost all moves are accepted, but the generated configurations are strongly correlated. The acceptance rate of about 50% in general provides a good choice.

The efficiency of a variational calculation can be highly improved by doing a complex move consisting of separate moves of one particle at a time. Each independent move allow a larger displacement at the fixed acceptance rate. Indeed, the amplitude of each individual move can be an order of magnitude larger and consequently leading to a faster convergence of the sampling.

## 2.3 Diffusion Monte Carlo

The Diffusion Monte Carlo method (DMC) can be successfully applied to the investigation of bosonic systems at low temperatures. It is based on solving the Schrödinger equation in the imaginary time and allows calculation of the exact (in statistical sense) value of the ground state energy.

### 2.3.1 Schrödinger equation

The evolution of a quantum system is described by Schrödinger equation

$$i\hbar \frac{\partial}{\partial t} \varphi(\mathbf{R}, t) = \hat{H} \varphi(\mathbf{R}, t), \quad (2.6)$$

Instead of considering the time-evolution we will look for the ground state properties. That can be done by introducing the *imaginary time*  $\tau = -it/\hbar$ . We rewrite the Schrödinger equation and introduce a constant energy shift  $E$ , whose meaning will become clearer later:

$$-\frac{\partial}{\partial \tau} \varphi(\mathbf{R}, \tau) = (\hat{H} - E) \varphi(\mathbf{R}, \tau), \quad (2.7)$$

The formal solution  $\psi(\mathbf{R}, \tau) = e^{-(\hat{H}-E)\tau} \psi(\mathbf{R}, 0)$  can be expanded in eigenstate functions of the Hamiltonian  $\hat{H} \phi_n = E_n \phi_n$ , where we order the eigennumbers in an increasing order  $E_0 < E_1 < \dots$

$$\psi(\mathbf{R}, \tau) = \sum_{n=0}^{\infty} c_n \phi_n(\mathbf{R}, \tau) = \sum_{n=0}^{\infty} c_n \phi_n(\mathbf{R}, 0) e^{-(E_n - E)\tau} \quad (2.8)$$

The amplitudes of the components change with time, either increasing or decreasing depending on the sign of  $(E_n - E)$ . At large times the term that corresponds to the projection on the ground state dominates the sum. In other words all excited states decay exponentially fast and only contribution from ground state survives

$$\psi(\mathbf{R}, \tau) \rightarrow c_0 \phi_0(\mathbf{R}, 0) e^{-(E_0 - E)\tau}, \quad \text{when } \tau \rightarrow \infty \quad (2.9)$$

In the long time limit the wave function remains finite only if  $E$  is equal to  $E_0$ . The ground state energy  $E_0$  will be estimated in a different way (Sec. 2.7.1), but the fact that its estimation used for the energy shift value  $E$  leads to a stable normalization of  $\psi(\mathbf{R}, \tau)$  proves in a different way that the estimator is correct (for the implementation see Eq. 2.34).

The Hamiltonian of a system of  $N$  particles interacting via pair-wise potential  $V_{int}$  and subjected to an external field  $V_{ext}$  in a most general form can be written as

$$\hat{H} = -\frac{\hbar^2}{2m} \sum_{i=1}^N \Delta_i + \sum_{i<j}^N V_{int}(|\vec{r}_i - \vec{r}_j|) + \sum_{i=1}^N V_{ext}(\vec{r}_i), \quad (2.10)$$

The Schrödinger equation (2.7) reads as<sup>2</sup>

$$-\frac{\partial}{\partial \tau} \psi(\mathbf{R}, \tau) = -D \Delta_{\mathbf{R}} \psi(\mathbf{R}, \tau) + V(\mathbf{R}) \psi(\mathbf{R}, \tau) - E \psi(\mathbf{R}, \tau), \quad (2.11)$$

where we introduced the notation  $D = \hbar^2/2m$  and terms depending only on particle coordinates are denoted as  $V(\mathbf{R}) = \sum_{i<j}^N V_{int}(|\vec{r}_i - \vec{r}_j|) + \sum_{i=1}^N V_{ext}(\vec{r}_i)$ .

The efficiency of the method can be significantly improved if additional information on the wave function is used. The idea is to approximate the true wave function  $\psi(\mathbf{R}, \tau)$  by a trial one  $\psi_T(\mathbf{R})$  and let the algorithm correct the guess done. This approach is called *importance sampling* and consists in solving the Schrödinger equation for the modified wave function

$$f(\mathbf{R}, \tau) = \psi_T(\mathbf{R}) \psi(\mathbf{R}, \tau) \quad (2.12)$$

Another reason for using the product of wave functions as the probability distribution instead of sampling  $\psi$  is that the average over the latter is ill defined  $\langle A \rangle = \int A \psi d\mathbf{R} / \int \psi d\mathbf{R}$ , on the contrary the average over the product of wave functions has the meaning of the mixed estimator  $\langle A \rangle = \int \psi_T A \psi d\mathbf{R} / \int \psi_T \psi d\mathbf{R}$ . From (2.11) it follows that the distribution function  $f$  satisfies the equation

$$-\frac{\partial}{\partial \tau} f(\mathbf{R}, \tau) = -D \Delta_{\mathbf{R}} f(\mathbf{R}, \tau) + D \nabla_{\mathbf{R}} (\mathbf{F} f(\mathbf{R}, \tau)) + (E^{loc}(\mathbf{R}) - E) f(\mathbf{R}, \tau), \quad (2.13)$$

here  $E^{loc}$  denotes the *local energy* which is the average of the Hamiltonian with respect to trial wave function<sup>3</sup>

$$E^{loc}(\mathbf{R}) = \psi_T^{-1}(\mathbf{R}) \hat{H} \psi_T(\mathbf{R}) \quad (2.14)$$

<sup>2</sup>The subscript  $\mathbf{R}$  of the differential operator indicates that the derivative has to be taken for every component of  $\mathbf{R}$ .

<sup>3</sup>for details of the calculation refer to Sec. 2.7

and  $\mathbf{F}$  is the *drift force* which is proportional to the gradient of the trial wave function and points in the direction of the maximal increase of  $\psi_T$ <sup>4</sup>

$$\mathbf{F} = \frac{2}{\psi_T(\mathbf{R})} \nabla_{\mathbf{R}} \psi_T(\mathbf{R}) \quad (2.15)$$

### 2.3.2 Green's function

The formal solution of the Schrödinger equation written in coordinate space is given by

$$\langle \mathbf{R} | f(\tau) \rangle = \sum_{\mathbf{R}'} \langle \mathbf{R} | e^{-(\hat{H}-E)\tau} | \mathbf{R}' \rangle \langle \mathbf{R}' | f(0) \rangle, \quad (2.16)$$

or, expressed in terms of the *Green's function*  $G(\mathbf{R}, \mathbf{R}', \tau) = \langle \mathbf{R} | e^{-(\hat{H}-E)t} | \mathbf{R}' \rangle$ , the above equation reads as

$$f(\mathbf{R}, \tau) = \int G(\mathbf{R}, \mathbf{R}', \tau) f(\mathbf{R}', 0) d\mathbf{R}' \quad (2.17)$$

In other words, the differential Schrödinger equation (2.6) corresponds to the integral equation (2.17), which can be integrated with help of Monte Carlo methods. Although the Green's function  $G(\mathbf{R}', \mathbf{R}, \tau)$  is not known, it can be approximated at small times  $\tau$ , and then equation (2.17) can be solved step by step

$$f(\mathbf{R}, \tau + \Delta\tau) = \int G(\mathbf{R}, \mathbf{R}', \Delta\tau) f(\mathbf{R}', \tau) d\mathbf{R}' \quad (2.18)$$

The asymptotic solution for large times can be obtained by propagating  $f(\mathbf{R}, \tau)$  for a large number of time steps  $\Delta\tau$ .

$$f(\mathbf{R}, \tau) \rightarrow \psi_T(\mathbf{R}) \phi_0(\mathbf{R}), \quad \tau \rightarrow \infty \quad (2.19)$$

For further convenience let us split the Hamiltonian into three pieces

$$\hat{H} = \hat{H}_1 + \hat{H}_2 + \hat{H}_3, \quad (2.20)$$

where

$$\begin{aligned} \hat{H}_1 &= -D\Delta, \\ \hat{H}_2 &= D((\nabla_{\mathbf{R}} \mathbf{F}) + \mathbf{F} \nabla_{\mathbf{R}}), \\ \hat{H}_3 &= E^{loc}(\mathbf{R}) - E \end{aligned} \quad (2.21)$$

Let us introduce the corresponding Green's functions:

$$G_i(\mathbf{R}, \mathbf{R}', \tau) = \langle \mathbf{R} | e^{-\hat{H}_i \tau} | \mathbf{R}' \rangle, \quad i = 1, 2, 3 \quad (2.22)$$

---

<sup>4</sup>The definition (2.15) of the drift force can be understood in a classical analogy. In a classical system the probability distribution has a Boltzman form. The coordinate part of the distribution function is related to the potential energy  $p(\mathbf{R}) = const \exp(-U(\mathbf{R}))$  (we put the fictitious temperature to one). The classical force is an antigradient of the potential energy  $\mathbf{F} = -\nabla_{\mathbf{R}} U(\mathbf{R}) = \nabla_{\mathbf{R}} \ln p(\mathbf{R})$ . If we approximate a quantum probability distribution by the square of a trial wave function (2.1), then the force equals exactly to (2.15).

The exponent of a sum of two operators (on the contrary to an exponent of  $c$ -numbers) in general can not be written as a product of two exponents. The exact relation takes into account the non-commutativity  $\exp\{-(\hat{A} + \hat{B})\tau + [\hat{A}, \hat{B}]\tau^2/2\} = \exp\{-\hat{A}\tau\} \exp\{-\hat{B}\tau\}$ . The primitive approximation consists in neglecting the noncommutativity

$$e^{-\hat{H}\tau} = e^{-\hat{H}_1\tau} e^{-\hat{H}_2\tau} e^{-\hat{H}_3\tau} + O(\tau^2) \quad (2.23)$$

This formula, rewritten in the coordinate representation, gives the expression for the Green's function

$$G(\mathbf{R}, \mathbf{R}', \tau) = \iint G_1(\mathbf{R}, \mathbf{R}_1, \tau) G_2(\mathbf{R}_1, \mathbf{R}_2, \tau) G_3(\mathbf{R}_2, \mathbf{R}', \tau) d\mathbf{R}_1 d\mathbf{R}_2$$

From Eq. 2.22 we find that the Green's function should satisfy Bloch differential equation:

$$\begin{cases} -\frac{\partial}{\partial\tau} G_i(\mathbf{R}, \mathbf{R}', \tau) = \hat{H}_i G_i(\mathbf{R}, \mathbf{R}', \tau), & i = 1, 2, 3 \\ G_i(\mathbf{R}, \mathbf{R}', 0) = \delta(\mathbf{R} - \mathbf{R}') \end{cases} \quad (2.24)$$

The equation for the kinetic term has the form

$$-\frac{\partial G_1(\mathbf{R}, \mathbf{R}', \tau)}{\partial\tau} = -D\Delta G_1(\mathbf{R}, \mathbf{R}', \tau) \quad (2.25)$$

This is the diffusion equation with diffusion constant  $D = \hbar^2/2m$ . It can be conveniently solved in a momentum representation where the kinetic energy operator is diagonal. Going back to the coordinate representation one finds that the solution is a Gaussian

$$G_1(\mathbf{R}, \mathbf{R}', \tau) = (4\pi D\tau)^{-3N/2} \exp\left\{-\frac{(\mathbf{R} - \mathbf{R}')^2}{4D\tau}\right\} \quad (2.26)$$

The equation for the drift force term is

$$-\frac{\partial G_2(\mathbf{R}, \mathbf{R}', \tau)}{\partial\tau} = -D\nabla_{\mathbf{R}}(\mathbf{F}G_2(\mathbf{R}, \mathbf{R}', \tau)) \quad (2.27)$$

and its solution is

$$G_2(\mathbf{R}, \mathbf{R}', \tau) = \delta(\mathbf{R} - \mathbf{R}(\tau)), \quad (2.28)$$

here  $\mathbf{R}(\tau)$  is the solution of the classical equation of motion

$$\begin{cases} \frac{d\mathbf{R}(\tau)}{d\tau} = D\mathbf{F}(\mathbf{R}(\tau)), \\ \mathbf{R}(0) = \mathbf{R}' \end{cases} \quad (2.29)$$

The last equation from (2.24) has a trivial solution, which describes the *branching* term

$$G_3(\mathbf{R}, \mathbf{R}', \tau) = \exp\{(E - E^{loc}(\mathbf{R}))\tau\} \delta(\mathbf{R} - \mathbf{R}') \quad (2.30)$$



### 2.3.3 Primitive algorithm

If the wave function of the system  $f(\mathbf{R}, \tau)$  is real and positive, as it happens in case of ground state of a bose system, it can be treated as population density distribution<sup>1</sup> (the algorithm for fermions, where the wave function has nodes will be discussed in Sec. 2.6)

$$f(\mathbf{R}, \tau) = \sum_{i=1}^{N_W} C \delta(\mathbf{R} - \mathbf{R}_i(\tau)), \quad (2.31)$$

here  $C$  is a positive constant,  $\mathbf{R}_i(\tau)$  are coordinates of a population element (so called *walker*) in  $3N$ -dimensional configuration space,  $f(\mathbf{R}, \tau) d\mathbf{R}$  gives the probability to find a walker at time  $\tau$  in the vicinity  $d\mathbf{R}$  of a point  $\mathbf{R}$ .

Let us now interpret the action of the each of the three terms of the Hamiltonian (2.20) on the population distribution or, being the same, the action of the corresponding Green's functions (2.26, 2.28, 2.30). In terms of Markov chains the Green's function is the  $G(\mathbf{R}, \mathbf{R}', \tau)$  is the transition matrix which determines the evolution of the distribution (see Eq. 2.18).

The first term means the *diffusion* of each of the walkers in the configuration space

$$\mathbf{R}^{(1)}(t + \Delta\tau) = \mathbf{R}(\tau) + \chi, \quad (2.32)$$

here  $\chi$  is a random value having a gaussian distribution  $\exp\{-\chi^2/(4D\Delta\tau)\}$ .

The second term describes the action of the drift force, which guides the walkers to places in the configuration space, where the trial wave function is maximal. This is the way how importance sampling acts in the algorithm

$$\mathbf{R}^{(2)}(t + \Delta\tau) = \mathbf{R}(\tau) + DF(\mathbf{R})\Delta\tau \quad (2.33)$$

The Green's functions of steps (2.26),(2.28) are normalized to unity  $\int G(\mathbf{R}, \mathbf{R}', \tau) d\mathbf{R} = 1$ . The normalization of wave function  $f$  is then conserved, which means that the number of walkers remains constant.

The third term is the *branching*

$$f^{(3)}(\mathbf{R}, \tau + \Delta\tau) = \exp\{-(E^{loc}(\mathbf{R}) - E) \Delta\tau\} f(\mathbf{R}, \tau) \quad (2.34)$$

The corresponding Green's function  $G_3(\mathbf{R}, \mathbf{R}', \tau)$  (2.30) is no longer normalized. That means that the weight of a walker  $\mathbf{R}$  changes on this step, thus walkers with lower local energy have larger weights and walkers with larger local energy have smaller weights. On this step each walker is to be duplicated  $b = \exp\{-(E^{loc}(\mathbf{R}) - E) \Delta\tau\}$  times. In general the number  $b$  is not an integer. A possible solution is to throw a random number  $\xi \in (0, 1)$  and duplicate the walker  $[b + \xi]$  times, where the brackets  $[ \cdot ]$  stand for the integer part of a number.

Now it is clear that by adjusting the value of  $E$  one can control the size of the population and keep it within the desired range. If the value of  $E$  is taken to be equal the estimator  $E_0$  (2.14) averaged over the population and the population size does not change, it means that  $E_0$  is equal to the ground state energy (see, also, Eq. 2.9).

---

<sup>1</sup>The formula (2.31) should be understood in the statistical sense, the average of any value  $A$  over the l.h.s. and r.h.s distributions are equal to each other in the limit when size of the population  $N_W$  tends to infinity  $\int A(\mathbf{R})f(\mathbf{R}, \tau) d\mathbf{R} =$

$$\lim_{N_W \rightarrow \infty} \int A(\mathbf{R}) \sum_{i=1}^{N_W} C \delta(\mathbf{R} - \mathbf{R}_i(\tau)) d\mathbf{R}$$

The branching is an essential part of the DMC algorithm as it “corrects” the trial wave function. Indeed, the first two steps (2.26), (2.28) alone without (2.30) are equivalent to sampling the trial wave function and provide the same result as the variational calculation (Sec. 2.2). If the trial wave function is an exact eigenfunction of the Hamiltonian, the local energy equals to the corresponding eigennumber and is independent of  $\mathbf{R}$ , thus the branching becomes irrelevant as it acts in the same way on all walkers.

### 2.3.4 Higher-order algorithm

The primitive approximation (2.23) for the Green’s function has a first-order of accuracy, *i.e.* the resulting energy has a linear dependence on the timestep. It means that measurements with different time-steps are necessary in order to make extrapolation to zero timestep  $\Delta\tau \rightarrow 0$  as the dependence on the timestep is very strong. Instead one can consider a higher order approximations. One of the possible second-order expansions is

$$e^{-\hat{H}\tau} = e^{-\hat{H}_3\tau/2} e^{-\hat{H}_2\tau/2} e^{-\hat{H}_1\tau} e^{-\hat{H}_2\tau/2} e^{-\hat{H}_3\tau/2} + O(\tau^3) \quad (2.35)$$

This expansion leads to a quadratic dependence of the energy on the timestep which makes this approximation very useful. The point is that each calculation has an intrinsic statistical error, which depends on the length of the calculation and on the variance of the measured quantity. Once the desired level of accuracy is chosen one can make a study of the dependence on the timestep and adjust it to the maximal value, which still gives an error smaller than the desired statistical error. Using this timestep one can avoid the extrapolation procedure at all.

Here is the summary of the higher order scheme used in the calculations. One step which propagates the system in the imaginary time from  $\tau$  to  $\tau + \Delta\tau$ . The walker is moved from position  $\mathbf{R}_{i-1}$  to position  $\mathbf{R}_i$  and is replicated with the weight calculated during the branching

1) Gaussian jump (2.26):

$$\mathbf{R} = \mathbf{R}_{i-1} + \chi, \quad f(\chi) = \exp\{-\mathbf{R}^2/4\Delta\tau\}$$

2) Drift force (2.28):

$$\begin{aligned} \mathbf{R}' &= \mathbf{R} + \mathbf{F}(\mathbf{R}) \Delta\tau/2 \\ \mathbf{R}'' &= \mathbf{R} + (\mathbf{F}(\mathbf{R}) + \mathbf{F}(\mathbf{R}')) \Delta\tau/4 \\ \mathbf{R}''' &= \mathbf{R} + \mathbf{F}(\mathbf{R}'') \Delta\tau \end{aligned}$$

3) Branching (2.30):

$$\mathbf{R}''' \rightarrow \mathbf{R}_i$$

## 2.4 Fixed-node Diffusion Monte Carlo method

The FN-DMC method [RCAJ82] modifies the DMC method to allow an approximate treatment of excited states of many-body systems. The idea of the FN-DMC method is to treat excited states by “enforcing” the positive definiteness of the probability distribution  $f(\mathbf{R}, \tau) = \psi_T(\mathbf{R})\psi(\mathbf{R}, \tau)$ . The function  $f(\mathbf{R}, \tau)$  is positive definite everywhere in configuration space, and can hence be interpreted as a probability distribution, if  $\psi_T(\mathbf{R})$  and  $\psi(\mathbf{R}, \tau)$  change sign together, and thus share the same (high-dimensional) nodal surface. To ensure positive definiteness of  $f(\mathbf{R}, \tau)$ , the trial wave function  $\psi_T(\mathbf{R})$  imposes a nodal constraint, which is fixed during the calculation. Within this constraint, the function  $f(\mathbf{R}, \tau)$  is propagated (following a scheme very similar to that outlined in Sec. 2.3), and reaches an asymptotic distribution for large  $\tau \rightarrow \infty$ ,  $f(\mathbf{R}, \tau) = \psi_T(\mathbf{R})\psi(\mathbf{R}, \tau)$ . In the FN-DMC

method,  $\psi_T(\mathbf{R})$  is an approximation to the exact excited eigenfunction of the many-body Schrödinger equation (and not the groundstate wave function as in the DMC method). It can be proven that, due to the nodal constraint, the fixed-node energy is a variational upper bound to the exact eigenenergy for a given symmetry [RCAJ82]. In particular, if the nodal surface of  $\psi_T(\mathbf{R})$  were exact, then  $\psi(\mathbf{R}, \tau)$  would be exact. Thus, the FN-DMC energy depends crucially on a good parameterization of the many-body nodal surface.

Thus, in a FN-DMC simulation the function  $f(\mathbf{R}, \tau) = \psi_T(\mathbf{R})\Psi(\mathbf{R}, \tau)$ , where  $\Psi(\mathbf{R}, \tau)$  denotes the wave function of the system and  $\psi_T(\mathbf{R})$  is a trial function used for importance sampling, is evolved in imaginary time according to the Schrödinger equation

$$-\frac{\partial f(\mathbf{R}, \tau)}{\partial \tau} = -D\nabla_{\mathbf{R}}^2 f(\mathbf{R}, \tau) + D\nabla_{\mathbf{R}}[\mathbf{F}(\mathbf{R})f(\mathbf{R}, \tau)] + [E_L(\mathbf{R}) - E_{ref}]f(\mathbf{R}, \tau) \quad (2.36)$$

In the above equation  $\mathbf{R} = (\mathbf{r}_1, \dots, \mathbf{r}_N)$ ,  $E_L(\mathbf{R}) = \psi_T(\mathbf{R})^{-1}H\psi_T(\mathbf{R})$  denotes the local energy,  $\mathbf{F}(\mathbf{R}) = 2\psi_T(\mathbf{R})^{-1}\nabla_{\mathbf{R}}\psi_T(\mathbf{R})$  is the quantum drift force,  $D = \hbar^2/(2m)$  plays the role of an effective diffusion constant, and  $E_{ref}$  is a reference energy introduced to stabilize the numerics. The energy and other observables of the state of the system are calculated from averages over the asymptotic distribution function  $f(\mathbf{R}, \tau \rightarrow \infty)$ . To ensure positive definiteness of the probability distribution  $f$  for fermions, the nodal structure of  $\psi_T$  is imposed as a constraint during the calculation. It can be proved that, due to this nodal constraint, the calculated energy is an upper bound to the eigenenergy for a given symmetry [RCAJ82]. In particular, if the nodal surface of  $\psi_T$  were exact, the fixed-node energy would also be exact.

Construction of the trial wave function, as well as evaluation of the energy, is described in Sec. 2.6.

## 2.5 Construction of trial wave functions: system of Bosons

### 2.5.1 Introduction

This Section is aimed to provide technical details on the construction of trial bosonic wave functions. First of all we will discuss the general Bijl-Jastrow trial wave function and then we will explain in details the construction of trial wave functions used to obtain properties of the bosonic systems. The idea of this section is to make a reference for the technical part of the calculations, in order to leave the subsequent discussion free for physical discussions.

### 2.5.2 Bijl-Jastrow wave function

The bosonic function must be symmetric with respect to exchange of two particles. The most natural way to construct the trial wave function of a system of Bosons is to consider a product of one-body and two-body terms (we neglect three-body and higher terms):

$$\Psi(\vec{r}_1, \dots, \vec{r}_N) = \prod_{i=1}^N f_1(\vec{r}_i) \prod_{j < k}^N f_2(|\vec{r}_j - \vec{r}_k|) \quad (2.37)$$

This construction is called Bijl-Jastrow trial wave function. The one-body term  $f_1(\vec{r})$  accounts for the external potential and, commonly, has the same structure as the solution of an ideal system in the same external potential. The interaction between particles is accounted by the two-body Bijl-Jastrow term  $f_2(r)$  which must go to a unity (uncorrelated value) at large distances. If the periodic

boundary conditions are used the restriction on the two-body term is stronger, the function must go to the unity already at the half size of the simulation box. This condition ensures that the particles do not interact with their own images and no artificial correlations are introduced.

Once the exact type of the Bijl-Jastrow terms is chosen, one should also calculate the first and second derivatives in order to implement the QMC method. Actually the algorithm can be optimized by noticing (see Sec. 2.7) that the trial wave function always comes in one of the three combinations:

1) the logarithm of the Bijl-Jastrow term (is necessary for the Metropolis algorithm in the variational calculation and calculations of the non-local quantities, *e.g.* the one-body density matrix)

$$u(r) = \ln f(r) \quad (2.38)$$

2) the logarithmic derivative of the Bijl-Jastrow term (is needed for the calculation of the drift force (2.15))

$$\mathcal{F}(r) = \frac{f'(r)}{f(r)} \quad (2.39)$$

3) the second derivative enters only in the calculation of the kinetic part of the local energy. The following combination is relevant:

$$\mathcal{E}^{loc}(r) = -\frac{f''(r)}{f(r)} + \left(\frac{f'(r)}{f(r)}\right)^2 + \frac{mV_{int}(r)}{\hbar^2} - \frac{D-1}{r} \frac{f'(r)}{f(r)}, \quad (2.40)$$

where  $D$  is number of dimensions.

### 2.5.3 One-body Bijl-Jastrow term in an anisotropic trap

Let the external field be an anisotropic trap with the aspect ratio  $\lambda$ :  $V_{ext}(\vec{r}) = \frac{1}{2}m\omega_{\perp}^2(x^2 + y^2 + \lambda^2 z^2)$ . We choose the one-body Bijl-Jastrow term (2.37) in form of a Gaussian with the widths  $\alpha$  and  $\beta$  being variational parameters:

$$f_1(\vec{r}) = \exp\{-\alpha(x^2 + y^2) - \beta\lambda z^2\} \quad (2.41)$$

Then the one body contribution to the drift force is

$$\vec{F}_1(\vec{r}_i) = -(2\alpha x, 2\alpha y, 2\beta\lambda z) \quad (2.42)$$

The local energy is

$$E^{loc}(\mathbf{R}) = N(2\alpha + \beta\lambda) + \sum_{j<k}^N \mathcal{E}_2^{loc}(|\vec{r}_j - \vec{r}_k|) - \frac{1}{2} \sum_{i=1}^N |\vec{F}_i(\vec{r}_1, \dots, \vec{r}_N)|^2 + \sum_{i=1}^N \frac{x_i^2 + y_i^2 + \lambda^2 z_i^2}{2} \quad (2.43)$$

where we used oscillator units: energy is measured in units of  $\hbar\omega_{\perp}$  and the distances in units of the oscillator length  $a_{\perp}$ .

### 2.5.4 One-dimensional wave functions

In this section we will discuss construction of a wave functions which are used to solve one-dimensional problems. Apart from the case of the Tonks-Girardeau and gas of hard rods, where the wave function is known exactly (Secs. 2.5.4.1, 2.5.4.2), the wave function are constructed in a Bijl-Jastrow form based on two-body solutions found in the Secs. 1.3.3 (the same method is used also in the construction of three-dimensional wave functions Secs. 2.5.5).

### 2.5.4.1 Tonks-Girardeau wave function

As was first shown by Girardeau[Gir60], the wave function of the Tonks-Girardeau gas is equal to the absolute value of the wave function of 1D ideal fermions. The interaction potential corresponds to  $\delta$ -function with infinite strength, or in other words the TG model describes impenetrable particles of a zero size. The component of an *exact wave function* is given by

$$f_2(z) = |\sin(\pi z/L)| \quad (2.44)$$

Strictly speaking the wave function (2.44) does not fall into the class of Bijl-Jastrow functions (2.37) as the term  $f_2(z)$  does not go to a constant even in the large-range limit, but always experience oscillations. At the same time it does not cause problems in our calculations as it turns out that the scattering energy  $\mathcal{E} = \pi^2 \hbar^2 / mL^2$  of the exact solution [Gir60] corresponds to lowest energy of one particle of reduced mass in a box with zero boundary conditions and the  $f_2(z)$  goes to one in a smooth way at the maximal allowed distance  $z = L/2$ .

The drift force contribution (2.39) is given by

$$\mathcal{F}_2(z) = \sqrt{\mathcal{E}} \cotan \sqrt{\mathcal{E}} z \quad (2.45)$$

and the 1D local energy (2.40) equals to

$$\mathcal{E}_{22}(z) = \mathcal{E}(1 + \cotan^2 \sqrt{\mathcal{E}} z) \quad (2.46)$$

### 2.5.4.2 Hard-rod wave function (exact)

In this section we will discuss the wave function of the hard-rod gas, *i.e.* the one-dimensional gas of impenetrable particles (1.79) of radius  $a_{1D}$ . Already in his original work[Gir60], Girardeau noted that the *exact* ground state wave function of a hard-rod system can be obtained from the wave function of the TG gas (Sec 2.5.4.1) by subtracting the excluded volume. That can be done by the transformation

$$z'_i = z_i - ia_{1D}, \quad i = \overline{1, N} \quad (2.47)$$

This exact wave function is used for calculation of correlation properties in the super-Tonks regime.

### 2.5.4.3 Hard-rod wave function (approximate)

The transformation (2.47) makes the implementation of the calculation quite sophisticated. Instead one can construct an approximate wave function in the same spirit as it will be done in the subsequent sections, *i.e.* by using the exact solution for the two particle scattering problem (1.60).

Using the solution (1.80) we propose

$$f_2(z) = \begin{cases} 0, & |z| \leq |a_{1D}| \\ \left| \frac{A}{z} \sin(\sqrt{\mathcal{E}}(|z| - |a_{1D}|)) \right|, & |z| > |a_{1D}| \end{cases} \quad (2.48)$$

The advantage of this wave function is that it is solution of a two-body problem, so the interaction energy is always constant, which is much easier to sample numerically. The force and local energy

can be easily obtained from 1D hard-sphere wave function. The difference is that  $\mathcal{E}$  is a variational parameter here.

The drift force contribution (2.39) is given by

$$\mathcal{F}_2(z) = \begin{cases} 0, & |z| \leq |a_{1D}| \\ \sqrt{\mathcal{E}} \cotan \sqrt{\mathcal{E}}(|z| - |a_{1D}|), & |z| > |a_{1D}| \end{cases} \quad (2.49)$$

The 1D local energy (2.40) is

$$\mathcal{E}_2^{loc}(z) = \begin{cases} 0, & |z| \leq |a_{1D}| \\ E(1 + \cotan^2 \sqrt{E}(|z| - |a_{1D}|)), & |z| > |a_{1D}| \end{cases} \quad (2.50)$$

#### 2.5.4.4 Wave function of the Lieb Liniger gas

In this section we will describe the construction of the wave function whis is used to solve the Lieb-Liniger equation in presence of an external confinement (refer to Sec. 3.2.5). The aim is to obtain a wave function suitable for the description of the gas in a wide range of the density, starting from the Tonks-Girardeau and up to the Gross-Pitaevskii regimes. The important point is that TG wave function always has nodes, although in GP regime the nodes are absent.

At the distances  $|z| > 0$  the interaction potential is absent and the solutions are are simple sinus and cosine functions. We want to choose a solution which goes to one at the matching distance  $R_m$ , which is treated as a variational parameter, and is a solution of a two-body problem (1.65) at a smaller distances. Also we want to have a symmetry in sign reversing. The solution that satisfies those conditions is

$$f_2(z) = \begin{cases} 1, & z < -R_m \\ \cos k(z - R_m), & -R_m \leq z < 0 \\ \cos k(z + R_m), & 0 \leq z < R_m \\ 1, & R_m \leq z \end{cases} \quad (2.51)$$

At the matching points  $\pm R_m$  the derivative is automatically equal to zero and the function matches smoothly to a constant. The phase  $\Delta(k) = kR_m$  is related to the scattering length  $a_{1D}$  by the boundary condition (1.70), which we will write as<sup>5</sup>

$$ka_{1D} \tan kR_m = 1 \quad (2.52)$$

Once  $k$  is obtained by solving numerically this equation the drift force contribution (2.39) can be calculated from formula

$$\mathcal{F}_2(z) = \begin{cases} -k \tan k(z - R_m), & 0 \leq |z| < R_m \\ 0, & |z| \geq R_m \end{cases} \quad (2.53)$$

The energy contribution (2.40) is then described by

$$\mathcal{E}_2(z) = \begin{cases} k^2(1 + \tan^2(k(z - R_m))), & 0 \leq |z| < R_m \\ 0, & |z| \geq R_m \end{cases} \quad (2.54)$$

---

<sup>5</sup>Note that for a repulsive gas  $a_{1D} < 0$  while for attractive  $a_{1D} > 0$ .

### 2.5.4.5 Phonon trial wave function ( $\delta$ -potential)

Here we shall construct a trial wave function which at distances short is a two-body solution of one-dimensional  $\delta$ -function scattering and has “phonon” like behavior at large distances (see [RC67]).

The trial wave function is chosen in the following form

$$f_2(z) = \begin{cases} A \cos k(z - B), & z < R \\ |\sin^\alpha(\pi z/L)|, & z \geq R \end{cases} \quad (2.55)$$

There are five undefined parameters  $A, B, k, \alpha, R$  and four continuity equations. One parameter is left free. We will chose matching distance  $R$  as the guiding parameter.

- 1) Continuity condition at zero is the same as in the Lieb-Liniger trial wave function (1.66) and is given by the formula (2.52)

$$ka_{1D} \tan kB = 1 \quad (2.56)$$

This equation fixes the value of the phase shift  $kB$ .

- 2) Continuity condition at the matching point

- a) continuity of the wave function:

$$A \cos k(R - B) = \sin^\alpha(\pi R/L) \quad (2.57)$$

- b) continuity of the first derivative, which together with the condition a) means continuity of the logarithmic derivative:

$$-k \tan k(R - B) = \alpha \frac{\pi}{L} \cotan(\pi R/L) \quad (2.58)$$

- c) continuity of the second derivative or, together with a) and b) means continuity of the local energy:

$$-k^2 = \alpha \left(\frac{\pi}{L}\right)^2 [(\alpha - 1) \cotan^2(\pi R/L) - 1] \quad (2.59)$$

One can prove that following relation holds  $kL/\pi \sin 2\pi R/L + \sin 2k(R - B) = 0$ . Another useful relation is  $\tan k(R - B) = (ka_{1D} \sin kR + \cos kR)/(ka_{1D} \cos kR - \sin kR)$ .

The value of the scattering momenta is a solution of the equation

$$\frac{(\sin kR - ka_{1D} \cos kR)(\cos kR + ka_{1D} \sin kR)}{k((ka_{1D})^2 + 1)} = \frac{L}{2\pi} \sin \frac{2\pi R}{L} \quad (2.60)$$

The maximal value of the l.h.s. is reached at  $k = 0$  and equals to  $R - a_{1D}$ . For matching distance much smaller than  $L$  the sinus function on the r.h.s. can be expanded and the condition for the existence of the solution is  $a_{1D} < 0$  which is always fulfilled for the repulsive gas.

All other parameters can be found from the following formulae:

$$\begin{cases} B &= \frac{1}{k} \operatorname{arccot} ka \\ \alpha &= 1 + \tan \frac{\pi R}{L} \left( \frac{kL}{\pi} \cotan k(R - B) + \tan \frac{\pi R}{L} \right) \\ A &= \frac{\sin^\alpha(\pi R/L)}{\cos(k(R-B))} \end{cases} \quad (2.61)$$

The contribution to the energy is given by

$$-\frac{f''}{f} + \left(\frac{f'}{f}\right)^2 = \begin{cases} k^2[1 + \tan^2 k(z - B)], & z < R \\ \alpha \left(\frac{\pi}{L}\right)^2 [1 + \cotan^2 \frac{\pi z}{L}], & z \geq R \end{cases} \quad (2.62)$$



### 2.5.4.6 Super-Tonks trial wave function (attractive $\delta$ -potential)

In this section we will describe the construction of the trial wave function  $\psi_T$  used for the investigation of the super-Tonks system (see Chapter 6).

We use Bijl-Jastrow construction (2.37) with the two-body term which is chosen to be similar to (2.51)

$$f_2(z) = \begin{cases} \cos[k(|z| - R_m)], & |z| \leq R_m \\ 1, & |z| > R_m \end{cases} \quad (2.63)$$

The cut-off length  $R_m$  is a variational parameter, while the wave vector  $k$  (for a given  $R_m$ ) is chosen in a such way that the boundary condition imposed by the  $\delta$ -function potential (2.52) at  $z = 0$  is satisfied:  $-k \tan(kR_m) = 1/a_{1D}$ . For distances smaller than the cut-off length,  $|z| \leq R_m$ , the above wave function corresponds to the exact solution with positive energy of the two-body problem with the interaction potential  $g_{1D}\delta(z)$  (see, formula 1.65).

### 2.5.4.7 Scattering on the resonance state of a Bose gas

In the case of the Hamiltonian (4.9) we use Gaussian construction for the one-body Bijl-Jastrow term

$$f_1(z) = \exp \left\{ -\frac{z^2}{2\alpha_z^2} \right\} \quad (2.64)$$

where the Gaussian width  $\alpha_z$  is treated as a variational parameter. The two-body correlation term  $f_2(z)$  (2.37) is chosen as

$$f_2(z) = \begin{cases} \cos[k_z(|z| - \bar{Z})], & |z| \leq \bar{Z} \\ 1, & |z| > \bar{Z} \end{cases} \quad (2.65)$$

The cut-off length  $\bar{Z}$  is fixed at  $\bar{Z} = 500a_{1D}$ , while the wave vector  $k_z$  is chosen such that the boundary condition at  $z = 0$  imposed by the  $\delta$ -function potential is satisfied:  $-k_z \tan(k_z \bar{Z}) = 1/a_{1D}$ . For negative  $a_{1D}$  ( $g_{1D} > 0$ ) the correlation function, Eq. 2.65, is positive everywhere. For positive  $a_{1D}$  ( $g_{1D} < 0$ ), in contrast,  $f_2(z)$  changes sign at  $|z| = a_{1D}$ . The parameterization given by Eq. 2.65 is used in our stability analysis performed within a VMC framework (see Sec. 4.5) and in our DMC calculations for  $g_{1D} > 0$ . To perform the FN-DMC calculations for negative  $g_{1D}$ , we need to construct a trial wave function that is positive definite everywhere. In the FN-DMC calculations, we thus use an alternative parameterization, which imposes the constraint  $f_2 = 0$  for  $a_{1D} \leq z$ ,

$$f_2(z) = \begin{cases} 0, & z \leq a_{1D} \\ \cos[k_z(|z| - \bar{Z})], & a_{1D} < z \leq \bar{Z} \\ 1, & z > \bar{Z} \end{cases} \quad (2.66)$$

## 2.5.5 Three-dimensional wave functions

### 2.5.5.1 Hard sphere trial wave function

The problem of scattering on a hard sphere potential (1.48) was studied in Sec. 1.3.2.2. In dilute systems for small interparticle distance  $r$  the two body Bijl Jastrow term  $f_2(r)$  is well approximated by the solution  $f(r)$  (1.51), *i.e.* by the wave function of a pair of particles in vacuum. At large distances the pair wave function asymptotically goes to a constant value, as the particles become uncorrelated.



Taking these facts into account we introduce the trial function in the following way[GBC99] (here we introduce dimensionless notation by measuring the distance  $r$  in units of the hard sphere radius  $a_{3D}$  and energy  $E$  in units of  $\hbar^2/(ma_{3D}^2)$ )

$$f_2(r) = \begin{cases} \frac{A \sin(\sqrt{2E}(r-1))}{r}, & |r| \leq R_m \\ 1 - B \exp\left\{-\frac{r}{\alpha}\right\}, & |r| > R_m \end{cases} \quad (2.67)$$

The request the function be smooth at the matching point  $R_m$ , *i.e.*

1) the function  $f_2(r)$  itself must be continuous:

$$\frac{A \sin(\sqrt{2E}(R_m-1))}{R_m} = 1 - B \exp\left\{-\frac{R_m}{\alpha}\right\} \quad (2.68)$$

2) derivative  $f_2'(r)$  must be continuous

$$\frac{A\sqrt{2E} \cos(\sqrt{2E}(R_m-1))}{R_m} - \frac{A \sin(\sqrt{E}(R_m-1))}{R_m^2} = \frac{B}{\alpha} \exp\left\{-\frac{R_m}{\alpha}\right\} \quad (2.69)$$

3) the local energy  $f_2(r)^{-1}(-\hbar^2\Delta_1/2m - \hbar^2\Delta_1/2m + V_{int}(\vec{r}_i - \vec{r}_j))f_2(r)$  must be continuous

$$2E = \frac{\left(\frac{1}{\alpha^2} - \frac{2}{R_m\alpha}\right) B \exp\left(-\frac{R_m}{\alpha}\right)}{1 - B \exp\left(-\frac{R_m}{\alpha}\right)} \quad (2.70)$$

The solution of this system is

$$\begin{cases} A = \frac{R}{\sin(u(1-1/R))} \frac{\xi^2 - 2\xi}{\xi^2 - 2\xi + u^2}, \\ B = \frac{u^2 \exp(\xi)}{\xi^2 - 2\xi + u^2}, \end{cases} \quad (2.71)$$

where we used the notation  $u = \sqrt{2E}R$  and  $\xi = R/\alpha$ . The value of  $\xi$  is obtained from the equation

$$1 - \frac{1}{R} = \frac{1}{u} \arctan \frac{u(\xi-2)}{u^2 + \xi - 2} \quad (2.72)$$

There are three conditions for the determination of five unknown parameters, consequently two parameters are left free. The usual way to define them is minimize the variational energy in Variational Monte Carlo which yields an optimized trial wave function.

### 2.5.5.2 Soft sphere trial wave function

At short distances the scattering solution  $f(r)$  (1.55) is expected to provide a good approximation for the two-body Bijl-Jastrow term  $f_2(r)$  (2.37) in a gas with the soft sphere interaction potential (1.52). At the larger distances  $f_2(r)$  should saturate to a constant in a smooth way. We choose an exponential type of decay:

$$f_2(r) = \begin{cases} \frac{A \sinh(\mathcal{K}r)}{r}, & r < R \\ \frac{B \sin(kr + \delta)}{r}, & R \leq r < R_m \\ 1 - C \exp\left(-\frac{r}{\alpha}\right), & R_m \leq \frac{L}{2} \end{cases} \quad (2.73)$$

The description of a continuous matching at the point  $R$  is described in Sec. 1.3.2.3. Now we shall discuss the matching procedure at the point  $R_m$ . As usual we have three matching conditions:

1. Continuity of the function  $f_2(r)$ :

$$f(R_m) = \frac{B \sin(kR_m + \delta)}{R_m} = 1 - C \exp\left(-\frac{R_m}{\alpha}\right) \quad (2.74)$$

2. Continuity of the logarithmic derivative  $f_2'(r)/f_2(r)$  which fixes the value of the parameter  $C$ :

$$C = \exp(R_m/\alpha) \frac{k \cotan(kR_m + \delta) - 1/R_m}{k \cotan(kR_m + \delta) - 1/R_m + 1/\alpha} \quad (2.75)$$

Substitution of (2.75) into (2.74) fixes value of  $B$

$$B = \frac{R_m/\alpha}{\sin(kR_m + \delta)} \frac{1}{k \cotan(kR_m + \delta) - 1/R_m + 1/\alpha} \quad (2.76)$$

3. The kinetic energy must be continuous at  $r = R_m$ . This condition yields

$$-\left(\frac{f''(R_m)}{f(R_m)} + \frac{2}{R_m} \frac{f'(R_m)}{f(R_m)}\right) = k^2 \quad (2.77)$$

After some mathematics the following procedure is obtained:

1. By choosing the value of the scattering length  $a_{3D}$  and the range of the potential  $R$  define the value of  $\varkappa$  (*i.e.* height of the potential  $V_0$  as related by (1.54)) by solving the transcendental equation (1.59)
2. Introduce  $x = kR_m$ ,  $y = R_m/\alpha$  and  $\bar{\delta} = \delta/x$ . Both equations (1.57) and

$$1 + \bar{\delta} = \frac{1}{x} \arctan\left(\frac{x(y-2)}{x^2 + y - 2}\right) \quad (2.78)$$

has to be satisfied in order to loop to determine  $x = kR_m$  and  $\delta$ . This can be done using iterative procedure:

- (a) Choose the value for the  $\bar{\delta}_a^{(i)}$  (the first time it is initialized with  $\bar{\delta}_a^{(0)} = -a/R_m$ ) and obtain the value of  $x^{(i)}$  as the solution of Eq. 2.78
- (b) Fix the scattering momentum  $k^{(i)} = x^{(i)}/R_m$  and obtain the phase  $\delta_b^{(i)}$  as a solution of (1.57)
- (c) Iterate  $(\bar{\delta}_a^{(i+1)} = (\delta_a^{(i)} + \delta_b^{(i)})/2$  until both numbers converge to the same value by repeating steps (a-c)

3. Then the the constants (A,B,C) are given by formulae

- (a)  $C = \exp(y)x^2/(x^2 + y^2 - 2y)$
- (b)  $B = R_m/\sin(x + \delta)$
- (c)  $A = B \sin(kR_m + \delta)/\sinh(kR_m)$

Once all parameters are fixed, the two-body term  $f_2(r)$  is given by (2.73), the drift force contribution (2.39) is given by

$$\mathcal{F}_2(r) = \begin{cases} \sqrt{V - \mathcal{E}} \frac{\text{cotanh}(\sqrt{V - \mathcal{E}} r)}{r} - \frac{1}{r}, & |r| \leq R \\ \sqrt{\mathcal{E}} \cotan(\sqrt{\mathcal{E}} r + \delta) - \frac{1}{r}, & R \leq |r| \leq R_m \\ \frac{C}{\alpha} \left( \exp\left(\frac{r}{\alpha} - C\right) \right)^{-1}, & |r| > R_m \end{cases} \quad (2.79)$$

Local energy (2.40) equals to

$$\mathcal{E}_2(r) = \begin{cases} \mathcal{E} + (V - \mathcal{E}) \left( \frac{\text{cotanh}(\sqrt{V - \mathcal{E}} r)}{r} \right)^2, & |r| < R \\ \mathcal{E}(1 + \cotan^2(\sqrt{\mathcal{E}} r + \delta)), & R \leq |r| \leq R_m \\ \frac{C}{\alpha} \left[ \frac{1}{\alpha} \left( 1 + \frac{C}{\exp(r/\alpha) - C} \right) - \frac{2}{r} \right] \frac{1}{\exp(r/\alpha) - C}, & |r| > R_m \end{cases} \quad (2.80)$$

### 2.5.5.3 Trial wave function of 3D zero range potential

We construct a wave function for a zero range potential in a three-dimensional case. The correct scattering length  $a$  is imposed on the trial wave function  $f(r)$  by corresponding boundary condition at zero distance.

$$\left. \frac{(rf(r))'}{rf(r)} \right|_{r=0} = -\frac{1}{a} \quad (2.81)$$

We choose the trial wave function in the form

$$f(r) = \frac{A}{r} \sin(kr + B) \quad (2.82)$$

for  $r < R$  and  $f(r) = 1$  otherwise.

The boundary condition at zero gives the constraint:

$$\tan B = -ka \quad (2.83)$$

We impose continuity of the derivative at the matching distance which gives us another condition on the parameters of the trial wave function

$$\tan(kR + B) = kR \quad (2.84)$$

The constant  $B$  can be easily eliminated providing an equation which fixes the momentum  $k$ :

$$\frac{\tan(kR - \arctan kR)}{kR} = \frac{a}{R} \quad (2.85)$$

Once it is solved, the equation (2.83) fixes the value of the  $B$ . Finally the value of  $A$  is fixed by continuity of the wave function itself

$$A = \frac{L/2}{\sin(kL/2 + B)} \quad (2.86)$$

The drift force is given by

$$\mathcal{F}_2(r) = k \cotan(kr + B) - \frac{1}{r} \quad (2.87)$$

The Bijl-Jastrow contribution to the 3D local energy depends on the distance  $r$  as

$$\mathcal{E}_2(r) = k^2 + \left( k \cotan(kr + B) - \frac{1}{r} \right)^2 \quad (2.88)$$

#### 2.5.5.4 Scattering on the resonance state of a Bose gas

To describe the lowest-lying gas-like state of the Hamiltonian (4.18), we use for the one-body Bijl-Jastrow term an *ansatz* similar to (2.41):

$$f_1(\vec{r}) = \exp \left\{ -\frac{x^2 + y^2}{2\alpha_\rho^2} - \frac{z^2}{2\alpha_z^2} \right\} \quad (2.89)$$

Here,  $\alpha_z$  and  $\alpha_\rho$  determine the Gaussian width of  $\psi_T$  in the longitudinal and transverse direction, respectively. These variational parameters  $\alpha_z$  and  $\alpha_\rho$  are optimized in the course of the VMC calculation by minimizing the energy expectation value. The two-body correlation factor  $f_2(r)$  (2.37) is chosen to reproduce closely the scattering behavior of two bosons at low energies. For the hard-sphere potential (1.48), we take

$$f_2(\vec{r}) = \begin{cases} 0, & |\vec{r}| \leq a_{3D} \\ 1 - a_{3D}/|\vec{r}|, & |\vec{r}| > a_{3D} \end{cases} \quad (2.90)$$

The constraint  $f_2 = 0$  for  $r \leq a_{3D}$  accounts for the boundary condition imposed by the hard-sphere potential, it is exact even for the many-body system. For the short-range potential (1.97), we use instead

$$f_2(\vec{r}) = \begin{cases} 0, & \frac{x^2 + y^2}{a^2} + \frac{z^2}{b^2} \leq 1 \\ 1 - 1/\sqrt{\frac{x^2 + y^2}{a^2} + \frac{z^2}{b^2}}, & \frac{x^2 + y^2}{a^2} + \frac{z^2}{b^2} > 1 \end{cases} \quad (2.91)$$

where  $a$  and  $b$  denote the lengths of the semi-axes of an ellipse. For two particles under highly-elongated confinement, the nodal surface is to a good approximation elliptically shaped as will be

discussed in Sec. 4.4.1. Thus, the parameters  $a$  and  $b$  are determined by fitting the elliptical surface to the nodal surface obtained by solving the Schrödinger equation for  $N = 2$ , Eqs. 4.7 and 4.8, by performing a B-spline basis set calculation. In contrast to  $V^{HS}$ , the constraint  $f_2 = 0$  in Eq. 2.91 parameterizes the many-body nodal surface for  $V^{SR}$  only approximately. We expect that our parameterization leads to an accurate description of quasi-1D Bose gases if the average distance between particles is much larger than the semi-axes of the ellipse. The trial wave functions discussed here in the context of our VMC calculations also enter our FN-DMC calculations.

## 2.6 Construction of trial wave functions: system of Fermions

### 2.6.1 Trial wave function in the BCS limit

In the construction of the trial function the antisymmetrization is included through the Slater determinant  $\mathcal{D}(\mathbf{R})$

$$\psi_T(\mathbf{R}) = \mathcal{D}(\mathbf{R}) \prod_{i=1}^N f_1(\vec{r}_i) \prod_{j < k}^N f_2(|\vec{r}_j - \vec{r}_k|) \quad (2.92)$$

Thus at the variational trial move one has to calculate the ratio of two determinants in addition to usual one- and two- body correlation terms present in the bosonic VMC algorithm (compare with (2.37) and see Sec. 2.2). An element of the Slater matrix is given by  $\mathcal{D}_{i\alpha} = \varphi_\alpha(\vec{r}_i)$ , where  $\varphi_\alpha(\vec{r})$  is a single particle orbital. In further latin indices will always refer to particle number and the greek indices to orbital number. During a trial move in which position of only one particle get changed, just one row of the Slater matrix changes. This means that instead of a direct calculation of the Slater determinant a more efficient method can be used. Before doing the trial move one should calculate the inverse matrix  $\overline{\mathcal{D}}$  such that  $\mathcal{D}\overline{\mathcal{D}} = I$  or in terms of the matrix elements

$$\sum_{\alpha=1}^N \mathcal{D}_{i\alpha} \overline{\mathcal{D}}_{j\alpha} = \delta_{ij} \quad (2.93)$$

If we denote the matrix with coordinate of the  $i^{th}$  particle changed as  $\mathcal{D}'$  then the ratio of interest becomes

$$\frac{|\mathcal{D}'|^2}{|\mathcal{D}|^2} = \frac{|\mathcal{D}\overline{\mathcal{D}}\mathcal{D}'|^2}{|\mathcal{D}|^2} = \frac{|\mathcal{D}|^2 |\overline{\mathcal{D}}\mathcal{D}'|^2}{|\mathcal{D}|^2} = |\mathcal{D}'\overline{\mathcal{D}}|^2 \quad (2.94)$$

The matrix  $\mathcal{D}'\overline{\mathcal{D}}$  is almost diagonal. Indeed, only  $i^{th}$  row is different from the one of a unitary matrix. It means that the determinant of such a matrix equals to the  $i^{th}$  element of this row, *i.e.*

$$q = \frac{|\mathcal{D}'|}{|\mathcal{D}|} = \sum_{\alpha=1}^N \varphi_\alpha(\vec{r}'_i) \overline{\mathcal{D}}_{i\alpha} \quad (2.95)$$

After the move is accepted the inverse matrix must be updated. There is a fast way of doing it. Instead of direct inversion of the determinant matrix one can use  $q$  from eq.(2.95):

$$\overline{\mathcal{D}}_{j\alpha} = \begin{cases} \overline{\mathcal{D}}_{j\alpha}/q, & j = i \\ \overline{\mathcal{D}}_{j\alpha} - \overline{\mathcal{D}}_{i\alpha} \sum_{\beta=1}^N \frac{\varphi_\beta(\vec{r}'_i) \overline{\mathcal{D}}_{j\beta}}{q}, & j \neq i \end{cases} \quad (2.96)$$

Differentiating the trial wave function (2.92) one finds the expression for the kinetic energy. It is equal to

$$T^{loc}(\mathbf{R}) = \frac{\hbar^2}{2m} \left\{ \sum_{i=1}^N \mathcal{E}_D^i + 2 \sum_{j<k}^N \mathcal{E}_2^{loc}(|\vec{r}_j - \vec{r}_k|) - \sum_{i=1}^N |\vec{F}_i(\mathbf{R})|^2 \right\}, \quad (2.97)$$

where the two-body contribution to the local energy is the same as in the bosonic case

$$\mathcal{E}_2^{loc}(r) = -\frac{f_2''(r)}{f_2(r)} - \frac{(D-1)f_2'(r)}{r f_2(r)} + \left( \frac{f_2'(r)}{f_2(r)} \right)^2 \quad (2.98)$$

and there is an additional term coming from the determinant part of the trial wave function.

$$\mathcal{E}_D^i(\vec{r}) = -\frac{\Delta_i \mathcal{D}(\mathbf{R})}{\mathcal{D}(\mathbf{R})} + \left( \frac{\nabla_i \mathcal{D}(\mathbf{R})}{\mathcal{D}(\mathbf{R})} \right)^2 \quad (2.99)$$

The drift force (2.15) appearing in (2.97) is given by

$$\vec{F}_i(\mathbf{R}) = \frac{\nabla_i \mathcal{D}(\mathbf{R})}{\mathcal{D}(\mathbf{R})} \frac{\vec{r}_i}{r_i} + \sum_{k \neq i}^N \frac{f_2'(|\vec{r}_i - \vec{r}_k|)}{f_2(|\vec{r}_i - \vec{r}_k|)} \frac{\vec{r}_i - \vec{r}_k}{|\vec{r}_i - \vec{r}_k|} \quad (2.100)$$

The derivatives of the determinant are related to the derivatives of the orbitals in an easy way (see formula (2.95))

$$\frac{\nabla_i \mathcal{D}(\mathbf{R})}{\mathcal{D}(\mathbf{R})} = \sum_{\alpha=1}^N \bar{D}_{i\alpha} \nabla_i \varphi_\alpha(\vec{r}_i) \quad (2.101)$$

## 2.6.2 Kinetic energy

We always use coordinate representation for the wave functions in our calculations, thus the calculation of the potential energy, which is diagonal in this representation, is trivial. Instead calculation of the kinetic energy demands knowledge of wave function derivatives. Let us calculate the first and second derivatives of the fermion wave function:

$$\vec{\nabla}_{\vec{r}_i} \Psi(\mathbf{R}) = \Psi(\mathbf{R}) \left( \frac{\vec{\nabla}_{\vec{r}_i} \mathcal{D}(\mathbf{R})}{\mathcal{D}(\mathbf{R})} + \sum_j \frac{\vec{\nabla}_{\vec{r}_i} f_2(|\vec{r}_i - \vec{r}_j|)}{f_2(|\vec{r}_i - \vec{r}_j|)} \right) \quad (2.102)$$

$$\Delta_{\vec{r}_i} \Psi(\mathbf{R}) = \Psi(\mathbf{R}) \left( \left[ \frac{\vec{\nabla}_{\vec{r}_i} \mathcal{D}(\mathbf{R})}{\mathcal{D}(\mathbf{R})} + \sum_j \frac{\vec{\nabla}_{\vec{r}_i} f_2(|\vec{r}_i - \vec{r}_j|)}{f_2(|\vec{r}_i - \vec{r}_j|)} \right]^2 + \mathcal{E}_i^{loc} + \mathcal{D}_i^{loc} \right) \quad (2.103)$$

The local energy is defined as

$$\mathcal{E}_i^{loc} = \sum_j \left[ \frac{\Delta_{\vec{r}_i} f_2(|\vec{r}_i - \vec{r}_j|)}{f_2(|\vec{r}_i - \vec{r}_j|)} - \left( \frac{\vec{\nabla}_{\vec{r}_i} f_2(|\vec{r}_i - \vec{r}_j|)}{f_2(|\vec{r}_i - \vec{r}_j|)} \right)^2 \right] \quad (2.104)$$

$$\mathcal{D}_i^{loc} = \frac{\Delta_{\vec{r}_i} \mathcal{D}(\mathbf{R})}{\mathcal{D}(\mathbf{R})} - \left( \frac{\vec{\nabla}_{\vec{r}_i} \mathcal{D}(\mathbf{R})}{\mathcal{D}(\mathbf{R})} \right)^2 \quad (2.105)$$

The second derivative of the determinant is calculated explicitly, while the second derivative of the two-body Jastrow term is calculated by assuming spherical symmetry:

$$\Delta_{\vec{r}_i} \mathcal{D}(\mathbf{R}) = \left( \frac{\partial^2}{\partial x_i^2} + \frac{\partial^2}{\partial y_i^2} + \frac{\partial^2}{\partial z_i^2} \right) \mathcal{D}(\mathbf{R}) \quad (2.106)$$

$$\Delta f_2(r) = f_2''(r) + \frac{2}{r} f_2'(r) \quad (2.107)$$

### 2.6.3 Calculation of the tail energy

A simulation of a homogeneous system is done by considering a finite box of size  $L$ . One restricts interaction between the particles to a distance of  $L/2$ . Larger distances should be avoided in order not to have a double counting of a same particle which would leave to artificial correlation. Thus one introduces a cut-off at  $L/2$  and a proper calculation of the energy is necessary.

The situation is different for a Bijl-Jastrow construction of the wave function and a Slater determinant. We will consider a generalization of the wave function containing a product of both terms. The energy per particle in the thermodynamic limit  $N \rightarrow \infty$  is given by the integral of the interaction energy from the cut-off length  $L/2$  to infinity.

$$E_{pot}^{tail} = \sum_i \sum_{j < i, |\vec{r}_i - \vec{r}_j| > L/2} V(|\vec{r}_i - \vec{r}_j|) \rightarrow n \int_{L/2}^{\infty} V(r) d^3r \quad (2.108)$$

In the thermodynamic limit  $N \rightarrow \infty$  the Jastrow force becomes zero as the summation on  $j$  is approximated by a symmetric uniform distribution of particles outside a sphere of  $L/2$  radius. So, the tail of a kinetic energy for a Jastrow wave function is

$$E_J^{tail} = \frac{\hbar^2 n}{m} \int_{L/2}^{\infty} \mathcal{E}^{loc}(r) d^3r = \frac{\hbar^2 n}{m} \int_{L/2}^{\infty} \left[ -\frac{f''(r)}{f(r)} - \frac{2}{r} \frac{f'(r)}{f(r)} + \left( \frac{f'(r)}{f(r)} \right)^2 \right] d^3r \quad (2.109)$$

On the opposite, there is no similar cancellation due to the symmetry in the Slater term, but instead due to linearity the square of the first derivative is exactly cancelled by the force squared term, thus

$$E_{Det}^{tail} = \frac{\hbar^2 n}{m} \int_{L/2}^{\infty} \left[ -\frac{g''(r)}{g(r)} - \frac{2}{r} \frac{g'(r)}{g(r)} \right] d^3r \quad (2.110)$$

### 2.6.4 Bijl-Jastrow term (square well trial wave function)

Now let us specify the Bijl-Jastrow term which will take care of the interactions between spin up and spin down particles. We consider an attractive interaction potential which supports a bound state. Thus we can describe resonant scattering with very large scattering lengths  $a_{3D}$ . It also means that for the unit of length it is preferable to take instead the range of potential  $R$  instead of  $a_{3D}$  which can be even diverging (the unitary regime).

We consider scattering on the square well (SW) potential (1.89). The scattering problem was studied in Sec. 1.3.5.1. Here we only summarize the construction of the Bijl-Jastrow term:

1) the equation for the scattering momentum is

$$\frac{1}{k} \left[ \arctan \frac{kL}{2} - \arctan \left( \frac{k}{\sqrt{\varkappa^2 + k^2}} \tan \sqrt{\varkappa^2 + k^2} R \right) \right] = \frac{L}{2} - R \quad (2.111)$$

2) the shift phase  $\delta$  is defined as

$$\delta = \arctan \left( \frac{kL}{2} \right) - \frac{kL}{2} \quad (2.112)$$

3) normalization factor  $B$

$$B = \frac{L/2}{\sin(kL/2 + \delta)} \quad (2.113)$$

4) normalization factor  $A$

$$A = B \frac{\sin(kR + \delta)}{\sin(\sqrt{\varkappa^2 + k^2} R)} \quad (2.114)$$

The Bijl-Jastrow contribution to the force and the local energy are given by following expressions:

$$\frac{f'(r)}{f(r)} = \begin{cases} \mathcal{K} \cotan(\mathcal{K}r) - \frac{1}{r}, & r < R \\ k \cotan(kr + \delta) - \frac{1}{r}, & r \geq R \end{cases} \quad (2.115)$$

$$E_{loc}^{3D} = \begin{cases} \mathcal{K}^2 - (\mathcal{K} \cotan(\mathcal{K}r) - \frac{1}{r})^2, & r < R \\ k^2 - (k \cotan(kr + \delta) - \frac{1}{r})^2, & r \geq R \end{cases} \quad (2.116)$$

### 2.6.5 Trial wave function: zero energy scattering state

On the BCS side of the resonance the scattering length is negative  $a < 0$ . Here the attractive square well potential well of strength  $V_0 = \hbar^2 \varkappa^2 / m$ . There is no bound state anymore and instead one has a solution with positive energy  $\mathcal{E} = \hbar^2 k^2 / m$ . The scattering solution is

$$f(r) = \begin{cases} \frac{A}{r} \sin \mathcal{K}r, & r < R \\ \frac{B}{r} \sin(kr + \delta), & r > R \end{cases} \quad (2.117)$$

The scattering length  $a$  phase is related to the phase of the scatters wave. In the low-energy limit the phase is simply  $\delta = -ka$ . In this limit  $\mathcal{K}\varkappa$  and we have simple solution

$$f(r) = \begin{cases} \frac{A}{r} \sin kr, & r < R \\ B(1 + \frac{|a|}{r}), & r > R \end{cases} \quad (2.118)$$

$$f'(r) = \begin{cases} \frac{A}{r} \sin kr \left( \varkappa \operatorname{ctg} - \frac{1}{r} \right), & r < R \\ -\frac{B|a|}{r^2}, & r > R \end{cases} \quad (2.119)$$



### 2.6.5.1 Matching to a constant

The wave function constructed in the previous section is long-ranged as it decays only as  $1/r$  at large distances. This leads to overestimation of the correlations in deep BCS limit. For example at  $a = -5R$  the variational energy is 8 times larger than the energy of a fermi gas. The fixed-node MC algorithm corrects this behavior and the resulting energy is close to the energy of a fermi gas.

$$f(r) = \begin{cases} \frac{A}{r} \sin \varkappa r, & r < R \\ B(1 + \frac{|a|}{r}), & R < r < R_m \\ 1 + C \exp(-k_m r), & R_m < r \end{cases} \quad (2.120)$$

The matching conditions fix values of the constants  $A, B, C$ :

$$\begin{cases} A = \frac{BR(1+|a|/R)}{\sin \varkappa R} \\ B = \left(1 + \frac{|a|}{R_m} \left(1 - \frac{1}{R_m k_m}\right)\right)^{-1} \\ C = \frac{B|a| \exp(k_m R_m)}{R_m^2 k_m} \end{cases} \quad (2.121)$$

## 2.7 Measured quantities

### 2.7.1 Local energy

The most general form of a Hamiltonian of a system of  $N$  interacting bosons in an external field is (2.10):

$$\hat{H} = -\frac{\hbar^2}{2m} \sum_{i=1}^N \Delta_{\vec{r}_i} + \sum_{i=1}^N V_{ext}(\vec{r}_i) + \sum_{j < k}^N V_{int}(|\vec{r}_j - \vec{r}_k|), \quad (2.122)$$

where  $m$  is mass of a particle,  $V_{ext}(\vec{r})$  is the external field,  $V_{int}(|\vec{r}|)$  is particle-particle interaction potential. Given the many-body wave function  $\Psi(\vec{r}_1, \dots, \vec{r}_N)$  the local energy is defined according to (2.14):

$$E^{loc}(\vec{r}_1, \dots, \vec{r}_N) = \frac{\hat{H}\Psi(\vec{r}_1, \dots, \vec{r}_N)}{\Psi(\vec{r}_1, \dots, \vec{r}_N)} \quad (2.123)$$

Operator of the external field and particle-particle interaction are diagonal in this representation and are calculated trivially as a summation over particles and pairs of the second and third terms of (2.122). Calculation of the kinetic energy, first term of (2.122) is more tricky, as the Laplacian operator is not diagonal.

#### 2.7.1.1 Local kinetic energy and the drift force

In this section we will find the expression of the local kinetic energy

$$T^{loc}(\vec{r}_1, \dots, \vec{r}_N) = -\frac{\hbar^2}{2m} \frac{\Delta\Psi(\vec{r}_1, \dots, \vec{r}_N)}{\Psi(\vec{r}_1, \dots, \vec{r}_N)} \quad (2.124)$$

Let us calculate the second derivative in two steps, as the first derivative is important for the calculation of the drift force. We consider the Bijl-Jastrow form (2.37) of the trial wave function

and will express the final results in terms of one- and two- body Bijl-Jastrow terms  $f_1$  and  $f_2$ . The gradient of the many-body trial wave function is given by

$$\vec{\nabla}_{\vec{r}_i} \Psi(\vec{r}_1, \dots, \vec{r}_N) = \Psi(\vec{r}_1, \dots, \vec{r}_N) \left( \frac{f_1'(\vec{r}_i) \vec{r}_i}{f_1(\vec{r}_i) r_i} + \sum_{k \neq i}^N \frac{f_2'(|\vec{r}_i - \vec{r}_k|) \vec{r}_i - \vec{r}_k}{f_2(|\vec{r}_i - \vec{r}_k|) |\vec{r}_i - \vec{r}_k|} \right) \quad (2.125)$$

The full expression for the Laplacian is

$$\begin{aligned} \Delta_{\vec{r}_i} \Psi(\vec{r}_1, \dots, \vec{r}_N) &= \Psi(\vec{r}_1, \dots, \vec{r}_N) \left( \frac{f_1'(\vec{r}_i) \vec{r}_i}{f_1(\vec{r}_i) r_i} + \sum_{k \neq i}^N \frac{f_2'(|\vec{r}_i - \vec{r}_k|) \vec{r}_i - \vec{r}_k}{f_2(|\vec{r}_i - \vec{r}_k|) |\vec{r}_i - \vec{r}_k|} \right)^2 + \\ &+ \Psi(\vec{r}_1, \dots, \vec{r}_N) \left( \frac{f_1''(\vec{r}_i)}{f_1(\vec{r}_i)} - \left( \frac{f_1'(\vec{r}_i)}{f_1(\vec{r}_i)} \right)^2 + \sum_{k \neq i}^N \left[ \frac{f_2''(|\vec{r}_i - \vec{r}_k|)}{f_2(|\vec{r}_i - \vec{r}_k|)} - \left( \frac{f_2'(|\vec{r}_i - \vec{r}_k|)}{f_2(|\vec{r}_i - \vec{r}_k|)} \right)^2 \right] \right) \end{aligned} \quad (2.126)$$

The kinetic energy can be written in a compact form

$$T^{loc}(\vec{r}_1, \dots, \vec{r}_N) = \frac{\hbar^2}{2m} \left\{ \sum_{i=1}^N \mathcal{E}_1^{loc}(\vec{r}_i) + 2 \sum_{j < k}^N \mathcal{E}_2^{loc}(|\vec{r}_j - \vec{r}_k|) - \sum_{i=1}^N |\vec{F}_i(\vec{r}_1, \dots, \vec{r}_N)|^2 \right\}, \quad (2.127)$$

where we introduced notation for the one- and two- body contribution to the local energy (see, also, (2.40))

$$\mathcal{E}_1^{loc}(\vec{r}) = -\frac{f_1''(\vec{r})}{f_1(\vec{r})} + \left( \frac{f_1'(\vec{r})}{f_1(\vec{r})} \right)^2 \quad (2.128)$$

$$\mathcal{E}_2^{loc}(r) = -\frac{f_2''(r)}{f_2(r)} + \left( \frac{f_2'(r)}{f_2(r)} \right)^2 \quad (2.129)$$

and introduced the drift force (see (2.39))

$$\vec{F}_i(\vec{r}_1, \dots, \vec{r}_N) = \frac{f_1'(\vec{r}_i) \vec{r}_i}{f_1(\vec{r}_i) r_i} + \sum_{k \neq i}^N \frac{f_2'(|\vec{r}_i - \vec{r}_k|) \vec{r}_i - \vec{r}_k}{f_2(|\vec{r}_i - \vec{r}_k|) |\vec{r}_i - \vec{r}_k|} \quad (2.130)$$

### 2.7.1.2 Exponentiation

It is convenient (see Eq.2.38) to do the exponentiation of the one- and two- body terms  $u_1(\vec{r}) = \ln f_1(\vec{r})$ ,  $u_2(r) = \ln f_2(r)$ . The point is that numerically a better precision is achieved by working with numbers of the same order. The formula for the kinetic energy becomes simpler

$$T^{loc}(\vec{r}_1, \dots, \vec{r}_N) = -\frac{\hbar^2}{2m} \left\{ \sum_{i=1}^N u_1''(\vec{r}_i) + 2 \sum_{j < k}^N u_2''(|\vec{r}_j - \vec{r}_k|) + \sum_{i=1}^N |\vec{F}_i(\vec{r}_1, \dots, \vec{r}_N)|^2 \right\} \quad (2.131)$$

with

$$\vec{F}_i(\vec{r}_1, \dots, \vec{r}_N) = u_1'(\vec{r}_i) \frac{\vec{r}_i}{r_i} + \sum_{k \neq i}^N u_2'(|\vec{r}_i - \vec{r}_k|) \frac{\vec{r}_i - \vec{r}_k}{|\vec{r}_i - \vec{r}_k|} \quad (2.132)$$

### 2.7.2 Static structure factor

It is natural to give the definition of the static structure factor  $S(\vec{k})$  in the momentum space as the correlation function of the momentum distribution between elements  $-\vec{k}$  and  $\vec{k}$  (1.29):

$$NS(\vec{k}) = \langle \rho_{-\vec{k}} \rho_{\vec{k}} \rangle - |\langle \rho_{\vec{k}} \rangle|^2, \quad (2.133)$$

Using the properties of the Fourier component  $\rho_{-\vec{k}} = (\rho_{\vec{k}})^*$  it can be rewritten in a different way

$$NS(\vec{k}) = \langle |\rho_{\vec{k}}|^2 \rangle - |\langle \rho_{\vec{k}} \rangle|^2 \quad (2.134)$$

In the Diffusion Monte Carlo calculation the density distribution is approximated by the density of walkers (see (2.31))

$$n(\vec{r}) = \sum_{i=1}^N \delta(\vec{r} - \vec{r}_i) \quad (2.135)$$

With the means of the Fourier transform we express it in the momentum space

$$\rho_{\vec{k}} = \int e^{i\vec{k}\vec{r}} n(\vec{r}) d\vec{r} = \sum_{i=1}^N e^{i\vec{k}\vec{r}_i} = \sum_{i=1}^N \cos \vec{k}\vec{r}_i + i \sum_{i=1}^N \sin \vec{k}\vec{r}_i \quad (2.136)$$

and obtain a simple expression for the static structure factor

$$NS(\vec{k}) = \left\langle \left( \sum_{i=1}^N \cos \vec{k}\vec{r}_i \right)^2 + \left( \sum_{i=1}^N \sin \vec{k}\vec{r}_i \right)^2 \right\rangle - \left| \left\langle \sum_{i=1}^N \cos \vec{k}\vec{r}_i \right\rangle \right|^2 - \left| \left\langle \sum_{i=1}^N \sin \vec{k}\vec{r}_i \right\rangle \right|^2 \quad (2.137)$$

In a trapped system there are no restrictions on the value of momentum  $\vec{k}$ , although, naturally, the momentum distribution vanishes for  $k \ll 1/R$ , where  $R$  is the size of the system. Instead, if periodic boundary conditions are used, the value of momenta is quantized and is dependent on the size of the box

$$k_{n_{x,y,z}} = \frac{2\pi}{L} n_{x,y,z} \quad (2.138)$$

At the same in a homogeneous system the two last terms in (2.137) are vanishing.

### 2.7.3 One body density matrix in a homogeneous system

The one body density matrix (OBDM)  $g_1$  of a homogeneous system described by the many body wave function  $\psi(\vec{r}_1, \dots, \vec{r}_N)$  according to (1.18) is equal to

$$g_1(|\vec{r}' - \vec{r}''|) = N \frac{\int \dots \int \psi^*(\vec{r}', \vec{r}_2, \dots, \vec{r}_N) \psi(\vec{r}'', \vec{r}_2, \dots, \vec{r}_N) d\vec{r}_2 \dots d\vec{r}_N}{\int \dots \int |\psi(\vec{r}_1, \dots, \vec{r}_N)|^2 d\vec{r}_1 \dots d\vec{r}_N} \quad (2.139)$$

Since in DMC calculation does not sample directly the ground-state probability distribution  $\phi_0^2$ , but instead the mixed probability  $\psi_T \phi_0$  (2.12) one obtains the *mixed* one-body density matrix as the output

$$g_1^{mixed}(\vec{r}) = N \frac{\int \dots \int \psi_T^*(\vec{r}_1 + \vec{r}, \vec{r}_2, \dots, \vec{r}_N) \phi_0(\vec{r}_1, \vec{r}_2, \dots, \vec{r}_N) d\vec{r}_2 \dots d\vec{r}_N}{\int \dots \int \psi_T^*(\vec{r}_1, \dots, \vec{r}_N) \phi_0(\vec{r}_1, \dots, \vec{r}_N) d\vec{r}_1 \dots d\vec{r}_N}, \quad (2.140)$$

This formula can be rewritten in a way convenient for the Monte Carlo sampling:

$$g_1^{mixed}(r) = n \frac{\int \dots \int [\psi_T^*(\vec{r}_1 + \vec{r}, \vec{r}_2, \dots, \vec{r}_N) (\psi_T^*(\vec{r}_1, \vec{r}_2, \dots, \vec{r}_N))^{-1}] f(\vec{r}_1, \dots, \vec{r}_N) d\vec{r}_1 \dots d\vec{r}_N}{\int \dots \int f(\vec{r}_1, \dots, \vec{r}_N) d\vec{r}_1 \dots d\vec{r}_N}, \quad (2.141)$$

where we have used the asymptotic formula (2.19) and have taken into account that in a homogeneous system  $g_2$  depends only on the module of the relative distance between two particles. If the trial wave function is chosen as a product of pair functions (2.37) then using the notation (2.38)  $u(|\vec{r}_i - \vec{r}_j|) = \ln f_2(|\vec{r}_i - \vec{r}_j|)$  and  $f_1 \equiv 0$  one has  $\psi_T(\vec{r}_1, \dots, \vec{r}_N) = \prod_{i < j} \exp\{u(|\vec{r}_i - \vec{r}_j|)\}$ . Then the ratio of the trial wave function appearing in (2.141) becomes

$$\frac{\psi_T(\vec{r}_1 + \vec{r}, \dots, \vec{r}_N)}{\psi_T(\vec{r}_1, \dots, \vec{r}_N)} = \exp \left\{ \sum_{j>1} \mu(|\vec{r}_1 + \vec{r} - \vec{r}_j|) - \mu(|\vec{r}_1 - \vec{r}_j|) \right\} \quad (2.142)$$

In order to gain better statistics it is convenient to average over all possible pairs of particles

$$g_1^{mixed}(r) = \frac{1}{N} \sum_{i=1}^N \frac{\psi_T(\vec{r}_1, \dots, \vec{r}_i + \vec{r}, \dots, \vec{r}_N)}{\psi_T(\vec{r}_1, \dots, \vec{r}_N)} = \frac{1}{N} \sum_{i=1}^N \exp \left\{ \sum_{j \neq i} u(|\vec{r}_i + \vec{r} - \vec{r}_j|) - u(|\vec{r}_i - \vec{r}_j|) \right\} \quad (2.143)$$

The asymptotic limit of the OBDM gives the condensate density

$$\lim_{r \rightarrow \infty} g_1(r) = \frac{N_0}{V} \quad (2.144)$$

and the condensate fraction is obtained by the calculating the asymptotic ratio

$$\lim_{r \rightarrow \infty} \frac{g_1(r)}{n} = \frac{N_0}{N} \quad (2.145)$$

### 2.7.4 One body density matrix in a harmonic trap

While in a homogeneous system the OBDM depends only on the relative distance, for a system in external potential it is no longer true (1.32). Instead one define the OBDM in a convenient way by integrating out the center of the mass motion.

$$\bar{g}_1(\vec{r}) = \int g_1 \left( \vec{R} + \frac{\vec{r}}{2}, \vec{R} - \frac{\vec{r}}{2} \right) d\vec{R}, \quad (2.146)$$

Here the standard notation for the center of the mass variables is used  $\vec{R} = (\vec{r}_1 + \vec{r}_2)/2$ ,  $\vec{r} = \vec{r}_1 - \vec{r}_2$ . The point in the definition (2.146) is that the momentum distribution can be obtained by the Fourier transform with respect to  $\vec{r}$

$$n(\vec{k}) = \int \bar{g}_1(\vec{r}) e^{i\vec{k}\vec{r}} d\vec{r} \quad (2.147)$$

For practical purposes it is convenient to change the notation

$$\begin{cases} \vec{R} &= \vec{r}_1 \\ \vec{r} &= \vec{r}_1 - \vec{r}_2 \end{cases} \quad (2.148)$$

Using this notation the mixed OBDM becomes

$$g_1^{mixed}(\vec{R}, \vec{r}) = N \frac{\int \dots \int \psi_T^*(\vec{R} + \vec{r}, \vec{r}_2, \dots, \vec{r}_N) \phi_0(\vec{R}, \vec{r}_2, \dots, \vec{r}_N) d\vec{r}_2 \dots d\vec{r}_N}{\int \dots \int \psi_T^*(\vec{r}_1, \dots, \vec{r}_N) \phi_0(\vec{r}_1, \dots, \vec{r}_N) d\vec{r}_1 \dots d\vec{r}_N}, \quad (2.149)$$

which reminds us the expression for the OBDM of a homogeneous system (1.18).

The function  $\bar{g}_1$  can be measured in the QMC simulation

$$\bar{g}_1^{mixed}(\vec{r}) = \frac{\int \dots \int [\psi_T^*(\vec{R} + \vec{r}, \vec{r}_2, \dots, \vec{r}_N) (\psi_T^*(\vec{R}, \vec{r}_2, \dots, \vec{r}_N))^{-1}] f(\vec{R}, \vec{r}_2, \dots, \vec{r}_N) d\vec{R} d\vec{r}_2 \dots d\vec{r}_N}{\int \dots \int f(\vec{r}_1, \dots, \vec{r}_N) d\vec{r}_1 \dots d\vec{r}_N}, \quad (2.150)$$

by taking an average of the following quantity

$$\frac{\psi_T(\vec{R} + \vec{r}, \dots, \vec{r}_N)}{\psi_T(\vec{R}, \dots, \vec{r}_N)} = \exp \left\{ u_1(\vec{R} + \vec{r}) - u_1(\vec{R}) + \sum_{j>1} u_2(|\vec{r}_1 + \vec{r} - \vec{r}_j|) - u_2(|\vec{r}_1 - \vec{r}_j|) \right\}, \quad (2.151)$$

where  $u_1(\vec{r})$  stands for the one-body exponent in the Jastrow-Bijl wave function (see Eq. 2.38), which for harmonic confinement is taken to be equal to (2.41).

### 2.7.5 Pair distribution

The pair distribution function (TBDM) in a homogeneous system is given by the formula (1.19)

$$g_2(|\vec{r}_2 - \vec{r}_1|) = \frac{N(N-1)}{n^2} \frac{\int |\psi(\mathbf{R})|^2 d\vec{r}_3 \dots d\vec{r}_N}{\int |\psi(\mathbf{R})|^2 d\mathbf{R}} \quad (2.152)$$

Let us explain now how this formula is implemented in Monte Carlo calculation. We make summation over all pairs of particles:

$$g_2(r) = \frac{N(N-1)}{n^2 L} \frac{\int \delta(\vec{r}_1 - \vec{r}_2 - \vec{r}) |\psi(\mathbf{R})|^2 d\mathbf{R}}{\int |\psi(\mathbf{R})|^2 d\mathbf{R}} = \frac{2}{nN} \frac{\int \sum_{i<j} \delta(r_{ij} - r) |\psi(\mathbf{R})|^2 d\mathbf{R}}{\int |\psi(\mathbf{R})|^2 d\mathbf{R}} \quad (2.153)$$

If we do a discretization of the coordinate with spacing  $h$  and introduce function  $\vartheta_h(z)$  which is one if  $z < h$  and zero otherwise, do summation over absolute value (the distribution is obviously symmetric) we obtain following expressions:

1) In one dimensional system:

$$g_2^{1D}(r) = \left\langle \frac{2}{2hnN} \sum_{i<j} \vartheta_h(|r_{ij} - r|) \right\rangle \quad (2.154)$$

In a uncorrelated system  $\vartheta_h(|z|) = 2h/L$  is constant and  $g_2(z) = 1 - 1/N$ .

2) In two-dimensional system distance  $z$  enters explicitly in the expression of the pair distribution function leading to larger numerical variance at small distances

$$g_2^{2D}(z) = \left\langle \frac{2}{2\pi z hnN} \sum_{i<j} \vartheta_h(|z_{ij} - z|) \right\rangle \quad (2.155)$$

3) In a three-dimensional system the corresponding expression is

$$g_2^{3D}(z) = \left\langle \frac{2}{4\pi z^2 hnN} \sum_{i<j} \vartheta_h(|z_{ij} - z|) \right\rangle \quad (2.156)$$

### 2.7.6 Pure estimators and extrapolation technique

As a result of the VMC calculation one obtains a *variational* estimator for a quantity (let it be described by an operator  $\hat{A}$ ), which corresponds to an average over the trial wave function  $\psi_T$ :

$$\langle \hat{A} \rangle_{var.} = \frac{\langle \psi_T | \hat{A} | \psi_T \rangle}{\langle \psi_T | \psi_T \rangle} \quad (2.157)$$

Instead, the DMC method asymptotically provides a more precise *mixed* estimator, which we denote as

$$\langle \hat{A} \rangle_{mix.} = \frac{\langle \phi_0 | \hat{A} | \psi_T \rangle}{\langle \phi_0 | \psi_T \rangle} \quad (2.158)$$

Still, this type of average can differ from the “pure” ground state average, which corresponds to the true quantum-mechanical equilibrium value at a zero temperature

$$\langle \hat{A} \rangle_{pure} = \frac{\langle \phi_0 | \hat{A} | \phi_0 \rangle}{\langle \phi_0 | \phi_0 \rangle} \quad (2.159)$$

The DMC method gives an exact result for the energy, as the mixed average of the local energy  $E_{loc} = \psi_T^{-1} \hat{H} \psi_T$  coincides with the pure estimator. This can be easily seen by noticing that when  $\langle \phi_0$  acts on  $\hat{H}$ , it gives exactly the ground state energy.

We will show that averages of local operators can be calculated in a “pure” way. This means that the pair distribution function, radial distribution, size of the condensate can be found essentially exactly. We assume that  $\langle \mathbf{R} | \hat{A} | \mathbf{R}' \rangle = A(\mathbf{R}) \langle \mathbf{R} | \mathbf{R}' \rangle$ . The “pure” average can be related to the mixed one in the following way

$$\langle \hat{A} \rangle_{pure} = \frac{\langle \phi_0 | A(\mathbf{R}) \frac{\phi_0(\mathbf{R})}{\psi_T(\mathbf{R})} | \psi_T \rangle}{\langle \phi_0 | \frac{\phi_0(\mathbf{R})}{\psi_T(\mathbf{R})} | \psi_T \rangle} = \frac{\langle A(\mathbf{R}) P(\mathbf{R}) \rangle_{mix}}{\langle P(\mathbf{R}) \rangle_{mix}}, \quad (2.160)$$

where  $P(\mathbf{R})$  is defined as

$$P(\mathbf{R}) = \frac{\phi_0(\mathbf{R})}{\psi_T(\mathbf{R})} \langle \phi_0 | \psi_T \rangle \quad (2.161)$$

and gives the number of descendants of a walker  $\mathbf{R}$  for large times  $\tau \rightarrow \infty$ . Practically it is enough to wait a sufficiently large, but a finite time  $T$ . One makes measurements of a local quantity for all of the walkers, but calculates the average after the time  $T$ , so that each walker was replicated according to the weight  $P(\mathbf{R})$ .

One of important examples of a non-local quantity is the non-diagonal element of the one-body density matrix (see (2.141)). This quantity deserves a special attention, so we will explain an extrapolation technique, which can be applied for finding averages of a non-local operators.

Let us denote the difference between the trial wave function and ground-state wave function as  $\delta\psi$

$$\phi_0 = \psi_T + \delta\psi \quad (2.162)$$

Then the ground-state average can be written as

$$\langle \hat{A} \rangle_{pure} = \langle \phi_0 | \hat{A} | \phi_0 \rangle = \langle \psi_T | \hat{A} | \psi_T \rangle + 2 \langle \phi_0 | \hat{A} | \delta\psi \rangle + \langle \delta\psi | \hat{A} | \delta\psi \rangle \quad (2.163)$$

If  $\delta\psi$  is small the second order term  $\langle\delta\psi|\hat{A}|\delta\psi\rangle$  can be neglected. After substitution  $\langle\phi_0|\hat{A}|\delta\psi\rangle = \langle\psi_T|\hat{A}|\phi_0\rangle - \langle\psi_T|\hat{A}|\psi_T\rangle$  the extrapolation formula becomes

$$\langle\hat{A}\rangle_{pure} \approx 2\langle\hat{A}\rangle_{mix.} - \langle\hat{A}\rangle_{var.} \quad (2.164)$$

It is possible to write another extrapolation formula of the same order of accuracy:

$$\langle\hat{A}\rangle_{pure} \approx \frac{\langle\hat{A}\rangle_{mix.}^2}{\langle\hat{A}\rangle_{var.}} \quad (2.165)$$

Of course, if the extrapolation technique is applicable, formulae (2.164) and (2.165) give the same result. The second formula is preferable for extrapolation of a non-negative quantity (*e.g.* the OBDM), if the function can be very close to zero, as (2.165) preserves the sign of the function.

In the end of this Section we will mention that it can be proven that the measurement of the superfluid density in DMC method is a pure estimator and to a large extent is not biased by the chose of a trial wave function [Ast01, AG02].





# Chapter 3

## 3D-1D crossover of a trapped Bose gas

### 3.1 Introduction

The study of trapped Bose systems in low dimensions is currently attracting a lot of interest. In particular, 1D systems are expected to exhibit remarkable properties which are far from the mean-field description and are not present in 2D and 3D. The peculiarity of 1D physics consists in the role played by fluctuations, which destroy long-range order even at zero temperature [Sch77, Hal81], and in the occurrence of characteristic effects due to correlations such as the fermionization of the gas in the Tonks-Girardeau regime [Gir60]. Recent experiments with highly anisotropic, quasi-one-dimensional traps have shown first evidences of 1D features in the aspect ratio and energy of the released cloud [GVL<sup>+</sup>01, SKC<sup>+</sup>01] as well as in the coherence properties of condensates with fluctuating phase [DHR<sup>+</sup>01]. From a theoretical viewpoint, the emergence of 1D effects in the properties of binary atomic collisions, by increasing the confinement in the transverse direction, has been pointed out by Olshanii [Ols98]. In the case of harmonically trapped gases, the occurrence of various regimes possessing true or quasi-condensate and the possibility of entering the Tonks-Girardeau gas regime of impenetrable bosons has been discussed in [PSW00].

The ground-state properties and excitation spectrum of a homogeneous 1D system of bosons interacting through a repulsive contact potential have been calculated exactly by Lieb and Liniger long time ago [LL63, Lie63]. For a fixed interaction strength the Lieb-Liniger equation of state reproduces in the high density regime the mean-field result obtained using the Bogoliubov model and in the opposite limit of low density coincides with the ground-state of impenetrable bosons [Gir60]. For 1D systems in harmonic traps, the exact many-body ground-state wave function in the Tonks-Girardeau regime has been recently calculated [GWT01], and the equation of state interpolating between the mean-field and the Tonks-Girardeau regime has been obtained within the local density approximation in [DLO01]. Methods based on local density approximation in the longitudinal direction and on the Gross-Pitaevskii equation for the transverse direction have been recently employed to predict the frequency of the collective excitations [MS02] and the ground-state energy in the 3D-1D cross-over as well as in the 1D mean field - Tonks-Girardeau gas cross-over [DGW02].

In this chapter we present exact Diffusion Monte-Carlo (see Sec. 2.3) results for the 3D-1D cross-over in harmonically trapped Bose gases. As a function of the anisotropy parameter of the trap we calculate the ground-state properties of the system and for highly anisotropic traps we point out the occurrence of important beyond mean-field effects including the fermionization of the gas.

## 3.2 Theory

### 3.2.1 Model Hamiltonian

In order to describe a cold bosonic gas in a trap we use the model Hamiltonian of type (2.122)

$$\hat{H} = -\frac{\hbar^2}{2m} \sum_{i=1}^N \Delta_i + \sum_{i<j} V_{int}(|\vec{r}_i - \vec{r}_j|) + \sum_{i=1}^N V_{ext}(\vec{r}_i), \quad (3.1)$$

Our system consists of  $N$  spinless bosons of mass  $m$  interacting through the two-body interatomic potential  $V_{int}(r)$  and is subject to the external field which is taken to be harmonic and axially symmetric:

$$V_{ext}(\vec{r}) = m(\omega_{\perp}^2 r_{\perp}^2 + \omega_z^2 z^2)/2, \quad (3.2)$$

where  $z$  is the axial coordinate,  $r_{\perp}$  is the radial transverse coordinate and  $\omega_z, \omega_{\perp}$  are the corresponding oscillator frequencies.

For the interatomic potential we use two different repulsive model potentials: the hard-sphere (HS) potential (1.48) and the soft-sphere (SS) potential (1.52). In the case of the HS potential the  $s$ -wave scattering length coincides with the radius of the sphere and in the case of the SS potential is given by (1.59). For finite  $V_0$  one always has  $R > a_{3D}$ , while for  $V_0 \rightarrow +\infty$  the SS potential coincides with the HS one with  $R = a_{3D}$ . The height  $V_0$  of the potential is fixed by the value of the range  $R$  in units of the scattering length, for which we choose  $R = 5a_{3D}$ . It is worth noticing that the HS and the SS model with  $R = 5a_{3D}$  represent two extreme cases for a repulsive interatomic potential. In the HS case, the energy is entirely kinetic, while for the SS potential  $a \simeq (m/\hbar^2) \int_0^{\infty} V(r)r^2 dr$ , according to Born approximation, and the energy is almost all potential. By comparing the results of the two model potentials we can investigate to what extent the ground-state properties of the system depend only on the  $s$ -wave scattering length and not on the details of the potential.

### 3.2.2 Relevant parameters and DMC approach

The relevant parameters of the problem are the number of particles  $N$ , the ratio  $a_{3D}/a_{\perp}$  of the scattering length to the transverse harmonic oscillator length  $a_{\perp} = \sqrt{\hbar/m\omega_{\perp}}$  and the anisotropy parameter  $\lambda = \omega_z/\omega_{\perp}$ . For a given set of parameters we solve exactly, using the Diffusion Monte-Carlo method (Sec. 2.3), the many-body Schrödinger equation (2.6) for the ground state and we calculate the energy per particle and the mean square radii of the cloud in the axial and radial directions. Importance sampling is used through the Bijl-Jastrow trial wave function (2.37). For the one-body term, which accounts for the external confinement, we use a simple gaussian *ansatz* (2.41)  $f_1(r_{\perp}, z) = \exp\{-\alpha_{\perp} r_{\perp}^2 - \alpha_z z^2\}$ , with  $\alpha_{\perp}$  and  $\alpha_z$  optimized variational parameters. The two-body term  $f_2(r)$  accounts instead for the particle-particle interaction and is chosen using the same technique employed in Ref. [GBC99] for a homogeneous system. Of course, since DMC is an exact method, the precise choice of  $\psi_T(\mathbf{R})$  is to a large extent unimportant and the results obtained are not biased by the choice of the trial wave function<sup>1</sup>.

---

<sup>1</sup>Mean square radii are calculated using the pure estimator technique developed in [CB95]

### 3.2.3 Mean-field approach

The DMC results are compared with the predictions of mean-field theory which are obtained from the stationary Gross-Pitaevskii (GP) equation (1.123)

$$\left( -\frac{\hbar^2}{2m}\Delta + V_{ext}(\vec{r}) + g(N-1)|\Phi(\vec{r})|^2 \right) \Phi(\vec{r}) = \mu\Phi(\vec{r}), \quad (3.3)$$

where  $\Phi(\vec{r})$  is the order parameter normalized to unity:  $\int |\Phi(\vec{r})|^2 d\vec{r} = 1$  and  $g = 4\pi\hbar^2 a_{3D}/m$  is the coupling constant (1.86). Further, finite size effects have been taken into account in the GP equation by the factor  $N-1$  in the interaction term [Esr97] (see, also, 1.113). In the case of anisotropic traps with  $\lambda < 1$ , the GP equation (3.3) is expected to provide a correct description of the system if the transverse confinement is weak  $a_{3D}/a_{\perp} \ll 1$ , and if the mean separation distance between particles is much smaller than the healing length  $1/n_{3D}^{1/3} \ll \xi$ , where  $\xi = 1/\sqrt{8\pi n_{3D} a_{3D}}$  and  $n_{3D}$  is the central density of the cloud. In terms of the linear density along  $z$ ,  $n_{1D}(z) = 2\pi \int_0^{\infty} r_{\perp} n_{3D}(r_{\perp}, z) dr_{\perp}$ , this latter condition reads  $1/n_{1D} \ll a_{\perp}^2/a_{3D}$ . If the mean separation distance between particles in the longitudinal direction becomes much larger than the effective 1D scattering length given by  $a_{\perp}^2/a_{3D}$  [PSW00], the mean-field approximation breaks down because of the lack of off diagonal long range order.

The system enters the 1D regime when the motion in the radial direction becomes frozen. In this regime the radial density profile of the cloud is fixed by the harmonic oscillator ground state, resulting in a mean square radius which coincides with the transverse oscillator length  $\sqrt{\langle r_{\perp}^2 \rangle} = a_{\perp}$ . Further, the energy per particle is dominated by the trapping potential and one has the condition  $E/N - \hbar\omega_{\perp} \ll \hbar\omega_{\perp}$ .

### 3.2.4 1D system: local density approximation

If the discretization of levels in the longitudinal direction can be neglected, *i.e.* if  $E/N - \hbar\omega_{\perp} \gg \hbar\omega_z$ , the 1D system can be described within the local density approximation (LDA). In this case, the chemical potential of the system is calculated through the local equilibrium equation (1.126) which we write separating in an explicit way the dominant contribution of the transverse confinement  $\hbar\omega_{\perp}$ :

$$\mu = \hbar\omega_{\perp} + \mu_{hom}(n_{1D}(z)) + \frac{m}{2}\omega_z^2 z^2, \quad (3.4)$$

Here  $\mu_{hom}(n_{1D})$  is the chemical potential corresponding to a homogeneous 1D system of density  $n_{1D}$ . If the ratio  $a_{3D}/a_{\perp} \ll 1$ , the local chemical potential can be obtained from the Lieb-Liniger (LL) equation (5.1) of state with the effective 1D coupling constant  $g_{1D} = g_{3D}/(2\pi a_{\perp}^2)$  (1.124). One finds:  $\mu_{hom} = \partial[n_{1D}\epsilon_{LL}(n_{1D})]/\partial n_{1D}$ , where  $\epsilon_{LL}$  is the LL energy per particle. The LDA problem in one-dimension was already studied in Sec. 1.6.2. The chemical potential  $\mu$  as a function of  $N$  and trap parameters is given by formula (1.140). The ground-state energy of the system with a given number of particles can then be calculated through direct integration of  $\mu(N)$ .

If  $n_{1D}a_{\perp}^2/a_{3D} \gg 1$ , the system is weakly interacting and the LL equation of state coincides with the mean-field prediction:  $\epsilon_{LL} = g_{1D}n_{1D}/2$ . In the notation of Sec. 1.6.2 it corresponds to  $C_1 = 2, \gamma_1 = 1, C_2 = 0$ . From formula (1.140) one finds the following results for the energy per particle

$$\frac{E}{N} - \hbar\omega_{\perp} = \frac{3}{10} \left( 3N\lambda \frac{a_{3D}}{a_{\perp}} \right)^{2/3} \hbar\omega_{\perp}, \quad (3.5)$$

and exploiting formula (1.138) one obtains an expression for the mean square radius of the cloud in the longitudinal direction

$$\sqrt{\langle z^2 \rangle} = \left( 3N\lambda \frac{a_{3D}}{a_{\perp}} \right)^{1/3} \frac{a_{\perp}}{\sqrt{5}\lambda}. \quad (3.6)$$

In the opposite limit,  $n_{1D}a_{\perp}^2/a \ll 1$ , the system enters the Tonks-Girardeau regime and the LL equation of state has the Fermi-like behavior (1.102)  $\epsilon_{LL} = \pi^2 \hbar^2 n_{1D}^2 / 6m$ . The energy per particle and the mean square radius of the trapped system are easily extracted from the results for a purely one-dimensional system (1.151),(1.153)

$$\frac{E}{N} - \hbar\omega_{\perp} = \frac{N\lambda}{2} \hbar\omega_{\perp}, \quad \sqrt{\langle z^2 \rangle} = \sqrt{\frac{N}{2\lambda}} a_{\perp}. \quad (3.7)$$

In terms of the parameters of the system, the two regimes can be identified by comparing the corresponding energies. The mean-field energy becomes favorable if  $N\lambda a_{\perp}^2 / a_{3D}^2 \gg 1$ , whereas the Tonks-Girardeau gas is preferred if the condition  $N\lambda a_{\perp}^2 / a_{3D}^2 \ll 1$  is satisfied<sup>2</sup>.

### 3.2.5 1D system: beyond local density approximation

In order to account for effects beyond local density approximation we have also applied the DMC method to a system of  $N$  particles interacting through the Lieb-Liniger Hamiltonian in the presence of harmonic confinement

$$\hat{H}_{LL}^{trap} = N\hbar\omega_{\perp} - \frac{\hbar^2}{2m} \sum_{i=1}^N \frac{\partial^2}{\partial z_i^2} + g_{1D} \sum_{i<j} \delta(z_i - z_j) + \sum_{i=1}^N \frac{m\omega_z^2 z_i^2}{2}. \quad (3.8)$$

When the number of particles is large, the properties of the ground state of the Hamiltonian (3.8) coincide with the ones obtained from the LL equation of state within LDA. However, for small systems one expects deviations and the DMC method provides us with a powerful tool. The relevant parameters are the same as for the 3D simulation with the Hamiltonian (3.1): the number of particles  $N$ , the ratio  $a_{3D}/a_{\perp}$  fixing the strength of the contact potential  $g_{1D}$  and the anisotropy parameter  $\lambda$  fixing the strength of the longitudinal confinement in units of  $\hbar\omega_{\perp}$ .

The importance sampling is realized through the Bijl-Jastrow trial wave function (2.37). The one-body term is of gaussian form (2.41)  $f_1(z) = \exp\{-\alpha_z z^2\}$ . The two-body term  $f_2(z)$  is given by the formula (2.51). The construction of the the discussed in details in Sec. 2.5.4.4. There are two variational parameters: gaussian width  $\alpha_z$  and the matching distance  $R_m$ . We fix them by minimizing the variational energy.

We notice that our choice of the two-body Jastrow factor reproduces both the weakly interacting and the Tonks-Girardeau regime. In fact, if  $kR_m$  is small,  $f_2(z) \simeq 1$ ,  $z = 0$  and the contact potential is almost transparent. On the other hand, if  $kR_m$  approaches  $\pi/2$ ,  $f_2(z) \rightarrow 0$ ,  $z = 0$  and the contact potential behaves as an impenetrable barrier.

---

<sup>2</sup>This characteristic for LDA parameter is universal, for example systems with different number of particles behave similarly if the combination  $N\lambda a_{\perp}^2 / a_{3D}^2$  is the same. It becomes clear from from equation (1.134) noting that  $N\lambda a_{\perp}^2 / a_{3D}^2 = \Delta_1^2$ .

### 3.3 Results

#### 3.3.1 Small system, medium scattering length

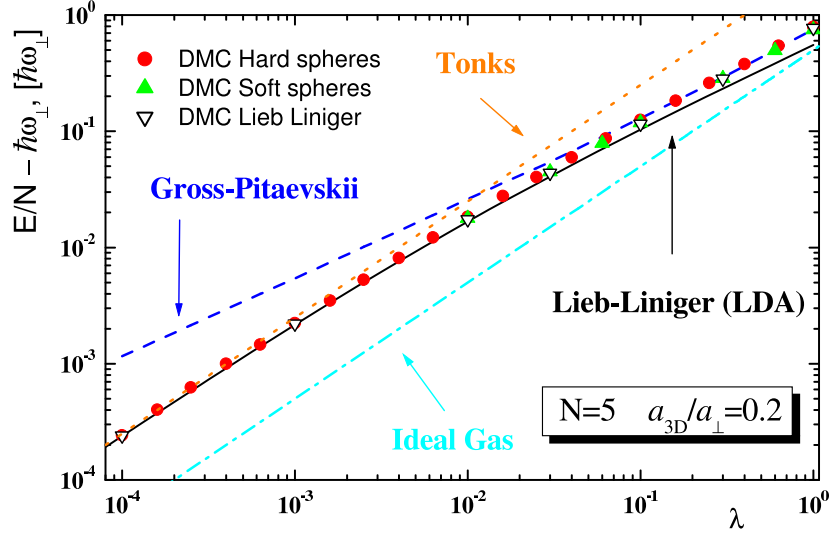


Figure 3.1: Energy per particle as a function of  $\lambda$ . DMC results: HS potential (solid circles), SS potential (solid triangles), LL Hamiltonian (3.8) (open triangles). Dashed line: GP equation (3.3), solid line: LL equation of states in LDA, dotted line: TG gas, dot-dashed line: non-interacting gas. Error bars are smaller than the size of the symbols.

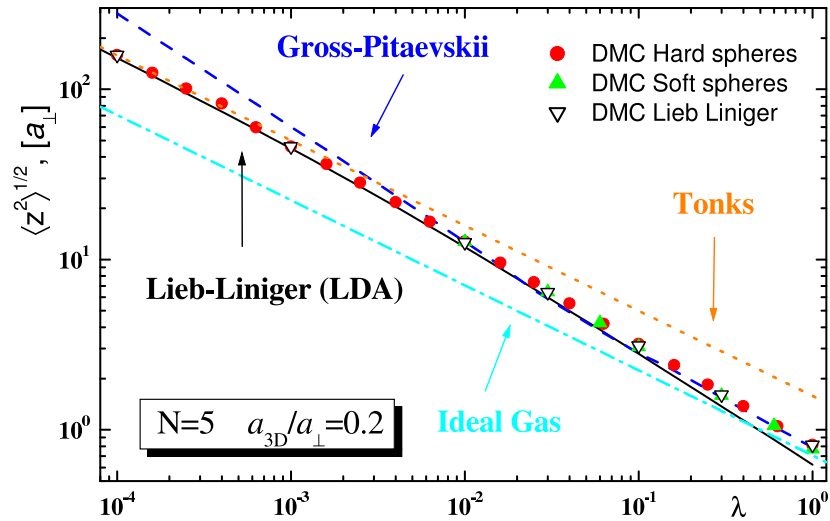


Figure 3.2: Mean square radius along  $z$  as a function of  $\lambda$ . Dashed line: GP equation (3.3), solid line: LL equation of states in LDA, dotted line: TG gas, dot-dashed line: non-interacting gas. Error bars are smaller than the size of the symbols.

We first consider a system of very few particles ( $N = 5$ ) and we consider different values of the ratio  $a_{3D}/a_{\perp}$ . Figs. 3.1-3.2 refer to  $a_{3D}/a_{\perp} = 0.2$ , and we present results for the energy per particle and the mean square radius of the cloud in the longitudinal direction as a function of the anisotropy parameter  $\lambda = \omega_z/\omega_{\perp}$ . Results from the GP equation (3.3) and from the Lieb-Liniger equation

of state in LDA are also shown. We find that the HS and SS potential give practically the same results even for the largest values of  $\lambda$ , showing that for these parameters we are well within the universal regime where the details of the potential are irrelevant. For large values of  $\lambda$  the DMC results agree well with the predictions of GP equation. By decreasing  $\lambda$  beyond mean-field effects become visible and both the energy per particle and the mean square radius approach the LL result when  $N\lambda a_{\perp}^2/a^2 \sim 1$ , corresponding to  $\lambda \sim 10^{-2}$ . Finally, for the smallest values of the anisotropy parameter ( $\lambda \sim 10^{-4}$ ) we find clear evidence of the Tonks-Girardeau gas behavior both in the energy and in the shape of the cloud. It is worth stressing that beyond mean-field effects occurring in the small  $\lambda$  regime can be only obtained by using DMC. A Variational Monte-Carlo (VMC) calculation based on the trial wave function  $\psi_T(\mathbf{R})$  described above, would yield results in good agreement with mean-field over the whole range of values of  $\lambda$ . DMC results using the Lieb-Liniger Hamiltonian  $H_{LL}$  of Eq. (3.8) are also shown and coincide with the results of the 3D Hamiltonian (3.1). This shows that the 3D interatomic potential is correctly described by the 1D  $\delta$ -potential even for the largest values of  $\lambda$ . In fact, due to the small number of particles, the density profile of the cloud in the transverse direction is correctly described by the harmonic oscillator ground-state wave function (see Fig. 3.9). The 1D character of the system is also evident from Fig. 3.1 which shows that  $E/N - \hbar\omega_{\perp}$  is always smaller than the transverse confining energy. Deviations of DMC results from the LL equation of state arise because of finite size effects. These effects become less and less important as  $\lambda$  decreases and one enters the regime  $(E/N - \hbar\omega_{\perp})/\hbar\omega_{\perp} \gg \lambda$  where LDA applies. In terms of the mean square radius of the cloud (see Fig. 3.2), the condition of applicability of LDA requires  $\langle z^2 \rangle^{1/2}$  much larger than the corresponding ideal gas (IG) value.

### 3.3.2 Small system, small scattering length

In Figs. 3.3-3.4 we present results for  $a_{3D}/a_{\perp} = 0.04$ , corresponding to a less tight transverse confinement or, equivalently, to a smaller scattering length. By decreasing  $a_{3D}/a_{\perp}$  we enter more deeply in the universal regime where the theory of pseudo-potentials applies and we find no difference between HS and SS results. Further, as for the  $a_{3D}/a_{\perp} = 0.2$  case, we find no difference between DMC results obtained starting from Hamiltonian (3.1) and from the 1D Hamiltonian (3.8). Compared to Figs. 3.1-3.2, the cross-over between mean field and Lieb-Liniger occurs for smaller values of  $\lambda$ . For the smallest values of  $\lambda$  beyond mean-field effects become evident, though one would need to decrease  $\lambda$  even further to enter the Tonks-Girardeau gas regime.

### 3.3.3 Small system, large scattering length

The results for  $a_{3D}/a_{\perp} = 1$  are shown in Figs. 3.5-3.6. In this case the HS and SS potential give significantly different results in the large  $\lambda$  regime. For both potentials the mean-field description is inadequate. By decreasing  $\lambda$  the HS system enters the Tonks-Girardeau regime before approaching the LL results, whereas the SS system crosses from the ideal gas (IG) regime to the Tonks-Girardeau regime. For this value of  $a_{3D}/a_{\perp}$  the DMC results with the Hamiltonian (3.8) coincide exactly with the ones of the LL equation of state in LDA due to the large coupling constant.

### 3.3.4 Large system

Figs. 3.7-3.8 refer to a much larger system with  $N = 100$  and  $a_{3D}/a_{\perp} = 0.2$ . In this case, we see a clear cross-over from 3D mean field, at large  $\lambda$ , to 1D LL at small  $\lambda$ . Important beyond mean-field



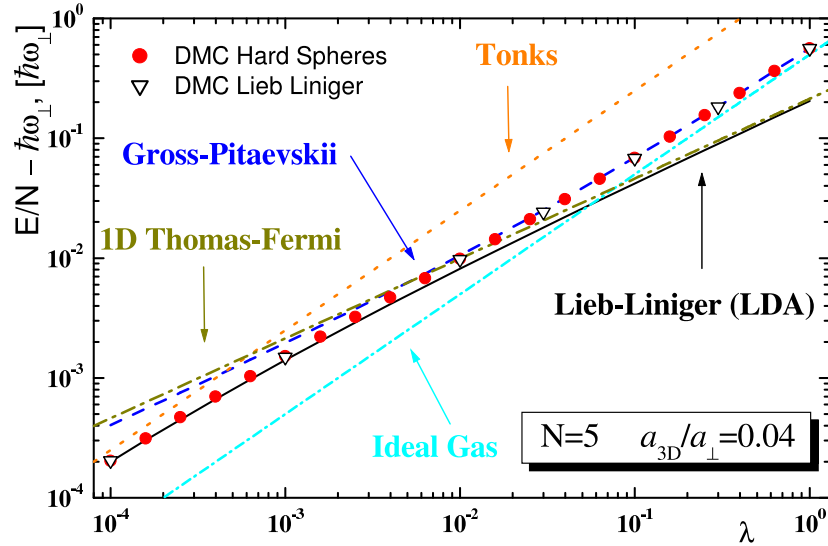


Figure 3.3: Energy per particle as a function of  $\lambda$ . DMC results: HS potential (solid circles), LL Hamiltonian (3.8) (open triangles), Dashed line: GP equation (3.3), solid line: LL equation of states in LDA, dotted line: TG gas, dot-dashed line: non-interacting gas.

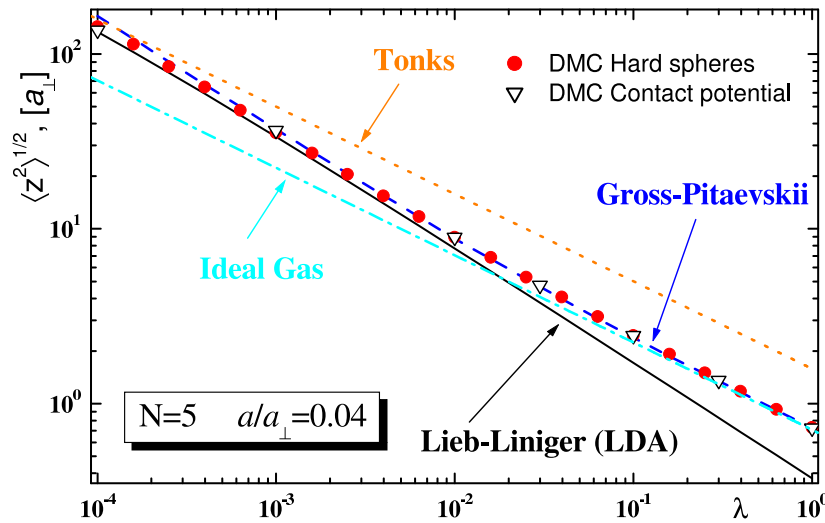


Figure 3.4: Mean square radius along  $z$  as a function of  $\lambda$ . Dashed line: GP equation (3.3), solid line: LL equation of states in LDA, dotted line: TG gas, dot-dashed line: non-interacting gas.

effects become evident in the energy per particle as  $N\lambda a_{\perp}^2/a^2 \sim 1$ , corresponding to  $\lambda \sim 10^{-3}$ . The Tonks-Girardeau regime would correspond to even smaller values of  $\lambda$  which are difficult to obtain in our simulation. However, for the smallest values of  $\lambda$  reported in Fig. 3.7 we find already very good agreement with the LL equation of state. One should notice that small deviations from mean field are also visible for  $\lambda \sim 1$ , and are due to high density corrections to the GP equation. The DMC results with the 1D Hamiltonian (3.8) follow exactly the LDA prediction showing that the deviations seen in Figs. 3.1-3.2 are due to finite size effects. In the cross-over region from the mean-field to the 1D LL regime, residual 3D effects are still present (see Fig. 3.9) and produce small deviations from the LL equation of state.

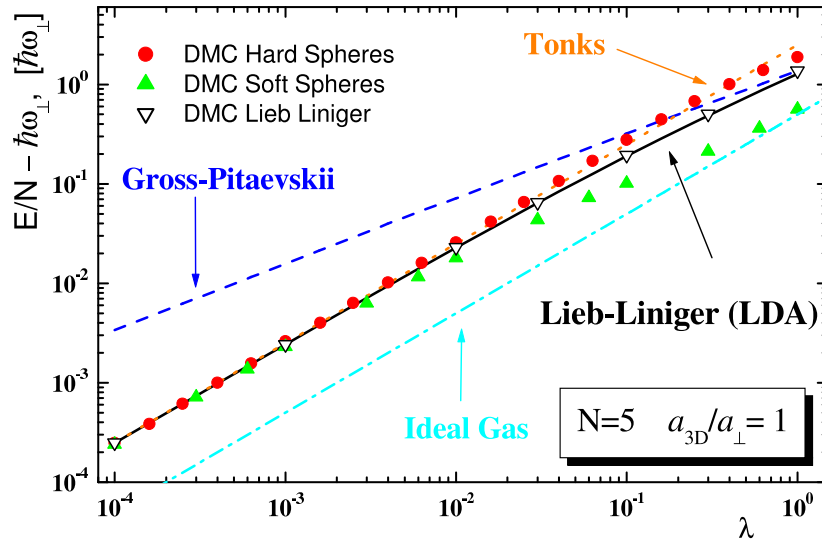


Figure 3.5: Energy per particle as a function of  $\lambda$ . Dashed line: GP equation (3.3), solid line: LL equation of states in LDA, dotted line: TG gas, dot-dashed line: non-interacting gas.

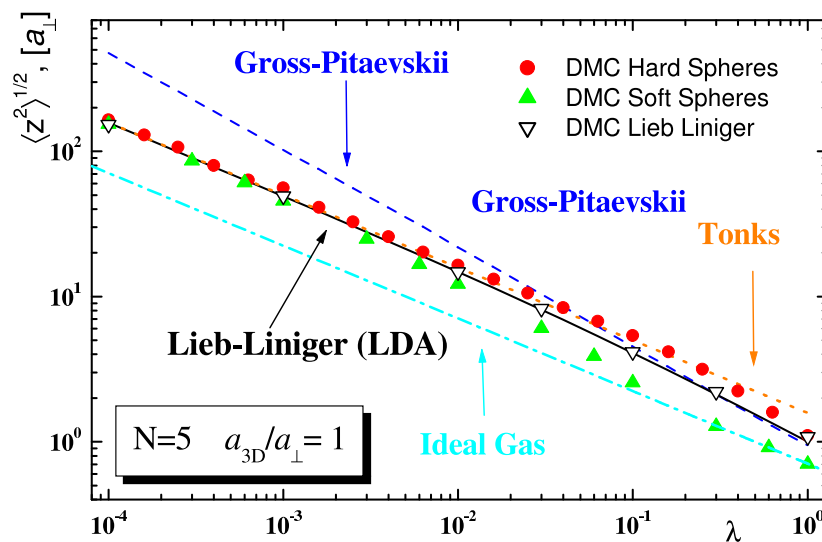


Figure 3.6: Mean square radius along  $z$  as a function of  $\lambda$ . Dashed line: GP equation (3.3), solid line: LL equation of states in LDA, dotted line: TG gas, dot-dashed line: non-interacting gas.

### 3.3.5 Radial size of the system

Finally, in Fig. 3.9, we show results for the mean square radius in the transverse direction. The cross-over from 3D to 1D is clearly visible in the case of  $N = 100$ , for both the HS and SS potential, and for the HS potential in the case of  $N = 5$  and  $a_{3D}/a_{\perp} = 1$ . For the system with  $N = 5$  and  $a_{3D}/a_{\perp} = 0.2$  we only see small deviations from  $\sqrt{\langle r_{\perp}^2 \rangle} = a_{\perp}$  for the largest values of  $\lambda$ . In the  $a_{3D}/a_{\perp} = 0.04$ , as well as in the  $a_{3D}/a_{\perp} = 1$  case with the SS potential, the transverse density profile is well described by the harmonic oscillator wave function and we find  $\sqrt{\langle r_{\perp}^2 \rangle} \simeq a_{\perp}$  over the whole range of values of  $\lambda$ . It is worth noticing that for the  $N = 5$  system with SS potential, the largest deviations from  $\sqrt{\langle r_{\perp}^2 \rangle} = a_{\perp}$  are achieved for  $a_{3D}/a_{\perp} = 0.2$ , corresponding to a transverse confinement  $a_{\perp} = R$  where  $R$  is the range of the SS potential.



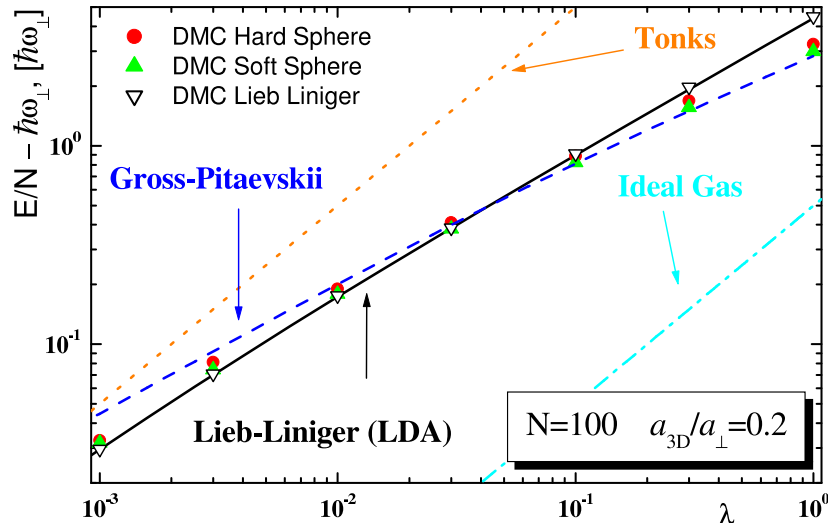


Figure 3.7: Energy per particle as a function of  $\lambda$ . Dashed line: GP equation (3.3), solid line: LL equation of states in LDA, dotted line: TG gas, dot-dashed line: non-interacting gas.

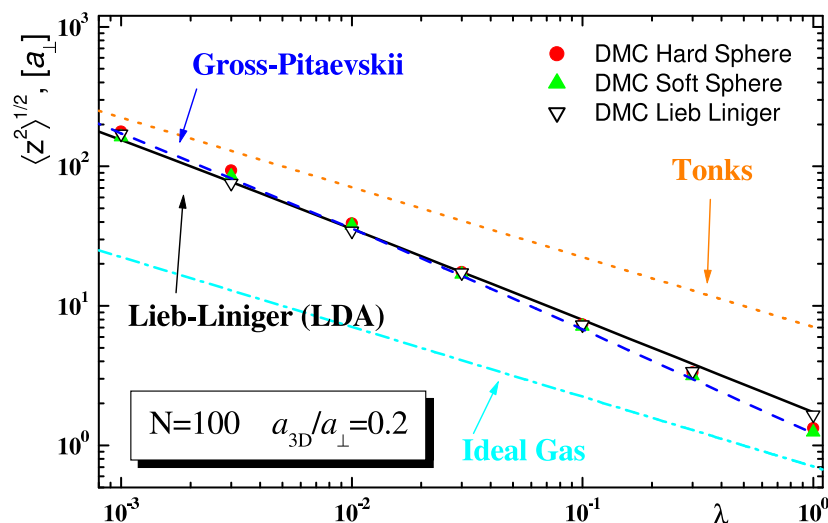


Figure 3.8: Mean square radius along  $z$  as a function of  $\lambda$ . Dashed line: GP equation (3.3), solid line: LL equation of states in LDA, dotted line: TG gas, dot-dashed line: non-interacting gas.

## 3.4 Conclusions

In this chapter we present exact Quantum Monte Carlo results of the ground-state energy and structure of a Bose gas confined in highly anisotropic harmonic traps. Starting from a 3D Hamiltonian, where interparticle interactions are model by a hard-sphere or a soft-sphere potential, we show that the system exhibits striking features due to particle correlations. By reducing the anisotropy parameter  $\lambda$ , while the number of particles  $N$  and the ratio  $a_{3D}/a_{\perp}$  of scattering to transverse oscillator length are kept fixed, the system crosses from a regime where mean-field theory applies to a regime which is well described by the 1D Lieb-Liniger equation of state in local density approximation. In the cross-over region both theories fail and one must resort to exact methods to account properly for both finite size effects and residual 3D effects. For very small values of  $\lambda$  we find clear evidence, both in the energy per particle and in the longitudinal size of the cloud, of the fermionization of the

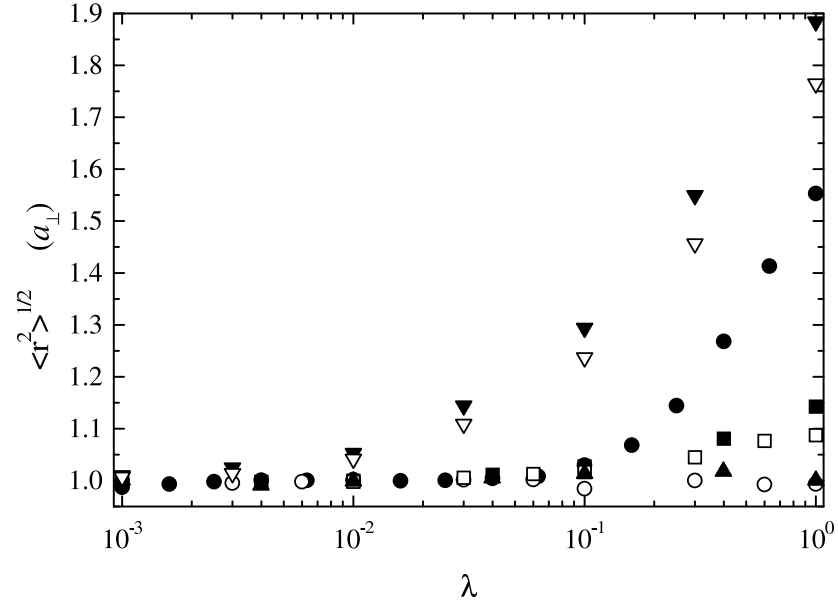


Figure 3.9: Mean square radius in the radial direction as a function of  $\lambda$ . Solid symbols: HS potential; open symbols: SS potential. Down triangles:  $N = 100$  and  $a_{3D}/a_{\perp} = 0.2$ ; circles:  $N = 5$  and  $a_{3D}/a_{\perp} = 1$ ; squares:  $N = 5$  and  $a_{3D}/a_{\perp} = 0.2$ ; up triangles:  $N = 5$  and  $a_{3D}/a_{\perp} = 0.04$ . Error bars are smaller than the size of the symbols.

system in the Tonks-Girardeau regime.

# Chapter 4

## Quasi 1D Bose gases with large scattering length

### 4.1 Introduction

Quasi-1D Bose gases have been realized in highly-elongated traps by tightly confining the transverse motion of the atoms to their zero point oscillations [GVL<sup>+</sup>01, SKC<sup>+</sup>01, GBM<sup>+</sup>01]. As compared to the 3D case, the role of quantum fluctuations is enhanced in 1D and these systems are predicted to exhibit peculiar properties, which cannot be described using traditional mean-field theories, but require more advanced many-body approaches. Particularly intriguing is the strong coupling regime, where, due to repulsion between particles, the quasi-one dimensional Bose gas behaves as if it consisted of fictitious spinless fermions (Tonks-Girardeau gas [Ton36, Gir60, Ols98, PSW00]). This regime has not been achieved yet, but is one of the main focus areas of present experimental investigations in this field [MSKE03, RT03]. An interesting possibility to approach the strongly correlated TG regime is provided by magnetic field induced atom-atom Feshbach resonances [IAS<sup>+</sup>98, CCR<sup>+</sup>00b, LRT<sup>+</sup>02, OHG<sup>+</sup>02, BCK<sup>+</sup>03]. By utilizing this technique one can tune the 3D *s*-wave scattering length  $a_{3D}$ , and hence the strength of atom-atom interactions, to essentially any value including zero and  $\pm\infty$ .

Degenerate quantum gases near a Feshbach resonance have recently received a great deal of interest both experimentally and theoretically. At resonance ( $|a_{3D}| \rightarrow \infty$ ) the 3D scattering cross-section  $\sigma$  is fixed by the unitary condition,  $\sigma = 4\pi/k^2$ , where  $k$  is the relative wave vector of the two atoms. In this regime it is predicted that, if the effective range  $R$  of the atom-atom interaction potential is much smaller than the average interparticle distance, the behavior of the gas is universal, *i.e.*, independent of the details of the interatomic potential and independent of the actual value of  $a_{3D}$  [Hei01, CHM<sup>+</sup>02]. This is known as the unitary regime [HM04]. In the case of 3D Bose gases, this unitary regime can most likely not be realized in experiments since three-body recombination is expected to set in when  $a_{3D}$  becomes comparable to the average interparticle distance. Three-body recombination leads to cluster formation and hence makes the gas-like state unstable. The situation is different for Fermi gases, for which the unitary regime has already been reached experimentally [OHG<sup>+</sup>02, BCK<sup>+</sup>03]. In this case, the Fermi pressure stabilizes the system even for large  $|a_{3D}|$ .

In quasi-one dimensional geometries a new length scale becomes relevant, namely, the oscillator length  $a_{\perp} = \sqrt{\hbar/(m\omega_{\perp})}$  of the tightly confined transverse motion, where  $m$  is the mass of the atoms and  $\omega_{\perp}$  is the angular frequency of the harmonic trapping potential. For  $|a_{3D}| \gg a_{\perp}$ , the gas is expected to exhibit a universal behavior if the effective range  $R$  of the atom-atom interaction

potential is much smaller than  $a_{\perp}$  and the mean interparticle distance is much larger than  $a_{\perp}$ . It has been predicted that three-body recombination processes are suppressed for strongly interacting 1D Bose gases (see Eq. 5.12). These studies raise the question whether the unitary regime can be reached in Bose gases confined in highly-elongated traps, that is, whether the quasi-one dimensional bosonic gas-like state is stable against cluster formation as  $a_{3D} \rightarrow \pm\infty$ .

This chapter is devoted to the investigation of the properties of a quasi-one dimensional Bose gas at zero temperature over a wide range of values of the 3D scattering length  $a_{3D}$  using Quantum Monte Carlo techniques (see Chapter 2). We find that the system 1) is well described by a 1D model Hamiltonian with contact interactions and renormalized coupling constant [Ols98] for any value of  $a_{3D}$ , 2) reaches the regime of a TG gas for a critical positive value of the 3D scattering length  $a_{3D}$ , 3) enters a unitary regime for large values of  $|a_{3D}|$ , that is, for  $|a_{3D}| \rightarrow \infty$ , where the properties of the quasi-one dimensional Bose gas become independent of the actual value of  $a_{3D}$  and are similar to those of a 1D gas of hard-rods and 4) becomes unstable against cluster formation for a critical value of the 1D gas parameter, or equivalently, for a critical negative value of the 3D scattering length  $a_{3D}$ .

The structure of this Chapter is as follows. Section 4.2 discusses the energetics of two bosons in quasi-one dimensional harmonic traps. to a 1D model Hamiltonian with contact interactions and renormalized coupling constant [Ols98]. The eigenenergies of the system are calculated by exact diagonalization of both the 3D and the 1D Hamiltonian. We use these results for two particles to benchmark our quantum MC calculations presented in Sec. 4.4. Section 4.3 discusses the relation between the 3D and the 1D Hamiltonian for  $N$  bosons under quasi-one dimensional confinement. Section 4.4 presents our MC results for  $N = 2$  and  $N = 10$  atoms in highly-elongated harmonic traps over a wide range of values of the 3D scattering length  $a_{3D}$ . A comparison of the energetics of the lowest-lying gas-like state for the 3D and the 1D Hamiltonian is carried out. In the  $N = 2$  case, we additionally compare with the essentially exact results presented in Sec. 4.2. In the  $N = 10$  case, we additionally compare with the energy of the lowest-lying gas-like state of the 1D Hamiltonian calculated using the local density approximation (LDA). Section 4.5 discusses the stability of the lowest-lying gas-like state against cluster formation when  $a_{3D}$  is negative using the variational Monte Carlo (VMC) method. We provide a quantitative estimate of the criticality condition. Finally, Sec. 4.6 draws our conclusions.

## 4.2 Two Bosons under quasi-one-dimensional confinement

Consider two interacting mass  $m$  bosons with position vectors  $\vec{r}_1$  and  $\vec{r}_2$ , where  $\vec{r}_i = (x_i, y_i, z_i)$ , in a waveguide with harmonic confinement in the radial direction. If we introduce the center of mass coordinate  $\vec{R}$  and the relative coordinate  $\vec{r} = \vec{r}_2 - \vec{r}_1$ , the problem separates. Since the solution to the center of mass Hamiltonian is given readily, we only consider the internal Hamiltonian  $H_{3D}^{int}$ , which can be conveniently written in terms of cylindrical coordinates  $\vec{r} = (\rho, \phi, z)$ ,

$$\hat{H}_{3D}^{int} = -\frac{\hbar^2}{2\mu}\Delta + V_{int}(\vec{r}) + \frac{1}{2}\mu\omega_{\perp}^2\rho^2, \quad (4.1)$$

where  $\mu$  denotes the reduced two-body mass,  $\mu = m/2$ , and  $V_{int}(\vec{r})$  denotes the full 3D atom-atom interaction potential.

Considering a regularized zero-range pseudo-potential  $V_{int}(\vec{r}) = 2\pi\hbar^2 a_{3D}/\mu\delta(\vec{r})\frac{\partial}{\partial r}r$ , where  $a_{3D}$  denotes the 3D scattering length, Olshanii [Ols98] derives an effective 1D Hamiltonian,

$$H_{1D}^{int} = -\frac{\hbar^2}{2\mu}\frac{d^2}{dz^2} + g_{1D}\delta(z) + \hbar\omega_{\perp}, \quad (4.2)$$

and renormalized coupling constant  $g_{1D}$ ,

$$g_{1D} = \frac{2\hbar^2 a_{3D}}{ma_{\perp}^2} \left[ 1 - |\zeta(1/2)| \frac{a_{3D}}{\sqrt{2}a_{\perp}} \right]^{-1}, \quad (4.3)$$

which reproduce the low energy scattering solutions of the full 3D Hamiltonian, Eq. 4.1. Here,  $\zeta(\cdot)$  denotes the Riemann zeta function,  $\zeta(1/2) = -1.4604$ . Alternatively,  $g_{1D}$  can be expressed through the effective 1D scattering length  $a_{1D}$  [Ols98],

$$g_{1D} = -\frac{2\hbar^2}{ma_{1D}}, \quad (4.4)$$

where

$$a_{1D} = -a_{\perp} \left( \frac{a_{\perp}}{a_{3D}} - \frac{|\zeta(1/2)|}{\sqrt{2}} \right) \quad (4.5)$$

Olshanii's result shows that the waveguide gives rise to an effective interaction, parameterized by the coupling constant  $g_{1D}$ , which can be tuned to any strength by changing the ratio between the 3D scattering length  $a_{3D}$  and the transverse oscillator length  $a_{\perp}$ .

The renormalized coupling constant, Eq. 4.3, can be compared with the unrenormalized coupling constant  $g_{1D}^0$  (1.124),

$$g_{1D}^0 = \frac{2\hbar^2 a_{3D}}{ma_{\perp}^2}, \quad (4.6)$$

Figure 4.1 shows the unrenormalized coupling constant  $g_{1D}^0$  [dashed line, Eq. 4.6] together with the renormalized coupling constant [solid line, Eq. 4.3]. For  $|a_{3D}| \ll a_{\perp}$ , the renormalized coupling constant  $g_{1D}$  is nearly identical to the unrenormalized coupling constant  $g_{1D}^0$ . For large  $|a_{3D}|$ , however, the confinement induced renormalization becomes important, and the effective 1D coupling constant  $g_{1D}$ , Eq. 4.3, has to be used. At the critical value  $a_{3D}^c = 0.9684a_{\perp}$  (indicated by a vertical arrow in Fig. 4.1),  $g_{1D}$  diverges. For  $a_{3D} \rightarrow \pm\infty$ ,  $g_{1D}$  reaches an asymptotic value,  $g_{1D} = -1.9368a_{\perp}\hbar\omega_{\perp}$  (indicated by a horizontal arrow in Fig. 4.1). Finally,  $g_{1D}$  is negative for all negative 3D scattering lengths. The inset of Fig. 4.1 shows the effective 1D scattering length  $a_{1D}$ , Eq. 4.5, as a function of  $a_{3D}$ . For small positive  $a_{3D}$ ,  $a_{1D}$  is negative and it changes sign at  $a_{3D} = a_{3D}^c$  ( $a_{1D} = 0$  for  $a_{3D} = a_{3D}^c$ ). Moreover,  $a_{1D}$  reaches, just as  $g_{1D}$ , an asymptotic value for  $|a_{3D}| \rightarrow \infty$ ,  $a_{1D} = 1.0326a_{\perp}$  (indicated by a horizontal arrow in the inset of Fig. 4.1). The renormalized 1D scattering length  $a_{1D}$  is positive for negative  $a_{3D}$ , and approaches  $+\infty$  as  $a_{3D} \rightarrow -0$ . Figure 4.1 suggests that tuning the 3D scattering length  $a_{3D}$  to large values allows a universal quasi-one dimensional regime, where  $g_{1D}$  and  $a_{1D}$  are independent of  $a_{3D}$ , to be entered.

The effective coupling constant  $g_{1D}$ , Eq. 4.3, has been derived for a wave guide geometry, that is, with no axial confinement. However, it also describes the scattering between two bosons confined to other quasi-one dimensional geometries. Consider, *e.g.*, a Bose gas under harmonic confinement. If the confinement in the axial direction is weak compared to that of the radial direction, the scattering properties of each atom pair are expected to be described accurately by the effective coupling constant  $g_{1D}$  and the effective scattering length  $a_{1D}$ .

The internal motion of two bosons under highly-elongated confinement can be described by the following 3D Hamiltonian

$$\hat{H}_{3D}^{int} = -\frac{\hbar^2}{2\mu}\Delta + V_{int}(\vec{r}) + \frac{1}{2}\mu(\omega_{\perp}^2\rho^2 + \omega_z^2z^2), \quad (4.7)$$

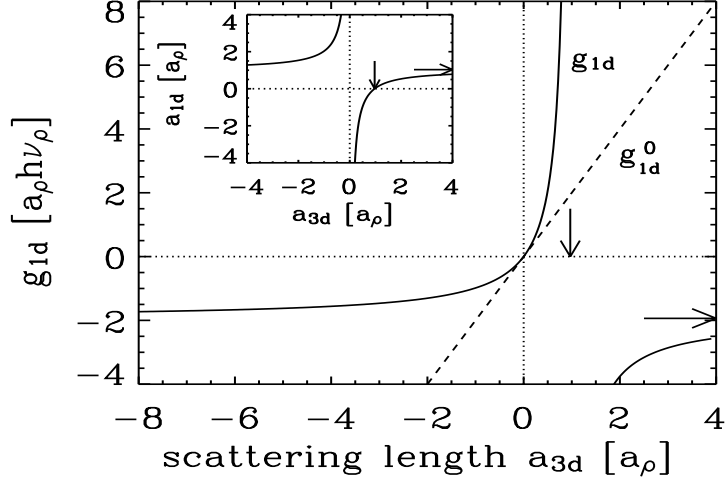


Figure 4.1: One-dimensional coupling constants  $g_{1D}$  [Eq. 4.3, solid line] and  $g_{1D}^0$  [Eq. 4.6, dashed line] as a function of the 3D scattering length  $a_{3D}/a_{\perp}$ . The vertical arrow indicates the value of  $a_{3D}$  for which  $g_{1D}$  diverges,  $a_{3D}^c = 0.9684a_{\perp}$ . The horizontal arrow indicates the asymptotic value of  $g_{1D}$  as  $|a_{3D}| \rightarrow \infty$ ,  $g_{1D} = -1.9368a_{\perp}\hbar\omega_{\perp}$ . Inset: One-dimensional scattering length  $a_{1D}$ , Eq. 4.5, as a function of  $a_{3D}/a_{\perp}$ . The vertical arrow indicates the value of  $a_{3D}$  for which  $a_{1D}$  goes through zero,  $a_{3D}^c = 0.9684a_{\perp}$ . The horizontal arrow indicates the asymptotic value of  $a_{1D}$  as  $|a_{3D}| \rightarrow \infty$ ,  $a_{1D} = 1.0326a_{\perp}$ . The angular frequency  $\omega_{\perp}$  determines the frequency  $\nu_{\perp}$ ,  $\omega_{\perp} = 2\pi\nu_{\perp}$  (also,  $\hbar\omega_{\perp} = h\nu_{\perp}$ ).

where  $\omega_z$  denotes the angular frequency in the longitudinal direction,  $\omega_z = \lambda\omega_{\perp}$  ( $\lambda$  denotes the aspect ratio,  $\lambda \ll 1$ ). The eigenenergies  $E_{3D}^{int}$  and eigenfunctions  $\psi_{3D}^{int}$  of this Hamiltonian satisfy the Schrödinger equation,

$$\hat{H}_{3D}^{int}\psi_{3D}^{int}(\rho, z) = E_{3D}^{int}\psi_{3D}^{int}(\rho, z). \quad (4.8)$$

The corresponding 1D Hamiltonian reads

$$H_{1D}^{int} = -\frac{\hbar^2}{2\mu} \frac{d^2}{dz^2} + g_{1D}\delta(z) + \frac{1}{2}\mu\omega_z^2 z^2 + \hbar\omega_{\perp} \quad (4.9)$$

The 1D eigenenergies  $E_{1D}^{int}$  of the stationary Schrödinger equation,

$$\hat{H}_{1D}^{int}\psi_{1D}^{int}(z) = E_{1D}^{int}\psi_{1D}^{int}(z), \quad (4.10)$$

can be determined semi-analytically by solving the transcendental equation [BEKW98],

$$g_{1D} = 2\sqrt{2} \frac{\Gamma(\chi_z + 1)}{\Gamma(\chi_z + 1/2)} \tan(\pi\chi_z) \hbar\omega_z a_z, \quad (4.11)$$

self consistently for  $\chi_z$  (for a given  $g_{1D}$ ). In the above equation,  $\chi_z$  is an effective (possibly non-integer) quantum number, which determines the energy  $E_z$ ,

$$\chi_z = \frac{E_z}{2\hbar\omega_z} - \frac{1}{4}. \quad (4.12)$$

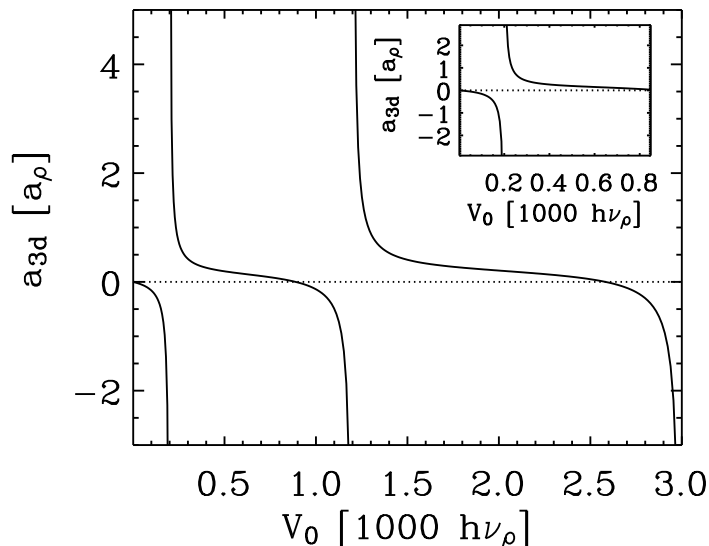


Figure 4.2: Three-dimensional  $s$ -wave scattering length  $a_{3D}$  as a function of the well depth  $V_0$  for the short-range model potential  $V^{SR}$ , Eq. 4.14. Each time the 3D scattering length diverges a new two-body  $s$ -wave bound state is created. Inset: Enlargement of the well depth region used in our calculations.

The energy  $E_z$ , in turn, determines the internal 1D eigenenergies  $E_{1D}^{int}$ ,

$$E_{1D}^{int} = \lambda E_z + \hbar\omega_{\perp}. \quad (4.13)$$

In Eq. 4.11,  $a_z$  denotes the characteristic oscillator length in the axial direction,  $a_z = \sqrt{\hbar/(m\omega_z)}$ .

To compare the eigenenergies  $E_{3D}^{int}$  and  $E_{1D}^{int}$ , we use, for the 3D atom-atom interaction potential  $V(r)$ , a short-range (SR) modified Pöschl-Teller potential (1.97)  $V^{SR}(r)$  that can support two-body bound states,

$$V^{SR}(r) = -\frac{V_0}{\cosh^2(r/R)} \quad (4.14)$$

In the above equation,  $V_0$  denotes the well depth, and  $R$  the range of the potential. In our calculations,  $R$  is fixed at a value much smaller than the transverse oscillator length,  $R = 0.1a_{\perp}$ . To simulate the behavior of  $a_{3D}$  near a field-dependent Feshbach resonance, we vary the well depth  $V_0$ , and consequently, the scattering length  $a_{3D}$ . It has been shown that such a model describes many atom-atom scattering properties near a Feshbach resonance properly [TWMJ00]. Figure 4.2 shows the dependence of the 3D scattering length  $a_{3D}$  on  $V_0$ . Importantly,  $a_{3D}$  diverges for particular values of the well depth  $V_0$ . At each of these divergencies, a new two-body  $s$ -wave bound state is created. The inset of Fig. 4.2 shows the range of well depths  $V_0$  used in our calculations.

To benchmark our MC calculations (see Chapter 2 and Sec. 4.4), we solve the 3D Schrödinger equation, Eq. 4.8, with  $\lambda = 0.01$  for various well depths  $V_0$  using a two-dimensional B-spline basis in  $\rho$  and  $z$ . Figure 4.3 shows the resulting 3D eigenenergies  $E_{3D}^{int}$  (diamonds) as a function of the 3D scattering length  $a_{3D}$ . We distinguish between two sets of states:



1) States with  $E_{3D}^{int} \geq \hbar\omega_{\perp}$  are referred to as gas-like states; their behavior is, to a good approximation, characterized by the 3D scattering length  $a_{3D}$ , and is hence independent of the detailed shape of the atom-atom potential. The energies of the gas-like states are shown in Fig. 4.3(a).

2) States with  $E_{3D}^{int} < \hbar\omega_{\perp}$  are referred to as molecular-like bound states; their behavior depends on the detailed shape of the atom-atom potential. The energies of these bound states are shown in Fig. 4.3(b). The well depth  $V_0$  of the short-range interaction potential  $V^{SR}$  is chosen such that  $V^{SR}$  supports — in the absence of the confining potential — no  $s$ -wave bound state for  $a_{3D} < 0$ , and one  $s$ -wave bound state for  $a_{3D} > 0$ . Figure 4.3(b) shows that the bound state remains bound for  $|a_{3D}| \rightarrow \infty$  and for negative  $a_{3D}$  if tight radial confinement is present. In addition, a dashed line shows the 3D binding energy,  $-\hbar^2/(ma_{3D}^2)$ , which accurately describes the highest-lying molecular bound state in the absence of any external confinement if  $a_{3D}$  is much larger than the range  $R$  of the potential  $V^{SR}$ .

The B-spline basis calculations yield not only the internal 3D eigenenergies  $E_{3D}^{int}$ , but also the corresponding wave functions  $\psi_{3D}^{int}$ . The nodal surface of the lowest-lying gas-like state, which is to a good approximation an ellipse in the  $\rho z$ -plane, is a crucial ingredient of our many-body calculations. Section 4.4 discuss in detail how this nodal surface is used to parametrize our trial wave function entering the MC calculations.

To compare the energy spectrum for  $N = 2$  of the effective 1D Hamiltonian with that of the 3D Hamiltonian, Fig. 4.3 additionally shows the 1D eigenenergies  $E_{1D}^{int}$  (solid lines) obtained by solving the Schrödinger equation for  $H_{1D}^{int}$ , Eq. 4.9, semi-analytically [using the renormalized coupling constant  $g_{1D}$ , Eq. 4.3]. Figure 4.3(a) demonstrates excellent agreement between the 3D and the 1D internal energies for all states with gas-like character. For positive  $a_{3D}$ , the effective 1D Hamiltonian fails to reproduce the energy spectrum of the molecular-like bound states of the 3D Hamiltonian accurately [see Fig. 4.3(b), and also [BMO03, BTJ03]].

Our main focus is in the lowest-lying energy level with gas-like character. This energy branch is shown in Fig. 4.3(c) on an enlarged scale. A horizontal dashed line shows the lowest internal 3D eigenenergy for two non-interacting spin-polarized fermions (where the anti-symmetry of the wave function enters in the  $z$  coordinate). Our numerical calculations confirm [BMO03] that for  $a_{3D} = a_{3D}^c$  ( $g_{1D} \rightarrow \infty$ ) the two boson system behaves as if it consisted of two non-interacting spin-polarized fermions (TG gas). The energy  $E_{3D}^{int}$  is larger than that of two non-interacting fermions for  $a_{3D} > a_{3D}^c$ , and approaches the first excited state energy of two non-interacting bosons for  $a_{3D} \rightarrow -0$  [indicated by a dotted line in Fig. 4.3(a)].

For positive  $g_{1D}$ , the 1D Schrödinger equation, Eq. 4.10, does not support molecular-like bound states. Consequently, the wave function of the lowest-lying gas-like state is positive definite everywhere. For negative  $g_{1D}$ , however, one molecular-like two-body bound state exists. If  $a_{1D} \ll a_z$  the bound-state wave function is approximately given by the eigenstate  $\psi_{1D}^{int}$  of the 1D Hamiltonian without confinement, Eq. 4.2,

$$\psi_{1D}^{int}(z) = \exp\left(-\frac{|z|}{a_{1D}}\right), \quad (4.15)$$

with eigenenergy  $E_{1D}^{int}$ ,

$$E_{1D}^{int} = -\frac{\hbar^2}{ma_{1D}^2} + \hbar\omega_{\perp}. \quad (4.16)$$

For the highly-elongated trap with  $\lambda = 0.01$  shown in Fig. 4.3(b) and positive  $a_{1D}$  the above binding energy nearly coincides with the exact eigenenergy of the molecular-like bound state obtained



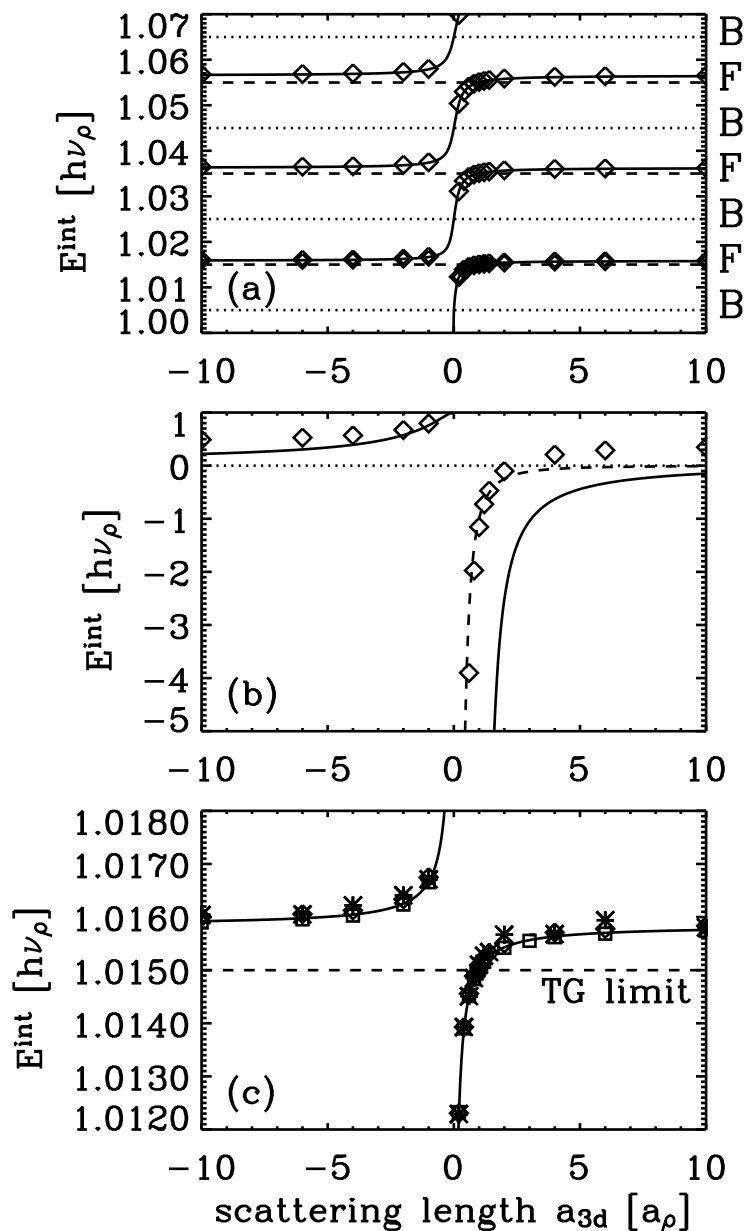


Figure 4.3: Internal eigenenergies  $E^{int}$  as a function of the 3D scattering length  $a_{3D}/a_{\perp}$  for two bosons under highly-elongated confinement with  $\lambda = 0.01$ . (a) 3D  $s$ -wave eigenenergies  $E_{3D}^{int}$  (diamonds) of gas-like states obtained using the short-range model potential  $V^{SR}$ , Eq. 4.14, in a B-spline basis set calculation together with internal 1D eigenenergies  $E_{1D}^{int}$  (solid lines). Excellent agreement between the 3D and 1D energies is found. Horizontal dotted lines show the lowest internal eigenenergies for two non-interacting spin-polarized bosons, while horizontal dashed lines show those for two non-interacting spin-polarized fermions (indicated respectively by “B” and “F” on the right hand side).

(b) Binding energy of molecular-like bound states. In addition to the 3D and 1D energies [diamonds and solid lines, respectively; see (a)], a dashed line shows the 3D binding energy  $-\hbar^2/(ma_{3D}^2)$ .

(c) Enlargement of the lowest-lying gas-like state. In addition to the 3D and 1D energies shown in (a), asterisks show the 3D energies for the interaction potential  $V^{SR}$  calculated using the FN-MC technique, and squares the 1D energies for the contact interaction potential calculated using the FN-MC technique. The statistical uncertainty of the FN-MC energies is smaller than the symbol size. Good agreement between the FN-MC energies (asterisks and squares) and the energies calculated by alternative means (diamonds and solid lines) is found.

from the solution of the transcendental equation (4.11) (solid line). The two-body binding energy, Eq. 4.16, is largest for  $a_{1D} \rightarrow +0$  ( $g_{1D} \rightarrow -\infty$ ); in this case, the molecular-like bound state wave function is tightly localized around  $z = 0$ , where  $z = z_2 - z_1$ . Consider a system with  $a_{1D} \ll a_z$ . For negative  $g_{1D}$  (positive  $a_{1D}$ ), the nodes along the relative coordinate  $z$  of the lowest-lying gas-like wave function (in this case, the first excited state) are then approximately given by  $\pm a_{1D}$ . Thus, imposing the boundary condition  $\psi_{1D}^{int} = 0$  at  $|z| = a_{1D}$  and restricting the configuration space to  $z > a_{1D}$  allows one to obtain an approximation to the eigenenergy of the first excited eigen state. Furthermore, imposing the boundary condition  $\psi_{1D}^{int} = 0$  at  $z = a_{1D}$  is identical to solving the 1D Schrödinger equation for a hard-rod interaction potential  $V^{HR}(z)$  (1.79),

$$V^{HR}(z) = \begin{cases} \infty & \text{for } z < a_{1D} \\ 0 & \text{for } z \geq a_{1D} . \end{cases} \quad (4.17)$$

For  $N = 2$ , asterisks in Fig. 4.3(c) show the fixed-node diffusion Monte Carlo (FN-MC) results obtained using the above fictitious hard-rod potential (see Sec. 4.4.2). Good agreement is found with the exact 1D eigenenergies obtained from Eqs. 4.11-4.12. For  $N > 2$  bosons, our 1D FN-MC algorithm and our usage of the hard-rod equation of state both take advantage of a reduction of configuration space similar to that discussed here for two bosons (see Sec. 4.3 and Chapter 2).

### 4.3 $N$ bosons under quasi-one-dimensional confinement

For tightly-confined trapped gases the 1D regime is reached if the transverse motion of the atoms is frozen, with all the particles occupying the ground state of the transverse harmonic oscillator. At zero temperature, this condition requires that the energy per particle is dominated by the trapping potential,  $E/N = \hbar\omega_{\perp} + \epsilon$ , where the excess energy  $\epsilon$  is much smaller than the separation between levels in the transverse direction,  $\epsilon \ll \hbar\omega_{\perp}$ . In the following we consider situations where the Bose gas is in the 1D regime for any value of the 3D scattering length  $a_{3D}$ . For a fixed trap anisotropy parameter  $\lambda$  and a fixed number of particles  $N$  the above requirement is satisfied if  $N\lambda \ll 1$ . For  $\lambda = 0.01$  and  $N = 10$  (as considered in Sec. 4.4.1) this condition is fulfilled.

To compare the 3D and 1D energetics of a Bose gas, we consider the 3D and 1D Hamiltonian describing  $N$  spin-polarized bosons,

$$\hat{H}_{3D} = \sum_{i=1}^N \left[ -\frac{\hbar^2}{2m} \Delta_i + \frac{1}{2}m (\omega_{\perp}^2 \rho_i^2 + \omega_z^2 z_i^2) \right] + \sum_{i<j}^N V(r_{ij}), \quad (4.18)$$

and

$$\hat{H}_{1D} = \sum_{i=1}^N \left( -\frac{\hbar^2}{2m} \frac{\partial^2}{\partial z_i^2} + \frac{1}{2}m\omega_z^2 z_i^2 \right) + g_{1D} \sum_{i<j}^N \delta(z_{ij}) + N\hbar\omega_{\perp}, \quad (4.19)$$

respectively. The corresponding eigenenergies and eigenfunctions are given by solving the Schrödinger equations,

$$\hat{H}_{3D}\psi_{3D}(\vec{r}_1, \dots, \vec{r}_N) = E_{3D}\psi_{3D}(\vec{r}_1, \dots, \vec{r}_N) \quad (4.20)$$

and

$$\hat{H}_{1D}\psi_{1D}(z_1, \dots, z_N) = E_{1D}\psi_{1D}(z_1, \dots, z_N), \quad (4.21)$$

respectively. In contrast to Sec. 4.2, here we do not separate out the center of mass motion since the MC calculations used to solve the 3D and 1D many-body Schrödinger equations can be most conveniently implemented in Cartesian coordinate space (see Sec. 2.3.2). In the following, we refer to eigenstates of the confined Bose gas with energy greater than  $N\hbar\omega_\perp$  as gas-like states, and to those with energy smaller than  $N\hbar\omega_\perp$  as cluster-like bound states.

Section 4.4.1 compares the energetics of the lowest-lying gas-like state of the 3D Schrödinger equation, Eq. 4.20, obtained using the short-range potential  $V^{SR}$ , Eq. 4.14, with that obtained using the hard-sphere potential  $V^{HS}$  Eq. 1.48. For  $V^{HS}$ , the  $s$ -wave scattering length  $a_{3D}$  coincides with the range of the potential (see Sec. 1.3.2.2). For  $V^{SR}$ , in contrast,  $R$  determines the range of the potential, while the scattering length  $a_{3D}$  is determined by  $R$  and  $V_0$ . For  $a_{3D} \ll a_\perp$ , both potentials give nearly identical results for the energetics of the lowest-lying gas-like state, which depend to a good approximation only on the value of  $a_{3D}$ . For  $a_{3D} \gtrsim a_\perp$ , instead, deviations due to the different effective ranges become visible and only  $V^{SR}$  yields results, which do not depend on the short-range details of the potential and which are compatible with a 1D contact potential.

Section 4.4.1 also discusses the energetics of the 1D Hamiltonian, Eq. 4.19. For small  $|g_{1D}|$ , the energetics of the many-body 1D Hamiltonian are described well by a 1D mean-field equation with non-linearity. For negative  $g_{1D}$ , the mean-field framework describes, for example, bright solitons [CCR00a, KSU03], which have been observed experimentally [SPTH02, KSF<sup>+</sup>02]. For large  $|g_{1D}|$ , in contrast, the system is highly-correlated, and any mean-field treatment will fail. Instead, a many-body description that incorporates higher order correlations has to be used. In particular, the limit  $|g_{1D}| \rightarrow \infty$  corresponds to the strongly-interacting TG regime.

For infinitely strong particle interactions ( $|g_{1D}| \rightarrow \infty$ ), Girardeau shows [Gir60], using the equivalence between the 1D  $\delta$ -function potential and a “1D hard-point potential”, that the energy spectrum of the 1D Bose gas coincides with that of  $N$  non-interacting spin-polarized fermions. The lowest eigenenergy per particle of the trapped 1D Bose gas, Eq. 4.21, is, in the TG limit, given by<sup>1</sup>

$$\frac{E_{1D}^{TG}}{N} = \left( \frac{\lambda N}{2} + 1 \right) \hbar\omega_\perp \quad (4.22)$$

The corresponding gas density is given by the sum of squares of single-particle wave functions

$$n_{1D}^{TG}(z) = \frac{1}{\sqrt{\pi}a_z} \sum_{k=0}^{N-1} \frac{1}{2^k k!} H_k^2(z/a_z) \exp\{-(z/a_z)^2\}, \quad (4.23)$$

with the normalization  $\int_{-\infty}^{\infty} n_{1D}^{TG}(z) dz = N$ . In Eq. 4.23, the  $H_k$  denote Hermite polynomials, and  $z$  denotes the distance measured from the center of the trap. For large numbers of atoms, the density expression in Eq. 4.23 can be calculated using the LDA [DLO01],

$$n_{1D}^{TG}(z) = \frac{\sqrt{2N}}{\pi a_z} \left( 1 - \frac{z^2}{2Na_z^2} \right)^{1/2}. \quad (4.24)$$

The above result cannot reproduce the oscillatory behavior of the exact density, Eq. 4.23, but it does describe the overall behavior properly (see Sec. 4.5).

To characterize the *inhomogeneous* 1D Bose gas further, we consider the many-body Hamiltonian of the *homogeneous* 1D Bose gas,

$$H_{1D}^{hom} = \sum_{i=1}^N -\frac{\hbar^2}{2m} \frac{\partial^2}{\partial z_i^2} + g_{1D} \sum_{i<j}^N \delta(z_{ij}) + N\hbar\omega_\perp \quad (4.25)$$

<sup>1</sup>See, also, footnote on p. 35

By introducing the energy shift  $N\hbar\omega_\perp$ , our classification of gas-like states and cluster-like bound states introduced after Eq. 4.21 remains valid. For positive  $g_{1D}$ ,  $H_{1D}^{hom}$  corresponds to the Lieb-Liniger (LL) Hamiltonian. The gas-like states of the LL Hamiltonian, including its thermodynamic properties, have been studied in detail [LL63, Lie63, YY69]. The energy per particle of the lowest-lying gas-like state, the ground state of the system, is given by

$$\frac{E_{1D}^{LL}(n_{1D})}{N} = \frac{\hbar^2}{2m} e(\gamma) n_{1D}^2, \quad (4.26)$$

where  $n_{1D}$  denotes the density of the homogeneous system, and  $e(\gamma)$  a function of the dimensionless parameter  $\gamma = 2/(n_{1D}|a_{1D}|)$ .

We use the known properties of the LL Hamiltonian to determine properties of the corresponding inhomogeneous system, Eq. 4.19, within the LDA. This approximation provides a correct description of the trapped gas if the size of the atomic cloud is much larger than the characteristic length scale  $a_z$  of the confinement in the longitudinal direction [DLO01]. Specifically, consider the local equilibrium condition,

$$\mu(N) = \hbar\omega_\perp + \mu_{local}[n_{1D}(z)] + \frac{1}{2}m\omega_z^2 z^2, \quad (4.27)$$

where  $\mu_{local}(n_{1D})$  denotes the chemical potential of the homogeneous system with density  $n_{1D}$ ,

$$\mu_{local}(n_{1D}) = \frac{\partial [n_{1D} E_{1D}^{LL}(n_{1D})/N]}{\partial n_{1D}}. \quad (4.28)$$

The chemical potential  $\mu(N)$ , Eq. 4.27, can be calculated using Eq. 4.28 together with the normalization of the density,  $\int_{-\infty}^{\infty} n_{1D}(z) dz = N$ . Integrating the chemical potential  $\mu(N)$  then determines the energy of the lowest-lying gas-like state of the inhomogeneous  $N$ -particle system within the LDA. The LDA treatment is computationally less demanding than solving the many-body Schrödinger equation, Eq. 4.21, using MC techniques. By comparing with our full 1D many-body results we establish the accuracy of the LDA (see Sec. 4.4.1).

For negative  $g_{1D}$ , the Hamiltonian given in Eq. 4.25 supports cluster-like bound states. The ground state energy and eigenfunction of the system are [McG64]

$$\frac{E_{1D}^{hom}}{N} = -\frac{\hbar^2}{6ma_{1D}^2}(N^2 - 1) + \hbar\omega_\perp, \quad (4.29)$$

and

$$\psi_{1D}^{hom}(z_1, \dots, z_N) = \prod_{i < j}^N \exp \left\{ \frac{-|z_i - z_j|}{a_{1D}} \right\}, \quad (4.30)$$

respectively. The eigenstate given by Eq. 4.30 depends only on the relative coordinates  $z_{ij}$ , that is, it is independent of the center of mass of the system. Adding a confinement potential [see Eq. 4.19] with  $\omega_z$  such that  $a_z \gg a_{1D}$  leaves the eigenenergy  $E_{1D}^{hom}$  of this cluster-like bound state to a good approximation unchanged, while the corresponding wave function becomes localized at the center of the trap. This state describes a bright soliton, whose energy can also be determined within a mean-field framework [KSU03]. An excited state of the many-body 1D Hamiltonian with confinement corresponds, *e.g.*, to a state, where  $N - 1$  particles form a cluster-like bound state, *i.e.*, a soliton with

$N - 1$  particles, and where one particle approximately occupies the lowest harmonic oscillator state, *i.e.*, has gas-like character. Similarly, molecular-like bound states can form with fewer particles.

The above discussion implies that the lowest-lying gas-like state of the 1D Hamiltonian with confinement, Eq. 4.19 with negative  $g_{1D}$ , corresponds to a highly-excited state. For dilute 1D systems with negative  $g_{1D}$ , the nodal surface of this excited state can be well approximated by the following nodal surface:  $\psi_{1D} = 0$  for  $z_{ij} = a_{1D}$ , where  $i, j = 1, \dots, N$  and  $i < j$ . As in the two-body case, the many-body energy can then be calculated approximately by restricting the configuration space to regions where the wave function is positive. This corresponds to treating a gas of hard-rods of size  $a_{1D}$ . In the low density limit, we expect that the lowest-lying gas-like state of the 1D many-body Hamiltonian with  $g_{1D} < 0$  is well described by a system of hard-rods of size  $a_{1D}$ .

In addition to treating the full 1D many-body Hamiltonian, we treat the inhomogeneous system with negative  $g_{1D}$  within the LDA. The equation of state of the *uniform* hard-rod gas with density  $n_{1D}$  is given by (1.103) [Gir60]:

$$\frac{E_{1D}^{HR}(n_{1D})}{N} = \frac{\pi^2 \hbar^2 n_{1D}^2}{6m(1 - n_{1D}a_{1D})^2} + \hbar\omega_{\perp}. \quad (4.31)$$

We use this energy in the LDA treatment (see Eqs. 4.26 through 4.28 with  $E_{1D}^{LL}$  replaced by  $E_{1D}^{HR}$ ). The hard-rod equation of state treated within the LDA provides a good description when  $g_{1D}$  is negative, but  $|g_{1D}|$  not too small (see Secs. 4.4.1 and 4.5). To gain more insight, we determine the expansion for inhomogeneous systems with  $N\lambda \ll 1$  using the equation of state for the homogeneous hard-rod gas,

$$\frac{E_{1D}}{N} - \hbar\omega_{\perp} = \hbar\omega_{\perp} \frac{N\lambda}{2} \left( 1 + \frac{128\sqrt{2}}{45\pi^2} \sqrt{N\lambda} \frac{a_{1D}}{a_{\perp}} + \dots \right). \quad (4.32)$$

The first term corresponds to the energy per particle in the TG regime (see Eq. 4.22), the other terms can be considered as small corrections to the TG energy. In the unitary limit, that is, for  $a_{1D}/a_{\perp} = 1.0326$ , expression (4.32) becomes independent of  $a_{3D}$ , and depends only on  $N\lambda$ . Similarly, the linear density in the center of the cloud,  $z = 0$ , is to lowest order given by the TG result,  $n_{1D}^{TG}(0) = \sqrt{2N\lambda}/(\pi a_{\perp})$  (see Eq. 4.24). Section 4.5 shows that the TG density provides a good description of inhomogeneous 1D Bose gases over a fairly large range of negative  $g_{1D}$ .

## 4.4 Energetics of quasi-one-dimensional Bose gases

Table 4.1 summarizes the techniques used to solve the 1D and 3D Hamiltonian, respectively. This table is meant to guide the reader through our result sections. Section 4.4.2 discusses our MC energies for two-particle systems, while Sec. 4.4.1 discusses the energetics for larger systems, calculated within various frameworks. Finally, Sec. 4.5 discusses the stability of quasi-one dimensional Bose gases.

### 4.4.1 Two-body system

Section 4.2 discusses the calculation of the energy spectrum related to the internal motion of two bosons under highly-elongated confinement, Eq. 4.7, using a B-spline basis, and the eigenspectrum related to the internal motion of two bosons under 1D confinement, Eq. 4.9, using Eqs. 4.11 through (4.13). We now use these essentially exact eigenenergies to benchmark our FN-MC calculations.

Hamiltonian	interaction	technique	Section
$\tilde{H}_{3D}$	$V^{HS}$	DMC	4.4.2
$\hat{H}_{3D}$	$V^{SR}$	FN-MC	4.4.1, 4.4.2
$\tilde{H}_{1D}$	$g_{1D} > 0$	DMC	4.4.1, 4.4.2
$\hat{H}_{1D}$	$g_{1D} > 0$	LDA, LL	4.4.2
$\hat{H}_{1D}$	$g_{1D} < 0$	FN-MC	4.4.1, 4.4.2
$\hat{H}_{1D}$	$g_{1D} > 0$	LDA, hard-rod	4.4.2
$\hat{H}_{1D}$	$g_{1D} < 0$	VMC	4.5

Table 4.1: Guide that summarizes the techniques used to solve the 3D and 1D Hamiltonian, Eqs. 4.18 and 4.19, respectively. Column 2 specifies the atom-atom interactions of the many-body Hamiltonian, column 3 lists the techniques used to solve the corresponding many-body Schrödinger equation, and column 4 lists the sections that discuss the results obtained using this approach.

Toward this end, we solve the 3D Schrödinger equation, Eq. 4.18, and the 1D Schrödinger equation, Eq. 4.19, for various interaction strengths for  $N = 2$  and  $\lambda = 0.01$  using FN-MC techniques. The resulting MC energies  $E_{3D}$  and  $E_{1D}$  include the center of mass energy of  $(1 + \lambda/2)\hbar\omega_{\perp}$ . To compare with the internal eigenenergies discussed in Sec. 4.2, we subtract the center of mass energy from the FN-MC energies.

For  $N = 2$ , the lowest-lying gas-like state of the 3D Hamiltonian for the short-range potential  $V^{SR}$  is the first excited eigenstate. Consequently, we solve the 3D Schrödinger equation by the FN-MC technique using the trial wave function  $\psi_T$  given by Eqs. 2.37 and 2.91. Figure 4.4 shows the elliptical nodal surface of the trial wave function  $\psi_T$  (solid lines) together with the essentially exact nodal surface calculated using a B-spline basis set (symbols; see also Sec. 4.2) for  $\lambda = 0.01$  and three different scattering lengths,  $a_{3D}/a_{\perp} = 1, 6$ , and  $-4$ . Notably, the semi-axes  $a$  along the  $\rho$  coordinate is larger than that along the  $z$  coordinate ( $a/b > 1$ ), “opposing” the shape of the confining potential, for which the characteristic length along the  $\rho$  coordinate is smaller than that along the  $z$  coordinate ( $a_{\perp}/a_z < 1$ ). Figure 4.4 indicates good agreement between the essentially exact nodal surface and the parameterization of the nodal surface by an ellipse for  $a_{3D}/a_{\perp} = 1$  and  $6$ ; some discrepancies become apparent for negative  $a_{3D}$ . Since the FN-MC method results in the exact energy if the nodal surface of  $\psi_T$  coincides with the nodal surface of the exact eigenfunction, comparing the FN-MC energies for two particles with those obtained from a B-spline basis set calculation provides a direct measure of the quality of the nodal surface of  $\psi_T$ . Figure 4.3(c) compares the internal 3D energy of the lowest-lying gas-like state calculated using a B-spline basis (diamonds, see Sec. 4.2) with that calculated using the FN-MC technique (asterisks). The agreement between these two sets of energies is — within the statistical uncertainty — excellent for all scattering lengths  $a_{3D}$  considered. We conclude that our parameterization of the two-body nodal surface, Eq. 2.91, is accurate over the whole range of interaction strengths  $a_{3D}$  considered.

We expect that our parameterization of the two-body nodal surface is to a good approximation independent of the confining potential in  $z$  (for small enough  $\lambda$ ). In fact, we expect our nodal surface to closely resemble that of the scattering wave function at low scattering energy of the 3D wave guide Hamiltonian given by Eq. 4.1. To quantify this statement, Fig. 4.5 shows the semi-axes  $a$  and  $b$  (pluses and asterisks, respectively) obtained by fitting an ellipse, see Eq. 2.91, to the nodal surface obtained by solving the Schrödinger equation for the two-body Hamiltonian, Eq. 4.7, using a B-spline basis for various aspect ratios  $\lambda = 0.001, \dots, 1$ , and fixed scattering length,  $a_{3D} = 2a_{\perp}$

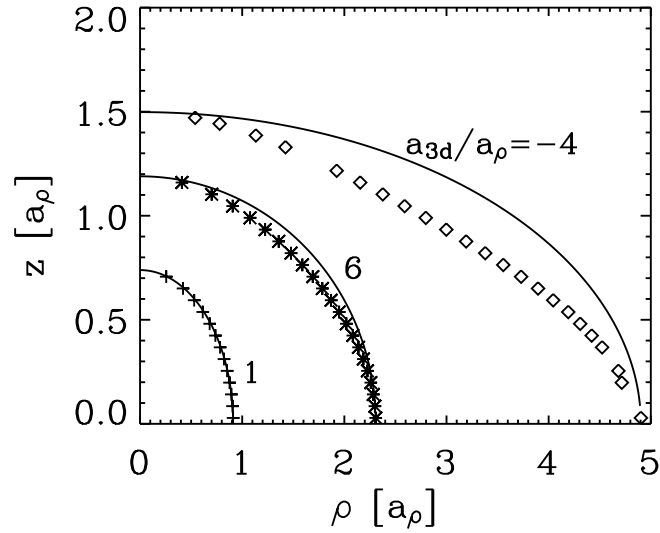


Figure 4.4: Nodal surface of the trial wave function  $\psi_T$  (solid lines, Eq. 2.91) together with the essentially exact nodal surface calculated using a B-spline basis set (symbols) for  $\lambda = 0.01$ ,  $N = 2$ , and three different scattering lengths,  $a_{3D}/a_{\perp} = 1$  (pluses),  $a_{3D}/a_{\perp} = 6$  (asterisks), and  $a_{3D}/a_{\perp} = -4$  (diamonds). The nodal surface is shown as a function of the internal coordinates  $z$  and  $\rho$ . Good agreement between the elliptical nodal surface (solid lines) and the essentially exact nodal surface (symbols) is visible for  $a_{3D}/a_{\perp} = 1$  and  $6$ . Small deviations are visible for  $a_{3D}/a_{\perp} = -4$ .



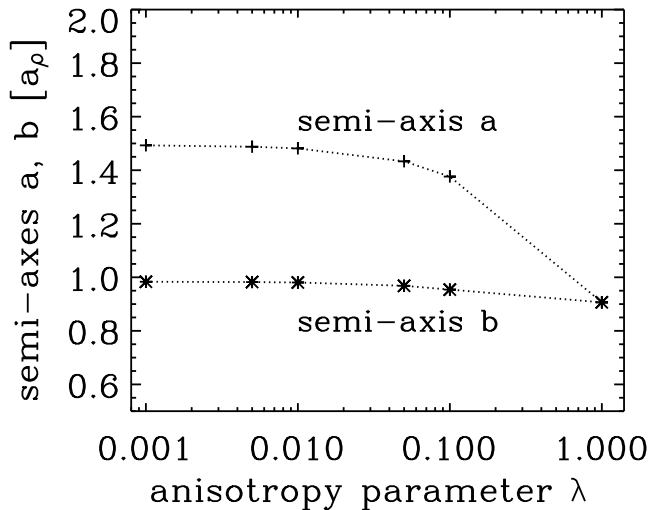


Figure 4.5: Semi-axes  $a$  (pluses) and  $b$  (asterisks) obtained by fitting an ellipse (see Eq. 2.91) to the essentially exact nodal surface for two bosons under cylindrical confinement, calculated using a B-spline basis set as a function of the anisotropy parameter  $\lambda$ , for  $a_{3D}/a_\perp = 2$ . Dotted lines are shown to guide the eye. For  $\lambda \leq 0.01$ , the nodal surface is nearly independent of the anisotropy parameter  $\lambda$ .

(similar results are found for other scattering lengths). Indeed, the nodal surface for a given  $a_{3D}/a_\perp$  is nearly independent of the aspect ratio  $\lambda$  for  $\lambda \leq 0.01$ . These findings for two particles imply that the parameterization of the nodal surface of  $\psi_T$  used in the FN-MC many-body calculations should be good as long as the density along  $z$  is small.

Next, consider the 1D Hamiltonian, Eq. 4.19, for  $N = 2$ . For positive  $g_{1D}$ , the lowest-lying gas-like state is the ground state of the two-body system and we hence use the DMC technique with  $\psi_T$  given by Eqs. 2.64 and 2.65; for  $g_{1D} < 0$ , the lowest-lying gas-like state is the first excited state, and we instead use the FN-MC technique with  $\psi_T$  given by Eqs. 2.64 and 2.66. Figure 4.3 shows the 1D energies of the lowest-lying gas-like state calculated using Eqs. 4.11 through 4.13 (solid line), together with those calculated by the FN-MC technique (squares). We find excellent agreement between these two sets of 1D energies.

The comparison for two bosons between the FN-MC energies and the energies calculated by alternative means serves as a stringent test of our MC codes, since these codes are implemented such that the number of particles enters simply as a parameter.

## 4.4.2 N-body system

This section presents our many-body study, which investigates the properties of quasi-one dimensional Bose gases over a wide range of scattering lengths  $a_{3D}$ . We focus specifically on three distinct regimes: 1)  $0 < a_{3D} < a_{3D}^c$  ( $g_{1D}$  is positive), 2)  $|a_{3D}| \rightarrow \infty$  ( $g_{1D}$  and  $a_{1D}$  are independent of  $a_{3D}$ ; unitary regime); and iii)  $a_{3D} \rightarrow -0$  ( $a_{1D}$  is large and positive; onset of instability). We discuss the energetics



of quasi-one dimensional Bose gases for  $N = 10$ . Our results presented here support our earlier conclusions, which are based on a study conducted for a smaller system, *i.e.*, for  $N = 5$  [ABGG04b].

For small  $\lambda$  ( $\lambda = 0.01$ ), the radial angular frequency  $\omega_\perp$  dominates the eigenenergies of the 3D and of the 1D Schrödinger equation. The shift of the eigenenergy of the lowest-lying gas-like state as a function of the interaction strength is, however, set by the axial angular frequency  $\omega_z$ . To emphasize the dependence of the eigenenergies of the lowest-lying gas-like state on  $\omega_z$ , we report the energy per particle subtracting the constant offset  $\hbar\omega_\perp$ , that is, we report the quantity  $E/N - \hbar\omega_\perp$ .

Consider the lowest-lying gas-like state of the 3D Schrödinger equation. Figure 4.6 shows the 3D energy per particle,  $E_{3D}/N - \hbar\omega_\perp$ , as a function of  $a_{3D}$  for  $N = 10$  under quasi-one dimensional confinement,  $\lambda = 0.01$ , for the hard-sphere two-body potential  $V^{HS}$  (diamonds) and the short-range potential  $V^{SR}$  (asterisks). The energies for  $V^{HS}$  are calculated using the DMC method [with  $\psi_T$  given by Eqs. 2.37 and 2.90], while those for  $V^{SR}$  are calculated using the FN-MC method [with  $\psi_T$  given by Eqs. 2.37 and 2.91]. For small  $a_{3D}/a_\perp$ , the energies for these two two-body potentials agree within the statistical uncertainty. For  $a_{3D} \gtrsim a_\perp$ , however, clear discrepancies are visible. The DMC energies for  $V^{SR}$  cross the TG energy per particle (indicated by a dashed horizontal line),  $E/N - \hbar\omega_\perp = \hbar\omega_\perp \lambda N/2$ , very close to the value  $a_{3D}^c = 0.9684a_\perp$  (indicated by a vertical arrow in Fig. 4.6(b)), while the energies for  $V^{HS}$  cross the TG energy per particle at a somewhat smaller value of  $a_{3D}$ .

For  $a_{3D} > a_{3D}^c$ , the energy for the short-range potential  $V^{SR}$  of the lowest-lying gas-like state increases slowly with increasing  $a_{3D}$ , and becomes approximately constant for large values of  $|a_{3D}|$ . The limit  $|a_{3D}| \rightarrow \infty$  corresponds to the unitary regime (see below). Notably, the 3D energy behaves smoothly as  $a_{3D}$  diverges. The 3D energy slowly increases further for increasing negative  $a_{3D}$ , and changes more rapidly as  $a_{3D} \rightarrow -0$ . The  $|a_{3D}| \rightarrow \infty$  regime and the  $a_{3D} \rightarrow -0$  regime are discussed in more detail below.

To compare our results obtained for the 3D Hamiltonian,  $H_{3D}$ , with those for the 1D Hamiltonian,  $H_{1D}$ , we also solve the Schrödinger equation for  $H_{1D}$ , Eq. 4.19, for the lowest-lying gas-like state. For positive coupling constants,  $g_{1D} > 0$ , the lowest-lying gas-like state is the many-body ground state, and we hence use the DMC method [with  $\psi_T$  given by Eqs. 2.64 and 2.65]. For  $g_{1D} < 0$ , however, the 1D Hamiltonian supports cluster-like bound states. In this case, the lowest-lying gas-like state corresponds to an excited many-body state, and we hence solve the 1D Schrödinger equation by the FN-MC method [with  $\psi_T$  given by Eqs. 2.64 and 2.66].

Figure 4.6 shows the resulting 1D energies per particle,  $E_{1D}/N - \hbar\omega_\perp$ , for the renormalized coupling constant  $g_{1D}$  [squares, Eq. 4.3], and the unrenormalized coupling constant  $g_{1D}^0$  [pluses, Eq. 4.6], respectively. The 1D energies calculated using the two different coupling constants agree well for small  $a_{3D}$ , while clear discrepancies become apparent for  $a_{3D} \gtrsim a_{3D}^c$ . In fact, the 1D energies calculated using the unrenormalized coupling constant  $g_{1D}^0$  approach the TG energy (dashed horizontal line) asymptotically for  $a_{3D} \rightarrow \infty$ , but do not become larger than the TG energy. The 1D energies calculated using the renormalized 1D coupling constant  $g_{1D}$  agree well with the 3D energies calculated using the short-range potential  $V^{SR}$  (asterisks) up to very large values of the 3D scattering length  $a_{3D}$ . In contrast, the 1D energies deviate clearly from the 3D energies calculated using the hard-sphere potential  $V^{HS}$  (diamonds) at large  $a_{3D}$ .

The 1D energies calculated using the renormalized coupling constant agree with the 3D energies calculated using the short-range potential  $V^{SR}$  also for  $|a_{3D}| \rightarrow \infty$ , that is, in the unitary regime, and for negative  $a_{3D}$ . Small deviations between the 1D energies calculated using the renormalized 1D coupling constant  $g_{1D}$  and the 3D energies calculated using the short-range potential  $V^{SR}$  are visible; we attribute these to the finite range of  $V^{SR}$ . The deviations should decrease with decreasing

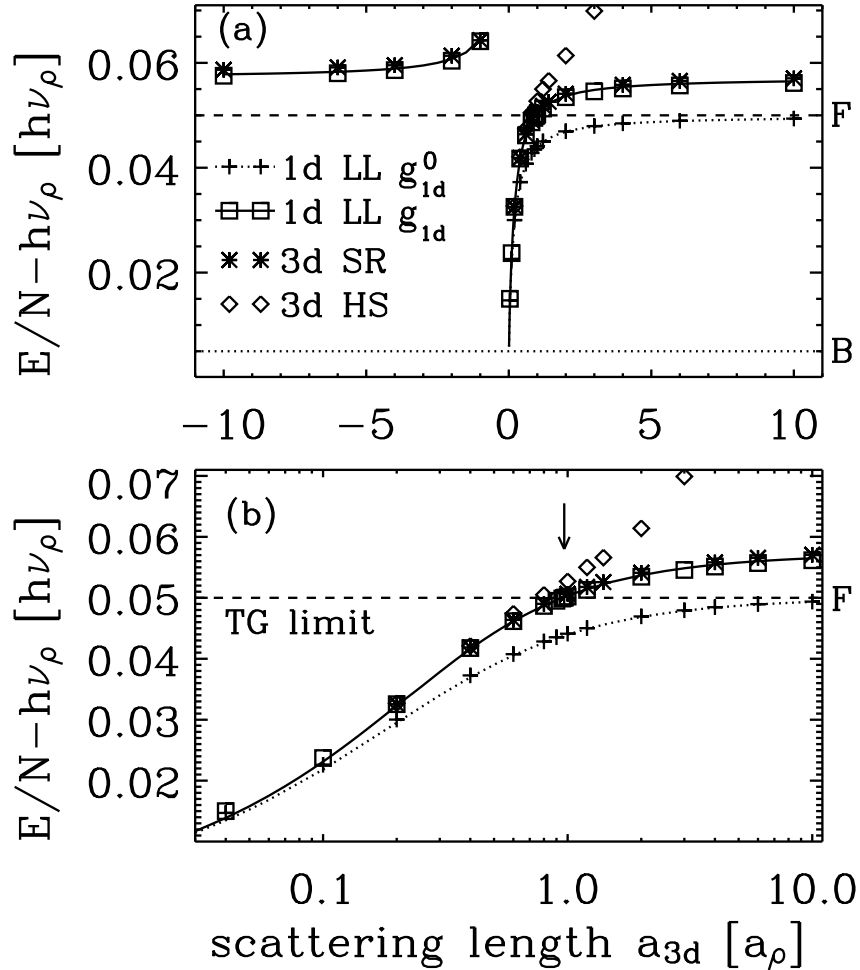


Figure 4.6: Three-dimensional FN-MC energy per particle,  $E_{3D}/N - \hbar\omega_{\perp}$ , calculated using  $V^{HS}$  (diamonds) and  $V^{SR}$  (asterisks), respectively, together with 1D FN-MC energy per particle,  $E_{1D}/N - \hbar\omega_{\perp}$ , calculated using  $g_{1D}$  [squares, Eq. 4.3] and  $g_{1D}^0$  [pluses, Eq. 4.6], respectively, as a function of  $a_{3D}$  [(a) linear scale; (b) logarithmic scale] for  $N = 10$  and  $\lambda = 0.01$ . The statistical uncertainty of the FN-MC energies is smaller than the symbol size. Dotted and solid lines show the 1D energy per particle calculated within the LDA for  $g_{1D}^0$ , Eq. 4.6 [using the LL equation of state] and for  $g_{1D}$ , Eq. 4.3 [using the LL equation of state for  $g_{1D} > 0$ , and the hard-rod equation of state for  $g_{1D} < 0$ ], respectively. A dotted horizontal line indicates the energy per particle of a non-interacting Bose gas, and a dashed horizontal line indicates the TG energy per particle. A vertical arrow the position where  $g_{1D}$ , Eq. 4.3, diverges.

range  $R$  of the short-range potential  $V^{SR}$ . On the other hand,  $R$  determines to first order the energy-dependence of the scattering length  $a_{3D}$ . Thus, usage of an energy-dependent coupling constant  $g_{1D}$  should also reduce the deviations between the 1D energies and the 3D energies calculated using the short-range potential  $V^{SR}$  [GB04]. Such an approach is, however, beyond the scope of this paper.

We conclude that the renormalization of the effective 1D coupling constant  $g_{1D}$  and of the 1D scattering length  $a_{1D}$  are crucial to reproduce the results of the 3D Hamiltonian  $H_{3D}$  when  $a_{3D} \gtrsim a_{\perp}$  and when  $a_{3D}$  is negative.

In addition to treating the 1D many-body Hamiltonian using the FN-MC technique, we solve the 1D Schrödinger equation using the LL equation of state ( $g_{1D} > 0$ ) and the hard-rod equation of state ( $g_{1D} < 0$ ) within the LDA (see Sec. 4.3). These treatments are expected to be good when the size of the cloud is much larger than the harmonic oscillator length  $a_z$ , where  $a_z = \sqrt{\hbar/m\omega_z}$ , that is, when  $a_{3D}$  is large and positive or when  $a_{3D}$  is negative.

Dotted lines in Fig. 4.6 show the 1D energy per particle calculated within the LDA for  $g_{1D}^0$  (using the LL equation of state), while solid lines show the 1D energy per particle calculated within the LDA for  $g_{1D}$ , Eq. 4.3 (using the LL equation of state for  $g_{1D} > 0$ , and the hard-rod equation of state for  $g_{1D} < 0$ ). Remarkably, the LDA energies nearly coincide with the 1D many-body DMC energies calculated using the unrenormalized coupling constant (pluses) and the renormalized coupling constant (squares), respectively. Finite-size effects play a minor role only for  $a_{3D} \ll a_{\perp}$ . Our calculations thus establish that a simple treatment, *i.e.*, a hard-rod equation of state treated within the LDA, describes inhomogeneous quasi-one dimensional Bose gases with negative coupling constant  $g_{1D}$  well over a wide range of 3D scattering lengths  $a_{3D}$ .

For  $a_{3D} \rightarrow -0$ , that is, for large  $a_{1D}$ , the hard-rod equation of state treated within the LDA, cannot properly describe trapped quasi-one dimensional Bose gases, which are expected to become unstable against formation of cluster-like many-body bound states for  $a_{1D} \approx 1/n_{1D}$ . Thus, Sec. 4.5 investigates the regime with negative  $a_{3D}$  in more detail within a many-body framework.

## 4.5 Stability of quasi-one-dimensional Bose gases

This section discusses the stability of *inhomogeneous* quasi-one dimensional Bose gases with negative  $g_{1D}$ , that is, with  $a_{3D} > a_{3D}^c$  and  $a_{3D} < 0$ , against cluster formation. Section 4.4.1 shows that the FN-MC results for the 1D Hamiltonian, Eq. (4.19), are in very good agreement with the FN-MC results for the 3D Hamiltonian. Hence, we carry our analysis out within the 1D model Hamiltonian, Eq. 4.19; we believe that our final conclusions also hold for the 3D Hamiltonian, Eq. 4.18. For the inhomogeneous 1D Hamiltonian  $H_{1D}$ , Eq. 4.19, the lowest-lying gas-like state is a highly-excited state (see Sec. 4.3). We now address the question whether this state is stable quantitatively using the VMC method.

We solve the 1D many-body Schrödinger equation for the Hamiltonian  $H_{1D}$ , Eq. 4.19, by the VMC method using the trial wave function  $\psi_T$  given by Eqs. 2.64 and 2.65. This many-body wave function has the same nodal constraint as a system of  $N$  hard-rods of size  $a_{1D}$ . However, contrary to hard-rods, for interparticle distances smaller than  $a_{1D}$  the amplitude of the wave function increases as  $|z|$  decreases. This effect arises from the attractive nature of the 1D effective potential and gives rise in the many-body framework to the formation of cluster-like bound states as the average interparticle distance is reduced below a certain critical value.

Figure 4.7 shows the resulting VMC energy per particle,  $E_{1D}/N - \hbar\omega_{\perp}$ , for  $N = 5$  and  $\lambda = 0.01$  as a function of the Gaussian width  $\alpha_z$  for four different values of  $a_{1D}$ . For  $a_{1D}/a_{\perp} = 1.0326$  and 2,

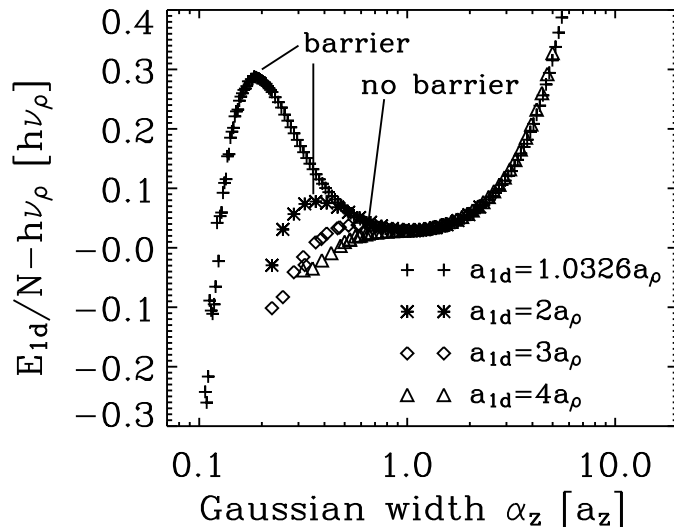


Figure 4.7: VMC energy per particle,  $E_{1D}/N - \hbar\nu_{\rho}$ , as a function of the variational parameter  $\alpha_z$  for  $N = 5$ ,  $\lambda = 0.01$  and  $a_{1D}/a_{\perp} = 1.0326$  (pluses), 2 (asterisks), 3 (diamonds) and 4 (triangles). An energy barrier is present for  $a_{1D}/a_{\perp} = 1.0326$  and 2, but not for  $a_{1D}/a_{\perp} = 4$ .

Fig. 4.7 shows a local minimum at  $\alpha_{z,min} \approx a_z$ . The minimum VMC energy nearly coincides with the FN-MC energy (see also Fig. 4.8), which suggests that our variational wave function provides a highly accurate description of the quasi-one dimensional many-body system. The energy barrier at  $\alpha_z \approx 0.2a_z$  decreases with increasing  $a_{1D}$ , and disappears for  $a_{1D}/a_{\perp} \approx 3$ . We interpret this vanishing of the energy barrier as an indication of instability [BEG98]. For small  $a_{1D}$ , the energy barrier separates the lowest-lying gas-like state from cluster-like bound states. Hence, the gas-like state is stable against cluster formation. For larger  $a_{1D}$ , this energy barrier disappears and the gas-like state becomes unstable against cluster formation.

We stress that our stability analysis should not be confused with that carried out for attractive inhomogeneous 3D systems at the level of mean-field Gross-Pitaevskii theory [BP96]. In fact, a mean-field type analysis of inhomogeneous 1D Bose gases does not predict stability of gas-like states [CKR01]. In our analysis, the emergence of local energy minima in configuration space is due to the structure of the two-body correlation factor  $f_2(z)$  entering the VMC trial wave function  $\psi_T$ , Eqs. 2.64 and 2.65. It is a many-body effect that cannot be described within a mean-field Gross-Pitaevskii framework.

To additionally investigate the dependence of stability on the number of particles, Fig. 4.8 shows the VMC energy for  $\lambda = 0.01$  as a function of the variational parameter  $\alpha_z$  for different values of  $N$ ,  $N = 5, 10$  and 20. The scattering length  $a_{1D}$  is fixed at the value corresponding to the unitary regime,  $a_{1D} = 1.0326a_{\perp}$ . Figure 4.8 shows that the height of the energy barrier decreases for increasing  $N$ . Figures 4.7 and 4.8 suggest that the stability of 1D Bose gases depends on  $a_{1D}$  and  $N$ . To extract a functional dependence, we additionally perform variational calculations for larger  $N$  and different values of  $\lambda$  and  $a_{1D}$ . We find that the onset of instability of the lowest-lying gas-like state can be

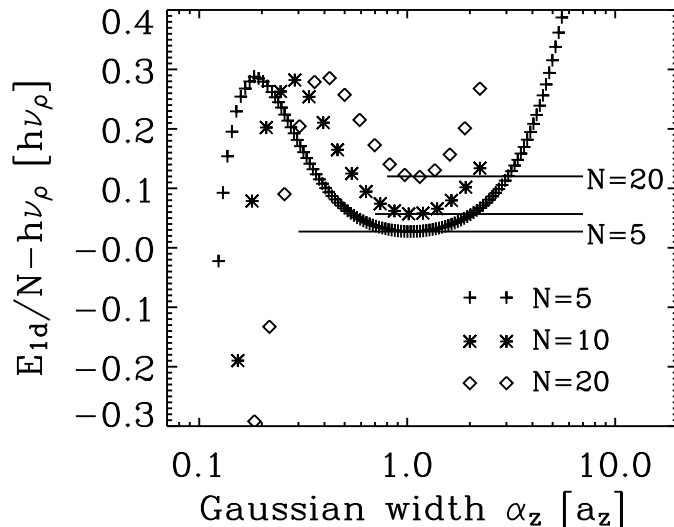


Figure 4.8: VMC energy per particle,  $E_{1D}/N - \hbar\nu_\rho$ , as a function of the variational parameter  $\alpha_z$  for  $a_{1D}/a_\perp = 1.0326$  (corresponding to the unitary regime),  $\lambda = 0.01$ , and  $N = 5$  (pluses), 10 (asterisks), and 20 (diamonds). (The  $N = 5$  data are also shown in Fig. 4.7.) The height of the energy barrier decreases with increasing  $N$ . Horizontal solid lines show the corresponding energies for  $N = 5, 10$  and 20 obtained using the FN-MC technique, which are in excellent agreement with the VMC energy obtained for  $\alpha_z = \alpha_{z,min}$ .

described by the following criticality condition

$$\sqrt{N\lambda} \frac{a_{1D}}{a_\perp} \simeq 0.78, \quad (4.33)$$

or, equivalently, by  $\sqrt{N}a_{1D}/a_z \simeq 0.78$ . Our 1D many-body calculations thus suggest that the lowest-lying gas-like state is stable if  $\sqrt{N\lambda}a_{1D}/a_\perp \lesssim 0.78$ , and that it is unstable if  $\sqrt{N\lambda}a_{1D}/a_\perp \gtrsim 0.78$ . The stability condition, Eq. (4.33), implies that reducing the anisotropy parameter  $\lambda$  should allow stabilization of relatively large quasi-one dimensional Bose gases.

To express the stability condition, Eq. 4.33, in terms of the 1D gas parameter  $n_{1D}a_{1D}$ , where  $n_{1D}$  denotes the linear density at the trap center, we approximate the density for negative  $g_{1D}$  by the TG density, Eq. 4.24. Figure 4.9 compares the TG density with that obtained from the VMC calculations for  $N = 5, 10$  and 20 and values of  $a_{1D}/a_\perp$  close to the criticality condition, Eq. 4.33. The density at the center of the trap is described by the TG density to within 10%. Since the TG density at the trap center is given by  $\sqrt{2N}/(\pi a_z)$  (see Eq. 4.24), the stability condition, Eq. 4.33, expressed in terms of the 1D gas parameter reads  $n_{1D}a_{1D} \lesssim 0.35$ .

## 4.6 Conclusions

This paper presents a thorough study of the properties of inhomogeneous, harmonically-confined quasi-one dimensional Bose gases as a function of the 3D scattering length  $a_{3D}$ . The behavior of

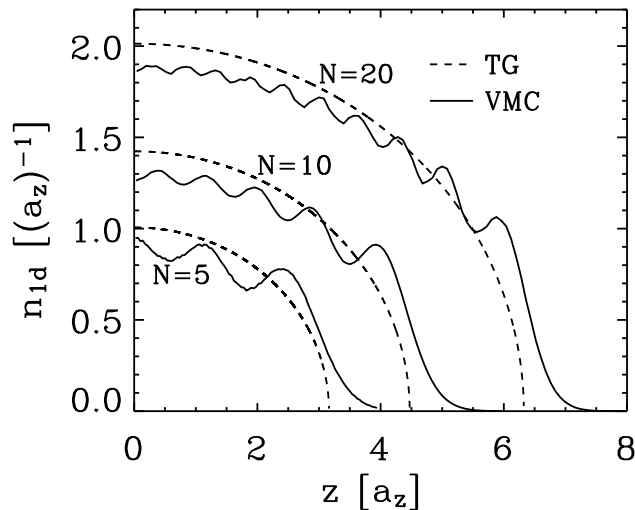


Figure 4.9: TG density [Eq. 4.24, dashed lines] as a function of  $z$  together with VMC density (solid lines), obtained by solving the 1D many-body Schrödinger equation, Eq. 4.21, for  $N = 5$  and  $a_{1D}/a_{\perp} = 3.6$ , for  $N = 10$  and  $a_{1D}/a_{\perp} = 2.6$ , and for  $N = 20$  and  $a_{1D}/a_{\perp} = 1.8$ . The TG density at the center of the trap,  $z = 0$ , deviates from the VMC density at the center of the trap by less than 10 %.

confined Bose gases strongly depends on the ratio of the harmonic oscillator length in the tight transverse direction,  $a_{\perp}$ , to the interaction range  $R$  and to the average interparticle distance  $1/n^{1/3}$ , where  $n$  denotes the 3D central density.

Quasi-1D bosonic gases have been realized experimentally in highly-elongated harmonic traps. The strength of atom-atom interactions can be varied over a wide range by tuning the value of the 3D  $s$ -wave scattering length  $a_{3D}$  through application of an external magnetic field in the proximity of a Feshbach resonance. For  $R \ll a_{\perp}$ , the scattering length  $a_{3D}$  determines to a good approximation the effective 1D scattering length  $a_{1D}$  and the effective 1D coupling constant  $g_{1D}$ , which can be, just as the 3D coupling constant, tuned to essentially any value including zero and  $\pm\infty$ . By exploiting Feshbach resonance techniques, one should be able to achieve strongly-correlated quasi-one dimensional systems. The strong coupling regime is achieved for  $1/n^{1/3} \gg a_{\perp}$ , it includes the TG gas, where a system of interacting bosons behaves as if it consisted of non-interacting spinless fermions, and the so-called unitary regime, where the properties of the gas become independent of the actual value of  $a_{3D}$ . In the unitary regime, the gas is dilute, that is,  $nR^3 \ll 1$ , and at the same time strongly-correlated, that is,  $n|a_{3D}|^3 \gg 1$ .

The present analysis is carried out within various theoretical frameworks. We obtain the 3D energetics of the lowest-lying gas-like state of the system using a microscopic FN-MC approach, which accounts for all degrees of freedom explicitly. The resulting energetics are then used to benchmark our 1D calculations. Full microscopic 1D calculations for contact interactions with renormalized coupling constant  $g_{1D}$  result in energies that are in excellent agreement with the full 3D energies. This agreement implies that a properly chosen many-body 1D Hamiltonian describes quasi-one dimensional

Bose gases well.

We also consider the LL and the hard-rod equation of state of a 1D system treated within the LDA. These approaches provide a good description of the energy of the lowest-lying gas-like state for as few as five or ten particles. Finite size effects are to a good approximation negligible. Our detailed microscopic studies suggest that these LDA treatments provide a good description of quasi-one dimensional Bose gases. In particular, we suggest a simple treatment of 1D systems with negative  $g_{1D}$  using the hard-rod equation of state.

Finally, we address the question of whether the lowest-lying gas-like state of inhomogeneous quasi-one dimensional Bose gases is actually stable. We find, utilizing a variational 1D many-body framework, that the lowest-lying gas-like state is stable for negative coupling constants, up to a minimum critical value of  $|g_{1D}|$ . Our numerical results suggest that the stability condition can be expressed as  $n_{1D}a_{1D} \simeq 0.35$ . Since our conclusions are derived from variational 1D calculations, more thorough microscopic calculations are needed to confirm our findings. We believe, however, that our findings will hold even in a 3D framework or when three-body recombination effects are included explicitly.

While our study was performed for inhomogeneous quasi-one dimensional Bose gases, many findings also apply to homogeneous quasi-one dimensional Bose gases. Furthermore, the Fermi-Bose mapping [Gir60, GB04, CS99, GO03], which allows one to map an interacting 1D gas of spin-polarized fermions to an interacting 1D gas of spin-polarized bosons, suggests that many of the results presented here for quasi-one dimensional Bose gases may directly apply to quasi-one dimensional Fermi gases.





# Chapter 5

## Ground state properties of a one-dimensional Bose gas

### 5.1 Introduction

Recent progress achieved in techniques of confining Bose condensates has lead to experimental realizations of quasi-one dimensional systems[GVL<sup>+</sup>01, SKC<sup>+</sup>01, DHR<sup>+</sup>01, RGT<sup>+</sup>03, MSKE03, TOH<sup>+</sup>04]. The 1D regime is reached in highly anisotropic traps, where the axial motion of the atoms is weakly confined while the radial motion is frozen to zero point oscillations by the tight transverse confinement. Another possible realization of a quasi one-dimensional system could be a cold gas on a chip. The possibility of an experimental observation revived interest in analytical description of the properties of a one-dimensional bose gas. To first approximation one parameter, the one-dimensional scattering length  $a_{1D}$ , is sufficient to describe the interatomic potential, which in this case can be modeled by repulsive  $\delta$ -function pseudopotential. Many properties of this integrable model like the ground state energy[LL63], excitation spectrum[Lie63], thermodynamic functions at finite temperature[YY69] were obtained exactly already in 60-ies using the Bethe *ansatz* method. Gaudin in his book [Gau83] devoted to this powerful method writes that so far almost nothing is known about the correlation functions, apart from the case of impenetrable bosons [Len64, VT79, JMMS80]. Lately active work was carried out in this direction, there are recent calculations of short-range expansion of the one-body density matrix[OD03], the value at zero of the two-body correlation function[GS03b]. Still there are no exact calculations of the correlation functions present in the literature.

We use Diffusion Monte Carlo method (Sec. 2.3), which is exact apart from the statistical uncertainty, in order to address the problem of  $\delta$ -interacting bosons in the ground state of a homogeneous system. We argue that the trial wave function we propose provides a very good description of the ground state wave function. As a benchmark test for our DMC calculation we recover the equation of state which is known exactly[LL63]. For the first time we find complete description of the one-body density matrix and pair distribution function. We show that our results are in agreement with known analytical predictions. We calculate momentum distribution and static structure factor which are accessible in an experiment. We calculate exactly the value of three-body correlation function which is very important quantity as it governs rates of inelastic processes. Also we address effects of the external confinement.

We present study of the correlation functions of a homogeneous system. We find the one-body density matrix at all densities. We calculate the pair-distribution function. Fourier transform relate those quantities to the momentum distribution and the static structure factor, which are accessible

experimentally. We calculate a momentum distribution in a trapped system. We expand our prediction on homogeneous three-body correlation function, relevant for the estimation of three-body collision rate, pair-distribution function and static structure factor in traps. We discuss in details known analytical limits and propose a precise expression for the decay coefficient of the one-body density matrix. We provide relevant details of our Monte Carlo study. In particular it is argued that the trial wave function we construct provides good description and variational energy is only slightly higher than the exact one.

The structure of this chapter is as follows. In section 5.2 we discuss a model used to describe a cold one-dimensional gas and make a summary of known analytical expressions for correlation functions. Section 5.3 is devoted to a brief description of the Monte Carlo scheme used for numerical solution of the Schrödinger equation and investigation of a finite size errors that is relevant for infinite system simulation. The trial wave function used for the importance sampling is discussed in detail. We present the result for a homogeneous system in section 5.4. One-body density matrix, pair distribution function and three-body correlation function are calculated and compared to known exact results and analytical expansions. The information about the momentum distribution and static structure factor is extracted by means of the Fourier transformation. In section 5.5 we discuss effects of the external trapping. Modifications to the construction of the trial wave function are discussed. The results for the pair distribution function and momentum distribution are presented. Finally, in Section 5.6 we draw our conclusions.

## 5.2 Lieb-Liniger Hamiltonian

A cold bosonic gas confined in a waveguide or in a very elongated trap can be described in terms of a one-dimensional model if the energy of the motion in the long longitudinal direction is insufficient to excite the levels of transverse confinement. Further, if the range of interparticle interaction potential is much smaller than the characteristic length of the external confinement, one parameter is sufficient to describe the interaction potential, namely the one-dimensional  $s$ -wave scattering length. In this case the particle-particle interactions can be safely modeled by a  $\delta$ -pseudopotential. Such a system is described by the homogeneous Lieb-Liniger Hamiltonian

$$\hat{H}_{LL} = -\frac{\hbar^2}{2m} \sum_{i=1}^N \frac{\partial^2}{\partial z_i^2} + g_{1D} \sum_{i<j} \delta(z_i - z_j), \quad (5.1)$$

where the positive one-dimensional coupling constant is related to the one-dimensional  $s$ -wave scattering length  $g_{1D} = -2\hbar^2/ma_{1D}$  (1.69) with  $m$  being mass of an atom. In the presence of tight harmonic transverse confinement (we denote the oscillator length as  $a_{\perp}$ , the one-dimensional scattering length  $a_{1D}$  was shown [Ols98] to experience a resonant behavior in terms of  $a_{3D}$  due to virtual excitations of transverse oscillator levels

$$a_{1D} = -a_{\perp} \left( \frac{a_{\perp}}{a_{3D}} - 1.0326 \right) \quad (5.2)$$

By tuning the  $a_{3D}$  by Feshbach resonance value of  $a_{1D}$  can be widely varied. Without using the Feshbach resonance one typically has  $a_{3D} \ll a_{\perp}$  condition fulfilled. In this situation the relation (5.2) simplifies  $a_{1D} = -a_{\perp}^2/a_{3D}$  (compare with the mean-field result (1.125)).

All properties in this model depend only on one parameter, the dimensionless density  $n_{1D}a_{1D}$ . On the contrary to 3D case, where at low density the gas is weakly interacting, in 1D system small

values of the gas parameter  $n_{1D}a_{1D}$  mean strongly correlated system. This peculiarity of 1D system can be easily seen by comparing the characteristic kinetic energy  $\hbar^2 n^{2/D}/2m$ , with  $D$  being number of dimensions, to the mean-field interaction energy  $gn$ . The equation of state of this model first was obtained Lieb and Liniger [LL63] by using the Bethe *ansatz* formulation. The energy of the system is conveniently expressed as

$$\frac{E}{N} = e(n_{1D}|a_{1D}|) \frac{\hbar^2 n_{1D}^2}{2m}, \quad (5.3)$$

where the function  $e(n_{1D}|a_{1D}|)$  is obtained by solving a system of LL integral equations. In the mean-field regime  $n_{1D}a_{1D} \gg 1$  the energy per particle is linear in the density  $E^{GP}/N = g_{1D}n_{1D}/2$ , although in the strongly correlated regime the dependence is quadratic (1.102):  $E^{TG}/N = \pi^2 n_{1D}^2/6m$ . Still an explicit general expression of the energy for an arbitrary value of  $n_{1D}a_{1D}$  is not known. The dependence of the energy on the density resulting from numerical solution of the LL integral equations is plotted in Fig. 5.1. On the same figure we present the energy obtained by a different method of solving the Schrödinger equation, the Diffusion Monte Carlo method (see section 5.3). Results of both methods are in perfect coincidence.

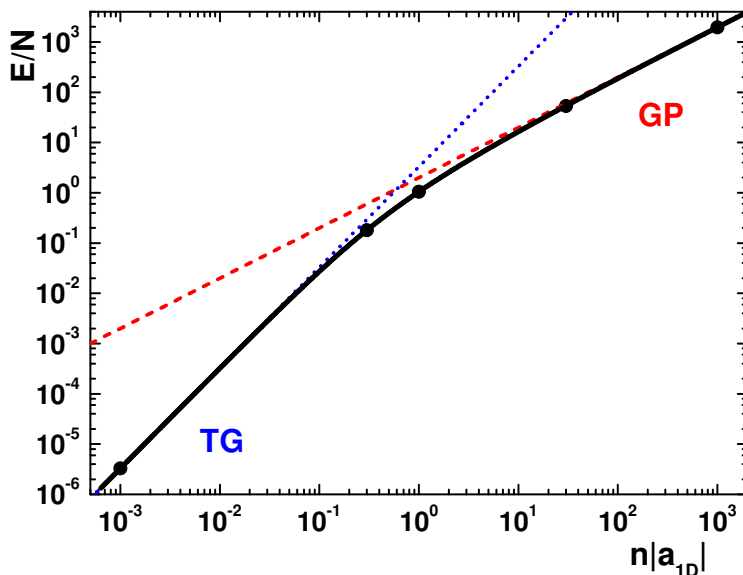


Figure 5.1: Energy per particle: Bethe *ansatz* solution (solid line), DMC (circles), GP limit (dashed line), TG limit (dotted line). Energies are in units of  $\hbar^2/(ma_{1D}^2)$ .

The chemical potential is defined as the derivative of the total energy with respect to the number of particles  $\mu = \partial E/\partial N$ . The healing length  $\xi = \hbar/(\sqrt{2}mc)$  is related to the speed of sound  $c$ , which in turn can be extracted from the chemical potential  $mc^2 = n_{1D} \frac{\partial}{\partial n_{1D}} \mu$ .

These quantities can be obtained in an explicit way in the regime of strong interactions  $n_{1D}a_{1D} \ll 1$ . In this limit the energy of incident particle is not sufficient to tunnel through the particle-particle interaction potential. Two particles can never be at the same point in space, which together with spatial peculiarity of 1D system acts as an effective Fermi exclusion principle. Indeed, in this limit the system of bosons acquires many fermi-like properties. There exist a direct mapping of the

wave function of strongly interacting bosons onto a wave function of noninteracting fermions due to Girardeau [Gir60]. We will refer to this limit as the Tonks-Girardeau limit. The speed of sound in this gas is related to the fermi momentum of the one-component fermi system at the same density  $c = p_F/m = \pi n_{1D} \hbar/m$ . The chemical potential equals to the fermi energy (1.101)  $\mu = \pi^2 n_{1D}^2 / 2m$  (see  $n_{1D} a_{1D} \ll 1$  limit in the Fig. 5.1).

Further, due to this mapping one knows the pair distribution function, which exhibits Friedel-like oscillations

$$g_2(z) = 1 - \frac{\sin^2 \pi n_{1D} z}{(\pi n_{1D} z)^2} \quad (5.4)$$

The static structure factor of the TG gas is given by

$$S(k) = \begin{cases} |k|/(2\pi n_{1D}), & |k| < 2\pi n_{1D} \\ 1, & |k| > 2\pi n_{1D} \end{cases} \quad (5.5)$$

The one-body density matrix  $g_1(z)$  was calculated in terms of series expansion at small and large distances [Len64, VT79, JMMS80]. Its slow long-range decay

$$g_1(z) = \frac{\sqrt{\pi} e 2^{-1/3} A^{-6}}{\sqrt{z n}}, \quad n_{1D} |a_{1D}| \ll 1 \quad (5.6)$$

leads to an infrared divergence in the momentum distribution  $n(k) \propto 1/\sqrt{|k|}$ .

Beyond the TG regime full expressions of the correlation functions are not known. The long-range asymptotics (*i.e.* distances much larger than the healing length  $\xi$ ) can be obtained from the hydrodynamic theory of the low-energy phonon-like excitations [RC67, Sch77, Hal81, KBI93]. One finds following power-law decay (1.199)

$$g_1(z) = \frac{C_{asympt}}{|z n_{1D}|^\alpha}, \quad (5.7)$$

where  $\alpha = mc/(2\pi \hbar n_{1D})$  and coefficient  $C_{asympt}$  is given by formula (5.15). In the TG regime  $c = \pi \hbar n_{1D}/m$  and thus  $\alpha = 1/2$  as anticipated above. In the opposite GP regime ( $n_{1D} |a_{1D}| \gg 1$ ), the result is  $\alpha = 1/(\pi \sqrt{2n_{1D} |a_{1D} d|})$  which decreases as  $n_{1D} |a_{1D}|$  increases. That means that in the Lieb-Liniger theory  $\alpha \leq 1/2$ . Instead in the super-Tonks regime one deals with special situation  $\alpha > 1/2$ . In the mean-field limit the relation of the coefficient of proportionality in Eq. 5.7 to  $\alpha$  was established by Popov [Pop80] Of course power-law decay of the non-diagonal element of the one-body density matrix (5.6,5.7) does not support long-range order and excludes the existence of Bose-Einstein condensation in one dimension even at zero temperature [Sch63]. The behavior of the momentum distribution for  $|k| \ll 1/\xi$  follows immediately from (5.7)

$$n(k) = C_{asympt} \left| \frac{2n_{1D}}{k} \right|^{1-\alpha} \frac{\sqrt{\pi} \Gamma(\frac{1}{2} - \frac{\alpha}{2})}{\Gamma(\frac{\alpha}{2})} \quad (5.8)$$

Furthermore, the hydrodynamic theory allows one to calculate the static structure factor in the long-wavelength regime  $|k| \ll 1/\xi$ . One finds the well-known Feynman result [Fey54]

$$S(k) = \frac{\hbar |k|}{2mc} \quad (5.9)$$

Recently, the short range behavior of the one-, two-, and three-body correlation functions has also been described. The value at  $z = 0$  of the pair correlation function at arbitrary density can be obtained from the equation of state through the Hellmann-Feynman theorem [GS03b]:

$$g_2(0) = -\frac{(n_{1D}|a_{1D}|)^2}{2}e', \quad (5.10)$$

where the derivative of  $e$  is taken with the respect to the gas parameter  $n_{1D}|a_{1D}|$ .

This quantity vanishes in the TG regime and approaches unity in the GP regime. The “excluded volume” correction (1.106) allows one to specify its behavior close to the TG region:

$$g_2(0) = \frac{\pi^2 n_{1D}^2 |a_{1D}|^2}{3}, \quad n_{1D}|a_{1D}| \ll 1 \quad (5.11)$$

The  $z = 0$  value of the three-body correlation function was obtained in a perturbative manner in the regions of strong and weak interactions [GS03b]. Similarly to  $g_2(0)$ , it quickly decays in the TG limit

$$g_3(0) = \frac{(\pi n a_{1D})^6}{60}, \quad n_{1D} a_{1D} \ll 1, \quad (5.12)$$

and goes to a constant value in the GP regime:

$$g_3 = 1 - \frac{6\sqrt{2}}{\pi\sqrt{n a_{1D}}}, \quad n_{1D} a_{1D} \gg 1. \quad (5.13)$$

Furthermore, recently the first few terms of the short-range series expansion of the one-body correlation function have been calculated in [OD03]

$$g_1(z) = 1 - \frac{1}{2}(e + e'n_{1D}|a_{1D}|)|n_{1D}z|^2 + \frac{e'}{6}|n_{1D}z|^3 \quad (5.14)$$

This expansion is applicable for distances  $|n_{1D}z| \ll 1$  and arbitrary densities.

## 5.3 Quantum Monte Carlo Method

We use Diffusion Monte Carlo (DMC) technique in order to obtain the ground state properties of the system. A good choice of the trial wave-function is crucial for the efficiency of the calculation. In order to prove that our trial wave-function is indeed very close to the true ground state wave function we perform calculation of the variational energy  $E_{VMC}$  which provides an upper-bound to the ground state energy (see Table 5.1). We find that the variational energy is at maximum 2% higher than the energy of the DMC calculation, which coincides with the exact solution based on the use of the Bethe *ansatz* (see, also, Fig. 5.1).

In a homogeneous system we use the Bijl-Jastrow construction (2.37) of the trial wave function. The construction of the two-body term  $f_2(z)$  is described in Sec. 2.5.4.5. The  $|z| < R$  part corresponds to the exact solution of the two-body problem and provides a correct description of short-range correlations. Long-range correlations arising from phonon excitations are instead accounted for by the functional dependence of  $f(z)$  for  $z > Z$  [RC67]. The value of the matching point  $R$  is a variational parameter which we optimize using the variational Monte Carlo (VMC). The TG wave

$n_{1D}a_{1D}$	$E_{LL}/N$	$E_{VMC}/N$
$10^{-3}$	$1.6408 \cdot 10^{-6}$	$1.64(1) \cdot 10^{-6}$
0.03	$1.3949 \cdot 10^{-3}$	$1.3956(3) \cdot 10^{-3}$
0.3	$9.0595 \cdot 10^{-2}$	$9.089(3) \cdot 10^{-2}$
1	0.5252	0.535(3)
30	26.842	27.121(3)
$10^3$	981.15	981.72(6)

Table 5.1: Energy per particle for different values of the dimensionless density  $n_{1D}a_{1D}$ : exact result  $E_{LL}$  obtained by solving Lieb-Liniger equations, variational result  $E_{VMC}$  obtained by optimization the trial wave function 2.55. Variational energy gives the upper bound to the exact energy. DMC calculation recovers the exact result  $E_{LL}$ .

function (2.5.4.1) is obtained as a special case of our trial wave function (2.55) for  $R = B = L/2$  and  $kL = \pi$ .

The level of accuracy of the trial wave function is particularly important for the calculation of the of  $g_1(z)$ . Instead, the pair distribution function  $g_2(z)$  is calculated using the method of “pure” estimators, unbiased by the choice of the trial wave function [CB95]. Due to non local property of the one-body density matrix, the function  $g_1(z)$  can instead be obtained only through the extrapolation technique. For an operator  $\hat{A}$ , which does not commute with the Hamiltonian, the output of the DMC method is a “mixed” estimator  $\langle \Psi_0 | \hat{A} | \psi_T \rangle$ . Combined together with the variational estimator  $\langle \psi_T | \hat{A} | \psi_T \rangle$  obtained from the VMC calculation it can be used for extrapolation to the “pure” estimator by the rule  $\langle \Psi_0 | \hat{A} | \Psi_0 \rangle = 2 \langle \Psi_0 | \hat{A} | \psi_T \rangle - \langle \psi_T | \hat{A} | \psi_T \rangle$ . Of course, this procedure is very accurate only if  $\psi_T \simeq \Psi_0$ . We find that DMC and VMC give results for  $g_1(z)$  which are very close and we believe that the extrapolation technique is in this case exact.

We consider  $N$  particles in a box of size  $L$  with periodic boundary conditions. In the construction of the trial wave function we have ensured that the two-body term  $f_2$  is uncorrelated at the boundaries  $f_2(\pm L/2) = 1$ . In order to estimate properties of an infinite system we we increase number of particles and study convergence in the quantities of interest. The dependence on the number of particles (finite size effects) are more pronounced at the large density where the correlations extend up to large distances. Out of the quantities we measured, the one-body density matrix is the most sensitive to finite size corrections. As an example in Fig. 5.2 we show  $g_1(z)$  at density  $n_{1D}a_{1D} = 30$  for 50, 100, 200 and 500 particles and make comparison it with the asymptotic  $z \rightarrow \infty$  behavior. We find largest finite size effects near the maximal distance  $L/2$  for which the one-body density matrix can be calculated. Also we see a dependence of the slope on the number of particles. Already for 500 particles we find the correct slope of the one-body density matrix. For the smaller densities, where finite size effects are smaller, it is sufficient to have  $N = 500$ .

## 5.4 Homogeneous system

We calculated the pair distribution matrix for a number of densities ranging from very small value of the gas parameter  $n_{1D}a_{1D} \ll 1$  (TG regime) up large densities  $n_{1D}a_{1D} \gg 1$  (GP regime). The results are presented in the Fig. 5.3. In the GP regime the correlations between particles are very weak and  $g_2(z)$  arrives very quickly at the bulk value. Decreasing the  $|a_{1D}|$  (thus making the coupling

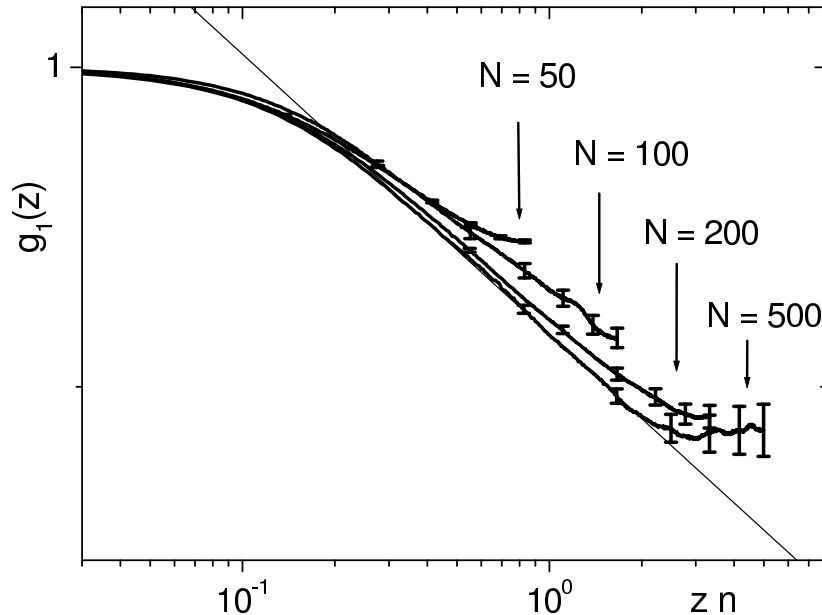


Figure 5.2: Example of the finite size effects in the calculation of the one-body density matrix at  $n_{1D}a_{1D} = 30$ .

constant  $g_{1D}$  larger) we enhance beyond-mean field effects and enforce correlations. For the smallest considered value of the gas parameter  $n_{1D}a_{1D} = 10^{-3}$  we see oscillations in the pair distribution function, which, in this sense becomes more similar to the one of a liquid, rather than of a gas. At the same density we compare the pair distribution function with the one of the TG gas and find no visible difference.

On the same Figure we plot predictions for the value of the pair distribution function at zero and find perfect agreement with the analytical prediction. In the TG regime particles never meet each other and consequently  $g_2(0) = 0$ . Making the interaction between the particles weaker we find finite probability of two particles coming close to each other according to the Eq. 5.10. As we go further into the direction of the GP the interaction potential becomes more transparent and we approach the ideal gas limit  $g_2(0) = 1$ .

In the Fig. 5.4 we present the static structure factor obtained from  $g_2(z)$  according to relation (1.31). At the smallest density  $n_{1D}|a_{1D}| = 10^{-3}$  our points lie exactly on the top of the  $S(k)$  of the TG gas (Eq. 5.5). For all densities the small-momenta part of the structure factor comes from generation of a phonon. We compare DMC results with the Feynman prediction (Eq. 5.9). We see that in the strongly correlated regime phononic description works well even to values of the momenta of the order of inverse density  $n_{1D}^{-1}$ , although in the MF regime the healing length becomes significantly larger than the mean interparticle distance leading to earlier deviations.

We calculate the value at zero of the three-body correlation function (1.22) over a large range of densities. At large density  $n_{1D}|a_{1D}| = 10^4$  the probability of three-body collisions is high. Making the density smaller we find decrease in the value of  $g_3(0)$ . Close to the MF limit the result of the Bogoliubov theory (Eq. 5.13) provides fairly good description of  $g_3(0)$  (see. Fig. 5.5). Further decrease in the density leads to fast decay of three-body collision rate and it becomes vanishing at values of the gas parameter smaller than one. In order to resolve the law of the decay we plot same data on the log-log scale (Fig. 5.6) and show that the decay goes with the forth power of the gas



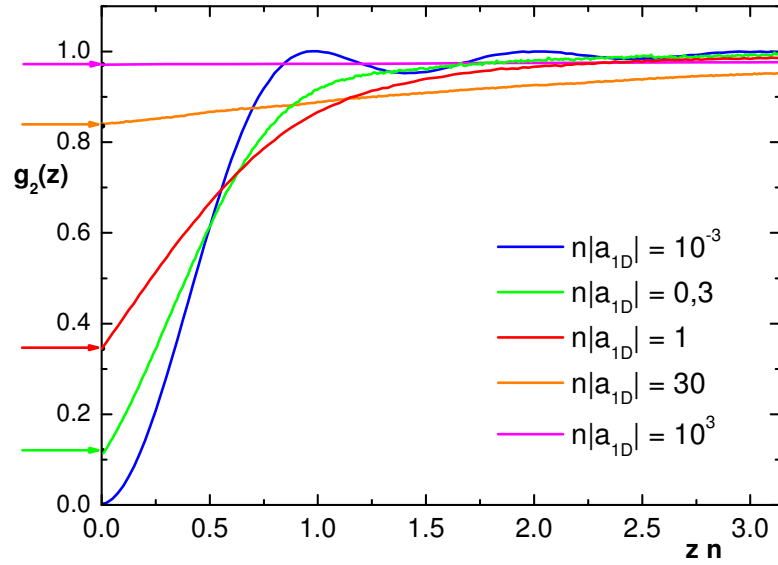


Figure 5.3: Pair distribution function for different values of the gas parameter. In ascending order of the value at zero  $n_{1D}|a_{1D}| = 10^{-3}, 0,3, 1, 30, 10^3$ . Arrows indicate the value of  $g_2(0)$  as obtained from Eq. 5.10.

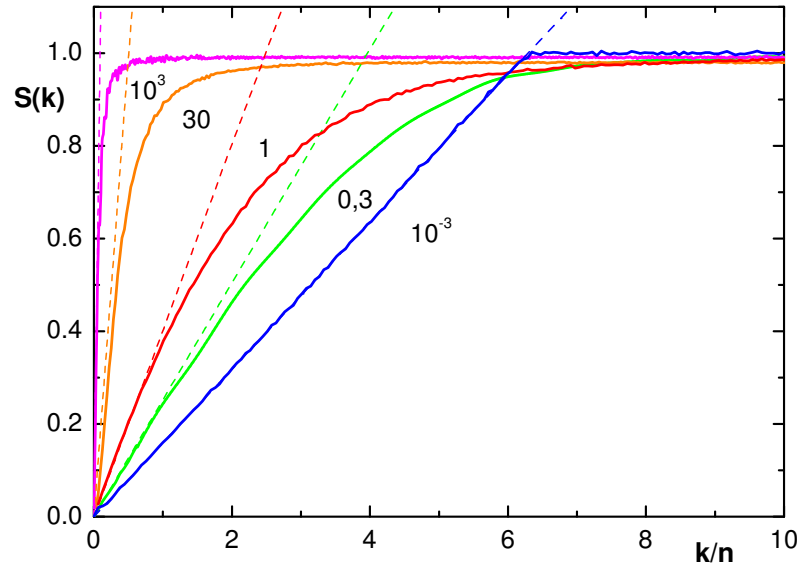


Figure 5.4: Static structure factor for the same values of  $n_{1D}|a_{1D}|$  as in Fig. 5.3 (solid lines). The dashed lines are the corresponding long-wavelength asymptotics from Eq. 5.9.

parameter in agreement with Eq. 5.12. Numerical estimation of  $g_3(0)$  at smaller densities becomes very difficult due to very small value of the measured quantity itself. It is interesting to note that  $g_2^3(0)$  follows closely to  $g_3(0)$ .



We compare the result of an experiment done in NIST [TOH<sup>+</sup>04] with the theoretical prediction of the Lieb-Liniger model, see Figs. 5.5,5.6. In this experiment the three body recombination rate was measured and the value of  $g_3(0)$  was extracted. We find an agreement between experiment and theory. The result of DMC calculation is slightly closer to the experimental data point than the estimation  $g_2^3(0)$ , although the error bars of the experimental measurement cover both values.

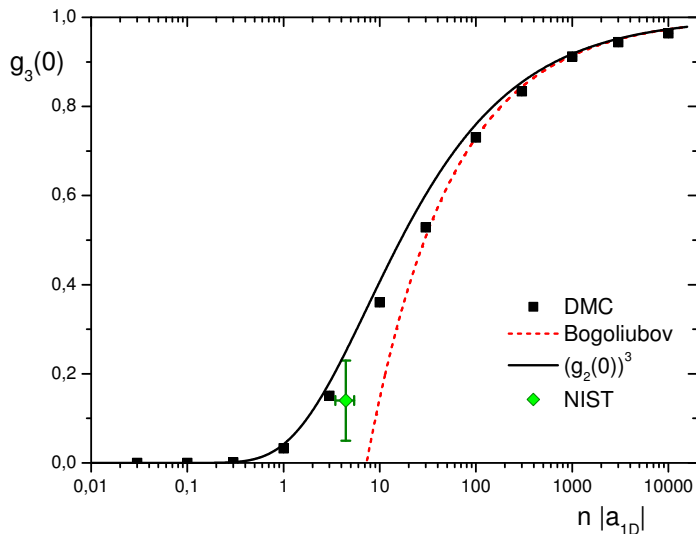


Figure 5.5: Value at zero of the three-body correlation function  $g_3(0)$  (squares), Bogoliubov limit Eq. 5.13 (dashed line),  $g_2^3(0)$  Eq. 5.10 (solid line), experimental result of [TOH<sup>+</sup>04] (diamond).

We calculated the spatial dependence of the one-body density matrix for different densities. At small distances we compare the function with the short range expansion (5.14) and find an agreement for  $zn_{1D} \ll 1$  (see Fig. 5.7). For distances larger than the healing length we expect the hydrodynamic theory to provide a correct description. Indeed, we see that the long-range decay has a power-law form in agreement with the prediction Eq. 5.7 (see Fig. 5.8). We fix the coefficient of proportionality in Eq. 5.7 by fitting the data. By doing it we conclude complete description of the one-body density matrix starting from small distances up to large ones. The deviations on Fig. 5.8 from power law-decay are at largest distances ( $z \approx L/2$ ) are due to finite size effects.

We derive a highly accurate expression for the coefficient  $C_{asympt}$  from a hydrodynamic approach considering weak interactions and low density fluctuations. In terms of Euler's constant  $\gamma = 0.577$  we have (1.199):

$$C_{asympt} = \left( \frac{e^{1-\gamma}}{8\pi\alpha} \right)^\alpha (1 + \alpha) \quad (5.15)$$

Although this constant is formally derived in the limit  $\alpha \ll 1$  (*i.e.* limit of weak interaction  $n_{1D}a_{1D} \gg 1$ ) it provides a very good description in the whole range of densities. Indeed, the coefficient defined by fitting  $g_1$  as shown in Fig. 5.8 is always in agreement with prediction (5.15) within the uncertainty errorbars we get from our DMC calculation. Further, in the most strongly

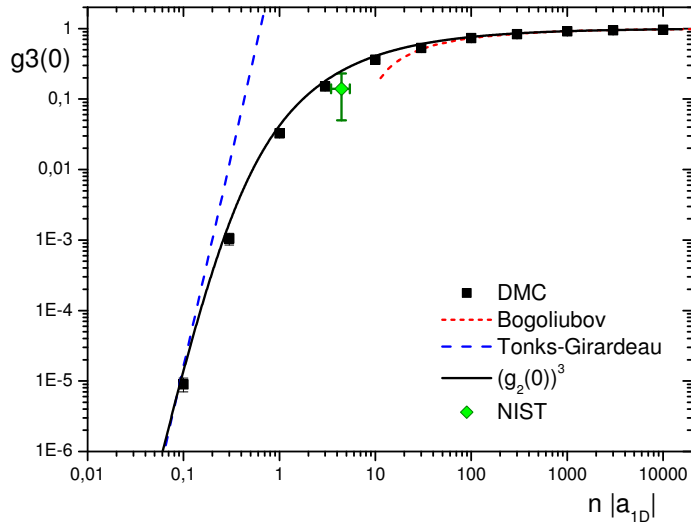


Figure 5.6: Value at zero of the three-body correlation function, log-log scale,  $g_3(0)$  (squares), TG limit Eq. 5.12 (dashed line), Bogoliubov limit Eq. 5.13 (short-dashed line),  $g_2^3(0)$  Eq. 5.10 (solid line), experimental result of [TOH<sup>+</sup>04] (diamond).

interacting TG regime we compare (5.15) with the exact result provided by formula (5.6) and find only 0.3% difference. A different expression was obtained by Popov [Pop80] (and later recovered in [MC02])  $C_{asympt}^{Popov} = \left(\frac{e^{2-\gamma}}{8\pi\alpha}\right)^\alpha$ . Both expressions coincide for small values of  $\alpha$ , but Popov's coefficient lead up to larger 10% maximal error, as it was pointed out in [Caz04]. The comparison of different coefficients is presented in Table 5.2.

We obtain the momentum distribution from the Fourier transform (see Eq. 1.26) of the one-body density matrix at short distances and the fit power-law decay at large distances. In an infinite homogeneous system the momentum distribution has an infrared divergence (Eq. 5.8). In order to present the momentum distribution in the most efficient way we plot in Fig. 5.9 a combination  $kn(k)$ , where this divergence is absent. We notice that the infrared asymptotic behavior is recovered for values of  $k$  considerably smaller than the inverse healing length  $1/\xi$ . At large  $k$  the numerical noise of our results is too large to extract evidences of  $1/k^4$  behavior predicted in [OD03].

## 5.5 Trapped system

Now let us consider effects of the external trap. We consider the trapping potential to be a harmonic oscillator. The effective one-dimensional Hamiltonian is then given by

$$\hat{H}_{LL}^{trap} = -\frac{\hbar^2}{2m} \sum_{i=1}^N \frac{\partial^2}{\partial z_i^2} + \frac{m\omega_z^2}{2} \sum_{i=1}^N z_i^2 + g_{1D} \sum_{i<j} \delta(z_i - z_j), \quad (5.16)$$

where the effective coupling constant depends both on the value of the 3D s-wave scattering length and the oscillator length of the transverse confinement  $a_\perp = \sqrt{\hbar/m\omega_\perp}$  through relation  $g_{1D} = 2\hbar^2 a/m a_\perp^2$

$n_{1D}a_{1D}$	$C_{asympt}^{DMC}$	$C_{asympt}^{Popov}$	$C_{asympt}$
1000	1.02	1.0226	1.0226
30	1.06	1.0588	1.0579
1	0.951	0.9646	0.9480
0.3	0.760	0.8145	0.7814
0.001	0.530	0.5746	0.5227

Table 5.2: Coefficient of the long-range decay of the one-body density matrix defined as in (5.7). First column is the one-dimensional gas parameter, second column is the fitting coefficient extracted from Eq. 5.8, third column is Popov's prediction, fourth column is formula 5.15. Density  $n_{1D}a_{1D} = 0.001$  is deeply in the TG regime and here one can apply Eq. 5.6 leading to  $C_{asympt}^{TG} = 0.5214$

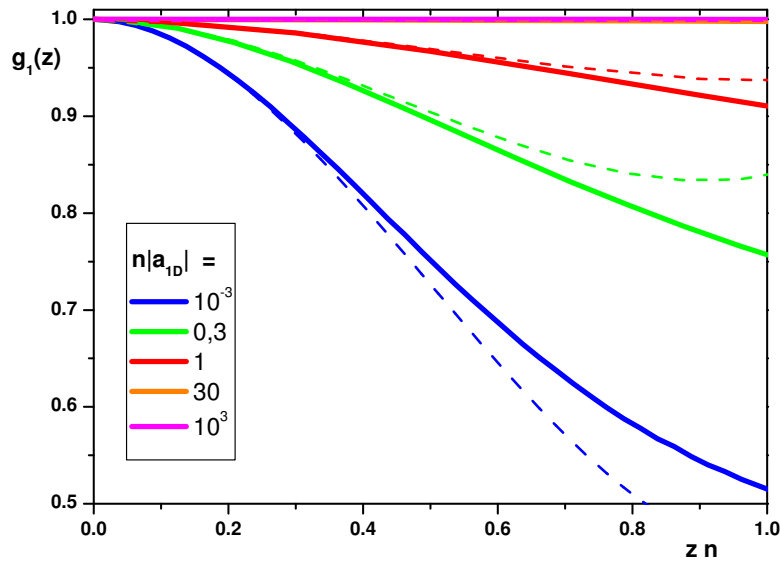


Figure 5.7: Short range behavior of the one-body density matrix for different values of the gas parameter  $n_{1D}|a_{1D}| = 10^{-3}, 0.3, 1, 30, 10^3$  (the lowest curve corresponds to  $n_{1D}|a_{1D}| = 10^{-3}$ , the uppermost to  $n_{1D}|a_{1D}| = 10^3$ ,  $g_1(z)$  (solid lines), series expansion at zero (eq. 5.14) (dashed lines).

(1.124). The relevant parameters are: the ratio  $a_{3D}/a_{\perp}$ , the anisotropy parameter  $\lambda = \omega_z/\omega_{\perp}$  and the number of particles  $N$ .

In the construction of the trial wave function used in our DMC calculation we introduce one-body Jastrow term  $f_1(z_i)$  in addition to the two-body terms  $f_2(z_{ij})$  already contained in homogeneous trial wave function (2.55). Taking into account the harmonic nature of the external potential we choose the one-body term in the Gaussian form  $f_1(z) = \exp(-\alpha_z z^2)$  with  $\alpha_z$  being the variational parameter. The correlations at distances much larger than the longitudinal oscillator length  $a_z = \sqrt{\hbar/m\omega_z}$  are dominated by the oscillator confinement and two-body correlations become irrelevant.

We consider the following configurations:  $a_{3D}/a_{\perp} = 0.2$ ,  $\lambda = 10^{-3}$  and number of particles  $N = 5, 20, 100$ . In Sec. 3 we have proven that in these conditions the ground-state energy and structure of the cloud is correctly described by the Lieb-Liniger equation of state in local density approximation.

In Fig. 5.10 we plot the pair distribution function (2.146) for 5, 20 and 100 particles. The short-

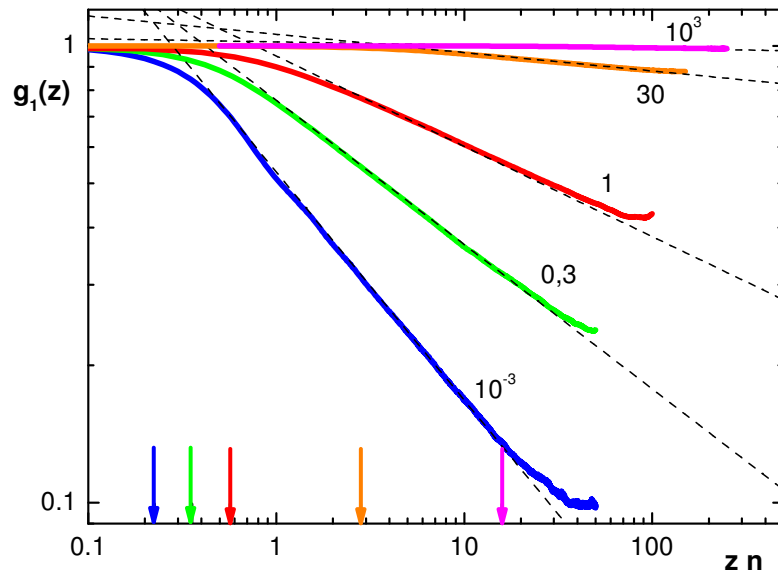


Figure 5.8: Large range behavior of the one-body density matrix (solid lines), fits to the long-wavelength asymptotics from eq. 5.7 (dashed lines). Values of the density are same as in Fig. 5.8. The arrows indicate the value of  $\xi n$ : the leftmost corresponds to  $n_{1D}|a_{1D}| = 10^{-3}$ , the rightmost to  $n_{1D}|a_{1D}| = 10^3$

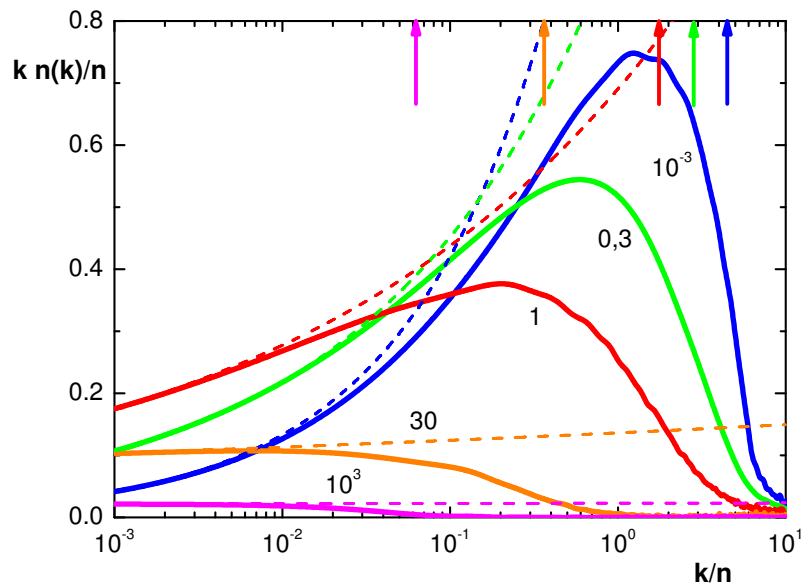


Figure 5.9: Momentum distribution for the same values of  $n_{1D}|a_{1D}|$  as in Fig. 5.8 (solid lines). The dashed lines correspond to the infrared behavior of Eq. 5.8. The arrows indicate the value of  $1/\xi n_{1D}$ : the rightmost corresponds to  $n_{1D}|a_{1D}| = 10^{-3}$ , the leftmost to  $n_{1D}|a_{1D}| = 10^3$ .

range dependence is dominated by two-body interactions. We do not find oscillations which means that strong shell structure is absent. At large distances the external trapping suppresses density.

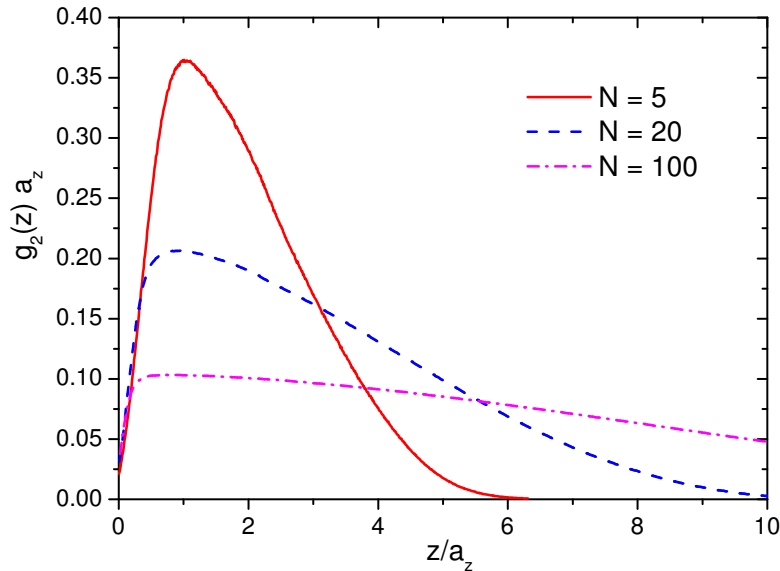


Figure 5.10: Pair distribution of a trapped system for 5, 20, 100 particles and  $a_{3D}/a_{\perp} = 0.2$ ,  $\lambda = 10^{-3}$ .

We refer to general definition of the static structure factor in terms of the momentum distribution  $n_k$  (2.133):

$$S(k) = \frac{1}{N}(\langle n_{-k}n_k \rangle - |\langle n_k \rangle|^2) \quad (5.17)$$

On the contrary uniform case, the last term is no longer vanishing for  $k \neq 0$  in a trap. In Fig. 5.11 we present the static structure factor obtained for the same set of parameters. We are interested in evidences of the linear behavior characteristic for the phonon propagation. We discover that Feynman formula (5.9) with the speed of sound taken at the center of the trap provides relatively good description also for the trapped systems. Of course, the very low momenta part is different due to the finite size effects.

For the smallest number of particles considered ( $N = 5$ ), the density is always small  $n_{1D}a_{1D} < 0.18$  and we can derive an explicit expression for the  $S(k)$  exploiting knowledge of the static structure factor in the limit of small density (5.5) as explained in Sec. 1.6.4. The resulting expression is given by formula (1.154). It can be calculated. We find that the linear behavior at small  $k$  matches the asymptotic constant in a smoother way than it happens in a homogeneous system (see TG static structure factor in Fig. 5.4).

In Fig. 5.12 we show the results for the momentum distribution  $n(k)$ . On the contrary to homogeneous case,  $n(k)$  in a finite system always remain finite due to natural limitations on the minimal possible value of wave vector  $k_{min} \simeq 1/R_z$ , where  $R_z$  is the size of the cloud in the axial direction. We are looking for traces of the divergent behavior at small momenta similar to (5.8). In the case of  $N = 5$  and  $N = 20$  the rounding off of  $n(k)$  at  $k \sim k_{min}$  washes out completely the divergent behavior. For the largest system with  $N = 100$  we find some evidence of the infrared behavior (see

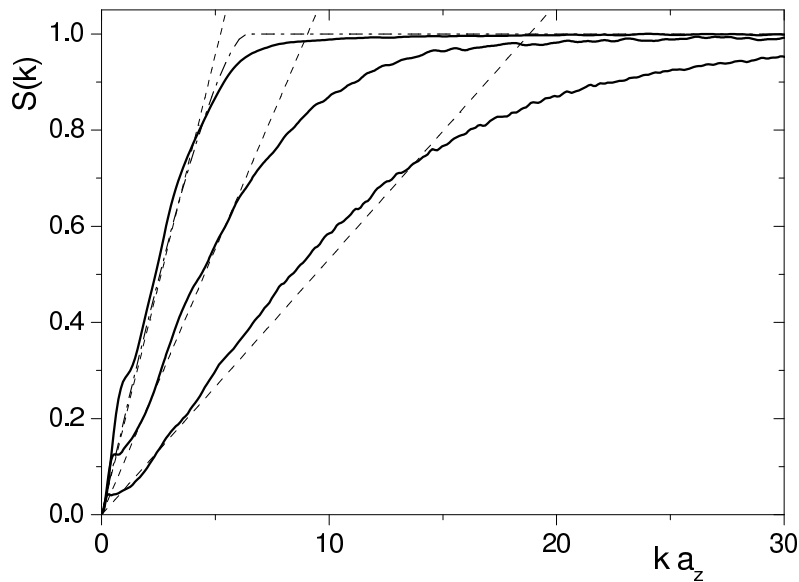


Figure 5.11: Static structure factor of a trapped system for  $a_{3D}/a_{\perp} = 0.2$ ,  $\lambda = 10^{-3}$  and 5, 20, 100 particles (solid lines from up to down). The dashed lines show linear behavior residual of the phononic part of  $S(k)$  in a homogeneous system and given by formula (5.9). We use the density in the center of the trap to estimate the sound velocity. The dash-dotted line for 5 particles is obtained within the local density approximation for the TG-equation of state and is given by Eq. 1.154.

inset in Fig. 5.12) in the region of wave vectors  $1/R_z < k < 1/\xi$ . The healing length is estimated by the density in the center of the trap  $n_0|a_{1D}| \simeq 1.1$ . We also plot a power law function with the exponent  $\alpha \simeq 0.19$  which corresponds to the value in a homogeneous system with same density and the coefficient of proportionality obtained by best fit. In order to see a cleaner signature of the infrared behavior one should consider much larger systems.

## 5.6 Conclusions

This paper presents a thorough study of correlation properties of a one-dimensional gas of bosons at zero temperature. In a homogeneous system the behavior is fixed by the product of linear density  $n_{1D}$  and one-dimensional scattering length  $a_{1D}$ . In the strongly interacting regime  $n_{1D}a_{1D} \ll 1$  the bosonic system behaves effectively as a system of non interacting fermions. In this limit the energy, pair distribution function  $g_2(z)$ , static structure factor  $S_k$  are known explicitly and are same as the ones of the corresponding fermionic system. For arbitrary value of the gas parameter no complete description was known so far. Switching on an external harmonic potential leads to modification in properties as new length, the oscillator length  $a_z$  is introduced.

Quasi one-dimensional systems have been already realized in a number of experiments with elongated traps. Many new experiments with condensates in a same geometry, in a waveguide or on a chip are expected to appear. The characteristic parameter  $n_{1D}a_{1D}$  can be varied by changing number of atoms in the condensate, trapping frequencies or by adjusting the scattering length using the Feshbach resonance. Momentum distribution is accessible from ballistic expansion and static factor can be measured by the Bragg scattering.

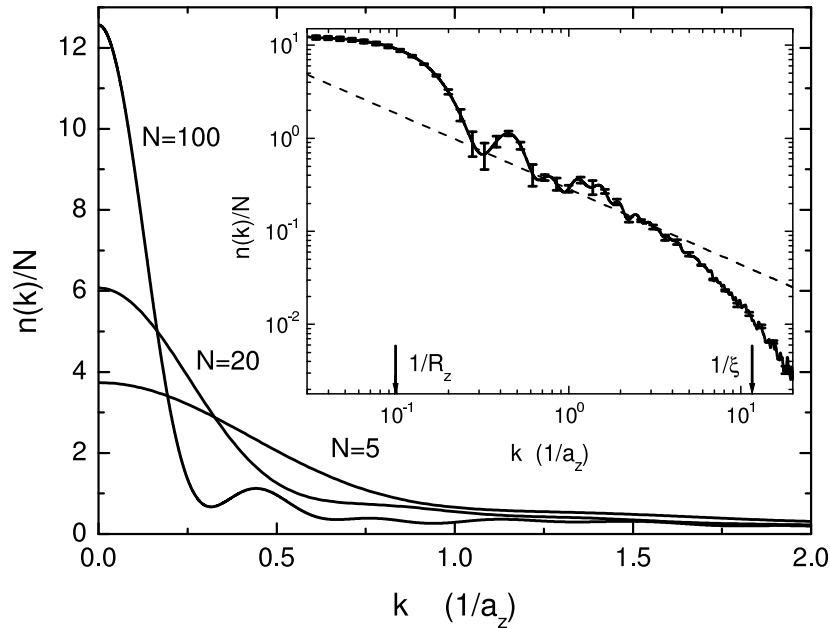


Figure 5.12: Momentum distribution of a trapped system. Inset: momentum distribution for  $N = 100$  (solid line) on a log-log scale. The dashed line is a fit to  $1/k^{1-\alpha}$  with  $\alpha = 0.19$ . The momentum distribution is in units of  $a_z = \sqrt{\hbar/(m\omega_z)}$ .

We find for the first time full description of the correlation functions in a wide range of the characteristic parameter  $n_{1D}a_{1D}$  starting from Tonks-Girardeau regime and up to Gross-Pitaevskii regime. We benchmark our Diffusion Monte Carlo calculations by recovering the ground state energy known from solution of the Lieb-Liniger integral equations. We completely recover all properties of the Tonks-Girardeau gas and known asymptotic behavior of the momentum distribution and correlation functions. We obtain the one-body density matrix  $g_1(z)$  and pair distribution function  $g_2(z)$  for all densities. In particular we have the description of the most nontrivial regime  $n_{1D}a_{1D} \approx 1$  which is relevant for current experiments.

We study the dependence of the value at zero of the three-body correlation function  $g_3(0)$  on the density  $n_{1D}a_{1D}$ . This function is of a great interest as it governs the three-body recombination rate, which leads to loss of the atoms out of the condensate. The data of an experimental measurement of  $g_3(0)$  is available [TOH<sup>+</sup>04] and is compared with the predictions of the Lieb-Liniger theory. An agreement between theory and experiment is found.

By the means of Fourier transform we extract the momentum distribution  $n(k)$  and static structure factor  $S(k)$ . Low momentum part is described by phonon hydrodynamic theory which is expected to be applicable at distances  $|z|$  larger than the healing length  $\xi$ . We judge that  $n(k)$  shows phononic power-law divergence for values of  $k$  considerably smaller than  $1/\xi$ .

Finally we discuss how the presence of a harmonic trapping modifies the correlation functions. We plot the pair distribution function in typical experimental configurations. We discuss possibility of finding in  $n(k)$  traces of divergent behavior, which is characteristic for a one-dimensional infinite system, in a trapped system.





# Chapter 6

## Beyond Tonks-Girardeau: super-Tonks gas

### 6.1 Introduction

The study of quasi-1D Bose gases in the quantum-degenerate regime has become a very active area of research. The role of correlations and of quantum fluctuations is greatly enhanced by the reduced dimensionality and 1D quantum gases constitute well suited systems to study beyond mean-field effects [PSW00]. Among these, particularly intriguing is the fermionization of a 1D Bose gas in the strongly repulsive Tonks-Girardeau (TG) regime, where the system behaves as if it consisted of noninteracting spinless fermions [Gir60]. The Bose-Fermi mapping of the TG gas is a peculiar aspect of the universal low-energy properties which are exhibited by bosonic and fermionic gapless 1D quantum systems and are described by the Luttinger liquid model [Voi95]. The concept of Luttinger liquid plays a central role in condensed matter physics and the prospect of a clean testing for its physical implications using ultracold gases confined in highly elongated traps is fascinating [MLE98, RFZZ03a].

Bosonic gases in 1D configurations have been realized experimentally. Complete freezing of the transverse degrees of freedom and fully 1D kinematics has been reached for systems prepared in a deep 2D optical lattice [MSKE03, TOH<sup>+</sup>04]. The strongly interacting regime has been achieved by adding a longitudinal periodic potential and the transition from a 1D superfluid to a Mott insulator has been observed [SMS<sup>+</sup>04]. A different technique to increase the strength of the interactions, which is largely employed in both bosonic and fermionic 3D systems [IAS<sup>+</sup>98, OHG<sup>+</sup>02] but has not yet been applied to 1D configurations, consists in the use of a Feshbach resonance. With this method one can tune the effective 1D coupling constant  $g_{1D}$  to essentially any value, including  $\pm\infty$ , by exploiting a confinement induced resonance [Ols98, BMO03]. For large and positive values of  $g_{1D}$  the system is a TG gas of point-like impenetrable bosons. On the contrary, if  $g_{1D}$  is large and negative, we will show that a new gas-like regime is entered (super-Tonks) where the hard-core repulsion between particles becomes of finite range and correlations are stronger than in the TG regime. In this Chapter we investigate using Variational Monte Carlo techniques (Sec. 2.2) the equation of state and the correlation functions of a homogeneous 1D Bose gas in the super-Tonks regime. We find that the particle-particle correlations decay faster than in the TG gas and that the static structure factor exhibits a pronounced peak. The momentum distribution and the structure factor of the gas are directly accessible in experiments by using, respectively, time-of-flight techniques and two-photon Bragg spectroscopy [SMS<sup>+</sup>04]. The study of collective modes also provides a useful experimental

technique to investigate the role of interactions and beyond mean-field effects [MSKE03]. Within a local density approximation (LDA) for systems in harmonic traps we calculate the frequency of the lowest compressional mode as a function of the interaction strength in the crossover from the TG gas to the super-Tonks regime.

## 6.2 The model and method

We consider a 1D system of  $N$  spinless bosons described by the following contact-interaction Hamiltonian

$$H = -\frac{\hbar^2}{2m} \sum_{i=1}^N \frac{\partial^2}{\partial z_i^2} + g_{1D} \sum_{i<j} \delta(z_{ij}), \quad (6.1)$$

where  $m$  is the mass of the particles,  $z_{ij} = z_i - z_j$  denotes the interparticle distance between particle  $i$  and  $j$  and  $g_{1D}$  is the coupling constant which we take large and negative. The study of the scattering problem of two particles in tight waveguides yields the a relation of the effective 1D coupling constant  $g_{1D}$  in terms of the 3D  $s$ -wave scattering length  $a_{3D}$  [Ols98]. The relation is given by the formula (8.4), where  $a_{\perp} = \sqrt{\hbar/m\omega_{\perp}}$  is the characteristic length of the transverse harmonic confinement producing the waveguide. The confinement induced resonance is located at the critical value  $a_{3D}^c$  and corresponds to the abrupt change of  $g_{1D}$  from large positive values ( $a_{3D} \lesssim a_{3D}^c$ ) to large negative values ( $a_{3D} \gtrsim a_{3D}^c$ ). The renormalization (8.4) of the effective 1D coupling constant has been recently confirmed in a many-body calculation of Bose gases in highly elongated harmonic traps using quantum Monte Carlo techniques [ABGG04b, ABGG04a].

For positive  $g_{1D}$ , the Hamiltonian (6.1) corresponds to the Lieb-Liniger (LL) model (5.1). The ground state and excited states of the LL Hamiltonian have been studied in detail [LL63, Lie63] and, in particular, the TG regime corresponds to the limit  $g_{1D} = +\infty$ . The ground state of the Hamiltonian (6.1) with  $g_{1D} < 0$  has been investigated by McGuire [McG64] and one finds a soliton-like state with energy  $E/N = -mg_{1D}^2(N^2 - 1)/24\hbar^2$ . The lowest-lying gas-like state of the Hamiltonian (6.1) with  $g_{1D} < 0$  corresponds to a highly-excited state that is stable if the gas parameter  $na_{1D} \ll 1$ , where  $n$  is the density and  $a_{1D}$  is the 1D effective scattering length defined in Eq. (8.4). This state can be realized in tight waveguides by crossing adiabatically the confinement induced resonance. The stability of the gas-like state can be understood from a simple estimate of the energy per particle. For a contact potential the interaction energy is given by (1.21)  $E_{int}/N = g_{1D}ng_2(0)/2$ , where the  $g_2(0) = \langle \hat{\Psi}^\dagger(z)\hat{\Psi}^\dagger(z)\hat{\Psi}(z)\hat{\Psi}(z) \rangle/n^2$ , is the value at zero of the two-body correlation function (1.12) and  $\hat{\Psi}^\dagger, \hat{\Psi}$  are the creation and annihilation particle operators (1.1). In the limit  $g_{1D} \rightarrow -\infty$  one can use for the correlation function the result in the TG regime (5.11)[GS03b], which does not depend on the sign of  $g_{1D}$ . In the same limit the kinetic energy can be estimated by (1.102):  $E_{kin}/N \simeq \pi^2\hbar^2n^2/(6m)$ , corresponding to the energy per particle of a TG gas. For the total energy  $E = E_{kin} + E_{int}$  one finds the result (1.105)  $E/N \simeq \pi^2\hbar^2n^2/(6m) - \pi^2\hbar^2n^3a_{1D}/(3m)$ , holding for  $na_{1D} \ll 1$ . For  $na_{1D} < 0.25$  this equation of state yields a positive compressibility  $mc^2 = n\partial\mu/\partial n$ , where  $\mu = dE/dN$  is the chemical potential and  $c$  is the speed of sound, corresponding to a stable gas-like phase. We will show that a more precise estimate gives that the gas-like state is stable against cluster formation for  $na_{1D} \lesssim 0.35$ .

The analysis of the gas-like equation of state is carried out using the VMC technique. The trial wave function employed in the calculation is of the form (2.63). For  $g_{1D} < 0$  ( $a_{1D} > 0$ ) the wave function  $f(z)$  changes sign at a nodal point which, for  $R_m \gg a_{1D}$ , is located at  $|z| = a_{1D}$ . In the attractive case the wave function has a node which means that the variational calculation can

be easily done, while without additional modifications the DMC can not be done. The variational energy is calculated through the expectation value of the Hamiltonian (6.1) on the trial wave function (2.14). In the calculations we have used  $N = 100$  particles with periodic boundary conditions and because of the negligible dependence of the variational energy on the parameter  $R_m$  we have used in all simulations the value  $R_m = L/2$ , where  $L$  is the size of the simulation box. Calculations carried out with larger values of  $N$  have shown negligible finite size effects.

## 6.3 Energy

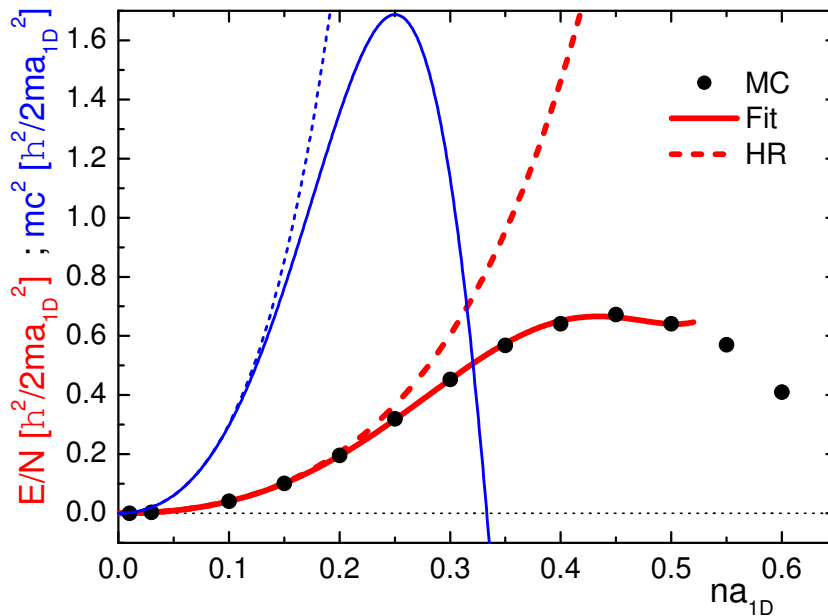


Figure 6.1: Energy per particle and compressibility as a function of the gas parameter  $na_{1D}$ . Solid symbols and thick solid line: VMC results and polynomial best fit; thick dashed line: HR equation of state [Eq. (1.103)]. Thin solid and dashed line: compressibility from the best fit to the variational equation of state and from the HR equation of state respectively.

The results for the variational energy as a function of the gas parameter  $na_{1D}$  are shown in Fig. 6.1 with solid symbols. For small values of the gas parameter our variational results agree very well with the equation of state of a gas of hard-rods (HR) of size  $a_{1D}$  (thick dashed line). The HR energy per particle can be calculated exactly from the energy of a TG gas by accounting for the excluded volume (1.103) [Gir60].

For larger values of  $na_{1D}$ , the variational energy increases with the gas parameter more slowly than in the HR case and deviations are clearly visible. By fitting a polynomial function to our variational results we obtain the best fit shown in Fig. 6.1 as a thick solid line. The compressibility obtained from the best fit is shown in Fig. 6.1 as a thin solid line and compared with  $mc^2$  of a HR gas (thin dashed line). As a function of the gas parameter the compressibility shows a maximum and then drops abruptly to zero. The vanishing of the compressibility implies that the system is mechanically unstable against cluster formation. Our variational estimate yields  $na_{1D} \simeq 0.35$  for the critical value

of the density where the instability appears. This value coincides with the critical density for collapse calculated in the center of the trap for harmonically confined systems [ABGG04a, ABGG04b]. It is worth noticing that the VMC estimate of the energy of the system can be extended beyond the instability point, as shown in Fig. 6.1. This is possible since the finite size of the simulation box hinders the long-range density fluctuations that would break the homogeneity of the gas. This feature is analogous to the one observed in the quantum Monte-Carlo characterization of the spinodal point in liquid  $^4\text{He}$  [BCN94].

As shown in Fig. 6.1, the HR model describes accurately the equation of state for small values of the gas parameter. A similar accuracy is therefore expected for the correlation functions of the system. The correlation functions of a HR gas of size  $a_{1D}$  can be calculated from the exact wave function [Nag40] (2.5.4.2). We calculate the static structure factor  $S(k)$  (2.137) and the one-body density matrix  $g_1(z)$  (2.139)

## 6.4 One-body density matrix and static structure factor

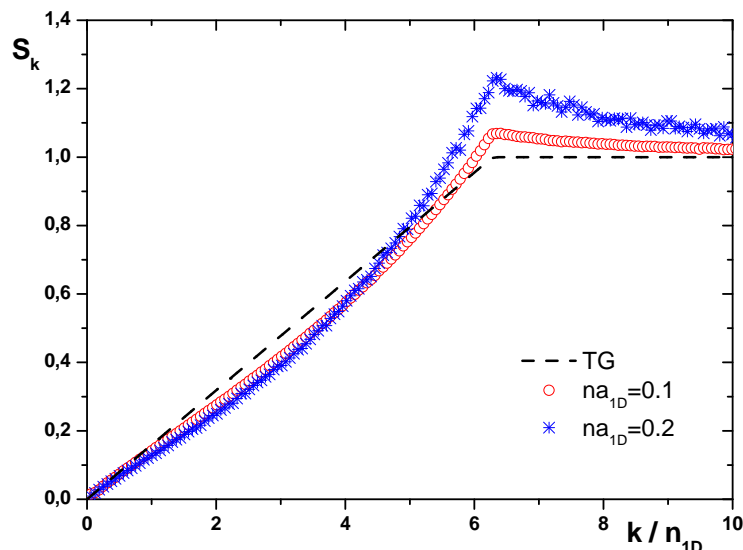


Figure 6.2: Static structure factor  $S(k)$  for a gas of HR at different values of the gas parameter  $na_{1D}$  (symbols) and for a TG gas (dashed line).

Contrarily to the TG case, it is not possible to obtain analytical expressions for  $g_1(z)$  and  $S(k)$  in the HR problem. We have calculated them using configurations generated by a Monte Carlo simulation according to the exact probability distribution function  $|\psi_{HR}|^2$ . The results for the static structure factor are shown in Fig. 6.2. Compared to  $S(k)$  in the TG regime, a clear peak is visible for values of  $k$  of the order of twice the Fermi wave vector  $k_F = \pi n$  and the peak is more pronounced as  $na_{1D}$  increases. The change of slope for small values of  $k$  reflects the increase of the speed of sound  $c$  with  $na_{1D}$ . The long-range behavior of  $g_1(z)$  can be obtained from the hydrodynamic theory of low-energy excitations [RC67, Sch77, Hal81]. For  $|z| \gg \xi$ , where  $\xi = \hbar/(\sqrt{2}mc)$  is the healing length of the system, one finds the following power-law decay (1.199):

$$g_1(z) \propto 1/|z|^\alpha, \quad (6.2)$$

where the exponent  $\alpha$  is given by  $\alpha = mc/(2\pi\hbar n)$ . For a TG gas  $mc = \pi\hbar n$ , and thus  $\alpha_{TG} = 1/2$ . For a HR gas one finds  $\alpha = \alpha_{TG}/(1 - na_{1D})^2$  and thus  $\alpha > \alpha_{TG}$ . This behavior at long range is clearly shown in Fig. 6.3 where we compare  $g_1(z)$  of a gas of HR with  $na_{1D} = 0.1, 0.2$  and  $0.3$  to the result of a TG gas [JMMS80]. The long-range power-law decay of  $g_1(z)$  is reflected in the infrared divergence of the momentum distribution  $n(k) \propto 1/|k|^{1-\alpha}$  holding for  $|k| \ll 1/\xi$ . A gas of HR exhibits a weaker infrared divergence compared to a TG gas. The correlation functions of a HR gas at  $na_{1D} = 0.1, 0.2$  should accurately describe the physical situation of a Bose gas with large and negative  $g_{1D}$ . For  $na_{1D} = 0.3$  we expect already some deviations from the HR model, as it is evident from the equation of state in Fig. 6.1, which should broaden the peak in  $S(k)$  and decrease the slope of the power-law decay in  $g_1(z)$  at large distances. The analysis of correlation functions clearly shows that the super-Tonks regime corresponds to a Luttinger liquid where short range correlations are significantly stronger than in the TG gas.

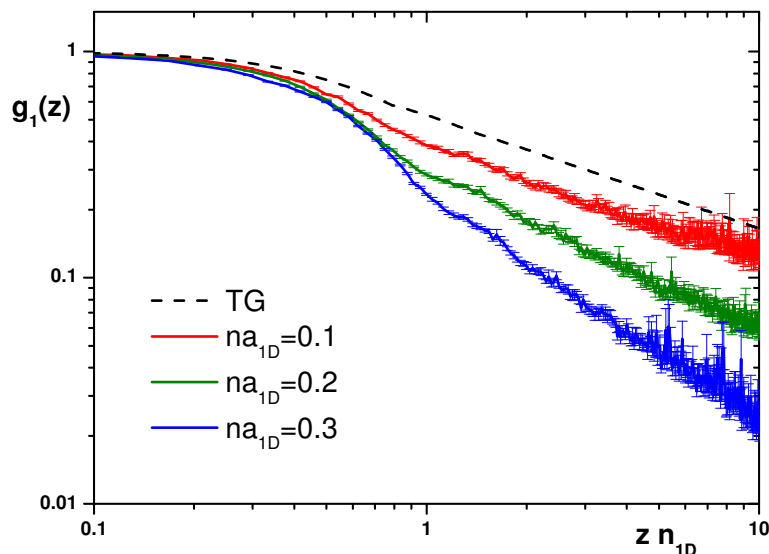


Figure 6.3: One-body density matrix  $g_1(z)$  for a gas of HR at different values of the gas parameter  $na_{1D}$  (solid lines) and for a TG gas (dashed line). Higher values of density correspond to a faster decay of  $g_1(z)$ .

## 6.5 Collective modes

Another possible experimental signature of the super-Tonks regime can be provided by the study of collective modes. To this aim, we calculate the frequency of the lowest compressional mode of a system of  $N$  particles in a harmonic potential  $V_{ext} = \sum_{i=1}^N m\omega_z^2 z_i^2/2$ . We make use of LDA (Sec. 1.6) which allows us to calculate the chemical potential of the inhomogeneous system  $\tilde{\mu}$  and the density profile  $n(z)$  from the local equilibrium equation  $\tilde{\mu} = \mu[n(z)] + m\omega_z^2 z^2/2$ , and the normalization condition  $N = \int_{-R}^R n(z) dz$ , where  $R = \sqrt{2\tilde{\mu}/(m\omega_z^2)}$  is the size of cloud. For densities  $n$  smaller than the critical density for cluster formation,  $\mu[n]$  is the equation of state of the homogeneous system derived from the fit to the VMC energies (Fig. 6.1). From the knowledge of the density profile  $n(z)$

one can obtain the mean square radius of the cloud  $\langle z^2 \rangle = \int_R^R n(z)z^2 dz/N$  and thus, making use of the result [MS02]

$$\omega^2 = -2 \frac{\langle z^2 \rangle}{d\langle z^2 \rangle/d\omega_z^2}, \quad (6.3)$$

one can calculate the frequency  $\omega$  of the lowest breathing mode. Within LDA, the result will depend only on the dimensionless parameter  $Na_{1D}^2/a_z^2$ , where  $a_z = \sqrt{\hbar/m\omega_z}$  is the harmonic oscillator length. For  $g_{1D} > 0$ , *i.e.* in the case of the LL Hamiltonian, the frequency of the lowest compressional mode increases from  $\omega = \sqrt{3}\omega_z$  in the weak-coupling mean-field regime ( $Na_{1D}^2/a_z^2 \gg 1$ ) to  $\omega = 2\omega_z$  in the strong-coupling TG regime ( $Na_{1D}^2/a_z^2 \ll 1$ ). The results for  $\omega$  in the super-Tonks regime are shown in Fig. 6.4 as a function of the coupling strength. In the regime  $Na_{1D}^2/a_z^2 \ll 1$ , where the HR model is appropriate, we can calculate analytically the first correction to the frequency of a TG gas (refer to Table 1.1). One finds the result  $\omega = 2\omega_z[1 + (16\sqrt{2}/15\pi^2)(Na_{1D}^2/a_z^2)^{1/2} + \dots]$ . Fig. 6.4 shows that this expansion accurately describes the frequency of the breathing mode when  $Na_{1D}^2/a_z^2 \ll 1$ , for larger values of the coupling strength the frequency reaches a maximum and drops to zero at  $Na_{1D}^2/a_z^2 \simeq 0.6$ . The observation of a breathing mode with a frequency larger than  $2\omega_z$  would be a clear signature of the super-Tonks regime.

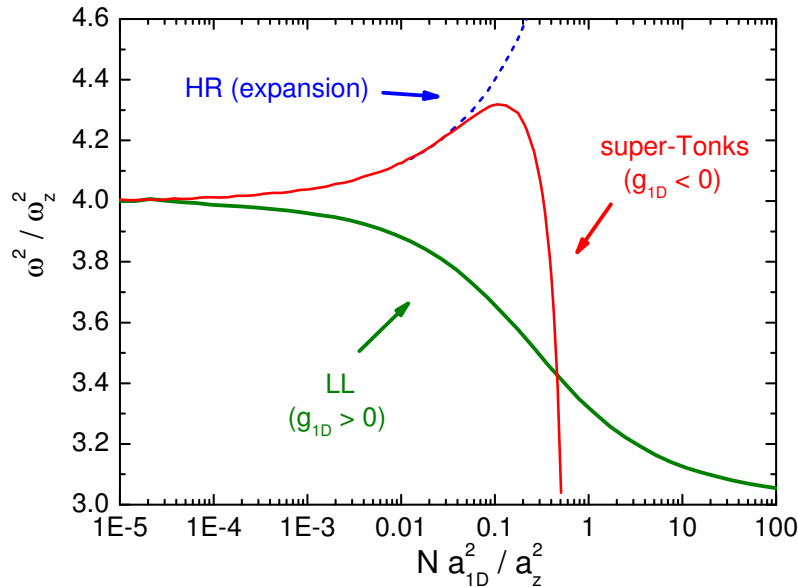


Figure 6.4: Square of the lowest breathing mode frequency,  $\omega^2$ , as a function of the coupling strength  $Na_{1D}^2/a_z^2$  for the LL Hamiltonian ( $g_{1D} > 0$ ) and in the super-Tonks regime ( $g_{1D} < 0$ ). The dashed line is obtained from the HR expansion (see Table 1.1).

## 6.6 Conclusions

In conclusion we have pointed out the existence of a strongly correlated regime in quasi-1D Bose gases beyond the Tonks-Girardeau regime. This regime can be entered by exploiting a confinement induced resonance of the effective 1D scattering amplitude. We calculate the equation of state of the gas in

the super-Tonks regime using VMC and we estimate the critical density for the onset of instability against cluster formation. The static structure factor and one-body density matrix are calculated exactly within the hard-rod model, which provides the correct description of the system for small values of the gas parameter. For harmonically trapped systems we provide explicit predictions for the frequency of the lowest compressional mode.





# Chapter 7

## Motion of a heavy impurity through a Bose-Einstein condensate

### 7.1 Introduction

One of the most important peculiarities of Landau theory superfluidity is the existence of a finite critical velocity. If a body moves in a superfluid at  $T = 0$  with velocity  $V$  less than  $v_c$ , the motion is dissipationless. At  $V > v_c$  a drag force arises because of the possibility of emission of elementary excitations. However, both theoretical and experimental investigation in superfluid  $^4\text{He}$  are difficult. The critical velocity in  $^4\text{He}$  is related to creation of rotons, for which one has no simple theoretical description. Further, an important role is played by complicated processes involving vortex rings production.

The situation in low-density weakly-interacting Bose-Einstein condensed (BEC) gases is simpler. The Landau critical velocity in this case is due to Cherenkov emission of phonons which can be described by mean-field theory. Due to the presence in the theory of an intrinsic length parameter, the correlation length  $\xi$ , the friction force for a small body does not depend on its structure. Vortex rings in the BEC cannot have radius less than  $\xi$  (see, *e.g.*, [JR82]) and it is reasonable to believe that probability of their creation by a small body is small. Thus quantitative investigation of critical velocities in BEC are very interesting and can be used to probe the superfluidity of a quantum gas.

Recently existence of the critical velocity in a Bose-Einstein Condensed gas was confirmed in a few experiments. At MIT a trapped condensate was stirred by a blue detuned laser beam [RKO<sup>+</sup>99] and the energy of dissipation was measured. The critical velocity was found to be smaller than the speed of sound due to emission of vortices. The diameter of the laser spot in this experiment was of a macroscopic size and was large compared to the healing length. An improved technique allowed measurement of the drag force acting on the condensate in a subsequent experiment [ORV<sup>+</sup>00].

The analytical study of flow of the condensate over an impurity is highly nontrivial due to the intrinsic nonlinearity of the problem arising from the interaction of the particles in the condensate. In one dimension the dissipation could occur at velocities smaller than predicted by Landau's approach due to emission of solitons [Hak97]. The dependence of the critical velocity on the type of the potential was studied both by using a perturbative approach and numerical integration in [LP01, Pav02]. The effective two dimensional problem was considered in [KM00]. In this work generation of excitations in the oscillating condensate in a time dependent parabolic trap in the presence of a static impurity was studied analytically. A three-dimensional flow of a condensate around an obstacle was calculated numerically by integration of the Gross-Pitaevskii (GP) equation and emission of vortices

was observed [FPR92, WMA99].

There are different definitions of the superfluidity. It is possible to make following experiment. Move a small body through the system. According to Landau if there is no normal part (we consider zero temperature or small enough) no dissipation will happen if the speed is smaller than the speed of sound. Our goal is to calculate effect of such a probe, a small impurity moving through a condensate which is described by the Gross-Pitaevskii equation.

We want to find an answer to a question which is rather complicated. From one side we know from usual considerations in the mean field regime that the system is superfluid. From the other side we know that in the Tonks-Girardeau regime the system is mapped on the fermions, which are, definitely, not superfluid. Indeed what we find is that the situation is somewhere between.

## 7.2 Three-dimensional system

Let us consider an impurity moving through a three-dimensional condensate at  $T = 0$ . One of the possible realizations of this model could be scattering of heavy neutral molecules by the condensate.

### 7.2.1 Perturbed solution

We start from the three-dimensional energy functional (1.110) of a homogeneous weakly-interacting Bose gas in the presence of a  $\delta$ -function perturbation (an impurity) moving with a constant velocity  $\mathbf{V}$

$$E = \int \left( \frac{\hbar^2}{2m} |\nabla\psi|^2 + (\mu - g_i \delta(\mathbf{r} - \mathbf{V}t)) |\psi|^2 + \frac{g}{2} |\psi|^4 \right) d^3r, \quad (7.1)$$

where  $\psi$  is the condensate wave function,  $\mu$  is the chemical potential,  $m$  mass of a particle in the condensate,  $g = 4\pi\hbar^2 a/m$  and  $g_i = 2\pi\hbar^2 b/m$  are particle-particle and particle-impurity coupling constants, with  $a$  and  $b$  being the respective scattering lengths<sup>1</sup>. We will assume that the interaction with impurity is small and we will use perturbation theory. By splitting the wave function into a sum of the unperturbed solution and a small correction  $\psi(\mathbf{r}, t) = \phi_0 + \delta\psi(\mathbf{r}, t)$  and linearizing the time-dependent GP equation with respect to  $\delta\psi$ , we obtain an equation describing the time evolution of  $\delta\psi$

$$i\hbar \frac{\partial}{\partial t} \delta\psi = \left( -\frac{\hbar^2}{2m} \Delta - \mu + 2g|\phi_0|^2 \right) \delta\psi + g|\phi_0|^2 \delta\psi^* + g_i \delta(\mathbf{r} - \mathbf{V}t) \phi_0 \quad (7.2)$$

In a homogeneous system  $\phi_0$  is a constant fixed by the particle density  $\phi_0 = \sqrt{n}$  and  $\mu = gn = mc^2$ .

The perturbation follows the moving impurity, *i.e.*  $\delta\psi$  is a function of  $(\mathbf{r} - \mathbf{V}t)$ , so the coordinate derivative is related to the time derivative

$$\partial \delta\psi(\mathbf{r} - \mathbf{V}t) / \partial t = -\mathbf{V} \vec{\nabla} \delta\psi(\mathbf{r} - \mathbf{V}t) \quad (7.3)$$

We shall work in the frame moving with the impurity  $\mathbf{r}' = \mathbf{r} - \mathbf{V}t$  and the subscript over  $\mathbf{r}$  will be dropped.

---

<sup>1</sup>Considering a homogenous condensate, we assume that its size is large enough, particularly that the gas is the Thomas-Fermi conditions. Then results for a homogenous gas will be approximately valid for a gas in a trap.

Eq. (7.2) for a perturbation in a homogeneous system can be conveniently solved in momentum space. In order to do this we introduce the Fourier transform of the wave function  $\delta\psi_{\mathbf{k}} = \int e^{-i\mathbf{k}\cdot\mathbf{r}}\delta\psi(\mathbf{r})d^3r$ . Eq. (7.2) becomes

$$\begin{cases} \left(-\hbar\mathbf{k}\cdot\mathbf{V} + \frac{\hbar^2k^2}{2m} + \mu\right)\delta\psi_{\mathbf{k}} + \mu(\delta\psi_{-\mathbf{k}})^* + g_i\phi_0 = 0 \\ \mu\delta\psi_{\mathbf{k}} + \left(\hbar\mathbf{k}\cdot\mathbf{V} + \frac{\hbar^2k^2}{2m} + \mu\right)(\delta\psi_{-\mathbf{k}})^* + g_i\phi_0 = 0 \end{cases} \quad (7.4)$$

Here the second equation is obtained by doing the substitution  $\mathbf{k} \rightarrow -\mathbf{k}$  and and complex conjugation. We also use property of the Fourier transformation  $\delta(\psi^*)_{\mathbf{k}} = \delta(\psi_{-\mathbf{k}})^*$ . The system of linear equations (7.4) can be easily solved

$$\delta\psi_{\mathbf{k}} = g_i\phi_0 \frac{\hbar\mathbf{k}\cdot\mathbf{V} + \frac{\hbar^2k^2}{2m}}{(\hbar\mathbf{k}\cdot\mathbf{V})^2 - \frac{\hbar^2k^2}{2m} \left(\frac{\hbar^2k^2}{2m} + 2\mu\right)} \quad (7.5)$$

## 7.2.2 Total energy

For a fixed value of the chemical potential  $\mu$  the energy  $E' = E - \mu N$  reaches minimum on the ground state function  $\phi_0$ . From this it follows that  $E'$  does not have terms linear in  $\delta\psi_{\mathbf{k}}$  and  $\delta\psi_{\mathbf{k}}^*$ , and

$$E' = E^{(0)} + E^{(2)} + g_i(\phi_0^*\delta\psi(0) + \phi_0\delta\psi^*(0)) \quad (7.6)$$

Here  $E^{(0)} = Ngn/2 + g_i\phi_0^2$  is the energy of the system in absence of the perturbation plus the mean-field shift in the energy due to the impurity. The next term comes from the linear expansion of the energy  $\int |\psi(\mathbf{r})|^2 g_i \delta(\mathbf{r}) d\mathbf{r}$ . The term  $E^{(2)}$  being quadratic in  $\delta\psi_{\mathbf{k}}$  and  $\delta\psi_{\mathbf{k}}^*$  satisfies the Euler identity:

$$2E^{(2)} = \int \left[ \delta\psi(\mathbf{r}) \frac{\delta E^{(2)}}{\delta(\delta\psi(\mathbf{r}))} + \delta\psi^*(\mathbf{r}) \frac{\delta E^{(2)}}{\delta(\delta\psi^*(\mathbf{r}))} \right] d\mathbf{r} \quad (7.7)$$

which using the variational equation

$$i\hbar \frac{\partial \delta(\delta\psi)}{\partial t} = \frac{\delta E^{(2)}}{\delta(\delta\psi^*)} + g_i\phi_0\delta(\mathbf{r}) \quad (7.8)$$

can be rewritten as

$$E^{(2)} = \frac{i\hbar}{2} \int \left[ \delta\psi^*(\mathbf{r}) \frac{\partial \delta\psi(\mathbf{r})}{\partial t} - \frac{\partial \delta\psi^*(\mathbf{r})}{\partial t} \delta\psi(\mathbf{r}) \right] d\mathbf{r} - \frac{g_i}{2} (\phi_0^*\delta\psi(0) + \phi_0\delta\psi^*(0)) \quad (7.9)$$

To start with, let us Fourier transform the first term. Exchanging time derivatives with gradients by the rule (7.3) one obtains

$$E^{(2)} = \int \hbar\mathbf{k}\cdot\mathbf{V} |\delta\psi_{\mathbf{k}}|^2 \frac{d^3k}{(2\pi)^3} + \frac{g_i\phi_0}{2} (\delta\psi + \delta\psi^*)_{\mathbf{r}=0} \quad (7.10)$$

In the energy calculation we assume that the velocity  $V$  is small and will make an expansion in powers of  $V$  up to quadratic terms. It means that in the calculation of  $|\delta\psi_{\mathbf{k}}|^2$  the term  $(\hbar\mathbf{k}\mathbf{V})^2$  in the denominator of (7.5) can be neglected and  $|\delta\psi_{\mathbf{k}}|^2$  is written as

$$|\delta\psi_{\mathbf{k}}|^2 = \frac{g_i^2 |\phi_0|^2 \left[ \left(\frac{\hbar^2k^2}{2m}\right)^2 + 2\frac{\hbar^2k^2}{2m} \hbar\mathbf{k}\mathbf{V} \right]}{\left[ \frac{\hbar^2k^2}{2m} \left(\frac{\hbar^2k^2}{2m} + 2\mu\right) \right]^2} + \mathcal{O}(V^4) \quad (7.11)$$

The energy does not have terms linear in  $\mathbf{V}$ , because all terms independent of  $\mathbf{V}$  in (7.11) are even in  $\mathbf{k}$ , so once multiplied by  $\mathbf{k}$  and integrated over momentum space they provide zero contribution to the energy. The only term that is left is the following

$$E^{(2)} = 2g_i^2 |\phi_0|^2 \int \frac{(\hbar \mathbf{k} \mathbf{V})^2}{\frac{\hbar^2 k^2}{2m} \left( \frac{\hbar^2 k^2}{2m} + 2\mu \right)^2} \frac{d\mathbf{k}}{(2\pi)^3} \quad (7.12)$$

For the calculation of  $\delta\psi(0)$  in (7.6) and (7.9) one should consider  $\delta\psi_{\mathbf{k}}$  taking into account that  $\hbar \mathbf{k} \mathbf{V} \ll \mu$  and then integrate it over the momentum space

$$\begin{aligned} \delta\psi_{\mathbf{k}} &= -\frac{g_i \left( \hbar \mathbf{k} \mathbf{V} + \frac{\hbar^2 k^2}{2m} \right) \phi_0}{\frac{\hbar^2 k^2}{2m} \left( \frac{\hbar^2 k^2}{2m} + 2\mu \right)} \left[ 1 - \frac{(\hbar \mathbf{k} \mathbf{V})^2}{\frac{\hbar^2 k^2}{2m} \left( \frac{\hbar^2 k^2}{2m} + 2\mu \right)} \right]^{-1} \approx \\ &\approx \frac{(\hbar \mathbf{k} \mathbf{V})^2}{\frac{\hbar^2 k^2}{2m} \left( \frac{\hbar^2 k^2}{2m} + 2\mu \right)^2} g_i \phi_0 - \left\{ \frac{\hbar \mathbf{k} \mathbf{V} \left[ \frac{\hbar^2 k^2}{2m} \left( \frac{\hbar^2 k^2}{2m} + 2\mu \right) \right] + (\hbar \mathbf{k} \mathbf{V})^3}{\left[ \frac{\hbar^2 k^2}{2m} \left( \frac{\hbar^2 k^2}{2m} + 2\mu \right) \right]^2} + \frac{1}{\frac{\hbar^2 k^2}{2m} + 2\mu} \right\} g_i \phi_0 \end{aligned} \quad (7.13)$$

The integral of the second term over momentum space is equal to zero.

The third term suffers from large- $k$  divergency and one should renormalize the scattering amplitude. It is sufficient to express the coupling constant in the 2<sup>nd</sup> term of eq. (7.10) in terms of the scattering amplitude  $b$  using the second order Born approximation:

$$g_i = \frac{2\pi \hbar^2 b}{m} \left( 1 + \frac{2\pi \hbar^2 b}{m} \int \left( \frac{\hbar^2 k^2}{2m} \right)^{-1} \frac{d^3 k}{(2\pi)^3} \right) \quad (7.14)$$

Now the third term in (7.10) is converging and can be calculated

$$g_i^2 n \int \frac{2\mu}{\frac{\hbar^2 k^2}{2m} \left( \frac{\hbar^2 k^2}{2m} + 2\mu \right)} \frac{d^3 k}{(2\pi)^3} = 8\pi \sqrt{\pi} (na^3)^{3/2} \left( \frac{b}{a} \right)^2 \frac{\hbar^2}{ma^2} \quad (7.15)$$

The energy shift quadratic in velocity  $V$  is defined by the following integral

$$\delta E = E^{(2)} g_i (\phi_0^* \delta\psi(0) + \phi_0 \delta\psi^*(0)) = g_i^2 n \int \frac{(\hbar \mathbf{k} \mathbf{V})^2}{\frac{\hbar^2 k^2}{2m} \left( \frac{\hbar^2 k^2}{2m} + 2\mu \right)^2} \frac{d\mathbf{k}}{(2\pi)^3} \quad (7.16)$$

Here we make use of relation  $\phi_0 = \sqrt{n}$ . In a three-dimensional case the term  $(\mathbf{k} \mathbf{V})^2 d\mathbf{k}$  in the integral (7.16) can be replaced by  $1/3 k^2 V^2 4\pi k^2 dk$  due to the equivalence of different directions.

$$\delta E = \frac{g_i^2 n \hbar^2 V^2}{6\pi^2 \left( \frac{\hbar^2}{2m} \right)^{5/2}} \int_0^\infty \frac{\frac{\hbar^2 k^2}{2m} d \left( \frac{\hbar k}{\sqrt{2m}} \right)}{\left( \frac{\hbar^2 k^2}{2m} + 2gn \right)^2} \quad (7.17)$$

This integral can be easily calculated if one recall the integral identity  $\int \frac{x^2 dx}{(x^2+a^2)^2} = -\frac{x}{2(x^2+a^2)^2} + \frac{1}{2a} \arctan \frac{x}{a}$ . Finally, by collecting everything together and considering  $N_{imp}$  impurities with a concentration given by  $\chi = N_{imp}/N$  we obtain the energy per particle

$$\frac{E}{N} = \left\{ 2\pi na^3 \left( 1 + \chi \frac{b}{a} \right) + 8\pi^{3/2} (na^3)^{3/2} \chi \left( \frac{b}{a} \right)^2 \right\} \frac{\hbar^2}{ma^2} + \frac{2\sqrt{\pi}}{3} (na^3)^{1/2} \chi \left( \frac{b}{a} \right)^2 \frac{mV^2}{2} \quad (7.18)$$

If we set  $V = 0$  we recover Bogoliubov's corrections to the energy in the presence of quenched impurities [HM92, ABCG02]. Note that even if the “mean-field” energy obtained from the GP equation in the absence of impurities ( $\chi = 0$ ) leaves out terms of the order of  $(na^3)^{3/2}$ , the equations we obtain in the presence of impurities in a perturbative manner still correctly describe the effect of the disorder up to the terms of the order of  $(na^3)^{3/2}$ .

### 7.2.3 Effective mass and normal fraction

If  $V \neq 0$  a quadratic term in the impurity contribution to the energy is present. It can be denoted as  $\chi m^* V^2/2$  with

$$m^* = \frac{2\sqrt{\pi}}{3} (na^3)^{1/2} \left(\frac{b}{a}\right)^2 m \quad (7.19)$$

being the induced mass, i. e. the mass of particles dragged by an impurity [Ast01]. Applicability of the perturbation theory demands  $m^*$  to be small compared to  $m$ . This gives the condition  $(na^3)^{1/2} \left(\frac{b}{a}\right)^2 \ll 1$ . At zero temperature the interaction between particles does not lead to depletion of the superfluid density and the suppression of the superfluidity comes only from the interaction of particles with impurities. Thus (7.19) defines the normal density

$$\frac{\rho_n}{\rho} = \frac{m^*}{m} \chi = \frac{2\sqrt{\pi}}{3} (na^3)^{1/2} \chi \left(\frac{b}{a}\right)^2 \quad (7.20)$$

This result is in agreement with the one obtained by the means of Bogoliubov transformation starting from the Hamiltonian written in the second-quantized form in the presence of disorder [HM92, ABCG02]. The normal density of a superfluid is an observable quantity. It was evaluated in liquid  $^4\text{He}$  by measuring of the moment of inertia of a rotating liquid or by measuring of the second sound velocity. Both methods can be, in principle, developed for BEC gases.

### 7.2.4 Drag force and energy dissipation

The force with which the impurity acts on the system is

$$\mathbf{F} = - \int |\psi(\mathbf{r})|^2 \vec{\nabla} (g_i \delta(\mathbf{r})) d^3r = g_i (\vec{\nabla} |\psi(\mathbf{r})|^2)_{\mathbf{r}=0} \quad (7.21)$$

Expanding the wave function into the sum of  $\phi_0$  and  $\delta\psi$  and neglecting terms of order  $\delta\psi^2$  we obtain

$$\mathbf{F} = g_i \phi_0 \int i\mathbf{k} [\delta\psi_{\mathbf{k}} + (\delta\psi_{-\mathbf{k}})^*] \frac{d^3k}{(2\pi)^3} = \int \frac{2(g_i \phi_0)^2 i\mathbf{k} (\hbar^2 k^2 / 2m)}{(\hbar\mathbf{k} \cdot \mathbf{V} + i0)^2 - \frac{\hbar^2 k^2}{2m} \left(\frac{\hbar^2 k^2}{2m} + 2\mu\right)} \frac{d^3k}{(2\pi)^3}, \quad (7.22)$$

where we added an infinitesimal positive imaginary part  $+i0$  to the frequency  $\mathbf{k} \cdot \mathbf{V}$  according to the usual Landau causality rule. The drag force is obviously directed along to the velocity  $\mathbf{V}$ . The integration (7.22) can be done by using the formula  $\frac{1}{x+i0} = \mathcal{P}\frac{1}{x} - i\pi\delta(x)$ . Due to the integration between symmetric limits, only the imaginary part contributes to the integral and the final value is real.

$$\mathbf{F} = 2(g_i \phi_0)^2 \int \frac{i\mathbf{k} \frac{\hbar^2 k^2}{2m} (-i\pi)}{2\hbar\mathbf{k}\mathbf{V}} \left[ \delta\left(\hbar\mathbf{k}\mathbf{V} - \sqrt{\frac{\hbar^2 k^2}{2m} \left(\frac{\hbar^2 k^2}{2m} + 2\mu\right)}\right) + \delta\left(\hbar\mathbf{k}\mathbf{V} + \sqrt{\frac{\hbar^2 k^2}{2m} \left(\frac{\hbar^2 k^2}{2m} + 2\mu\right)}\right) \right] \frac{d^3k}{(2\pi)^3} \quad (7.23)$$

It is convenient to do the integration in spherical coordinates with  $\vartheta$  being angle between  $\mathbf{k}$  and  $\mathbf{V}$ . There is no dependence on the angle  $\phi$  and it can be immediately integrated out

$$\int f(\mathbf{k}) d^3k = \int_0^\infty \int_0^\pi f(k, \vartheta) 2\pi k^2 \sin \vartheta dk d\vartheta = \int_0^\infty \int_{-1}^1 f(k, \cos \vartheta) 2\pi k^2 dk d(\cos \vartheta) \quad (7.24)$$

The  $\delta$ -function can be further developed

$$\delta\left(\hbar\mathbf{k}\mathbf{V} \pm \sqrt{\frac{\hbar^2 k^2}{2m} \left(\frac{\hbar^2 k^2}{2m} + 2\mu\right)}\right) = \frac{1}{\hbar k V} \delta\left(\cos \vartheta \pm \frac{1}{\hbar k V} \sqrt{\frac{\hbar^2 k^2}{2m} \left(\frac{\hbar^2 k^2}{2m} + 2\mu\right)}\right) \quad (7.25)$$

The poles in the integration over  $\cos \vartheta$  appear if the square root in the denominator is smaller than one, which leads to the restriction on the values of momentum which contribute

$$|k| \leq k_{\max} = 2m(V^2 - c^2)^{1/2}/\hbar \quad (7.26)$$

Thus the energy dissipation takes place only if the impurity moves with a speed larger than the speed of sound.

Let us calculate the projection  $F_V$  of the force  $\mathbf{F}$  to the direction  $\mathbf{V}$  of the movement of the perturbation. It means that we have to multiply formula (7.23) on  $\mathbf{V}/V$

$$F_V = (g_i \phi_0)^2 2 \int_0^{2m(V^2 - c^2)} \frac{\frac{\hbar^2 k^2}{2m} \pi}{\hbar V} \frac{1}{\hbar k V} \frac{2\pi k^2 dk}{(2\pi)^3} = \frac{(g_i \phi_0)^2 m}{2\pi \hbar^4 V^2} \frac{1}{2} (2m(V^2 - c^2))^2$$

Now we can use that square of the unperturbed wave function gives the density  $\phi_0^2 = n$  and the coupling constant can be expressed as

$$g_i = \frac{2\pi \hbar^2 b}{m}, \quad (7.27)$$

which can be obtained from the formula (1.86) recalling that the reduced mass is  $\mu = m$  for the scattering on a quenched impurity.

Finally, we obtain following expression for the projection of the force

$$F_V = 4\pi n b^2 m V^2 (1 - c^2/V^2)^2 \quad (7.28)$$

The energy dissipation,  $\dot{E} = -F_V V$ , can be evaluated by measuring the heating of the gas.

For large  $V$  the force is proportional to  $V^2$ . The energy dissipation per unit time can then be presented as  $\dot{E} = -\gamma E$  with the damping rate  $\gamma \sim n b^2 V$ .

Note in conclusion that our perturbative calculations can not describe processes involving dissipation of energy due to creation of quantized vortex rings. Such a creation is possible at  $V < c$  but has a small probability for low velocity and for a weak point-like impurity.

## 7.3 Low dimensional systems

In this type of experiment the role of the impurity can also be played by a laser beam with small enough size and intensity. The Fourier components of the perturbed wave function  $\delta\psi_{\mathbf{k}}$  are given by the formula (7.5), which is derived in an arbitrary number of dimensions. The only difference is in the substitution of  $d^3k/(2\pi)^3$  with  $d^Dk/(2\pi)^D$  in the integrals:

$$F_V = \frac{2ig_i^2\phi_0^2}{V} \int \frac{\mathbf{kV} \frac{\hbar^2 k^2}{2m}}{(\hbar\mathbf{kV})^2 - \frac{\hbar^2 k^2}{2m} \left( \frac{\hbar^2 k^2}{2m} + 2mc^2 \right)} \frac{d\mathbf{k}}{(2\pi)^D} \quad (7.29)$$

In the expression for the energy (7.13), the term quadratic in velocity is of a great interest, as the coefficient in front of  $V^2/2$  has physical meaning of an effective mass. We develop further this term:

$$\Delta E = g_i^2\phi_0^2 \int \frac{(\hbar\mathbf{kV})^2}{\frac{\hbar^2 k^2}{2m} \left( \frac{\hbar^2 k^2}{2m} + 2mc^2 \right)^2} \frac{d^Dk}{(2\pi)^D} = \frac{g_i^2\phi_0^2(2m)^3V^2}{D\hbar^4} \int \frac{1}{(k^2 + (2mc/\hbar)^2)^2} \frac{d^Dk}{(2\pi)^D}, \quad (7.30)$$

where we used symmetry properties  $\int f(k)(\mathbf{kV})^2 d^Dk = \frac{1}{D} \int f(k)(kV)^2 d^Dk$ .

### 7.3.1 Two-dimensional system

There are different possible geometries of the experiment. One can create a two-dimensional perturbation in the three-dimensional condensate. Such a two-dimensional impurity can be created, analogously to the MIT experiment [RKO<sup>+</sup>99, ORV<sup>+</sup>00], by a thin laser beam. Such a beam creates a cylindrical hole in the condensate, which is stirred by moving the position of the laser beam. Another possibility is to fix the position of the laser beam along the long axis of an elongated condensate, so that the dissipation can be studied by shaking the trap and exciting the breathing modes. The problem is to create a beam with a diameter which is small with compared to the correlation length. The theory can be easily generalized for beams of finite diameter. The intensity of the beam can be tuned to satisfy the condition of a weak perturbation.

The more interesting possibility is the investigation of true two-dimensional condensates, which can be created in plane optical traps, produced by a standing light wave. If the light intensity is large enough, tunneling between planes is small and the condensates behave as independent two dimensional systems. The impurity can again be created by a laser beam perpendicular to the condensate plane. Another possibility is to use impurity atoms, which can be drive by a laser beam, with a frequency close to the atomic resonance of the impurity.

We expand the two dimensional differential  $d^2k$  by its representation in the polar coordinates  $d^2k = kdkd\vartheta = -\frac{k}{\sqrt{1-\cos^2\vartheta}} dk d\cos\vartheta$ . The 3D integrate rule (7.24) should be substituted by

$$\int_{-\infty}^{\infty} dk_x \int_{-\infty}^{\infty} dk_y f(k_x, k_y) = 2 \int_0^{\infty} dk \int_{-1}^1 d\cos\vartheta \left( \frac{k f(k, \cos\vartheta)}{\sqrt{1-\cos^2\vartheta}} \right) \quad (7.31)$$

#### 7.3.1.1 Drag force

Now the projection of the force  $\mathbf{F}$  onto the direction of motion  $\mathbf{V}$  is given by the integral (7.29)

$$F_V^{2D} = -\frac{4ig_i^2\phi_0^2}{V} \int_0^{\infty} \int_{-1}^1 \frac{kV \cos\vartheta \frac{\hbar^2 k^2}{2m}}{(\hbar kV \cos\vartheta)^2 - \frac{\hbar^2 k^2}{2m} \left( \frac{\hbar^2 k^2}{2m} + 2mc^2 \right)} \frac{k}{\sqrt{1-\cos^2\vartheta}} \frac{dk d\cos\vartheta}{(2\pi)^2} = \quad (7.32)$$



$$= \frac{ig_i^2 \phi_0^2}{4\pi^2 m V^2} \int_{-1}^1 \int_0^{2\pi} \left( \frac{1}{\cos \vartheta + \sqrt{(\frac{\hbar^2 k^2}{2m} + 2mc^2) / 2mV^2}} + \frac{1}{\cos \vartheta - \sqrt{(\frac{\hbar^2 k^2}{2m} + 2mc^2) / 2mV^2}} \right) \frac{k^2 dk d\cos \vartheta}{\sqrt{1 - \cos^2 \vartheta}}$$

In the following we will introduce a two-dimensional density  $n_{2D} = N/L^2$ . The square of the unperturbed homogeneous solution equals to it  $\phi_0^2 = n_{2D}$ . The integral (7.32) is different from zero only if integrand has poles, which means that the velocity  $V$  must be larger than the speed of sound  $c$ . Only momenta smaller than  $k_{max}$  (see eq.(7.26)) contribute to the integral

$$F_V^{2D} = -\frac{ig_i^2 n_{2D}}{4\pi^2 m V^2} \int_0^{k_{max}} \frac{2\pi i k^2 dk}{\sqrt{1 - (\frac{\hbar^2 k^2}{2m} + 2mc^2) / 2mV^2}} = \frac{g_i^2 n_{2D}}{2\pi m V^2} \int_0^{k_{max}} \frac{2mV k^2 dk}{\hbar \sqrt{\frac{4m^2(V^2 - c^2)}{\hbar^2} - k^2}} \quad (7.33)$$

We recall simple integral equality  $\int_0^{\mathcal{Z}} \frac{k^2 dk}{\sqrt{\mathcal{Z}^2 - k^2}} = \frac{\pi}{4} \mathcal{Z}^2$  and finally have

$$F_V^{2D} = \frac{g_i^2 n_{2D}}{\hbar^3 V} (V^2 - c^2). \quad (7.34)$$

In a quasi two-dimensional system, *i.e.* when the gas is confined in the  $z$ -direction by the harmonic potential  $m\omega_z^2 z^2/2$ , the two-dimensional coupling constant equals (see 1.122)

$$g_i^{2D} = \sqrt{2\pi} \frac{\hbar^2 b}{m a_z}, \quad (7.35)$$

where  $a_z = \sqrt{\hbar/m\omega_z}$  is the oscillator length and  $b$  is the three-dimensional scattering length. We consider here only the mean-field 2D situation. See [PS03],§17 and [PGS04] for a more detail discussion.

Notice again that our calculations do not take into account creation of vortex pairs which is possible at  $V < c$ .

### 7.3.1.2 Effective mass

The energy depending on the velocity contribution is given by an integral (7.30), which can be easily calculated

$$\Delta E^{2D}(V) = \frac{g_i^2 n_{2D} (2m)^3 V^2}{2\hbar^4} \int_0^\infty \frac{1}{(k^2 + (2mc/\hbar)^2)^2} \frac{k dk}{(2\pi)^2} = \frac{g_i^2 n_{2D} m V^2}{4\pi^2 \hbar^2 c^2} \frac{1}{2} \quad (7.36)$$

From this result we infer the effective mass

$$m^* = g_i^2 n_{2D} m / (4\pi^2 \hbar^2 c^2) \quad (7.37)$$

## 7.3.2 One-dimensional system. Mean-field theory

### 7.3.2.1 Drag force

In one dimension the integration is straightforward. From (7.29) we find

$$F^{1D} = -\frac{imng_i^2}{\pi \hbar^2} \int_{-\infty}^{\infty} \left( \frac{1}{k + 2m\sqrt{V^2 - c^2}/\hbar} + \frac{1}{k - 2m\sqrt{V^2 - c^2}/\hbar} \right) dk \quad (7.38)$$



The integration over  $k$  gives  $2\pi i$  if  $V > c$  and zero otherwise. So, the force is

$$F^{1D} = \frac{2g_i^2 n_{1D} m}{\hbar^2}, \quad (7.39)$$

where  $n_{1D} = N/L$  is the linear density. In a quasi one dimensional system (*i.e.* a very elongated trap or a waveguide) there are no excitations in the radial harmonic confinement and the coupling constant is obtained from (1.69) keeping in mind that the reduced mass equals to the mass of an incident particle  $\mu = m$  for the scattering on a heavy impurity

$$g_i = -\frac{\hbar^2}{mb_{1D}} \quad (7.40)$$

For the non-resonance scattering  $b_{1D} = -a_{\perp}^2/b$ , where  $a_{\perp} = \sqrt{\hbar/m\omega_{\perp}}$ . The expression of the force in terms of the scattering length reads as

$$F^{1D} = 2n_{1D}\hbar^2/mb_{1D}^2 \quad (7.41)$$

An interesting peculiarity is that the result does not depend on the velocity  $V$  (where, of course, the velocity must be larger than the speed of sound). This phenomenon comes from particular properties of a  $\delta$ -potential, namely that the Fourier transform of this potential is a constant. Numerical solutions by Pavloff[Pav02] for finite-range potentials in 1D show no friction for  $V < c$ , maximal friction for  $V \geq c$  and smaller friction for  $V \gg c$ , although the constant result (7.41) was found for the  $\delta$ -potential.

In a 1D system energy dissipation is possible at  $V < c$  due to creation of the ‘‘gray solitons’’ first considered in [Tsu71]. Non-linear calculations [Hak97] show that the critical velocity for this process decreases with increasing coupling constant  $g_i$ .

This theory can be checked in an experiment in a three-dimensional condensate. The impurity can be presented by a moving light sheet.

### 7.3.2.2 Effective mass

The energy term (7.30), which depends on the velocity  $\mathbf{V}$  can be trivially calculated by using of the integral equality  $\int \frac{dx}{(x^2+a^2)^2} = \frac{1}{2a^3} \arctan \frac{x}{a} + \frac{x}{2a^2(x^2+a^2)}$ . The result of the integration is  $\Delta E^{1D}(V) = \frac{g_i^2 n V^2}{4\hbar c^3}$  and the effective mass is given by

$$m^* = g_i^2 n_{1D} / 2\hbar c^3. \quad (7.42)$$

It can be expressed in terms of the particle-particle  $a$  and particle-impurity  $b$  scattering lengths  $m^* = \frac{1}{\sqrt{3}2n_{1D}a} \left(\frac{a}{b}\right)^2 m$

### 7.3.2.3 Density profile

The wave function of the perturbation,  $\delta\psi_k$ , was obtained in the momentum representation and is given by expression (7.5). The spatial dependence,  $\delta\psi(x)$ , is related to  $\delta\psi_k$  by means of the Fourier transformation. We will find the density profile  $n(x) = |\psi(x)|^2$ . Within the same level of accuracy, as in the calculations above,  $n(x)$  is given by

$$n(x) \approx \phi_0^2 + \phi_0(\delta\psi(x) + \delta\psi^*(x)) \quad (7.43)$$

In terms of Fourier components one has  $\delta\psi(x) = \int e^{ikx} \delta\psi_k \frac{dk}{2\pi}$

$$n(x) = n_0 + \phi_0 \int e^{ikx} (\delta\psi_k + (\delta\psi_{-k})^*) \frac{dk}{2\pi} \quad (7.44)$$

where we used property of the Fourier transform  $(\delta\psi^*)_k = (\delta\psi_{-k})^*$ . Together with (7.5) and (7.40) we obtain a simple expression

$$n(x) = n_0 \left( 1 + \frac{4}{b_{1D}} \int_{-\infty}^{\infty} \frac{e^{ikx}}{k^2 + \frac{4m^2(c^2 - V^2)}{\hbar^2}} \frac{dk}{2\pi} \right) \quad (7.45)$$

There are two cases to be considered separately:

- 1) The impurity moves with velocity smaller than the speed of sound. We introduce the notation  $\varkappa = 2m\sqrt{c^2 - V^2}/\hbar > 0$  and note that the integral has form of the inverse Fourier transform of the Yukawa potential:

$$\int_{-\infty}^{\infty} \frac{e^{ikx}}{k^2 + \varkappa^2} \frac{dk}{2\pi} = \frac{\exp\{-\varkappa|x|\}}{2\varkappa} \quad (7.46)$$

Thus, the density perturbation has a form of a bump and decays exponentially fast:

$$n(x) = n_0 \left( 1 + \frac{2e^{-\varkappa|x|}}{\varkappa b_{1D}} \right) \quad (7.47)$$

For a repulsive interaction with the impurity the scattering length is negative  $b_{1D} < 0$  and the density is suppressed by the presence of the impurity. Instead an attractive interaction  $b_{1D} > 0$  leads to an increase in the density.

- 2) The impurity moves with velocity larger than the speed of sound. In this case we introduce  $\varkappa$  in the following way  $\varkappa = 2m\sqrt{V^2 - c^2}/\hbar > 0$ . There are poles appearing in the function in the integral. We use Landau causality rule  $k \rightarrow k + i0$  in order to modify the integration contour. In this case for  $x > 0$  the pole is absent and the integral vanishes. This means that there is no perturbation in front of the impurity (impurity moves to the right).

Instead for  $x < 0$  the pole is present and the integral is different from zero.

$$\int_{-\infty}^{\infty} \frac{e^{ikx}}{k^2 - \varkappa^2} \frac{dk}{2\pi} = \frac{\sin \varkappa x}{\varkappa} \quad (7.48)$$

so the density profile behind the perturbation is oscillating and corresponds to the wake generated by the moving impurity

$$n(x) = \begin{cases} n_0 \left( 1 + \frac{4}{\varkappa b_{1D}} \sin \varkappa x \right) & x < 0 \\ n_0 & x > 0 \end{cases} \quad (7.49)$$

The condition of the applicability of the perturbation theory demands the perturbation  $|n(x) - n_0|$  be small compared to the unperturbed solution  $n_0$ . This condition is satisfied if the velocity of the impurity  $V$  is not too close to the speed of sound  $c$ .

### 7.3.3 One-dimensional system. Bethe-ansatz theory

We saw in the previous subsection that for a weakly interacting impurity the drag force appears only when the impurity velocity  $V$  is larger than the Landau critical velocity, which is equal to the velocity of sound  $c$ . The situation is, however, different in the Bethe-ansatz Lieb-Liniger theory of a 1D Bose gas [LL63]. According to this theory excitations in the system actually have a fermionic nature. Even a low frequency perturbation can create a particle-hole pair with a total momentum near  $2p_F \equiv 2\hbar k_F = \hbar 2\pi n_{1D}$ . To calculate the drag force for this case we will use the dynamic form factor of the system  $\sigma(\omega, k)$  (we follow notation of [LP80], §87). The dissipated energy at  $T = 0$  can be calculated as

$$\dot{E} = - \int_{-\infty}^{\infty} \frac{dk}{2\pi} \int_0^{\infty} \frac{d\omega}{\pi} \omega \frac{n_{1D}}{2\hbar} \sigma(\omega, k) |U(\omega, k)|^2, \quad (7.50)$$

where  $U(\omega, k) = 2\pi g_i \delta(\omega - kV)$  is the Fourier transform of the impurity potential  $U(t, z) = g_i \delta(z - Vt)$ . One has  $|U(\omega, k)|^2 = 2\pi g_i^2 t \delta(\omega - kV)$ , where  $t$  is "time of observation". Thus the energy dissipation per unit of time is

$$\dot{E} = -F_V V = -\frac{g_i^2 n_{1D} V}{\hbar} \int_0^{\infty} \frac{dk}{2\pi} k \sigma(kV, k), \quad (7.51)$$

where  $F_V$  is the drag force. We will try to estimate the velocity dependence of  $F_V$ .

For low frequency dissipation the important values of  $k$  are near  $2k_F$ . According to [NLCC94]

$$\sigma(\omega, 2k_F) \sim \omega^{(\eta-2)}, \omega \rightarrow 0, \quad (7.52)$$

where  $\eta = \frac{2\hbar k_F}{mc} = \frac{2\pi\hbar n_{1D}}{mc} \geq 2$  is the characteristic parameter of a 1D Bose gas. In the mean-field limit when  $n_{1D} \rightarrow \infty$  the parameter  $\eta \rightarrow \infty$ . In the opposite case of a small density bosons behave as impenetrable particles (Tonks-Girardeau limit [Gir60]) and the dynamic form-factor coincides with the one of an ideal Fermi gas. In this limit  $\eta = 2$ .

In the general case one can calculate  $\sigma(\omega, k)$  at small  $\omega$  and  $k \approx 2k_F$  generalizing the method of Haldane [Hal81] for the case of time-dependent correlation functions. Calculations give

$$\sigma(\omega, k) = \frac{n_{1D} c}{\omega^2} \left( \frac{\hbar\omega}{mc^2} \right)^\eta f\left(\frac{c\Delta k}{\omega}\right), \omega > 0, k > 0, \quad (7.53)$$

where  $k = 2k_F + \Delta k$  and the function  $f(x)$  is

$$f(x) = A(\eta) (1 - x^2)^{\eta/2-1} \quad (7.54)$$

in the interval  $|x| < 1$  and is equal to zero at  $|x| \geq 1$  (see also [KBI93]). The constant  $A(\eta)$  can be calculated in two limiting cases:  $A(\eta = 2) = \pi/4$  (see [PS03] §17.3) and  $A(\eta) \approx 4\pi^2 / [(8C)^\eta \Gamma^2(\frac{\eta}{2})]$ , where  $C = 1.78\dots$  is the Euler's constant (see Eq. 1.186), for  $\eta \gg 1$ .

Substituting (7.53) into (7.51) we finally find velocity dependence of the drag force:

$$F_V = \frac{\Gamma(\frac{\eta}{2})}{2\sqrt{\pi}\Gamma(\frac{\eta+1}{2})} A(\eta) \frac{g_i^2 n_{1D}^2}{\hbar V} \left( \eta \frac{V}{c} \right)^\eta \quad (7.55)$$

Equation (7.55) is valid for the condition  $V \ll c$ .

Thus in the Tonks-Girardeau strong-interaction limit  $F_V \sim V$  and Bose gas behaves, from the point of view of friction, as a normal system, where the drag force is proportional to the velocity. On the contrary, in the mean-field limit the force is very small and the behavior of the system is analogous to a 3D superfluid. However, even in this limit the presence of the small force makes a great difference. Let us imagine that our system is twisted into a ring, and that the impurity rotates around the ring with a small angular velocity. If the system is superfluid in the usual sense of the word, the superfluid part must stay at rest. Presence of the drag force means that equilibrium will be reached only when the gas as a whole rotates with the same angular velocity. From this point of view the superfluid part of the 1D Bose gas is equal to zero even at  $T = 0$ . Notice that in an earlier paper [Son71] the author concluded that  $\rho_s = \rho$  at  $T = 0$  for arbitrary  $\eta$ . We believe that this difference results from different definitions of  $\rho_s$  and reflects the non-standard nature of the system.

Equation (7.55) is equivalent to a result which was obtained by a different method in [BGB01], with a model consisting of an impurity considered as a Josephson junction. Notice that the process of dissipation, which in the language of fermionic excitations can be described as creation of a particle-hole pair, corresponds in the mean-field limit to creation of a phonon and a small-energy soliton. It seems that such a process cannot be described in the mean-field approach in the linear approximation.

Experimental confirmation of these quite non-trivial predictions demands a true one-dimensional condensate, where non mean-field effects can be sufficiently large. Such condensates have been investigated for the first time in experiments [SKC<sup>+</sup>01, GVL<sup>+</sup>01]. In experiments [GVL<sup>+</sup>01, SMS<sup>+</sup>04] condensates have been created in the form of elongated independent "needles" in optical traps, consisting of two perpendicular standing laser waves. The role of an impurity in this case must be played by a light sheet, perpendicular to the axis of condensates and moving along them.

Notice also, that application of the additional light waves in this experiments of this type allows one to create a harmonic perturbation of the form

$$U(t, z) = U_0 \cos(\omega t - kz), \quad k = 2k_F + \Delta k \quad (7.56)$$

with small  $\omega$  and  $\Delta k$ . Such potential with was used in [GVL<sup>+</sup>01, SMS<sup>+</sup>04] for experiments with 1D condensate in a periodic lattice. However, for a small amplitude  $U_0$ , measurement of the dissipation energy  $Q$  gives, according to (7.50), the dynamic form-factor  $S(\omega, k)$  directly.

## 7.4 Conclusions

We have studied motion of an impurity through the condensate at zero temperature by considering the perturbation of a stationary solution of the GP equation. We calculated the induced mass which contributes to the mass of normal component. We find that the motion at small velocities is dissipationless in one-, two-, and three- dimensional systems, although movement with velocities larger than the speed of sound leads to a non-zero drag force due to Cherenkov radiation of phonons. The expressions for the drag force are calculated. We used results for the dynamic form factor of exact Lieb-Liniger theory to investigate the velocity dependence of the drag force in a 1D system. The form factor was calculated with the help of the Haldane method of calculations of correlation functions. The drag force exists at an arbitrarily small velocity of motion, but is very small in the mean-field limit. The dynamic form-factor can be also directly measured by applying a harmonic time-dependent perturbation on one-dimensional condensates [GVL<sup>+</sup>01, SMS<sup>+</sup>04].

# Chapter 8

## Interacting fermions in highly elongated harmonic traps

### 8.1 Introduction

The study of cold quasi one dimensional atomic quantum gases presents a very active area of research. So far, most of the experimental [GVL<sup>+</sup>01, SKC<sup>+</sup>01, GBM<sup>+</sup>01, TOH<sup>+</sup>04, MSKE03] and theoretical [Ols98, PSW00, DLO01, MS02, GWT01] investigations have been devoted to quasi-one dimensional Bose gases and, in particular, to the strongly-interacting Tonks-Girardeau gas, which can be mapped to a gas of non-interacting fermions [Gir60, Ols98, RT03]. Quasi-1D two-component atomic Fermi gases have not been realized experimentally yet; however, their realization in highly-elongated, needle-shaped traps is within reach of present-day techniques. The behavior of quasi one dimensional two-component Fermi gases can, if the confinement is chosen properly, be characterized to a very good approximation by an effective 1D coupling constant,  $g_{1D}$ , which encapsulates the interspecies atom-atom interaction strength. This coupling constant can be tuned to essentially any value, including zero and  $\pm\infty$ , by varying the 3d  $s$ -wave scattering length  $a_{3d}$  through application of an external magnetic field in the proximity of a Feshbach resonance.

The role of interactions in quasi one dimensional atomic Fermi gases has been studied mainly in connection with Luttinger liquid theory [XW02, GW04, RFZZ03a, RFZZ03b]. Recati *et al.* [RFZZ03a, RFZZ03b] investigate the properties of a two-component Fermi gas with *repulsive* interspecies interactions confined in highly-elongated harmonic traps. In the limit of weak and strong coupling these authors relate the parameters of the Luttinger Hamiltonian, which describe the low-energy properties of the gas, to the microscopic parameters of the system. The prospect of realizing Luttinger liquids with cold fermionic atoms is fascinating since it would allow detailed investigations of strongly correlated many-body systems, which play a central role in condensed matter physics<sup>1</sup>, to be conducted.

In homogeneous 1D Fermi gases with attractive interactions, sound waves propagate with a well defined velocity, while spin waves exhibit a gap [KO75]. Furthermore, in the strong-coupling regime, the ground state is comprised of bosonic molecules (consisting of two fermions with different spin), whose spatial size is much smaller than the average intermolecular distance [KO75]. Consequently, BCS-type equations have been discussed for effectively attractive 1D interactions [CEE<sup>+</sup>91]. The quasi one dimensional molecular Bose gas discussed here (see also Ref. [Tok04, FRZ04]) has similar-

---

<sup>1</sup>See, *e.g.*, [Voi95]

ities with the formation of a molecular Bose-Einstein condensate (BEC) from a 3d Fermi sea close to a magnetic atom-atom Feshbach resonance [GRJ03, ZSS<sup>+</sup>03].

This Chapter investigates the properties of inhomogeneous quasi one dimensional two-component Fermi gases under harmonic confinement with *attractive* and *repulsive* interspecies interactions. Our study is based on the exact equation of state of a homogeneous 1D system of fermions with zero-range attractive [Gau67, KO75] and repulsive [Yan67] interactions treated within the local density approximation (Sec. 1.6). We calculate the energy per particle, the size of the cloud, and the frequency of the lowest compressional mode as a function of the effective 1D coupling constant, including infinitely strong attractive and repulsive interactions. Our predictions for the size of the cloud and for the breathing mode frequency have immediate implications for experimental studies. It has been shown recently for quasi one dimensional Bose gases [MSKE03] that precise measurements of collective mode frequencies can provide evidence for beyond mean-field effects. For attractive interactions we discuss the cross-over from the weak- to the strong-coupling regime and point out the possibility of forming a mechanically stable molecular Tonks-Girardeau gas.

## 8.2 Model

Consider a two-component atomic Fermi gas confined in a highly-elongated trap. The fermionic atoms are assumed to belong to the same atomic species, that is, to have the same mass  $m$ , but to be trapped in different hyperfine states  $\sigma$ , where  $\sigma$  represents a generalized spin or angular momentum,  $\sigma = \uparrow$  or  $\downarrow$ . The trapping potential is assumed to be harmonic and axially symmetric,

$$V_{trap} = \sum_{i=1}^N \frac{1}{2} m (\omega_\rho^2 \rho_i^2 + \omega_z^2 z_i^2) \quad (8.1)$$

Here,  $\rho_i = \sqrt{x_i^2 + y_i^2}$  and  $z_i$  denote, respectively, the radial and longitudinal coordinate of the  $i$ th atom;  $\omega_\rho$  and  $\omega_z$  denote, respectively, the angular frequency in the radial and longitudinal direction; and  $N$  denotes the total number of atoms. We require the anisotropy parameter  $\lambda$ ,  $\lambda = \omega_z/\omega_\rho$ , to be so small that the transverse motion is “frozen” to zero point oscillations. At zero temperature this implies that the Fermi energy associated with the longitudinal motion of the atoms in the absence of interactions,  $\epsilon_F = N\hbar\omega_z/2$ , is much smaller than the separation between the levels in the transverse direction,  $\epsilon_F \ll \hbar\omega_\rho$ . This condition is fulfilled if  $\lambda \ll 1/N$ . The outlined scenario can be realized experimentally with present-day technology using optical traps.

If the Fermi gas is kinematically in 1D, it can be described by an effective 1D Hamiltonian with contact interactions,

$$H = N\hbar\omega_\rho + H_{1D}^0 + \sum_{i=1}^N \frac{1}{2} m \omega_z^2 z_i^2, \quad (8.2)$$

where

$$H_{1D}^0 = -\frac{\hbar^2}{2m} \sum_{i=1}^N \frac{\partial^2}{\partial z_i^2} + g_{1D} \sum_{i=1}^{N_\uparrow} \sum_{j=1}^{N_\downarrow} \delta(z_i - z_j) \quad (8.3)$$

and  $N = N_\uparrow + N_\downarrow$ . This effective Hamiltonian accounts for the interspecies atom-atom interactions, which are parameterized by the 3d  $s$ -wave scattering length  $a_{3d}$ , through the effective 1D coupling constant  $g_{1D}$  [Ols98, BMO03],

$$g_{1D} = \frac{2\hbar^2 a_{3d}}{m a_\rho^2} \frac{1}{1 - A a_{3d}/a_\rho}, \quad (8.4)$$

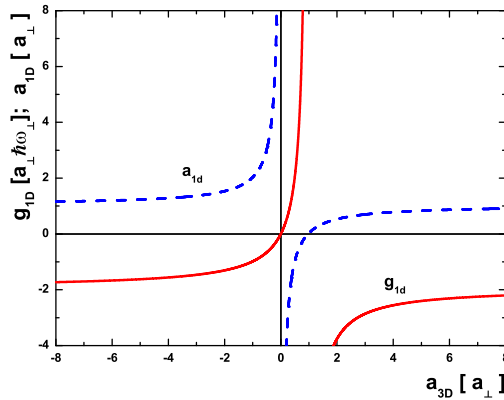


Figure 8.1: Effective 1D coupling constant  $g_{1D}$  [solid line, Eq. 8.4], together with effective 1D scattering length  $a_{1D}$  [dashed line, Eq. 8.5] as a function of  $a_{3d}$ .

but neglects the typically much weaker  $p$ -wave interactions. In Eq. 8.4,  $a_{\rho} = \sqrt{\hbar/m\omega_{\rho}}$  is the characteristic oscillator length in the transverse direction and  $A = |\zeta(1/2)|/\sqrt{2} \simeq 1.0326$ . Alternatively,  $g_{1D}$  can be expressed through the effective 1D scattering length  $a_{1D}$ ,  $g_{1D} = -2\hbar^2/(ma_{1D})$ , where

$$a_{1D} = -a_{\rho} \left( \frac{a_{\rho}}{a_{3d}} - A \right) \quad (8.5)$$

Figure 8.1 shows  $g_{1D}$  and  $a_{1D}$  as a

function of the 3d  $s$ -wave scattering length  $a_{3d}$ , which can be varied continuously by application of an external field. The effective 1D interaction is repulsive,  $g_{1D} > 0$ , for  $0 < a_{3d} < a_{3d}^c$  ( $a_{3d}^c = 0.9684a_{\rho}$ ), and attractive,  $g_{1D} < 0$ , for  $a_{3d} > a_{3d}^c$  and for  $a_{3d} < 0$ . By varying  $a_{3d}$ , it is possible to go adiabatically from the weakly-interacting regime ( $g_{1D} \sim 0$ ) to the strongly-interacting repulsive regime ( $g_{1D} \rightarrow +\infty$  or  $a_{3d} \lesssim a_{3d}^c$ ), as well as from the weakly-interacting regime to the strongly-interacting attractive regime ( $g_{1D} \rightarrow -\infty$  or  $a_{3d} \gtrsim a_{3d}^c$ )<sup>2</sup>

For two fermions with different spin the Hamiltonian  $H_{1D}^0$ , Eq. 8.3, supports one bound state with binding energy  $\epsilon_{bound} = -\hbar^2/(ma_{1D}^2)$  and spatial extent  $\sim a_{1D}$  for  $g_{1D} < 0$ , and no bound state for  $g_{1D} > 0$ , that is, the molecular state becomes exceedingly weakly-bound and spatially-delocalized as  $g_{1D} \rightarrow 0^-$  [Ols98, BMO03]. In the following we investigate the properties of a gas with  $N$  fermions,  $N_{\uparrow} = N_{\downarrow}$ , for both effectively *attractive and repulsive* 1D interactions *with and without* longitudinal confinement.

## 8.3 Homogeneous system

Consider the Hamiltonian  $H_{1D}^0$ , Eq. 8.3, which describes a homogeneous 1D two-component Fermi gas. The ground state energy  $E_{hom}$  of  $H_{1D}^0$  has been calculated exactly using Bethe's ansatz for attractive [Gau67] and repulsive [Yan67] interactions, and can be expressed in terms of the linear number density  $n_{1D} = N/L$ , where  $L$  is the size of the system,

$$\frac{E_{hom}}{N} = \frac{\hbar^2 n_{1D}^2}{2m} e(\gamma) \quad (8.6)$$

<sup>2</sup>Note that Eqs. 1.69-8.5 are valid only if the condition  $|a_{1D}| \gg a_{\rho}^3 n_{1D}^2$  is satisfied [Ols98].



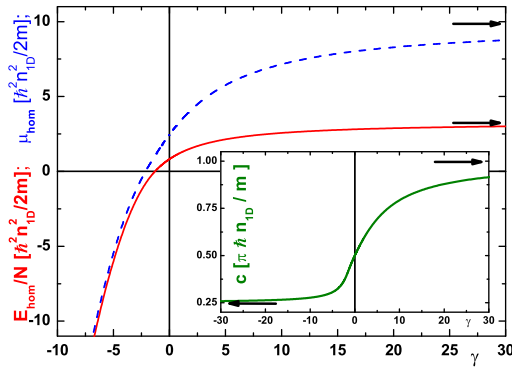


Figure 8.2:  $E_{hom}/N$  (solid line),  $\mu_{hom}$  (dashed line) and  $c$  (inset) for a homogeneous two-component 1D Fermi gas as a function of  $\gamma$  (horizontal arrows indicate the asymptotic values of  $E_{hom}/N$ ,  $\mu_{hom}$  and  $c$ , respectively).

The dimensionless parameter  $\gamma$  is proportional to the coupling constant  $g_{1D}$ ,  $\gamma = mg_{1D}/(\hbar^2 n_{1D})$ , while its absolute value is inversely proportional to the 1D gas parameter  $n_{1D}|a_{1D}|$ ,  $|\gamma| = 2/n_{1D}|a_{1D}|$ . The function  $e(\gamma)$  is obtained by solving a set of integral equations<sup>3</sup>, which is similar to that derived by Lieb and Liniger [LL63] for 1D bosons with repulsive contact interactions. To obtain the energy per particle, Eq. 8.6, we solve these integral equations for  $\gamma < 0$  [Gau67] and for  $\gamma > 0$  [Yan67].

Figure 8.2 shows the energy per particle,  $E_{hom}/N$  (solid line), the chemical potential  $\mu_{hom}$ ,  $\mu_{hom} = dE_{hom}/dN$  (dashed line), and the velocity of sound  $c$  (inset), which is obtained from the inverse compressibility  $mc^2 = n_{1D}\partial\mu_{hom}/\partial n_{1D}$ , as a function of the interaction strength  $\gamma$ . In the weak coupling limit,  $|\gamma| \ll 1$ ,  $\mu_{hom}$  is given by

$$\mu_{hom} = \frac{\pi^2}{4} \frac{\hbar^2 n_{1D}^2}{2m} + \gamma \frac{\hbar^2 n_{1D}^2}{2m} + \dots, \quad (8.7)$$

where the first term on the right hand side is the energy of an ideal two-component atomic Fermi gas, and the second term is the mean-field energy, which accounts for interactions. The chemical potential increases with increasing  $\gamma$ , and reaches an asymptotic value for  $\gamma \rightarrow \infty$  (indicated by a horizontal arrow in Fig. 8.2),

$$\mu_{hom} = \pi^2 \frac{\hbar^2 n_{1D}^2}{2m} - \frac{16\pi^2 \ln(2)}{3\gamma} \frac{\hbar^2 n_{1D}^2}{2m} + \dots. \quad (8.8)$$

The first term on the right hand side coincides with the chemical potential of a one-component ideal 1D Fermi gas with  $N$  atoms, the second term has been calculated in [RFZZ03a]. Interestingly, for  $\gamma \gg 1$ , the strong atom-atom repulsion between atoms with different spin plays the role of an effective Pauli principle [RFZZ03a, RFZZ03b].

For attractive interactions and large enough  $|\gamma|$  the energy per particle is negative (see Fig. 8.2), reflecting the existence of a molecular Bose gas, which consists of  $N/2$  diatomic molecules with binding energy  $\epsilon_{bound}$ . Each molecule is comprised of two atoms with different spin. In the limit

<sup>3</sup>Details on the numerical solution of the integral equations and a table for the function  $e(\gamma)$  can be downloaded from <http://www.science.unitn.it/~astra/1Dfermions/>.



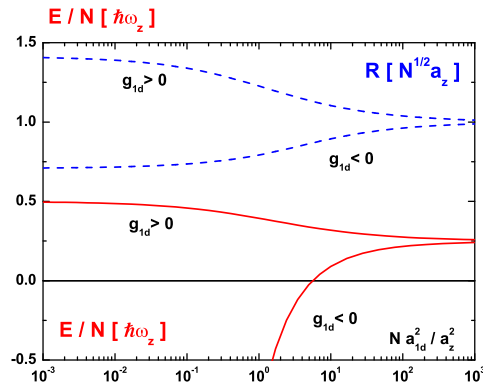


Figure 8.3: Energy per particle,  $E/N - \hbar\omega_\rho$  (solid lines), and size of the cloud,  $R$  (dashed lines), for an inhomogeneous two component 1D Fermi gas as a function of  $Na_{1D}^2/a_z^2$  for repulsive ( $g_{1D} > 0$ ) and attractive ( $g_{1D} < 0$ ) interactions.

$\gamma \rightarrow -\infty$ , the chemical potential becomes

$$\mu_{hom} = -\frac{\hbar^2}{2ma_{1D}^2} + \frac{\pi^2}{16} \frac{\hbar^2 n_{1D}^2}{2m} - \frac{\pi^2}{12\gamma} \frac{\hbar^2 n_{1D}^2}{2m} + \dots \quad (8.9)$$

The first term is simply  $\epsilon_{bound}/2$ , one half of the binding energy of the 1D molecule, while the second term is equal to half of the chemical potential of a bosonic Tonks-Girardeau gas with density  $n_{1D}/2$ , consisting of  $N/2$  molecules with mass  $2m$ <sup>4</sup>. Importantly, the compressibility remains positive for  $\gamma \rightarrow -\infty$  [a horizontal arrow in the inset of Fig. 8.2 indicates the asymptotic value of  $c$ ,  $c = \pi\hbar n_{1D}/(4m)$ ], which implies that two-component 1D Fermi gases are mechanically stable even in the strongly-attractive regime. In contrast, the ground state of 1D Bose gases with  $g_{1D} < 0$  has negative compressibility [McG64] and is hence mechanically unstable.

## 8.4 Trapped system

Using the solutions for the homogeneous two-component 1D Fermi gas, we now describe the inhomogeneous gas, Eq. 8.2, within the LDA [DLO01, MS02, RFZZ03a]. This approximation is applicable if the size  $R$  of the cloud is much larger than the harmonic oscillator length  $a_z$  in the longitudinal direction,  $a_z = \sqrt{\hbar/m\omega_z}$ , implying  $\epsilon_F \gg \hbar\omega_z$  and  $N \gg 1$ . The chemical potential  $\mu$  of the inhomogeneous system can be determined from the local equilibrium condition,

$$\mu = \mu_{hom}[n_{1D}(z)] + \frac{1}{2}m\omega_z^2 z^2, \quad (8.10)$$

and the normalization condition  $N = \int_{-R}^R n_{1D}(z) dz$ , where  $z$  is measured from the center of the trap,  $R = \sqrt{2\mu'/(m\omega_z^2)}$ , and  $\mu' = \mu$  for  $g_{1D} > 0$  and  $\mu' = \mu + |\epsilon_{bound}|/2$  for  $g_{1D} < 0$ . The normalization condition can be reexpressed in terms of the dimensionless chemical potential  $\tilde{\mu}$  and the dimensionless

<sup>4</sup>The coefficient and sign of the third term on the right hand side of Eq. 8.9 differ from Eq. A7 in Ref. [CEE<sup>+</sup>91].

density  $\tilde{n}_{1D}$  [ $\tilde{\mu} = \mu' / (\hbar^2 / 2ma_{1D}^2)$ ] and  $\tilde{n}_{1D} = |a_{1D}|n_{1D}$ ,

$$N \frac{a_{1D}^2}{a_z^2} = \int_0^{\tilde{\mu}} \frac{\tilde{n}_{1D}(\tilde{\mu} - x)}{\sqrt{x}} dx. \quad (8.11)$$

This expression emphasizes that the coupling strength is determined by  $Na_{1D}^2/a_z^2$ ;  $Na_{1D}^2/a_z^2 \gg 1$  corresponds to the weak coupling and  $Na_{1D}^2/a_z^2 \ll 1$  to the strong coupling regime, irrespective of whether the interactions are attractive or repulsive [MS02].

Figure 8.3 shows the energy per particle  $E/N$  and the size  $R$  of the cloud as a function of the coupling strength  $Na_{1D}^2/a_z^2$  for positive and negative  $g_{1D}$  calculated within the LDA for an inhomogeneous two-component 1D Fermi gas. Compared to the non-interacting gas, for which  $R = \sqrt{N}a_z$ ,  $R$  increases for repulsive interactions and decreases for attractive interactions. For  $Na_{1D}^2/a_z^2 \ll 1$ ,  $R$  reaches the asymptotic value  $\sqrt{2N}a_z$  for the strongly repulsive regime,  $g_{1D} \rightarrow +\infty$ , and the value  $\sqrt{N/2}a_z$  for the strongly attractive regime,  $g_{1D} \rightarrow -\infty$ . The shrinking of the cloud for attractive interactions reflects the formation of tightly bound molecules. In the limit  $g_{1D} \rightarrow -\infty$ , the energy per particle approaches  $\epsilon_{bound}/2 + N\hbar\omega_z/8 + \hbar\omega_\rho$ , indicating the formation of a molecular bosonic Tonks-Girardeau gas, consisting of  $N/2$  molecules. The size of the cloud shrinks from  $R = \sqrt{2N}a_z$  in the strongly repulsive regime ( $Na_{1D}^2/a_z^2 \ll 1$  and  $g_{1D} > 0$ ) to  $R = \sqrt{N/2}a_z$  in the strongly attractive regime ( $Na_{1D}^2/a_z^2 \ll 1$  and  $g_{1D} < 0$ ). We also notice that, similarly to the homogeneous case, for large attractive interactions the energy per particle approaches the molecular binding energy  $\epsilon_{bound}$ .

Using a sum rule approach, the frequency  $\omega$  of the lowest compressional (breathing) mode of harmonically trapped 1D gases can be calculated from the mean-square size of the cloud  $\langle z^2 \rangle$  [MS02],

$$\omega^2 = -2 \frac{\langle z^2 \rangle}{d\langle z^2 \rangle/d\omega_z^2} \quad (8.12)$$

In the weak and strong coupling regime ( $Na_{1D}^2/a_z^2 \gg 1$  and  $\ll 1$ , respectively),  $\langle z^2 \rangle$  has the same dependence on  $\omega_z$  as the ideal 1D Fermi gas. Consequently,  $\omega$  is in these limits given by  $2\omega_z$ , irrespective of whether the interaction is repulsive or attractive. Solid lines in Fig. 8.3 show  $\omega^2$ , determined numerically from Eq. 8.12, as a function of the interaction strength  $Na_{1D}^2/a_z^2$ . A non-trivial behavior of  $\omega^2$  as a function of  $Na_{1D}^2/a_z^2$  is visible. To gain further insight, we calculate the first correction  $\delta\omega$  to the breathing mode frequency  $\omega$  [ $\omega = 2\omega_z(1 + \delta\omega/\omega_z + \dots)$ ] analytically for weak repulsive and attractive interactions, as well as for strong repulsive and attractive interactions. For the weak coupling regime, we find  $\delta\omega/\omega_z = \pm(4/3\pi^2)/(Na_{1D}^2/a_z^2)^{1/2}$ , where the minus sign applies to repulsive interactions and the plus sign to attractive interactions. For the strong coupling regime, we find  $\delta\omega/\omega_z = -[16\sqrt{2}\ln(2)/15\pi^2](Na_{1D}^2/a_z^2)^{1/2}$  for repulsive interactions and  $\delta\omega/\omega_z = (8\sqrt{2}/15\pi^2)(Na_{1D}^2/a_z^2)^{1/2}$  for attractive interactions (see Table 1.1). Dashed lines in Fig. 8.4 show the resulting analytic expansions for  $\omega^2$ , which describe the lowest breathing mode frequency quite well over a fairly large range of interaction strengths but break down for  $Na_{1D}^2/a_z^2 \sim 1$ .

## 8.5 Conclusions

In conclusion, we have investigated the cross-over from weak to strong coupling of quasi one dimensional harmonically trapped two-component Fermi gases with both repulsive and attractive effective interactions. The frequency of the lowest breathing mode, which can provide an experimental signature of the cross-over, is calculated. We predict the existence of a stable molecular Tonks-Girardeau gas in the strongly attractive regime.

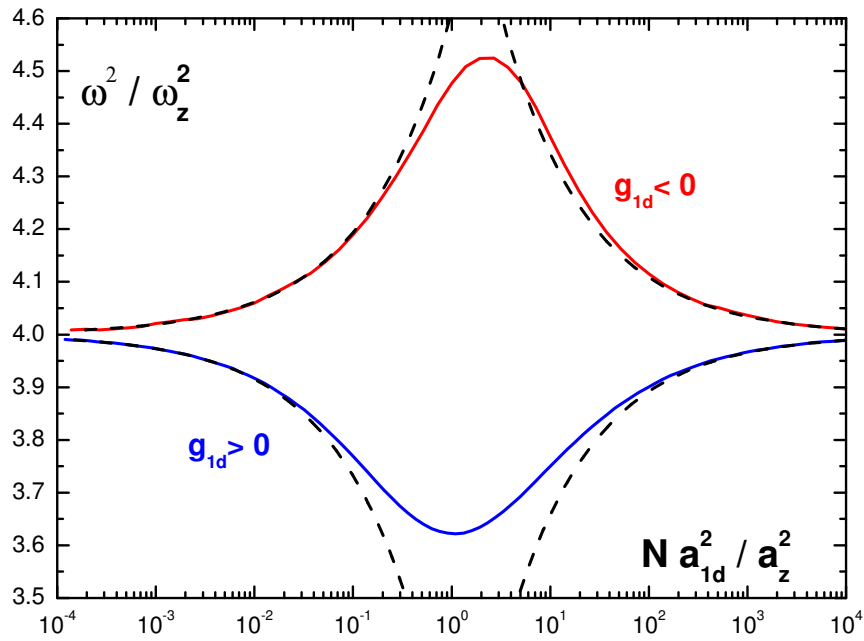


Figure 8.4: Square of the lowest breathing mode frequency,  $\omega^2$ , as a function of the coupling strength  $Na_{1D}^2/a_z^2$  for an inhomogeneous two-component 1D Fermi gas with repulsive ( $g_{1D} > 0$ ) and attractive ( $g_{1D} < 0$ ) interactions determined numerically from Eq. 8.12 (solid lines). Dashed lines show analytic expansions.



# Chapter 9

## BEC-BCS crossover

### 9.1 Introduction

Recent experiments on two-component ultracold atomic Fermi gases near a Feshbach resonance have opened the possibility of investigating the crossover from a Bose-Einstein condensate (BEC) to a Bardeen-Cooper-Schrieffer (BCS) superfluid. In these systems the strength of the interaction can be varied over a very wide range by magnetically tuning the two-body scattering amplitude. For positive values of the  $s$ -wave scattering length  $a$ , atoms with different spins are observed to pair into bound molecules which, at low enough temperature, form a Bose condensate [JBA<sup>+</sup>03, GRJ03, ZSS<sup>+</sup>03]. The molecular BEC state is adiabatically converted into an ultracold Fermi gas with  $a < 0$  and  $k_F|a| \ll 1$  [BAR<sup>+</sup>04a, BKC<sup>+</sup>04], where standard BCS theory is expected to apply. In the crossover region the value of  $|a|$  can be orders of magnitude larger than the inverse Fermi wave vector  $k_F^{-1}$  and one enters a new strongly-correlated regime known as unitary limit [OHG<sup>+</sup>02, BAR<sup>+</sup>04b, BKC<sup>+</sup>04]. In dilute systems, for which the effective range of the interaction  $R_0$  is much smaller than the mean interparticle distance,  $k_F R_0 \ll 1$ , the unitary regime is believed to be universal [Hei01, Bru04, PCHK04, DH04]. In this regime, the only relevant energy scale should be given by the energy of the noninteracting Fermi gas,

$$\epsilon_{FG} = \frac{3}{10} \frac{\hbar^2 k_F^2}{m}. \quad (9.1)$$

The unitary regime presents a challenge for many-body theoretical approaches because there is not any obvious small parameter to construct a well-posed theory. The first theoretical studies of the BEC-BCS crossover at zero temperature are based on the mean-field BCS equations [Leg80, NSR85, ERdM97]. More sophisticated approaches take into account the effects of fluctuations [PS00, PPS04], or include explicitly the bosonic molecular field [HKCW01, OG03]. These theories provide a correct description in the deep BCS regime, but are only qualitatively correct in the unitary limit and in the BEC region. In particular, in the BEC regime the dimer-dimer scattering length has been calculated exactly from the solution of the four-body problem, yielding  $a_m = 0.6a$  [PSS04]. Available results for the equation of state in this regime do not describe correctly the repulsive molecule-molecule interactions [HMOV04].

Quantum Monte Carlo techniques are the best suited tools for treating strongly-correlated systems. These methods have already been applied to ultracold degenerate Fermi gases in a recent work by Carlson *et al.* [CCPS03]. In this study the energy per particle of a dilute Fermi gas in the unitary limit is calculated with the fixed-node Green's function Monte Carlo method (FN-GFMC) giving the result  $E/N = \xi \epsilon_{FG}$  with  $\xi = 0.44(1)$ . In a subsequent work [CPCS04], the same authors

have extended the FN-GFMC calculations to investigate the equation of state in the BCS and BEC regimes. Their results in the BEC limit are compatible with a repulsive molecular gas, but the equation of state has not been extracted with enough precision.

In the present Chapter, we report results for the equation of state of a Fermi gas in the BEC-BCS crossover region using the fixed-node diffusion Monte Carlo method (FN-DMC). The interaction strength is varied over a very broad range from  $-6 \leq -1/k_F a \leq 6$ , including the unitary limit and the deep BEC and BCS regimes. In the unitary and in the BCS limit we find agreement, respectively, with the results of Ref. [CCPS03] and with the known perturbation expansion of a weakly attractive Fermi gas [HY57, LY57]. In the BEC regime, we find a gas of molecules whose repulsive interactions are well described by the dimer-dimer scattering length  $a_m = 0.6a$ . Results for the pair correlation functions of parallel and antiparallel spins are reported in the various regimes. In the BEC regime we find agreement with the pair correlation function of composite bosons calculated using the Bogoliubov approximation.

## 9.2 Model

The homogeneous two-component Fermi gas is described by the Hamiltonian

$$\hat{H} = -\frac{\hbar^2}{2m} \left( \sum_{i=1}^{N_\uparrow} \nabla_i^2 + \sum_{i'=1}^{N_\downarrow} \nabla_{i'}^2 \right) + \sum_{i,i'} V(r_{ii'}), \quad (9.2)$$

where  $m$  denotes the mass of the particles,  $i, j, \dots$  and  $i', j', \dots$  label, respectively, spin-up and spin-down particles and  $N_\uparrow = N_\downarrow = N/2$ ,  $N$  being the total number of atoms. We model the interspecies interatomic interactions using an attractive square-well potential:  $V(r) = -V_0$  for  $r < R_0$ , and  $V(r) = 0$  otherwise. In order to ensure that the mean interparticle distance is much larger than the range of the potential we use  $nR_0^3 = 10^{-6}$ , where  $n = k_F^3/(3\pi^2)$  is the gas number density. By varying the depth  $V_0$  of the potential one can change the value of the  $s$ -wave scattering length, which for this potential is given by  $a = R_0[1 - \tan(K_0 R_0)/(K_0 R_0)]$ , where  $K_0^2 = mV_0/\hbar^2$ . We vary  $K_0$  in the range:  $0 < K_0 < \pi/R_0$ . For  $K_0 R_0 < \pi/2$  the potential does not support a two-body bound state and  $a < 0$ . For  $K_0 R_0 > \pi/2$ , instead, the scattering length is positive,  $a > 0$ , and a molecular state appears whose binding energy  $\epsilon_b$  is determined by the transcendental equation  $\sqrt{|\epsilon_b| m/\hbar^2} R_0 \tan(\bar{K} R_0)/(\bar{K} R_0) = -1$ , where  $\bar{K}^2 = K_0^2 - |\epsilon_b| m/\hbar^2$ . The value  $K_0 = \pi/(2R_0)$  corresponds to the unitary limit where  $|a| = \infty$  and  $\epsilon_b = 0$ .

In the present study we resort to the Fixed Node Monte Carlo technique described in Sec. 2.4. We make use of the following trial wave functions. A BCS wave function

$$\psi_{BCS}(\mathbf{R}) = \mathcal{A} \left( \phi(r_{11'}) \phi(r_{22'}) \dots \phi(r_{N_\uparrow N_\downarrow}) \right), \quad (9.3)$$

and a Jastrow-Slater (JS) wave function

$$\psi_{JS}(\mathbf{R}) = \prod_{i,i'} \varphi(r_{ii'}) \left[ \mathcal{A} \prod_{i,\alpha} e^{i\mathbf{k}_\alpha \cdot \mathbf{r}_i} \right] \left[ \mathcal{A} \prod_{i',\alpha} e^{i\mathbf{k}_\alpha \cdot \mathbf{r}_{i'}} \right], \quad (9.4)$$

where  $\mathcal{A}$  is the antisymmetrizer operator ensuring the correct antisymmetric properties under particle exchange. In the JS wave function, Eq. (9.4), the plane wave orbitals have wave vectors  $\mathbf{k}_\alpha =$

$2\pi/L(\ell_{\alpha x}\hat{x} + \ell_{\alpha y}\hat{y} + \ell_{\alpha z}\hat{z})$ , where  $L$  is the size of the periodic cubic box fixed by  $nL^3 = N$ , and  $\ell$  are integer numbers. The correlation functions  $\phi(r)$  and  $\varphi(r)$  in Eqs. (9.3)-(9.4) are constructed from solutions of the two-body Schrödinger equation with the square-well potential  $V(r)$ . In particular, in the region  $a > 0$  we take for the function  $\phi(r)$  the bound-state solution  $\phi_{bs}(r)$  with energy  $\epsilon_b$  and in the region  $a < 0$  the unbound-state solution corresponding to zero scattering energy:  $\phi_{us}(r) = (R_0 - a)\sin(K_0r)/[r\sin(K_0R_0)]$  for  $r < R_0$  and  $\phi_{us}(r) = 1 - a/r$  for  $r > R_0$ . In the unitary limit,  $|a| \rightarrow \infty$ ,  $\phi_{bs}(r) = \phi_{us}(r)$ .

The JS wave function  $\psi_{JS}$ , Eq. (9.4), is used only in the region of negative scattering length,  $a < 0$ , with a Jastrow factor  $\varphi(r) = \phi_{us}(r)$  for  $r < \bar{R}$ . In order to reduce possible size effects due to the long range tail of  $\phi_{us}(r)$ , we have used  $\varphi(r) = C_1 + C_2 \exp(-\alpha r)$  for  $r > \bar{R}$ , with  $\bar{R} < L/2$  a matching point. The coefficients  $C_1$  and  $C_2$  are fixed by the continuity condition for  $\varphi(r)$  and its first derivative at  $r = \bar{R}$ , whereas the parameter  $\alpha > 0$  is chosen in such a way that  $\varphi(r)$  goes rapidly to a constant. Residual size effects have been finally determined carrying out calculations with an increasing number of particles  $N = 14, 38$ , and  $66$ . In the inset of Fig. 9.1 we show the dependence of the energy per particle  $E/N$  on  $N$  in the unitary limit. Similar studies carried out in the BEC and BCS regime show that the value  $N = 66$  is optimal since finite-size corrections in the energy are below the reported statistical error in the whole BEC-BCS crossover. We have also checked that effects due to the finite range  $R_0$  of the potential are negligible.

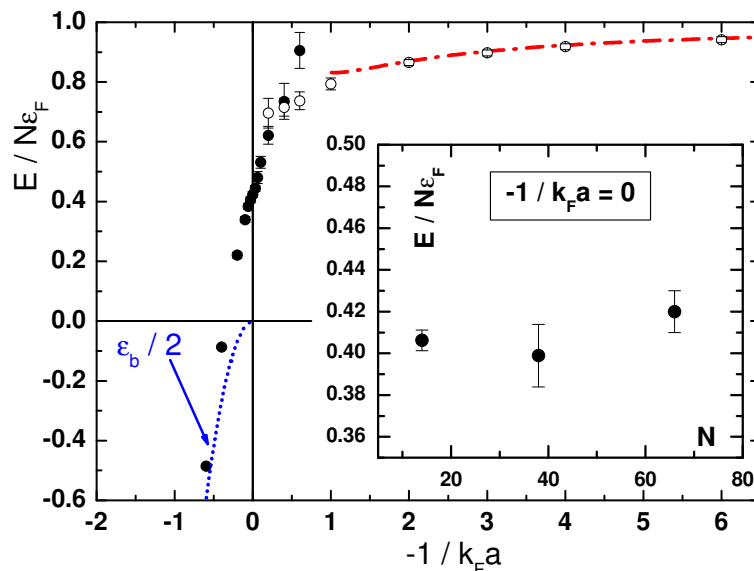


Figure 9.1: Energy per particle in the BEC-BCS crossover. Solid symbols refer to results obtained with the trial wave function  $\psi_{BCS}$ , open symbols refer to the ones obtained with  $\psi_{JS}$ . The red dot-dashed line is the expansion (9.5) holding in the BCS region and the blue dotted line corresponds to the binding energy  $\epsilon_b/2$ . Inset: finite size effects in the unitary limit  $-1/k_F a = 0$ .

### 9.3 Results

The FN-DMC energies for  $N = 66$  atoms and the potential  $V(r)$  with  $nR_0^3 = 10^{-6}$  are shown in Fig. 9.1 and in Table 9.3 as a function of the interaction parameter  $-1/k_F a$ . The numerical simulations are carried out both with the BCS wave function, Eq. (9.3), and with the JS wave function, Eq. (9.4). For  $-1/k_F a > 0.4$  we find that  $\psi_{JS}$  gives lower energies, whereas for smaller values of  $-1/k_F a$ , including the unitary limit and the BEC region, the function  $\psi_{BCS}$  is preferable. This behavior reflects the level of accuracy of the variational *ansatz* for the nodal structure of the trial wave function. We believe that in the intersection region,  $-1/k_F a \sim 0.4$ , both wave functions  $\psi_{BCS}$  and  $\psi_{JS}$  give a poorer description of the exact nodal structure of the state, resulting in a less accurate estimate of the energy. In the BCS region,  $-1/k_F a > 1$ , our results for  $E/N$  are in agreement with the perturbation expansion of a weakly attractive Fermi gas<sup>1</sup> [HY57, LY57]

$$\frac{E}{N\epsilon_{FG}} = 1 + \frac{10}{9\pi}k_F a + \frac{4(11 - 2\log 2)}{21\pi^2}(k_F a)^2 + \dots \quad (9.5)$$

$-1/k_F a$	$E/N$	$\epsilon_b/2$	$E/N - \epsilon_b/2$
-6	-73.170(2)	-73.1804	0.010(2)
-4	-30.336(2)	-30.3486	0.013(2)
-2	-7.071(2)	-7.1018	0.031(2)
-1	-1.649(3)	-1.7196	0.071(3)
-0.4	-0.087(6)	-0.2700	0.183(6)
-0.2	0.223(1)	-0.0671	0.29(1)
0	0.42(1)	0	0.42(1)
0.2	0.62(3)	0	0.62(3)
0.4	0.72(3)	0	0.72(3)
1	0.79(2)	0	0.79(2)
2	0.87(1)	0	0.87(1)
4	0.92(1)	0	0.92(1)
6	0.94(1)	0	0.94(1)

Table 9.1: Energy per particle and binding energy in the BEC-BCS crossover (energies are in units of  $\epsilon_{FG}$ ).

In the unitary limit we find  $E/N = \xi\epsilon_{FG}$ , with  $\xi = 0.42(1)$ . This result is compatible with the findings of Refs. [CCPS03, CPCS04] obtained using a different trial wave function which includes both Jastrow and BCS correlations. The value of the parameter  $\beta = \xi - 1$  has been measured in experiments with trapped Fermi gases [OHG<sup>+</sup>02, BAR<sup>+</sup>04b, BKC<sup>+</sup>04], but the precision is too low to make stringent comparisons with theoretical predictions. In the region of positive scattering length  $E/N$  decreases by decreasing  $k_F a$ . At approximately  $-1/k_F a \simeq -0.3$ , the energy becomes negative, and by further decreasing  $k_F a$  it rapidly approaches the binding energy per particle  $\epsilon_b/2$  indicating the formation of bound molecules [CPCS04]. The results with the binding energy subtracted from  $E/N$  are shown in Fig. 9.2. In the BEC region,  $-1/k_F a < -1$ , we find that the FN-DMC energies

<sup>1</sup>Note that for  $k_F|a| \ll 1$  the nonanalytic correction to the ground-state energy due to the superfluid gap is exponentially small.



agree with the equation of state of a repulsive gas of molecules

$$\frac{E/N - \epsilon_b/2}{\epsilon_{FG}} = \frac{5}{18\pi} k_F a_m \left[ 1 + \frac{128}{15\sqrt{6\pi^3}} (k_F a_m)^{3/2} + \dots \right], \quad (9.6)$$

where the first term corresponds to the mean-field energy of a gas of molecules of mass  $2m$  and density  $n/2$  interacting with the positive molecule-molecule scattering length  $a_m$ , and the second term corresponds to the first beyond mean-field correction [LHY57]. If for  $a_m$  we use the value calculated by Petrov *et al.* [PSS04]  $a_m = 0.6a$ , we obtain the curves shown in Fig. 9.2. If, instead, we use  $a_m$  as a fitting parameter to our FN-DMC results in the region  $-1/k_F a \leq -1$ , we obtain the value  $a_m/a = 0.62(1)$ . From a best fit to the equation of state we calculate the chemical potential  $\mu = dE/dN$  and the inverse compressibility  $mc^2 = n\partial\mu/\partial n$ , where  $c$  is the speed of sound. The results in units of the Fermi energy  $\mu_F = \hbar^2 k_F^2/2m$  and of the Fermi velocity  $v_F = \hbar k_F/m$  are shown in Fig. 9.3. A detailed knowledge of the equation of state of the homogeneous system is important for the determination of the frequencies of collective modes in trapped systems [Str04], which have been recently measured in the BEC-BCS crossover regime [KTT04, KHG<sup>+</sup>04, BAR<sup>+</sup>04a].

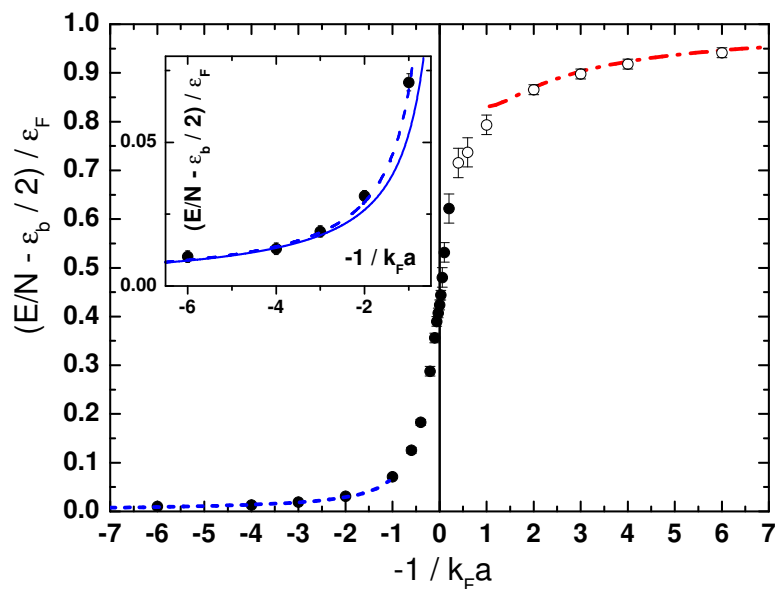


Figure 9.2: Energy per particle in the BEC-BCS crossover with the binding energy subtracted from  $E/N$ . Solid symbols: results with  $\psi_{BCS}$ , open symbols: results with  $\psi_{JS}$ . The red dot-dashed line is as in Fig. 9.1 and the blue dashed line corresponds to the expansion (9.6) holding in the BEC regime. Inset: enlarged view of the BEC regime  $-1/k_F a \leq -1$ . The solid blue line corresponds to the mean-field energy [first term in the expansion (9.6)], the dashed blue line includes the beyond mean-field correction Eq. 9.6).

In Fig. 9.4 we show the results for the pair correlation function of parallel,  $g_2^{\uparrow\uparrow}(r)$ , and antiparallel spins,  $g_2^{\uparrow\downarrow}(r)$ . For parallel spins,  $g_2^{\uparrow\uparrow}(r)$  must vanish at short distances due to the Pauli principle. In the BCS regime the effect of pairing is negligible and  $g_2^{\uparrow\uparrow}(r)$  coincides with the prediction of a noninteracting Fermi gas  $g_2^{\uparrow\uparrow}(r) = 1 - 9/(k_F r)^4 [\sin(k_F r)/k_F r - \cos(k_F r)]^2$ . This result continues to hold in the case  $-1/k_F a = 0$ , where it is consistent with the picture of a gas in the unitary regime as a

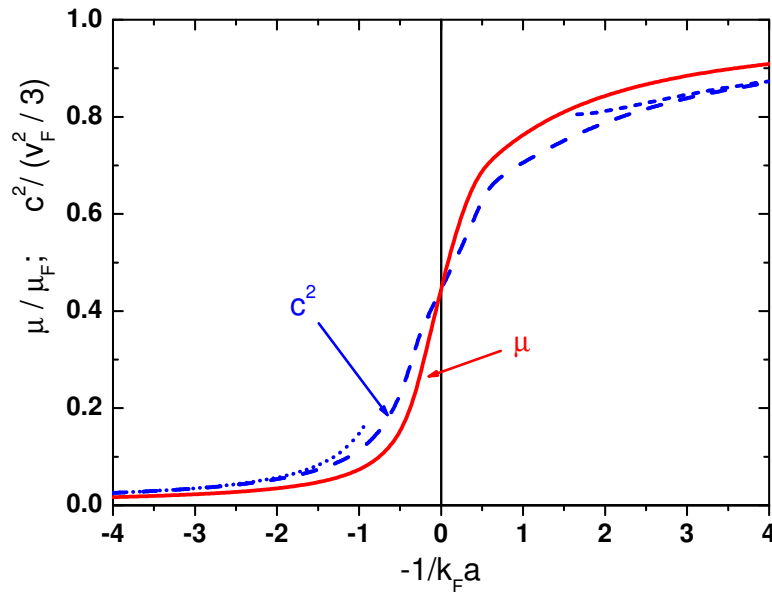


Figure 9.3: Chemical potential  $\mu$  (red solid line) and square of the speed of sound  $c^2$  (blue long dashed line) in the BEC-BCS crossover calculated from a best fit to the equation of state. The blue short-dashed line and the blue dotted line correspond to  $c^2$  calculated respectively from the expansion (9.5) and (9.6).

noninteracting Fermi gas with effective mass  $m^* = m/\xi$ . In the BEC regime the static structure factor  $S(k)$  of composite bosons can be estimated using the Bogoliubov result:  $S(k) = \hbar^2 k^2 / [2M\omega(k)]$ , where  $\omega(k) = (\hbar^4 k^4 / 4M^2 + gn_m \hbar^2 k^2 / M)^{1/2}$  is the Bogoliubov dispersion relation for particles with mass  $M = 2m$ , density  $n_m = n/2$  and coupling constant  $g = 4\pi \hbar^2 a_m / M$ . The pair distribution function  $g_2(r)$  of composite bosons, obtained through  $g_2(r) = 1 + 2/N \sum_{\mathbf{k}} [S(k) - 1] e^{-i\mathbf{k}\cdot\mathbf{r}}$  using the value  $a_m = 0.6a$ , is shown in Fig. 9.4 for  $-1/k_F a = -4$  and compared with the FN-DMC result. For large distances  $r \gg a_m$ , where Bogoliubov approximation is expected to hold, we find a remarkable agreement. This result is consistent with the equation of state in the BEC regime and shows that structural properties of the ground state of composite bosons are described correctly in our approach. For antiparallel spins,  $g_2^{\uparrow\downarrow}(r)$  exhibits a large peak at short distances due to the attractive interaction. In the BEC regime the short range behavior is well described by the exponential decay  $g_2^{\uparrow\downarrow}(r) \propto \exp(-2r\sqrt{|\epsilon_b|m}/\hbar)/r^2$  fixed by the molecular wave function  $\phi_{bs}(r)$ . In the unitary regime correlations extend over a considerably larger range compared to the tightly bound BEC regime. In the BCS regime the range of  $g_2^{\uparrow\downarrow}(r)$  is much larger than  $k_F^{-1}$  and is determined by the coherence length  $\xi_0 = \hbar^2 k_F / (m\Delta)$ , where  $\Delta$  is the gap parameter. In this regime the wave function we use does not account for pairing and is inadequate to investigate the behavior of  $g_2^{\uparrow\downarrow}(r)$ .

## 9.4 Conclusions

In conclusion, we have carried out a detailed study of the equation of state of a Fermi gas in the BEC-BCS crossover using FN-DMC techniques. In the BCS regime and in the unitary limit our results are in agreement with known perturbation expansions and with previous FN-GFMC cal-

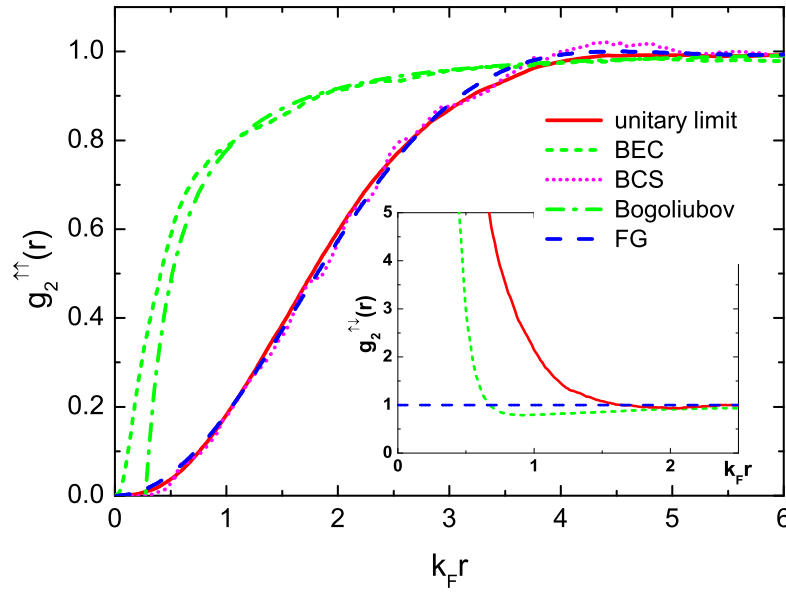


Figure 9.4: Pair correlation function of parallel,  $g_2^{\uparrow\uparrow}(r)$ , and (inset) of antiparallel spins,  $g_2^{\uparrow\downarrow}(r)$ , for  $-1/k_F a = 0$  (unitary limit),  $-1/k_F a = -4$  (BEC regime),  $-1/k_F a = 4$  (BCS regime) and for a noninteracting Fermi gas (FG). The dot-dashed line corresponds to the pair correlation function of a Bose gas with  $a_m = 0.6a$  and  $-1/k_F a = -4$  calculated using the Bogoliubov approximation.

culations [CCPS03, CPCS04], respectively. In the BEC regime, we recover the equation of state of a gas of composite bosons with repulsive effective interactions which are well described by the molecule-molecule scattering length  $a_m = 0.6a$  recently calculated in Ref. [PSS04].



# Conclusions

This Dissertation presents results of a thorough study of ultracold bosonic and fermionic gases in three-dimensional and quasi-one-dimensional systems. Although the analyses are carried out within various theoretical frameworks (Gross-Pitaevskii, Bethe *ansatz*, local density approximation, etc.) the main tool of the study is the Quantum Monte Carlo method in different modifications (variational MC, diffusion MC, fixed-node MC). We benchmark our Monte Carlo calculations by recovering known analytical results (perturbative theories in dilute limits, exactly solvable models, etc.) and extend calculations to regimes, where the results are so far unknown. In particular we calculate the equation of state and correlation functions for gases in various geometries and with various interatomic interactions.

The main novel results can be summarized as follows.

We present exact Quantum Monte Carlo results of the ground-state energy and structure of a Bose gas confined in highly anisotropic harmonic traps. Starting from a 3D Hamiltonian, where interparticle interactions are modeled by a hard-sphere or a soft-sphere potentials, we show that the system exhibits striking features due to particle correlations. By reducing the anisotropy parameter  $\lambda$ , while the number of particles  $N$  and the ratio  $a/a_{\perp}$  of scattering to transverse oscillator length are kept fixed, the system crosses from a regime where Gross-Pitaevskii mean-field theory applies to a regime which is well described by the 1D Lieb-Liniger equation of state in local density approximation. In the cross-over region both theories fail and one must resort to exact methods to account properly for both finite size effects and residual 3D effects. For very small values of  $\lambda$  we find clear evidence, both in the energy per particle and in the longitudinal size of the cloud, of the fermionization of the system in the Tonks-Girardeau regime.

We use different methods for studying the resonant scattering of a Bose gas in a highly elongated trap, when the system enters a quasi one dimensional regime. We make a fully three dimensional calculation of the lowest-lying gas-like state of the many body system using a microscopic Fixed-Node Monte Carlo method. In order to prove the presence of the confined induced resonance predicted by Olshanii in a many-body system we make a full microscopic one-dimensional calculation for contact interactions with renormalized coupling constant  $g_{1D}$ . The resulting energies are in excellent agreement. This agreement proves that a properly chosen many-body 1D Hamiltonian describes well 3D Bose gases in the quasi-one dimensional regime. We consider the Lieb-Liniger and the hard-rod equation of state of a 1D system treated within the local density approximation, which is expected to be correct for large number of particles. Our detailed microscopic studies suggest that these LDA treatments provide a good description of quasi-1D Bose gases. In particular, we suggest a simple treatment of 1D systems with negative  $g_{1D}$  using the hard-rod equation of state. We address the question of stability of an inhomogeneous gas in this regime utilizing a variational many-body framework. We find that the lowest-lying gas-like state is stable for negative coupling constants, up to a minimum critical value of  $|g_{1D}|$ . Our numerical results suggest that the stability condition can be expressed as  $n_{1D}a_{1D} \simeq 0.35$ .

Properties of the Lieb-Liniger gas are investigated in details. We calculate for the first time the behaviour of correlation functions in a wide range of the characteristic parameter  $na_{1D}$  covering Gross-Pitaevskii and Tonks-Girardeau regimes. We obtain the one-body density matrix  $g_1(z)$  and pair distribution function  $g_2(z)$  for all densities. In particular we investigate the nontrivial regime  $na_{1D} \approx 1$  which is relevant for current experiments. We study the dependence of the value at zero of the three-body correlation function  $g_3(0)$  on the gas parameter  $na_{1D}$  and compare it with experimental results obtained at NIST[TOH<sup>+</sup>04]. We find agreement between theory and experiment. We extract the momentum distribution  $n(k)$  and static structure factor  $S(k)$  for all densities. We discuss how the presence of a harmonic trapping modifies the properties of the system. Using the Haldane approach for one-dimensional liquids we calculate the asymptotic behaviour of the one-body density matrix, density-density correlation function, dynamic form factor. In particular a direct comparison with the DMC calculation shows that the accuracy of the obtained coefficient of the one-body density matrix decay is better than 0.3% in the whole range of densities.

We propose a novel technique of creating a metastable gas-like state of attractive bosons by crossing a confinement induced resonance. Such a gas has correlations even stronger than in the Tonks-Girardeau regime where the coupling constant is very large  $g_{1D} \rightarrow \infty$ . We calculate the equation of state in this “super-Tonks” regime using the Variational Monte Carlo method and estimate the critical density for the onset of instability against cluster formation. The static structure factor and one-body density matrix are calculated exactly within the hard-rod model, which provides the correct description of the system for small values of the gas parameter. For harmonically trapped systems we provide explicit predictions for the frequency of the lowest compressional mode.

We have studied the motion of an impurity through the condensate at zero temperature by solving the Gross-Pitaevskii equation in a perturbative way. We calculated the energy of a slow impurity. We find that the  $V = 0$  energy agrees with Bogoliubov theory, the velocity contribution can be written as  $m^*V^2/2$ , where the effective mass  $m^*$  contributes to the mass of the normal component. We find that the motion at small velocities is dissipationless in one-, two-, and three- dimensional systems, although motion with velocities larger than the speed of sound leads to a non-zero drag force due to Cherenkov radiation of phonons. The expressions for the drag force are calculated. We used results for the dynamic form factor of the exact Lieb-Liniger theory to investigate the velocity dependence of the drag force in a 1D system. The form factor is calculated with the help of the Haldane method[Hal81]. The drag force exists for arbitrarily small velocity of motion, but is very small in the mean-field limit.

We considered a quasi-one-dimensional system of two component Fermi gas with contact potential between fermions of different spins. We have investigated the cross-over from weak to strong coupling of harmonically trapped gases with both repulsive and attractive effective interactions. The frequency of the lowest breathing mode, which can provide an experimental signature of the cross-over, is calculated. We predict the existence of a stable molecular Tonks-Girardeau gas in the strongly attractive regime. We obtain description of trapped one- and three- dimensional gas in the local density approximation for a perturbative equation of state. Obtained predictions for the frequencies of the lowest breathing mode are compared with numerical solutions.

We have carried out a detailed study of the equation of state of a Fermi gas in the BEC-BCS crossover using Fixed Node Monte Carlo techniques. In the BCS regime and in the unitary limit our results are in agreement with known perturbation expansions and with previous Fixed Node Green Function MC calculations [CCPS03, CPCS04]. In the BEC regime, in our many body calculation we recover the equation of state of a gas of composite bosons with repulsive effective interactions which are well described by the molecule-molecule scattering length  $a_m = 0.6a$  recently calculated in

Ref. [PSS04].

The results obtained in this dissertation are relevant for present and future experiments. We make direct comparison the three-body loss rate of a 1D Bose system measured in experiments[TOH<sup>+</sup>04] finding good agreement. The equation of state obtained here for the BEC-BCS crossover in a two component Fermi gas can be used to determine frequencies of collective modes, which have been recently measured in experiments[BAR<sup>+</sup>04a, KHG<sup>+</sup>04, KTT04]. It is important to note that the methods of obtaining quasi-one-dimensional cigar-shaped systems have been developed considerably in the last years and it is expected that many more experiments on low-dimensional systems will appear soon. Another important point is that the strength of interactions can be tuned in a controlled way through the application of an external magnetic field in the proximity of a Feshbach resonance. Strengths of interaction in quasi-one-dimensional systems can be controlled by means of confinement induced resonance. This allows to hope that many new properties of low-dimensional quantum systems will be measured soon and compared to theoretical predictions.





# Bibliography

- [ABCG02] G. E. Astrakharchik, J. Boronat, J. Casulleras and S. Giorgini, *Superfluidity versus Bose-Einstein condensation in a Bose gas with disorder*, Phys. Rev. A **66**, 023603 (2002).
- [ABCG04a] G. Astrakharchik, J. Boronat, J. Casulleras and S. Giorgini, *Beyond Tonks-Girardeau: strongly correlated regime in quasi-one-dimensional Bose gases*, (2004), cond-mat/0405225.
- [ABCG04b] G. Astrakharchik, J. Boronat, J. Casulleras and S. Giorgini, *Equation of state of a Fermi gas in the BEC-BCS crossover: a quantum Monte Carlo study*, Phys. Rev. Lett. **93**, 200404 (2004), cond-mat/0406113.
- [ABGG04a] G. E. Astrakharchik, D. Blume, S. Giorgini and B. E. Granger, *Quantum Monte Carlo study of quasi-one-dimensional Bose gases*, J. Phys. B **37**(7), S205 (2004).
- [ABGG04b] G. E. Astrakharchik, D. Blume, S. Giorgini and B. E. Granger, *Quasi-one-dimensional Bose gases with large scattering length*, Phys. Rev. Lett. **92**, 030402 (2004), cond-mat/0308585.
- [ABGP04] G. Astrakharchik, D. Blume, S. Giorgini and L. Pitaevskii, *Interacting fermions in quasi-one-dimensional harmonic traps*, Phys. Rev. Lett. **93**, 050402 (2004), cond-mat/0312538.
- [AEM<sup>+</sup>95] M. H. Anderson, J. R. Ensher, M. R. Matthews, C. E. Wieman and E. A. Cornell, *Observation of Bose-Einstein Condensation in a Dilute Atomic Vapor*, Science **269**, 198 (1995).
- [AG02] G. E. Astrakharchik and S. Giorgini, *Quantum Monte Carlo study of the three- to one-dimensional crossover for a trapped Bose gas*, Phys. Rev. A **66**, 053614 (2002), cond-mat/0207613.
- [AG03] G. E. Astrakharchik and S. Giorgini, *Correlation functions and momentum distribution of one-dimensional Bose systems*, Phys. Rev. A **68**, 031602 (2003), cond-mat/0212512.
- [AP02] G. E. Astrakharchik and L. P. Pitaevskii, *Motion of a heavy impurity through a Bose-Einstein condensate*, Phys. Rev. A **70**, 013608 (2002), cond-mat/0307247.
- [Ast01] G. E. Astrakharchik, *Properties of a Bose Gas in the Presence of Disorder*, *Laurea thesis*, Università di Trento, 2001, <http://www.science.unitn.it/~astra/thesis/>.

- [BAR<sup>+</sup>04a] M. Bartenstein, A. Altmeyer, S. Riedl, S. Jochim, C. Chin, J. H. Denschlag and R. Grimm, *Collective Excitations of a Degenerate Gas at the BEC-BCS Crossover*, Phys. Rev. Lett. **92**, 203201 (2004).
- [BAR<sup>+</sup>04b] M. Bartenstein, A. Altmeyer, S. Riedl, S. Jochim, C. Chin, J. H. Denschlag and R. Grimm, *Crossover from a Molecular Bose-Einstein Condensate to a Degenerate Fermi Gas*, Phys. Rev. Lett. **92**, 120401 (2004).
- [BCK<sup>+</sup>03] T. Bourdel, J. Cubizolles, L. Khaykovich, K. M. F. Magalhaes, S. J. J. M. F. Kokkelmans, G. V. Shlyapnikov and C. Salomon, *Measurement of interaction energy near a Feshbach resonance in a <sup>6</sup>Li Fermi gas*, Phys. Rev. Lett. **91**, 020402 (2003), cond-mat/0303079.
- [BCN94] J. Boronat, J. Casulleras and J. Navarro, Phys. Rev. **B 50**, 3427 (1994).
- [BEG98] J. Bohn, B. Esry and C. Greene, Phys. Rev. **A 68**, 584 (1998).
- [BEKW98] T. Busch, B. Englert, K. Rzazewski and M. Wilkens, Found. Phys. **28**, 549 (1998).
- [BGB01] H. P. Büchler, V. B. Geshkenbein and G. Blatter, Phys. Rev. Lett. **87**, 100403 (2001).
- [BKC<sup>+</sup>04] T. Bourdel, L. Khaykovich, J. Cubizolles, J. Zhang, F. Chevy, M. Teichmann, L. Tarruell, S. J. J. M. F. Kokkelmans and C. Salomon, *Experimental Study of the BEC-BCS Crossover Region in Lithium 6*, Phys. Rev. Lett. **93**, 050401 (2004).
- [BMO03] T. Bergeman, M. Moore and M. Olshanii, *Atom-Atom Scattering under Cylindrical Harmonic Confinement: Numerical and Analytic Studies of the Confinement Induced Resonance*, Phys. Rev. Lett. **91**, 163201 (2003).
- [BP96] G. Baym and C. Pethick, Phys. Rev. Lett. **76**, 6 (1996).
- [Bru04] G. Bruun, *Two-component Fermi gas with a resonant interaction*, (2004), cond-mat/0401497.
- [BTJ03] E. Bolda, E. Tiesinga and P. Julienne, Phys. Rev. **A 68**, 032702 (2003).
- [BW52] J. M. Blatt and V. F. Weisskopf, *Theoretical Nuclear Physics*, Willey, New York, 1952.
- [Cal69] F. Calogero, *Solution of a three-body problem in one-dimension*, J. Math. Phys. **10**, 2191 (1969).
- [Caz04] M. Cazalilla, *Bosonizing one-dimensional cold atomic gases*, Journal of Physics B: AMOP **37**, S1 (2004), cond-mat/0307033.
- [CB95] J. Casulleras and J. Boronat, *Unbiased estimators in quantum Monte Carlo methods: Application to liquid <sup>4</sup>He*, Phys. Rev. **B 52**, 3654 (1995).
- [CCPS03] J. Carlson, S.-Y. Chang, V. Pandharipande and K. Schmidt, Phys. Rev. Lett. **91**, 050401 (2003).
- [CCR00a] L. Carr, C. Clark and W. Reinhardt, Phys. Rev. **A 62**, 063611 (2000).

- [CCR<sup>+</sup>00b] S. L. Cornish, N. R. Claussen, J. L. Roberts, E. A. Cornell and C. E. Wieman, *Stable  $^{85}\text{Rb}$  Bose-Einstein Condensates with Widely Tunable Interactions*, Phys. Rev. Lett. **85**, 1795 (2000).
- [CEE<sup>+</sup>91] M. Casas, C. Esebbag, A. Extremera, J. M. Getino, M. de Llano, A. Plastino and H. Rubio, *Cooper pairing in a soluble one-dimensional many-fermion model*, Phys. Rev. A **44**, 4915 (1991).
- [Cep95] D. M. Ceperley, *Path integrals in the theory of condensed helium*, Reviews of Modern Physics **67**, 279 (1995).
- [CHM<sup>+</sup>02] S. Cowell, H. Heiselberg, I. E. Mazets, J. Morales, V. R. Pandharipande and C. J. Pethick, *Cold Bose Gases with Large Scattering Lengths*, Phys. Rev. Lett. **88**, 210403 (2002).
- [CKR01] L. Carr, J. Kutz and W. Reinhardt, Phys. Rev. E **63**, 066604 (2001).
- [Col74] C. F. Coll, *Excitation spectrum of the one-dimensional Hubbard model*, Phys. Rev. B **9**, 2150 (1974).
- [CPCS04] S.-Y. Chang, V. Pandharipande, J. Carlson and K. Schmidt, *Quantum Monte Carlo Studies of Superfluid Fermi Gases*, (2004), physics/0404115.
- [CS99] T. Cheon and T. Shigehara, Phys. Rev. Lett. **82**, 2536 (1999).
- [DGW02] K. K. Das, M. D. Girardeau and E. M. Wright, *Crossover from one to three dimensions for a gas of hard-core bosons*, Phys. Rev. Lett. **89**, 110402 (2002), cond-mat/0204317.
- [DH04] R. B. Diener and T.-L. Ho, *The Condition for Universality at Resonance and Direct Measurement of Pair Wavefunctions Using rf Spectroscopy*, (2004), cond-mat/0405174.
- [DHR<sup>+</sup>01] S. Dettmer, D. Hellweg, P. Ryytty, J. J. Arlt, W. Ertmer, K. Sengstock, D. S. Petrov, G. V. Shlyapnikov, H. Kreutzmann, L. Santos and M. Lewenstein, *Observation of Phase Fluctuations in Elongated Bose-Einstein Condensates*, Phys. Rev. Lett. **87**, 160406 (2001).
- [DLO01] V. Dunjko, V. Lorent and M. Olshanii, Phys. Rev. Lett. **86**, 5413 (2001).
- [DMA<sup>+</sup>95] K. B. Davis, M.-O. Mewes, M. R. Andrews, N. J. van Druten, D. S. Durfee, D. M. Kurn and W. Ketterle, *Bose-Einstein condensation in a gas of sodium atoms*, Phys. Rev. Lett. **75**, 3969 (1995).
- [Ein24] A. Einstein, Sitzber. Kgl. Preuss. Akad. Wiss. **261** (1924).
- [Ein25] A. Einstein, Sitzber. Kgl. Preuss. Akad. Wiss. **3** (1925).
- [ERdM97] J. Engelbrecht, M. Randeria and C. S. de Melo, Phys. Rev. B **55**, 15153 (1997).
- [Esr97] B. Esry, Phys. Rev. A **55**, 1147 (1997).
- [Fer36] E. Fermi, Ricerca Sci. **7**, 13 (1936).

- [Fey54] R. P. Feynman, *Phys. Rev.* **94**, 262 (1954).
- [Flu71] S. Flügge, *Practical Quantum Mechanics I*, Springer-Verlag, Berlin-Heidelberg-New York, 1971.
- [FPR92] T. Frisch, Y. Pomeau and S. Rica, *Transition to dissipation in a model of superflow*, *Phys. Rev. Lett.* **69**, 1644 (1992).
- [FRZ04] J. Fuchs, A. Recati and W. Zwerger, *Exactly solvable model of the BCS-BEC crossover*, *Phys. Rev. Lett.* **93**, 090408 (2004), cond-mat/0402448.
- [Gau67] M. Gaudin, *Phys. Lett.* **24A**, 55 (1967).
- [Gau83] M. Gaudin, *La Fonction d'Onde de Bethe*, Paris, Masson, 1983.
- [GB04] B. E. Granger and D. Blume, *Tuning the interactions of spin-polarized fermions using quasi-one-dimensional confinement*, *Phys. Rev. Lett.* **92**, 133202 (2004), cond-mat/0307358.
- [GBC99] S. Giorgini, J. Boronat and J. Casulleras, *Ground state of a homogeneous Bose gas: A diffusion Monte Carlo calculation*, *Phys. Rev. A* **60**, 5129 (1999).
- [GBM<sup>+</sup>01] M. Greiner, I. Bloch, O. Mandel, T. W. Hänsch and T. Esslinger, *Exploring Phase Coherence in a 2D Lattice of Bose-Einstein Condensates*, *Phys. Rev. Lett.* **87**, 160405 (2001).
- [GGMB04] P. Gori-Giorgi, S. Moroni and G. B. Bachelet, *Pair-distribution functions of the two-dimensional electron gas*, *Phys. Rev. B* **70**, 115102 (2004).
- [Gir60] M. Girardeau, *J. Math. Phys. (N.Y.)* **1**, 516 (1960).
- [Gla63] R. J. Glauber, *The Quantum Theory of Optical Coherence*, *Phys. Rev.* **130**, 2529 (1963).
- [GO03] M. Girardeau and M. Olshanii, *Fermi-Bose mapping and N-particle ground state of spin-polarized fermions in tight atom waveguides*, (2003), cond-mat/0309396.
- [GR80] I. S. Gradshteyn and I. M. Ryzhik, *Tables of Integrals, Series and Products*, Academic, New York, 1980.
- [GRJ03] M. Greiner, C. Regal and D. Jin, *Nature* **426**, 537 (2003).
- [Gro61] E. P. Gross, *Nuovo Cimento* **20**, 454 (1961).
- [GS03a] D. M. Gangardt and G. V. Shlyapnikov, *Local correlations in a strongly interacting one-dimensional Bose gas*, *New Journal of Physics* **5**, 79 (2003).
- [GS03b] D. Gangardt and G. Shlyapnikov, *Phys. Rev. Lett.* **90**, 010401 (2003).
- [Gua98] R. Guardiola, *Microscopic Quantum Many-Body Theories and Their Applications*, Springer, Berlin, 1998.

- [GVL<sup>+</sup>01] A. Görlitz, J. M. Vogels, A. E. Leanhardt, C. Raman, T. L. Gustavson, J. R. Abo-Shaeer, A. P. Chikkatur, S. Gupta, S. Inouye, T. Rosenband and W. Ketterle, *Realization of Bose-Einstein Condensates in Lower Dimensions*, Phys. Rev. Lett. **87**, 130402 (2001).
- [GW04] F. Gleisberg and W. Wonneberger, J. Phys. B: At. Mol. Opt. Phys. **37**, S59 (2004).
- [GWT01] M. Girardeau, E. Wright and J. Triscari, Phys. Rev. A **63**, 033601 (2001).
- [Hak97] V. Hakim, Phys. Rev. E **55**, 2835 (1997).
- [Hal81] F. Haldane, Phys. Rev. Lett. **47**, 1840 (1981).
- [Hei01] H. Heiselberg, Phys. Rev. A **63**, 043606 (2001).
- [HKCW01] M. Holland, S. Kokkelmans, M. Chiofalo and R. Walser, Phys. Rev. Lett. **87**, 120406 (2001).
- [HM92] K. Huang and H. Meng, Phys. Rev. Lett. **69**, 644 (1992).
- [HM04] T.-L. Ho and E. J. Mueller, *High temperature expansion applied to fermions near Feshbach resonance*, Phys. Rev. Lett. **92**, 160404 (2004), cond-mat/0306187.
- [HMV04] M. Holland, C. Menotti and L. Viverit, *The role of boson-fermion correlations in the resonance theory of superfluids*, (2004), cond-mat/0404234.
- [Hua87] K. Huang, *Statistical Mechanics (2Ed)*, Wiley, 1987.
- [HY57] K. Huang and C. Yang, Phys. Rev. **105**, 767 (1957).
- [IAS<sup>+</sup>98] S. Inouye, M. Andrews, J. Stenger, H.-J. Miesner, D. Stamper-Kurn and W. Ketterle, *Observation of Feshbach resonances in a Bose-Einstein condensate*, Nature **392**, 151 (1998).
- [JBA<sup>+</sup>03] S. Jochim, M. Bartenstein, A. Altmeyer, G. Hendl, S. Riedl, C. Chin, J. H. Denschlag and R. Grimm, *Bose-Einstein Condensation of Molecules*, Science **302**, 2101 (2003).
- [JMMS80] M. Jimbo, T. Miwa, Y. Mori and M. Sato, Physica (Amsterdam) **1D**, 80 (1980).
- [JR82] C. Jones and P. Roberts, J. Phys. A **15**, 2599 (1982).
- [KBI93] V. E. Korepin, N. M. Bogoliubov and A. G. Izergin, *Quantum Inverse Scattering Method and Correlation Functions*, Cambridge University Press, Cambridge, 1993.
- [KHG<sup>+</sup>04] J. Kinast, S. L. Hemmer, M. E. Gehm, A. Turlapov and J. E. Thomas, *Evidence for Superfluidity in a Resonantly Interacting Fermi Gas*, Phys. Rev. Lett. **92**, 150402 (2004).
- [KM00] Y. Kagan and L. Maksimov, Phys. Rev. Lett. **85**, 3075 (2000).
- [KMJ99] E. Krotscheck, M.D.Miller and J.Wojdylo, *Variational approach to the many-boson problem in one dimension*, Phys. Rev. B **60**, 13028 (1999).
- [KO75] V. Krivnov and A. Ovchinnikov, Sov. Phys. JETP **40**, 781 (1975).

- [KSF<sup>+</sup>02] L. Khaykovich, F. Schreck, G. Ferrari, T. Bourdel, J. Cubizolles, L. Carr and C. S. Y. Castin, *Formation of a Matter-Wave Bright Soliton*, *Science* **296**, 1290 (2002), cond-mat/0205378.
- [KSU03] R. Kanamoto, H. Saito and M. Ueda, *Phys. Rev. A* **67**, 115208 (2003).
- [KTT04] J. Kinast, A. Turlapov and J. E. Thomas, *Breakdown of Hydrodynamics in the Radial Breathing Mode of a Strongly-Interacting Fermi Gas*, (2004), cond-mat/0408634.
- [Leg80] A. Leggett, *Modern Trends in the Theory of Condensed Matter*, Springer-Verlag, Berlin, 1980.
- [Len64] A. Lenard, *J. Math. Phys.* **5**, 930 (1964).
- [LHY57] T. Lee, K. Huang and C. Yang, *Phys. Rev.* **106**, 1135 (1957).
- [Lie63] E. Lieb, *Exact Analysis of an Interacting Bose Gas. II. The Excitation Spectrum*, *Phys. Rev.* **130**, 1616 (1963).
- [LL63] E. H. Lieb and W. Liniger, *Exact Analysis of an Interacting Bose Gas. I. The General Solution and the Ground State*, *Phys. Rev.* **130**, 1605 (1963).
- [LP80] E. Lifshitz and L. Pitaevskii, *Statistical Physics, Part 2*, Pergamon Press, Oxford, 1980.
- [LP01] P. Leboeuf and N. Pavloff, *Phys. Rev. A* **64**, 033602 (2001).
- [LRT<sup>+</sup>02] T. Loftus, C. A. Regal, C. Ticknor, J. L. Bohn and D. S. Jin, *Resonant Control of Elastic Collisions in an Optically Trapped Fermi Gas of Atoms*, *Phys. Rev. Lett.* **88**, 173201 (2002).
- [LY57] T. Lee and C. Yang, *Phys. Rev.* **105**, 1119 (1957).
- [MC02] C. Mora and Y. Castin, *Phys. Rev. A* **67**, 053615 (2002).
- [McG64] J. McGuire, *J. Math. Phys. (N.Y.)* **5**, 622 (1964).
- [MFS95] S. Moroni, S. Fantoni and G. Senatore, *Euler Monte Carlo calculations for liquid <sup>4</sup>He and <sup>3</sup>He*, *Phys. Rev. B* **52**, 13547 (1995).
- [MLE98] H. Monien, M. Linn and N. Elstner, *Phys. Rev. A* **58**, R3395 (1998).
- [MRR<sup>+</sup>53] N. Metropolis, A. W. Rosenbluth, M. N. Rosenbluth, A. H. Teller and E. Teller, *J. Chem. Phys.* **21**, 1087 (1953).
- [MS02] C. Menotti and S. Stringari, *Collective oscillations of a 1D trapped Bose gas*, *Phys. Rev. A* **66**, 043610 (2002), cond-mat/0201158.
- [MSKE03] H. Moritz, T. Stöferle, M. Kohl and T. Esslinger, *Exciting Collective Oscillations in a Trapped 1D Gas*, *Phys. Rev. Lett.* **91**, 250402 (2003), cond-mat/0307607.
- [Nag40] T. Nagamiya, *Proc. Phys. Math. Soc. Jpn.* **22**, 705 (1940).



- [NG99] M. Naraschewski and R. J. Glauber, *Phys. Rev. A* **59**, 4595 (1999).
- [NLCC94] A. H. C. Neto, H. Q. Lin, Y. Chen and J. M. P. Carmelo, *Pseudoparticle-operator description of an interacting bosonic gas*, *Phys. Rev. B* **50**, 14032 (1994).
- [NSR85] P. Nozières and S. Schmitt-Rink, *J. Low Temp. Phys* **59**, 195 (1985).
- [OD03] M. Olshanii and V. Dunjko, *Short-Distance Correlation Properties of the Lieb-Liniger System and Momentum Distributions of Trapped One-Dimensional Atomic Gases*, *Phys. Rev. Lett.* **91**, 090401 (2003).
- [OG03] Y. Ohashi and A. Griffin, *Phys. Rev. A* **67**, 063612 (2003).
- [OHG<sup>+</sup>02] K. O'Hara, S. Hemmer, M. Gehm, S. Granade and J. Thomas, *Science* **298**, 2179 (2002).
- [Ols98] M. Olshanii, *Atomic Scattering in the Presence of an External Confinement and a Gas of Impenetrable Bosons*, *Phys. Rev. Lett.* **81**, 938 (1998).
- [ORV<sup>+</sup>00] R. Onofrio, C. Raman, J. M. Vogels, J. R. Abo-Shaeer, A. P. Chikkatur and W. Ketterle, *Observation of Superfluid Flow in a Bose-Einstein Condensed Gas*, *Phys. Rev. Lett.* **85**, 2228 (2000).
- [Pav02] N. Pavloff, *Phys. Rev. A* **66**, 013610 (2002).
- [PCHK04] S. D. Palo, M. Chiofalo, M. Holland and S. Kokkelmans, (2004), cond-mat/0404672.
- [PGS04] D. Petrov, D. Gangardt and G. Shlyapnikov, *Low-dimensional trapped gases*, *J. Phys. IV France* **116**, 3 (2004).
- [Pit61] L. P. Pitaevskii, *Zh. Eksp. Teor. Fiz.* **40**, 646 (1961).
- [Pop80] V. Popov, *Pis'ma Zh. Eksp. Teor. Fiz* **31**, 560 (1980).
- [PPS04] P. Pieri, L. Pisani and G. Strinati, *BCS-BEC crossover at finite temperature in the broken-symmetry phase*, (2004), cond-mat/0406099.
- [PS00] P. Pieri and G. Strinati, *Phys. Rev. B* **61**, 15370 (2000).
- [PS03] L. P. Pitaevskii and S. Stringari, *Bose-Einstein Condensation*, Oxford University Press, Oxford, 2003.
- [PSS04] D. Petrov, C. Salomon and G. Shlyapnikov, *Phys. Rev. Lett.* **93**, 090404 (2004).
- [PSW00] D. Petrov, G. Shlyapnikov and J. Walraven, *Regimes of Quantum Degeneracy in Trapped 1D Gases*, *Phys. Rev. Lett.* **85**, 3745 (2000).
- [RC67] L. Reatto and G. Chester, *Phonons and the Properties of a Bose System*, *Phys. Rev.* **155**, 88 (1967).
- [RCAJ82] P. Reynolds, D. Ceperley, B. Alder and W. L. Jr., *J. Chem. Phys* **77**, 5593 (1982).
- [RFZZ03a] A. Recati, P. Fedichev, W. Zwerger and P. Zoller, *Phys. Rev. Lett.* **90**, 020401 (2003).

- [RFZZ03b] A. Recati, P. Fedichev, W. Zwerger and P. Zoller, *J. Opt. B - Quantum and Semiclassical Opt.* **5**, S55 (2003).
- [RGT<sup>+</sup>03] S. Richard, F. Gerbier, J. H. Thywissen, M. Hugbart, P. Bouyer and A. Aspect, *Phys. Rev. Lett.* **91**, 010405 (2003).
- [RKO<sup>+</sup>99] C. Raman, M. Köhl, R. Onofrio, D. S. Durfee, C. E. Kuklewicz, Z. Hadzibabic and W. Ketterle, *Evidence for a Critical Velocity in a Bose-Einstein Condensed Gas*, *Phys. Rev. Lett.* **83**, 2502 (1999).
- [RT03] J. Reichel and J. H. Thywissen, *Using magnetic chip traps to study Tonks-Girardeau quantum gases*, (2003), cond-mat/0310330.
- [Sch63] T. Schultz, *J. Math. Phys.* **4**, 666 (1963).
- [Sch77] M. Schwartz, *Phys. Rev. B* **15**, 1399 (1977).
- [SKC<sup>+</sup>01] F. Schreck, L. Khaykovich, K. L. Corwin, G. Ferrari, T. Bourdel, J. Cubizolles and C. Salomon, *Quasipure Bose-Einstein Condensate Immersed in a Fermi Sea*, *Phys. Rev. Lett.* **87**, 080403 (2001).
- [SMS<sup>+</sup>04] T. Stöferle, H. Moritz, C. Schori, M. Köhl and T. Esslinger, *Transition from a strongly interacting 1D superfluid to a Mott insulator*, *Phys. Rev. Lett.* **92**, 130403 (2004), cond-mat/0312440.
- [Son71] E. B. Sonin, *Sov. Phys. JETP* **32**, 773 (1971).
- [SPTH02] K. Strecker, G. Partridge, A. Truscott and R. Hulet, *Nature (London)* **417**, 150 (2002).
- [Str04] S. Stringari, *Europhys. Lett.* **65**, 749 (2004).
- [Sut71] B. Sutherland, *Quantum Many Body Problem in One Dimension: Ground State*, *J. Math. Phys.* **12**(2), 246 (1971).
- [TOH<sup>+</sup>04] B. L. Tolra, K. M. O'Hara, J. H. Huckans, W. D. Phillips, S. L. Rolston and J. V. Porto, *Observation of Reduced Three-Body Recombination in a Correlated 1D Degenerate Bose Gas*, *Phys. Rev. Lett.* **92**, 190401 (2004), 0312003.
- [Tok04] I. Tokatly, *Dilute Fermi gas in quasi-one-dimensional traps: From weakly interacting fermions via hard core bosons to weakly interacting Bose gas*, *Phys. Rev. Lett.* **93**, 090405 (2004), cond-mat/0402276.
- [Ton36] L. Tonks, *Phys. Rev.* **50**, 955 (1936).
- [Tsu71] T. Tsuzuki, *J. Low Temp. Phys.* **4**, 441 (1971).
- [TWMJ00] E. Tiesinga, C. Williams, F. Mies and P. Julienne, *Phys. Rev. A* **61**, 063416 (2000).
- [Voi95] J. Voit, *Rep. Prog. Phys.* **58**, 977 (1995).
- [VT79] H. G. Vaidya and C. A. Tracy, *Phys. Rev. Lett.* **42**, 3 (1979).



- [WMA99] T. Winiecki, J. F. McCann and C. S. Adams, *Pressure Drag in Linear and Nonlinear Quantum Fluids*, Phys. Rev. Lett. **82**, 5186 (1999).
- [XW02] G. Xianlong and W. Wonneberger, Phys. Rev. **A 65**, 033610 (2002).
- [Yan67] C. Yang, Phys. Rev. Lett. **19**, 1312 (1967).
- [YY69] C. Yang and C. Yang, J. Math. Phys. **10**, 1115 (1969).
- [ZSS<sup>+</sup>03] M. W. Zwierlein, C. A. Stan, C. H. Schunck, S. M. F. Raupach, S. Gupta, Z. Hadzibabic and W. Ketterle, *Observation of Bose-Einstein Condensation of Molecules*, Phys. Rev. Lett. **91**, 250401 (2003).



# Appendix A

## Bethe *ansatz* solutions

In this Section the integral equations of exactly solvable bosonic and fermionic one-dimensional models are presented. The equations were derived by using Bethe *ansatz* method (see, for example, book [Gau83]).

### A.1 Lieb-Liniger equations

A gas of repulsive bosons interacting via  $\delta$ -potential in one-dimensional system is described by the Hamiltonian (5.1) with the relation between the coupling constant  $g_{1D}$  and the scattering length  $a_{1D}$  given by (1.69). It was shown by Lieb and Liniger [LL63] that the ground state energy can be found from the solution of the integral equation (see for example, [LL63, DLO01]):

$$\rho(k) = \frac{1}{2\pi} + \int_{-1}^1 \frac{2\lambda\rho(\varkappa)}{\lambda^2 + (k - \varkappa)^2} \frac{d\varkappa}{2\pi} \quad (\text{A.1})$$

Normalization of the function  $\rho(k)$  is related to the density  $n|a_{1D}|$ :

$$\gamma = \frac{2}{n|a_{1D}|} = \frac{\lambda}{\int_{-1}^1 \rho(k) dk}, \quad (\text{A.2})$$

here we use parameter  $\gamma$  which is often introduced for solving the Bethe equations and is inversely proportional to the density.

The energy per particle  $E/N = n^2 e(n|a_{1D}|) \hbar^2 / 2m$  is obtained from integral

$$e(n|a_{1D}|) = \frac{\gamma^3}{\lambda^3} \int_{-1}^1 k^2 \rho(k) dk \quad (\text{A.3})$$

The procedure of solving the integral equations can be following:

1. Fix some value of  $\lambda$
2. Obtain  $\rho(k)$  from (A.1)
3. Obtain density  $n|a_{1D}|$  from (A.2)
4. Obtain energy  $e(n|a_{1D}|)$  from (A.3)

## A.2 Attractive Fermi gas

The Hamiltonian of a two-component fermi gas reads as follows:

$$\hat{H} = \frac{\hbar^2 n^2}{m} \left[ - \sum_{i,\sigma} \frac{1}{2} \frac{\partial^2}{\partial z_{i,\sigma}^2} + \frac{g_{1D} m}{\hbar^2 n} \sum_{i < j} \delta(z_{i,\uparrow} - z_{j,\downarrow}) \right] \quad (\text{A.4})$$

In following we will express all energies in units of  $\hbar^2 n^2 / 2m$  and all distances in units of  $|a_{1D}|$ . Let us introduce notation  $\gamma = -\frac{g_{1D} m}{\hbar^2 n} > 0$ .

The integral equation for the equation of state is (see [KO75] with notation  $\gamma = u/2$ ,  $\rho = \sigma/2$ ):

$$\rho(k) = \frac{2}{\pi} - \int_{-K}^K \frac{2\gamma \rho(\varkappa)}{\gamma^2 + (k - \varkappa)^2} \frac{d\varkappa}{2\pi} \quad (\text{A.5})$$

The normalization condition is written as

$$n a_{1D} = \int_{-K}^K \rho(k) dk \quad (\text{A.6})$$

Once the density  $\rho(k)$  is known, the energy can be written as

$$e(\gamma) = \frac{1}{n a_{1D}} \int_{-K}^K k^2 \rho(k) dk - \frac{\gamma^2}{4} \quad (\text{A.7})$$

## A.3 Repulsive Fermi gas

This Hamiltonian can be solved for an arbitrary number of particles spin up  $N_\uparrow$  and spins down  $N_\downarrow$ . The corresponding integral equations are ( $\gamma = \frac{g_{1D} m}{\hbar^2 n} > 0$ ) [Yan67]:

$$\begin{cases} \sigma(k) &= - \int_{-B}^B \frac{2\gamma\sigma(\varkappa)}{\gamma^2 + (k - \varkappa)^2} \frac{d\varkappa}{2\pi} + \int_{-Q}^Q \frac{4\gamma\rho(y)}{\gamma^2 + 4(k - \varkappa)^2} \frac{d\varkappa}{2\pi} \\ \rho(k) &= 1 + \int_{-B}^B \frac{4\gamma\sigma(\varkappa)}{\gamma^2 + 4(k - \varkappa)^2} \frac{d\varkappa}{2\pi} \end{cases} \quad (\text{A.8})$$

The limit  $B \rightarrow \infty$  correspond to  $N_\downarrow = N_\uparrow$ . In this limit one can simplify further the system of integral equations by introducing a Fourier transformation (see also discrete lattice model [Col74]):

$$\sigma(x) = \int_{-\infty}^{\infty} e^{-ikx} \sigma(k) \frac{dk}{2\pi} \quad (\text{A.9})$$

$$\sigma(k) = \int_{-\infty}^{\infty} e^{ikx} \sigma(x) dx \quad (\text{A.10})$$

By multiplying first equation from (A.8) by  $e^{-ikx}/2\pi$  and integrating over  $k$  one obtains expression for the  $\sigma(x)$ <sup>1</sup>

$$\sigma(x) = \frac{1}{2 \cosh \frac{\gamma|x|}{2}} \int_{-Q}^Q e^{-ikx} \rho(k) \frac{dk}{2\pi} \quad (\text{A.11})$$

Setting  $x = 0$  one immediately sees that number of spin-down particles is half of the total number of particles  $\int \sigma(k) dk = \frac{1}{2} \int \rho(k) dk$ .

Inserting (A.10) into second equation from (A.8), taking into account formula (A.11) and carrying out two integrations one obtains the integral equation involving only  $\rho(x)$

$$\rho(k) = \frac{1}{2\pi} + \int_{-Q}^Q K(k - \varkappa) \rho(\varkappa) \frac{d\varkappa}{2\pi}, \quad (\text{A.12})$$

where the kernel is

$$K(\xi) = 2 \int_0^\infty \frac{\cos \xi x}{1 + e^{\gamma x}} dx \quad (\text{A.13})$$

Once this equation is solved the density and energy are given by

$$na_{1D} = \int_{-Q}^Q \rho(k) dk, \quad (\text{A.14})$$

$$e(\gamma) = \frac{1}{na_{1D}} \int_{-Q}^Q k^2 \rho(k) dk \quad (\text{A.15})$$

In the strongly interacting limit  $\gamma \rightarrow \infty$  and the kernel can be simplified

$$K(\xi) = 2 \int_0^\infty \frac{\cos \xi x}{1 + e^{\gamma x}} dx = 2 \sum_{n=1}^\infty (-1)^{n+1} \frac{n\gamma}{(n\gamma)^2 + \xi^2} \approx \frac{2}{\gamma} \sum_{n=1}^\infty \frac{(-1)^{n+1}}{n} = \frac{2 \ln 2}{\gamma} \quad (\text{A.16})$$

The energy per particle in units of  $\left[ \frac{\hbar^2}{2ma^2} \right]$  is given by

$$E = \frac{\pi^2 n^2}{3} - \frac{2 \ln(2) \pi^3 n}{3} \quad (\text{A.17})$$

which equals to the energy of gas of  $N$  free fermions of the same spin.

---

<sup>1</sup> It is convenient to use following equality  $\int_{-\infty}^\infty \frac{e^{\pm ikx}}{c^2 + a^2(\varkappa - k)^2} \frac{dk}{2\pi} = \frac{1}{2ac} e^{\pm i\varkappa x - \frac{c}{a}|x|}$

It is possible to express the kernel in terms of  $\beta$ -function (see Gradstein-Ryzhik). Taking into account the series representation  $\beta(z) = \sum_{k=0}^{\infty} \frac{(-1)^k}{z+k}$  one obtain following result from the (exact) sum (A.16)

$$K(\xi) = -\frac{1}{\gamma} \left( \beta \left( \frac{i\xi}{\gamma} \right) + \beta \left( -\frac{i\xi}{\gamma} \right) \right). \quad (\text{A.18})$$

The  $\beta$ -function is defined using the digamma function  $\beta(z) = \frac{1}{2} (\Psi(\frac{x+1}{2}) - \Psi(\frac{x}{2}))$ . The digamma function is defined as logarithmic derivative of the Gamma function  $\Psi(z) = \frac{\partial}{\partial z} \ln \Gamma(z)$ .

The kernel can be expanded at small and large values of the argument:

$$K(\xi) = \frac{2}{\gamma} \ln 2 - \frac{3}{2\gamma^3} \xi^2 + \mathcal{O}(\xi^4), \quad (\text{A.19})$$

$$K(\xi) = \frac{\gamma}{2} \xi^{-2} + \frac{2\gamma^3}{4} \xi^{-4} + \mathcal{O}(\xi^{-6}) \quad (\text{A.20})$$

## A.4 Numerical solution

In the most general form the integral equations we have to solve is written as

$$f(x) + \int_{-Y}^Y K(x-y)f(y) dy = g(x), \quad (\text{A.21})$$

where  $f(x)$  is so far unknown solution,  $K(x)$  is the kernel,  $Y$  defines the integration limit,  $g(x)$  defines the normalization (in LL case it is constant). The function  $f(x)$  enters twice: once inside the integral and second time outside, this can be remedied inserting the  $\delta$ -function:

$$\int_{-Y}^Y (\delta(x-y) + K(x-y))f(y) dy = g(x), \quad (\text{A.22})$$

Now we do discretization with spacing  $\Delta x$ . The equation (A.22) now can be expressed in the matrix form:

$$(I + K\Lambda)\vec{f}\Delta x = \vec{g}, \quad (\text{A.23})$$

here  $I$  stands for a unity matrix and the diagonal matrix  $\Lambda$  is defined by the integration method. Now the vector  $f$  is obtained by multiplication of the inverse matrix on  $\vec{g}$ :

$$\vec{f} = \frac{1}{\Delta x} (I + K\Lambda)^{-1} \vec{g}, \quad (\text{A.24})$$

For a uniform grid very good precision is achieved using the Simpson method. The matrix  $\Lambda$  in this case is defined as  $\Lambda = \text{diag}\{\frac{1}{3}, \frac{1}{3}, \frac{4}{3}, \frac{2}{3}, \frac{4}{3}, \dots, \frac{4}{3}, \frac{2}{3}, \frac{4}{3}, \frac{1}{3}\}$ . The residual term of the integration is very small and can be estimated as  $I_{err} = \max f^{(4)}(x) \frac{(\Delta x)^5}{2880}$  and the error in the energy (which is defined by integrating the solution  $f(x)$  with the weight proportional to  $x^2$ ) is proportional to the spacing  $\Delta x$  to the forth power.

## A.5 Expansions

Energy expansion, unit of energy  $\hbar^2/2ma_{1D}^2$ :

<i>term</i>	0th	1st	2nd	3rd
Attractive gas: strong interaction	-1	$\frac{\pi^2(na_{1D})^2}{48}$	$\frac{\pi^2(na_{1D})^3}{96}$	$\frac{\pi^2(na_{1D})^4}{256}$
Attractive gas: weak interaction	$\frac{\pi^2(na_{1D})^2}{12}$	$-n a_{1D} $	$-\frac{\ln^2(na_{1D}/2)}{\pi^2}$	
Repulsive gas: strong interaction	$\frac{\pi^2(na_{1D})^2}{3}$	$-\frac{2\ln(2)\pi^2(na_{1D})^3}{3}$		
Repulsive gas: weak interaction	$\frac{\pi^2(na_{1D})^2}{12}$	$n a_{1D} $		

Expansion of the chemical potential, unit of energy  $\hbar^2/2ma_{1D}^2$ :

<i>term</i>	0th	1st	2nd	3rd
Attr. gas: strong interaction	-1	$\frac{\pi^2(na_{1D})^2}{16}$	$\frac{\pi^2(na_{1D})^3}{24}$	$\frac{5\pi^2(na_{1D})^4}{256}$
Attr. gas: weak interaction	$\frac{\pi^2(na_{1D})^2}{4}$	$-2 na_{1D} $	$-\frac{\ln^2(\frac{na_{1D}}{2}) + 2\ln(\frac{na_{1D}}{2})}{\pi^2}$	
Rep. gas: strong interaction	$\pi^2(na_{1D})^2$	$-\frac{8\pi^2\ln(2)(na_{1D})^3}{3}$		
Rep. gas: weak interaction	$\frac{\pi^2(na_{1D})^2}{4}$	$2 na_{1D} $		
LL gas: strong interaction	$\pi^2(na_{1D})^2$	$-\frac{8\pi^2}{3}(na_{1D})^3$		
HR gas (small density)	$\pi^2(na_{1D})^2$	$\frac{8\pi^2}{3}(na_{1D})^3$		

The frequency of the oscillations  $\frac{\omega^2}{\omega_z^2} = 4(1 + \Delta\omega)$

limit	$\Delta\omega$
Attractive gas: strong interaction	$\frac{16\sqrt{2}\sqrt{N}a_{1D}}{15\pi^2 a_z}$
Attractive gas: weak interaction	$\frac{8}{3\pi^2} \frac{\sqrt{N}a_{1D}}{a_z}$
Repulsive gas: strong interaction	$-\frac{32\sqrt{2}\ln 2\sqrt{N}a_{1D}}{15\pi^2 a_z}$
Repulsive gas: weak interaction	$-\frac{8}{3\pi^2} \frac{\sqrt{N}a_{1D}}{a_z}$
Lieb-Liniger gas: strong interaction	$-\frac{32\sqrt{2}\sqrt{N}a_{1D}}{15\pi^2 a_z}$
Gas of Hard-Rods	$\frac{32\sqrt{2}\sqrt{N}a_{1D}}{15\pi^2 a_z}$

Speed of sound in units of  $m/\pi\hbar n$

<i>term</i>	0th	1st	2nd	3rd
Attractive gas: strong interaction	$\frac{1}{4}$	$\frac{na_{1D}}{8}$	$\frac{3(na_{1D})^2}{64}$	$-\frac{3(na_{1D})^3}{128}$
Attractive gas: weak interaction	$\frac{1}{2}$	$-\frac{1}{\pi^2 na_{1D}}$	$\frac{\ln(2/na_{1D}) - 2}{\pi^4 (na_{1D})^2}$	
Repulsive gas: strong interaction	1	$-2 \ln 2 na_{1D}$		
Repulsive gas: weak interaction	$\frac{1}{2}$	$\frac{1}{\pi^2 na_{1D}}$		

Energy and chemical potential (LDA) in units of  $N\hbar\omega_z$

limit	$\mu$	$E/N$
Repulsive gas: strong interaction	$1 - \frac{32\sqrt{2} \ln 2 \sqrt{N} a_{1D}}{9\pi^2 a_z}$	$\frac{1}{2} \left( 1 - \frac{128\sqrt{2} \ln 2 \sqrt{N} a_{1D}}{45\pi^2 a_z} \right)$
Attractive gas: strong interaction	$\frac{1}{4} \left( 1 + \frac{16\sqrt{2} \sqrt{N} a_{1D}}{9\pi^2 a_z} \right)$	$\frac{1}{8} \left( 1 + \frac{64\sqrt{2} \sqrt{N} a_{1D}}{45\pi^2 a_z} \right)$
Repulsive: weak interaction	$\frac{1}{2} \left( 1 + \frac{8}{\pi^2} \frac{\sqrt{N} a_{1D}}{a_z} \right)$	$\frac{1}{4} \left( 1 + \frac{32}{3\pi^2} \frac{\sqrt{N} a_{1D}}{a_z} \right)$
Attractive gas: weak interaction	$\frac{1}{2} \left( 1 - \frac{8}{\pi^2} \frac{\sqrt{N} a_{1D}}{a_z} \right)$	$\frac{1}{4} \left( 1 - \frac{32}{3\pi^2} \frac{\sqrt{N} a_{1D}}{a_z} \right)$

Size of the condensate and mean  $z^2$  in units of  $a_z^2$

limit	$R^2$	$z^2$
Repulsive gas: strong interaction	$2N \left( 1 - \frac{32\sqrt{2} \ln 2 \sqrt{N} a_{1D}}{9\pi^2 a_z} \right)$	$\frac{N}{2} \left( 1 - \frac{64\sqrt{2} \ln 2 \sqrt{N} a_{1D}}{15\pi^2 a_z} \right)$
Attractive gas: strong interaction	$\frac{N}{2} \left( 1 + \frac{16\sqrt{2} \sqrt{N} a_{1D}}{9\pi^2 a_z} \right)$	$\frac{N}{8} \left( 1 + \frac{32\sqrt{2} \sqrt{N} a_{1D}}{15\pi^2 a_z} \right)$
Repulsive: weak interaction	$N \left( 1 + \frac{8}{\pi^2} \frac{\sqrt{N} a_{1D}}{a_z} \right)$	$\frac{N}{4} \left( 1 + \frac{16}{3\pi^2} \frac{\sqrt{N} a_{1D}}{a_z} \right)$
Attractive gas: weak interaction	$N \left( 1 - \frac{8}{\pi^2} \frac{\sqrt{N} a_{1D}}{a_z} \right)$	$\frac{N}{4} \left( 1 - \frac{16}{3\pi^2} \frac{\sqrt{N} a_{1D}}{a_z} \right)$



# Appendix B

## Obtaining the momentum distribution from $g_1(r)$

The asymptotic behaviour of the one body density matrix of the Lieb gas is

$$\rho(x) = \frac{C}{x^\alpha}, \quad x \gg 1 \quad (\text{B.1})$$

In order to calculate the momentum distribution one has to calculate the Fourier transform of it

$$n(k) = 2 \int_0^\infty \cos kx \rho(x) dx \quad (\text{B.2})$$

This integral can be calculated numerically up to some cut-off distance  $L$ . Let us suppose, that at distances larger than  $L$  the asymptotic behavior is valid (B.1). Then one can calculate the “tail” integral analytically<sup>1</sup> by a substitution  $t = e^{i\pi/2} kx$

$$\int_L^\infty \frac{\cos kx}{x^\alpha} dx = \text{Re} \int_{ikL}^\infty \frac{e^{-i\frac{\pi}{2}(1-\alpha)}}{k^{1-\alpha}} e^{-t} t^{-\alpha} dt = \text{Re} \frac{e^{-i\frac{\pi}{2}(1-\alpha)} \Gamma(1-\alpha, ikL)}{k^{1-\alpha}} \quad (\text{B.3})$$

Here the incomplete Gamma function is defined as

$$\Gamma(\alpha, L) = \int_L^\infty e^{-t} t^{\alpha-1} dt \quad (\text{B.4})$$

If the if set  $L = 0$  then the integral can be simplified<sup>2</sup>

$$\int_0^\infty \frac{\cos kx}{x^\alpha} dx = \frac{\Gamma(1-\alpha)}{k^{1-\alpha}} \cos \frac{\pi(1-\alpha)}{2}, \quad k > 0, 0 < \alpha < 1 \quad (\text{B.5})$$

Let us derive an expansion of the incomplete Gamma function in terms of  $1/(kL)$ . For us it is convenient to use following definition of the function

$$f(k, L, \alpha) = \int_L^\infty \frac{\cos kx}{x^\alpha} dx \quad (\text{B.6})$$

<sup>1</sup>Compare with [GR80]  $\int_L^\infty x^{\mu-1} \cos ax dx = \frac{1}{2} [e^{-i\mu\pi/2} \Gamma(\mu, iL) + e^{i\mu\pi/2} \Gamma(\mu, -iL)]$

<sup>2</sup>See [GR80] 3.761.7  $\int_0^\infty x^{\mu-1} \cos(ax) dx = \frac{\Gamma(\mu)}{a^\mu} \cos \frac{\mu\pi}{2}, a > 0, 0 < \text{Re}\mu < 1$

Integrating it by parts two times we obtain<sup>3</sup>

$$f(k, L, \alpha) = \frac{1}{kL^\alpha} \left( -\sin kL + \frac{\alpha}{kL} \cos kL \right) - \frac{\alpha(\alpha+1)}{k^2} \int_L^\infty \frac{\cos kx}{x^{\alpha+2}} dx \quad (\text{B.7})$$

Here the last term has the same form as (B.6). And can be expanded in a similar way. Continuation of this expansion leads to formula

$$f(k, K, \alpha) = \sum_{n=0}^{\infty} \frac{(-1)^n}{kL^\alpha} \left( \cos kL \frac{\alpha(\alpha+1)\dots(\alpha+2n)}{(kL)^{2n+1}} - \sin kL \frac{\alpha(\alpha+1)\dots(\alpha+2n-1)}{(kL)^{2n}} \right) \quad (\text{B.8})$$

Another way to present it is

$$f(k, K, \alpha) = \frac{1}{kL^\alpha} \sum_{n=0}^{\infty} \frac{\text{Im } i^n e^{-ikL}}{(kL)^n} \frac{(\alpha+n-1)!}{(\alpha-1)!} \quad (\text{B.9})$$

Let us write explicitly

$$\text{Im } i^n e^{-ikL} = (-1)^{\text{mod}(n+1,2)+1} f_n(kL) \quad (\text{B.10})$$

where mod operation is integer division and the function  $f_n$  is defined as

$$f_n(x) = \begin{cases} \sin x, & n = 0, 2, 4, \dots \\ \cos x, & n = 1, 3, 5, \dots \end{cases} \quad (\text{B.11})$$

Looking at the structure of the expansion (B.9) one finds out that the sum converges only is  $kL > 1$ . The factorial dependence of the numerator on the order of the term  $n$  leads to divergence of the entire sum. Let us find order of the term  $n_{cr}$  when the summation procedure should be stopped. The condition is

$$\frac{\partial}{\partial n} \frac{(\alpha+1-n)!}{(kL)^n} = 0 \quad (\text{B.12})$$

In order to proceed further we will take use of the Stirling formula

$$n! = \sqrt{2\pi n} n^n e^{-n} \quad (\text{B.13})$$

Simple calculation gives

$$\ln(\alpha + n_{cr} - 1) + \frac{1}{2(\alpha + n_{cr} - 1)} = \ln kL - 1 \quad (\text{B.14})$$

Now we assume that  $n$  is much larger than one, so we can neglect the second term. Finally we obtain

$$n_{cr} = kL/e \quad (\text{B.15})$$

---

<sup>3</sup>In dimensionless units  $y = kL$  formulae (B.6, B.7) look like  $f(k, L, \alpha) = k^{\alpha-1} \int_{kL}^\infty \frac{\cos y}{y^\alpha} dy$  and  $f(k, L, \alpha) = \frac{1}{kL^\alpha} \left( -\sin kL + \frac{\alpha}{kL} \cos kL \right) - \alpha(\alpha+1)k^{\alpha-1} \int_{kL}^\infty \frac{\cos y}{y^{\alpha+2}} dy$

Another approach for the calculation of the integral is by modifying the integration contour. First of all, let us expand the cosine into sum of complex exponents

$$\int_L^\infty \frac{\cos x \, dx}{x^\alpha} = \frac{1}{2} \int_L^\infty \frac{e^{ix} \, dx}{x^\alpha} + \frac{1}{2} \int_L^\infty \frac{e^{-ix} \, dx}{x^\alpha} \quad (\text{B.16})$$

Let us calculate the first integral in this sum.

$$I_1 = \int_L^\infty \frac{e^{ix} \, dx}{x^\alpha} = \int_0^\infty \frac{e^{-y} e^{iL} \, idy}{(iy + L)^\alpha}, \quad (\text{B.17})$$

where we introduced notation  $x = iy + L$ , which is a complex variable  $x = \sqrt{y^2 + L^2} e^{i \arctan \frac{y}{L}}$ , so

$$I_1 = \int_0^\infty e^{-y} (y^2 + L^2)^{-\frac{\alpha}{2}} e^{i(L - \alpha \arctan \frac{y}{L})} \, idy = \quad (\text{B.18})$$

$$= \int_0^\infty e^{-y} (y^2 + L^2)^{-\frac{\alpha}{2}} \left[ \sin \left( \alpha \arctan \frac{y}{L} - L \right) + i \cos \left( \alpha \arctan \frac{y}{L} - L \right) \right] \, dy \quad (\text{B.19})$$

The second integral in (B.16) can be calculated by means of the substitution  $x = -iy + L = \sqrt{y^2 + L^2} e^{-i \arctan \frac{y}{L}}$

$$I_2 = \int_L^\infty \frac{e^{-ix} \, dx}{x^\alpha} = \int_0^\infty \frac{e^{-y} e^{-iL} (-i) \, dy}{(iy - L)^\alpha} = \int_0^\infty e^{-y} (y^2 + L^2)^{-\frac{\alpha}{2}} e^{i(-L + \alpha \arctan \frac{y}{L})} (-i) \, dy = \quad (\text{B.20})$$

$$= \int_0^\infty e^{-y} (y^2 + L^2)^{-\frac{\alpha}{2}} \left[ \sin \left( \alpha \arctan \frac{y}{L} - L \right) - \cos \left( \alpha \arctan \frac{y}{L} - L \right) \right] \, dy \quad (\text{B.21})$$

The imaginary parts of the integrals (B.19, B.21) cancel each other and the result is real

$$\int_L^\infty \frac{\cos kx \, dx}{x^\alpha} = k^{\alpha-1} \int_0^\infty e^{-y} (y^2 + (kL)^2)^{-\frac{\alpha}{2}} \sin \left( \alpha \arctan \frac{y}{kL} - kL \right) \, dy \quad (\text{B.22})$$

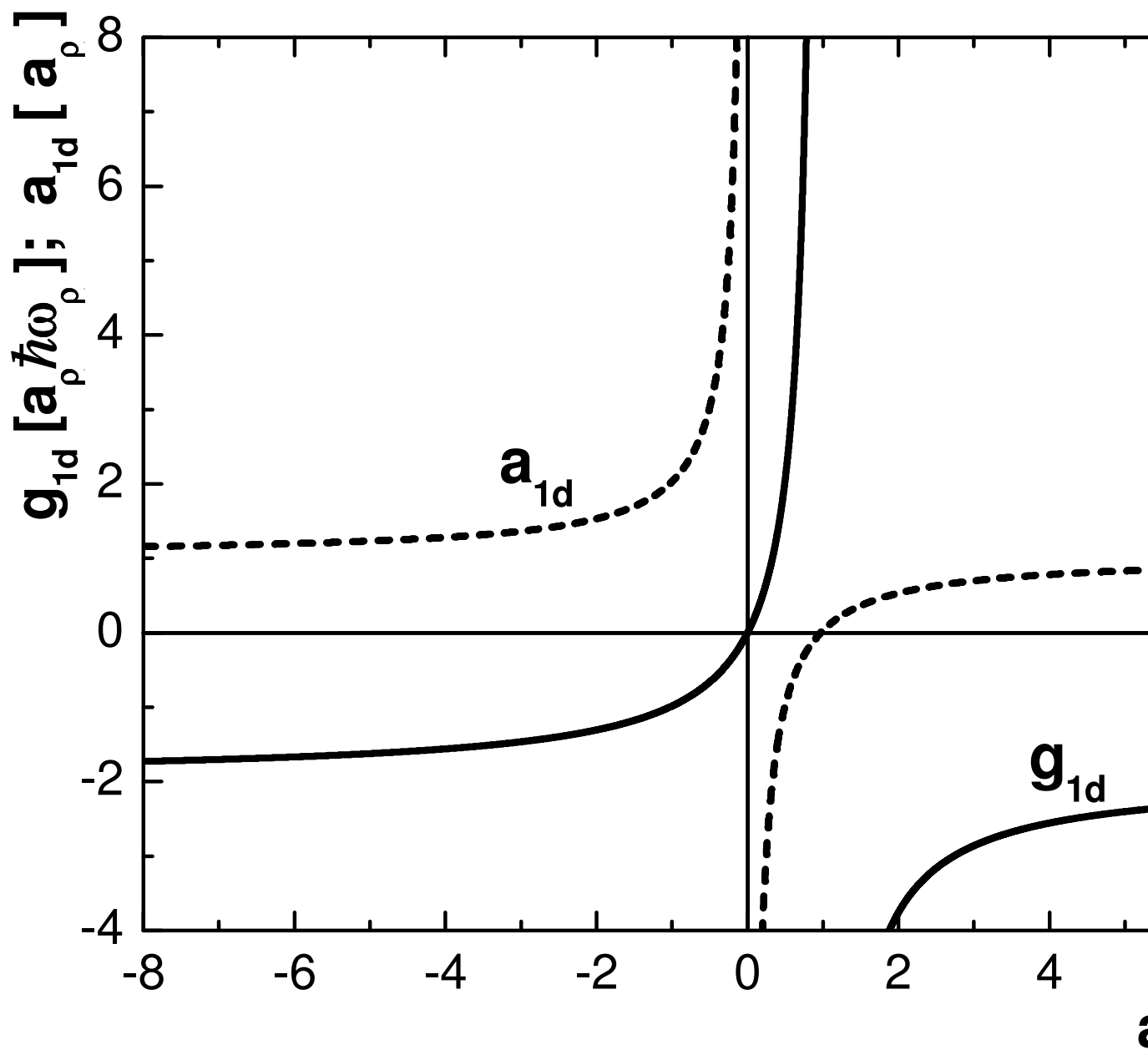


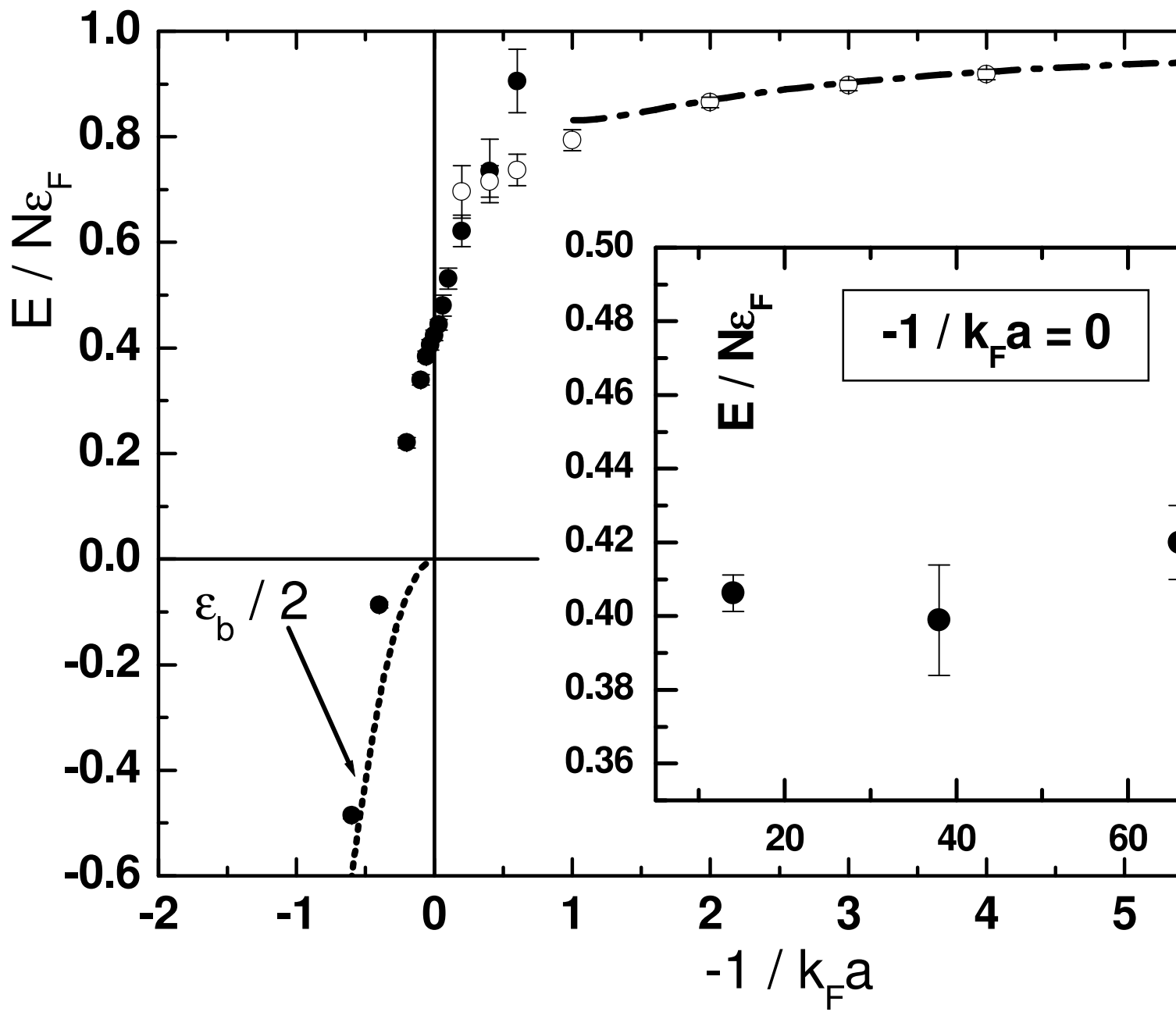
# Acknowledgements

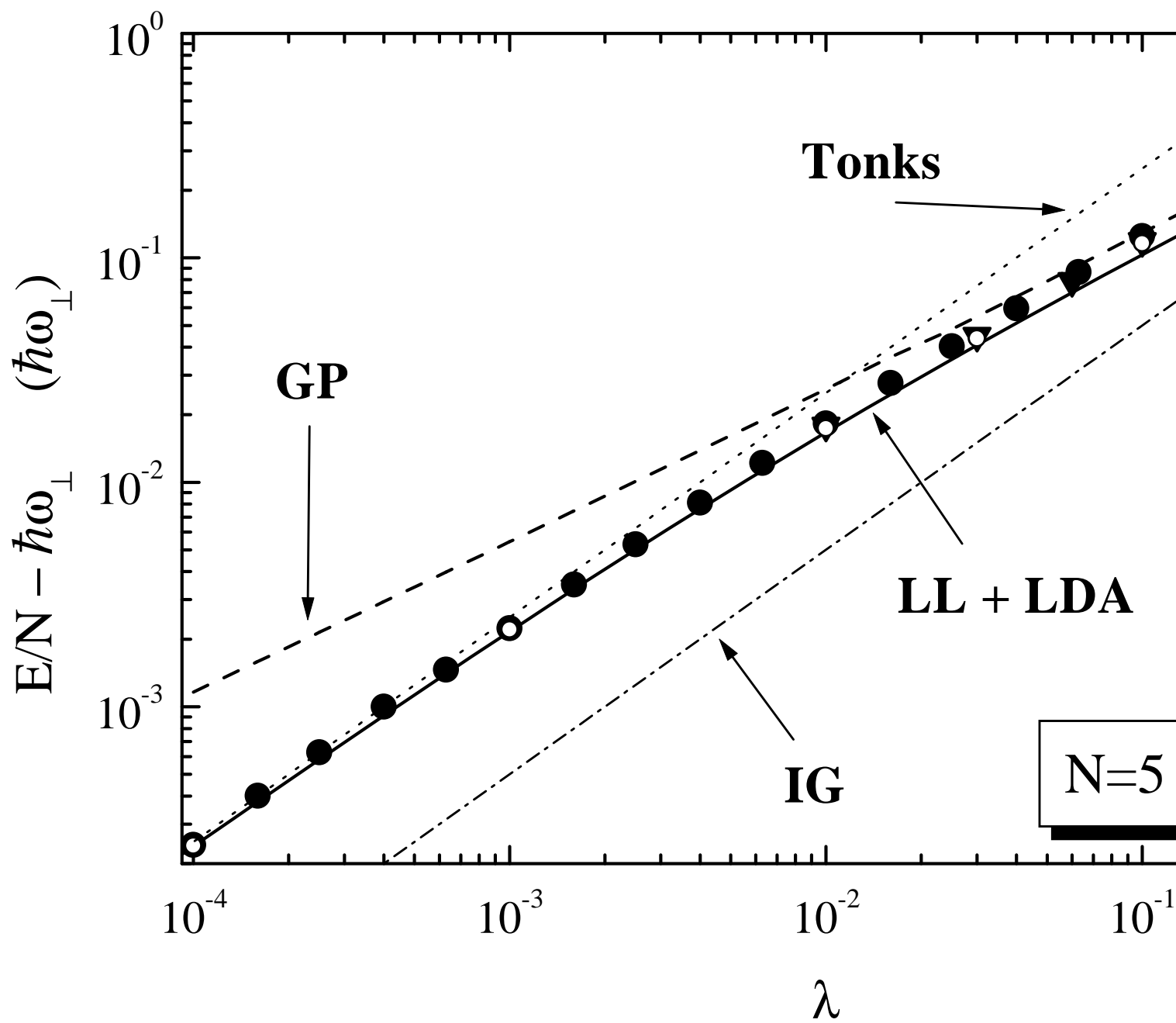
I would like to gratefully acknowledge the enthusiastic supervision of Dr. Stefano Giorgini and Prof. Lev P. Pitaevskii. They taught me so many new things and were always ready to answer any of my countless questions.

I owe special thanks to Prof. Sandro Stringari without whom this Dissertation would not exist. I want to thank him for giving me the opportunity to work in his group, for being a great mentor, for giving me invaluable help in solving the organizational problems.

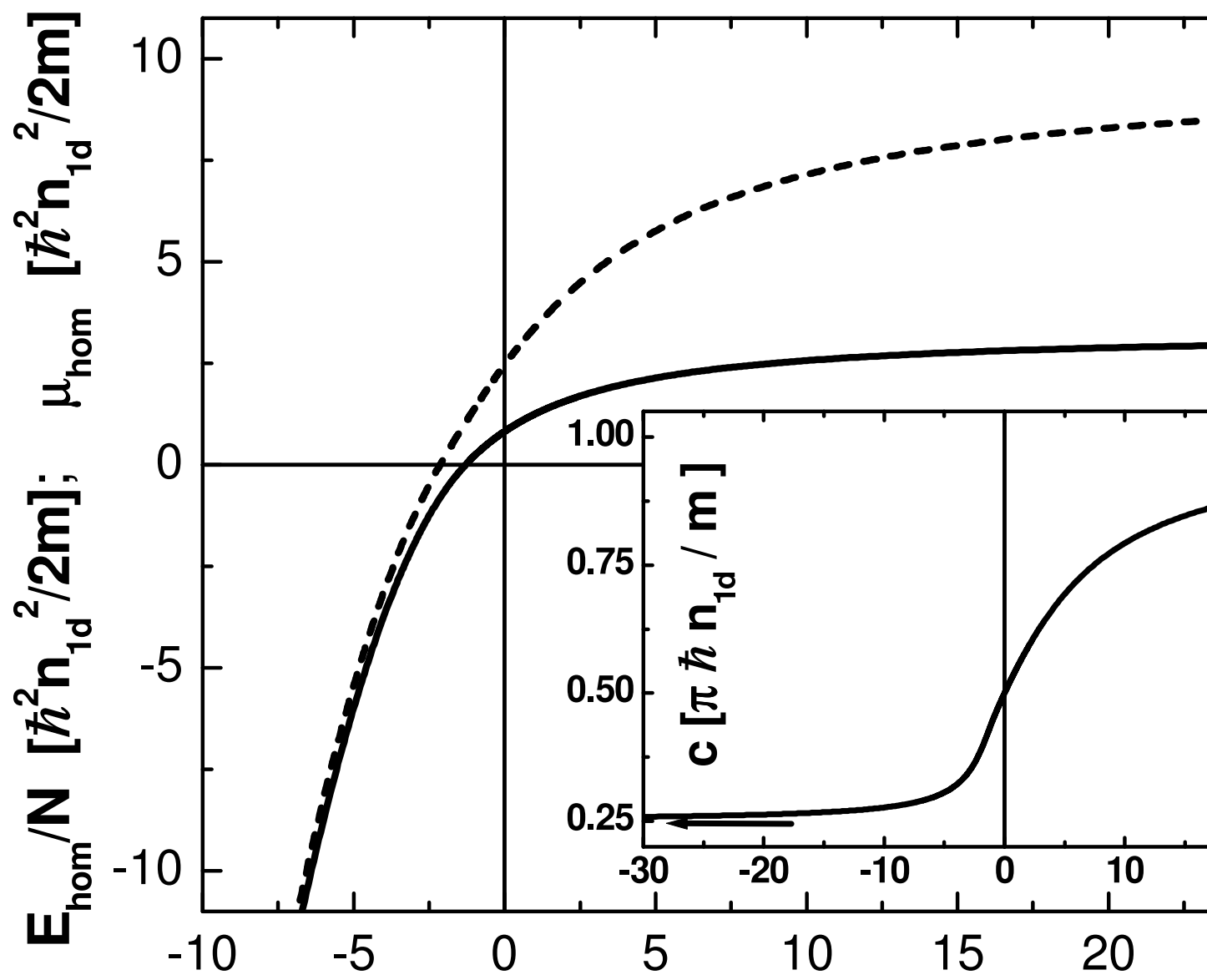
I am grateful to the many people I have met in the Trento BEC group, in the University of Trento and who have assisted me so much in the course of this work.

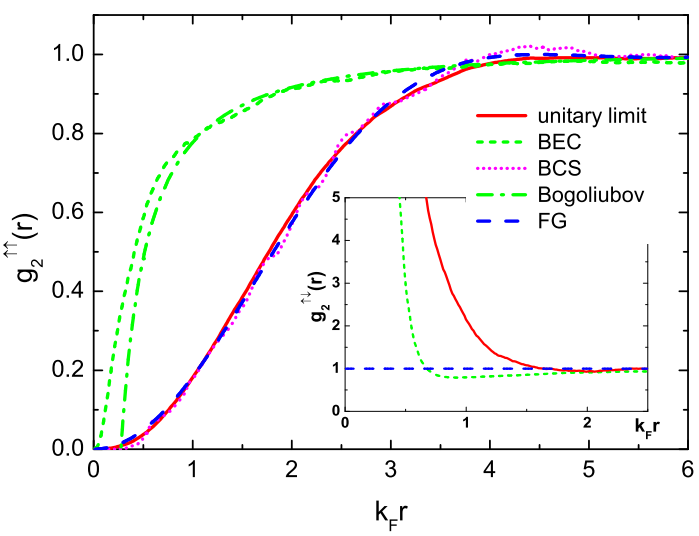


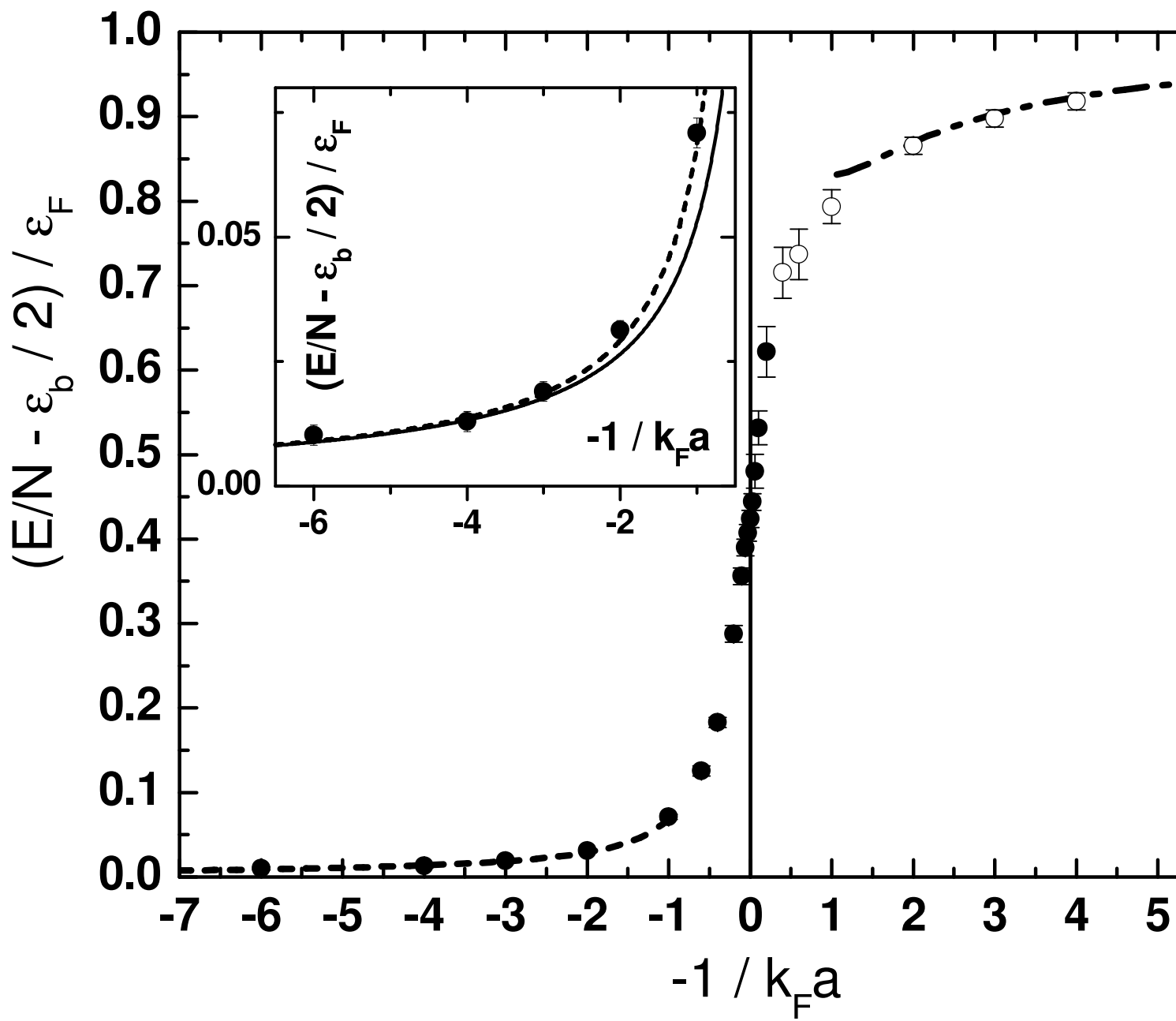


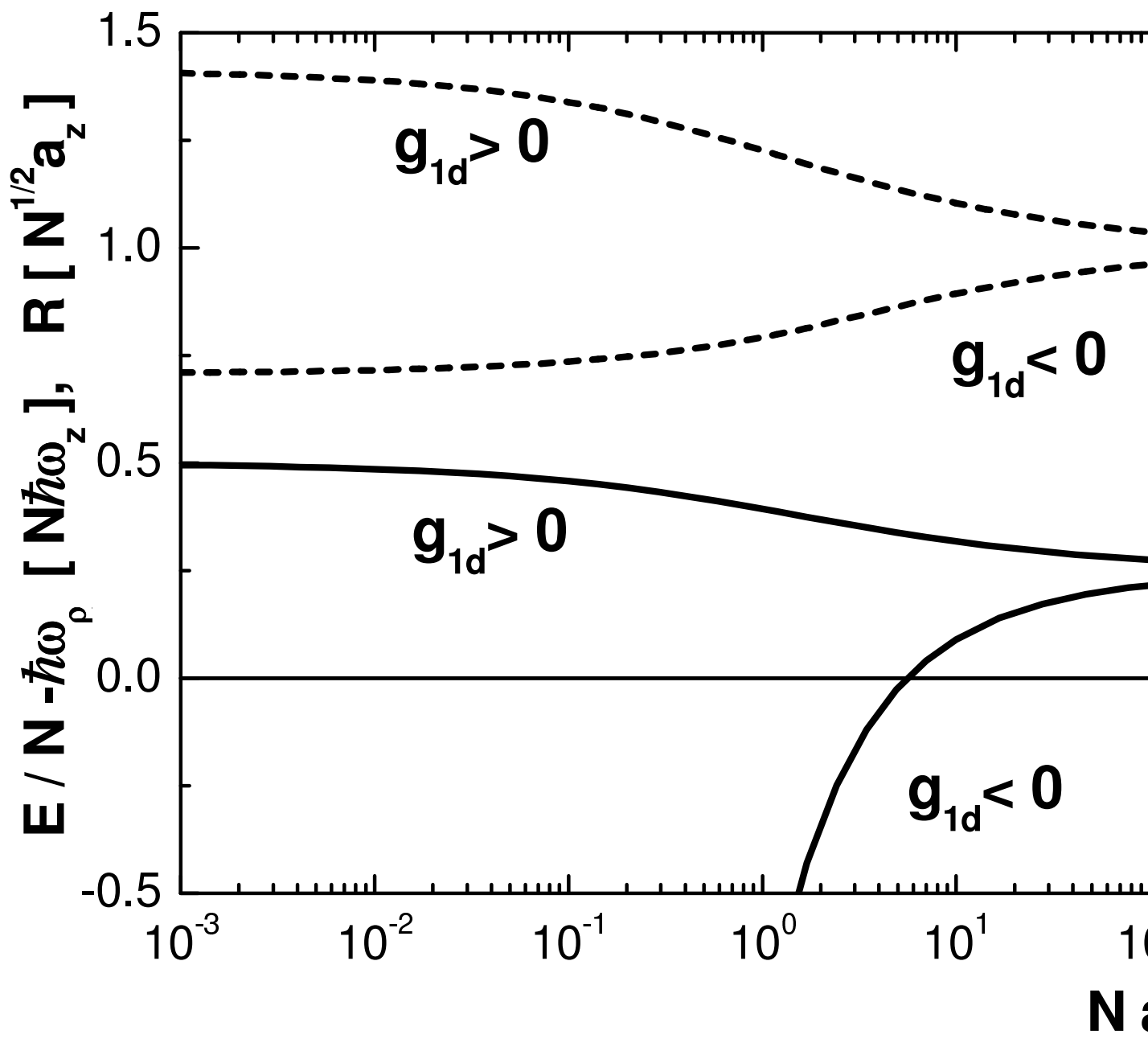


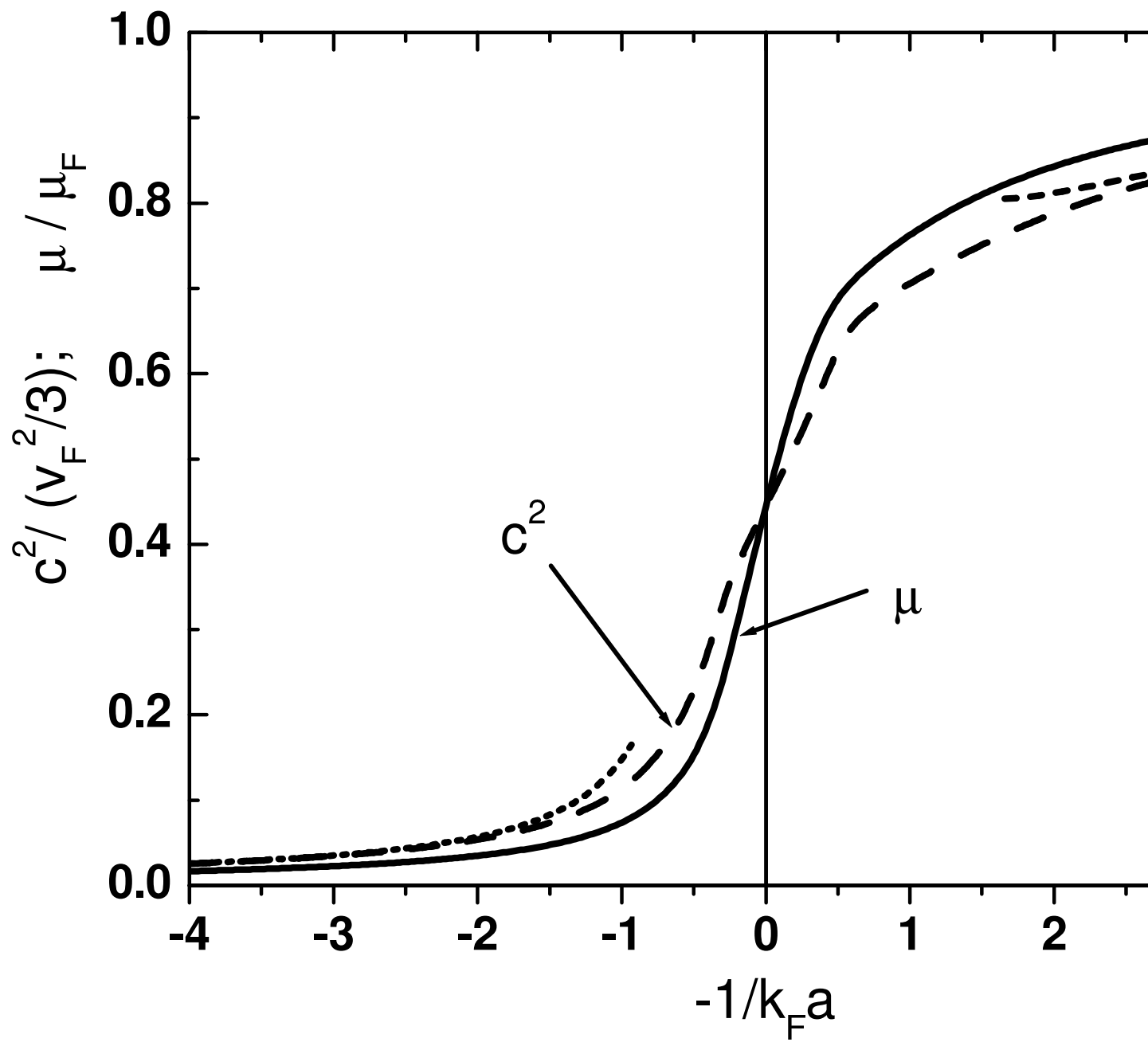


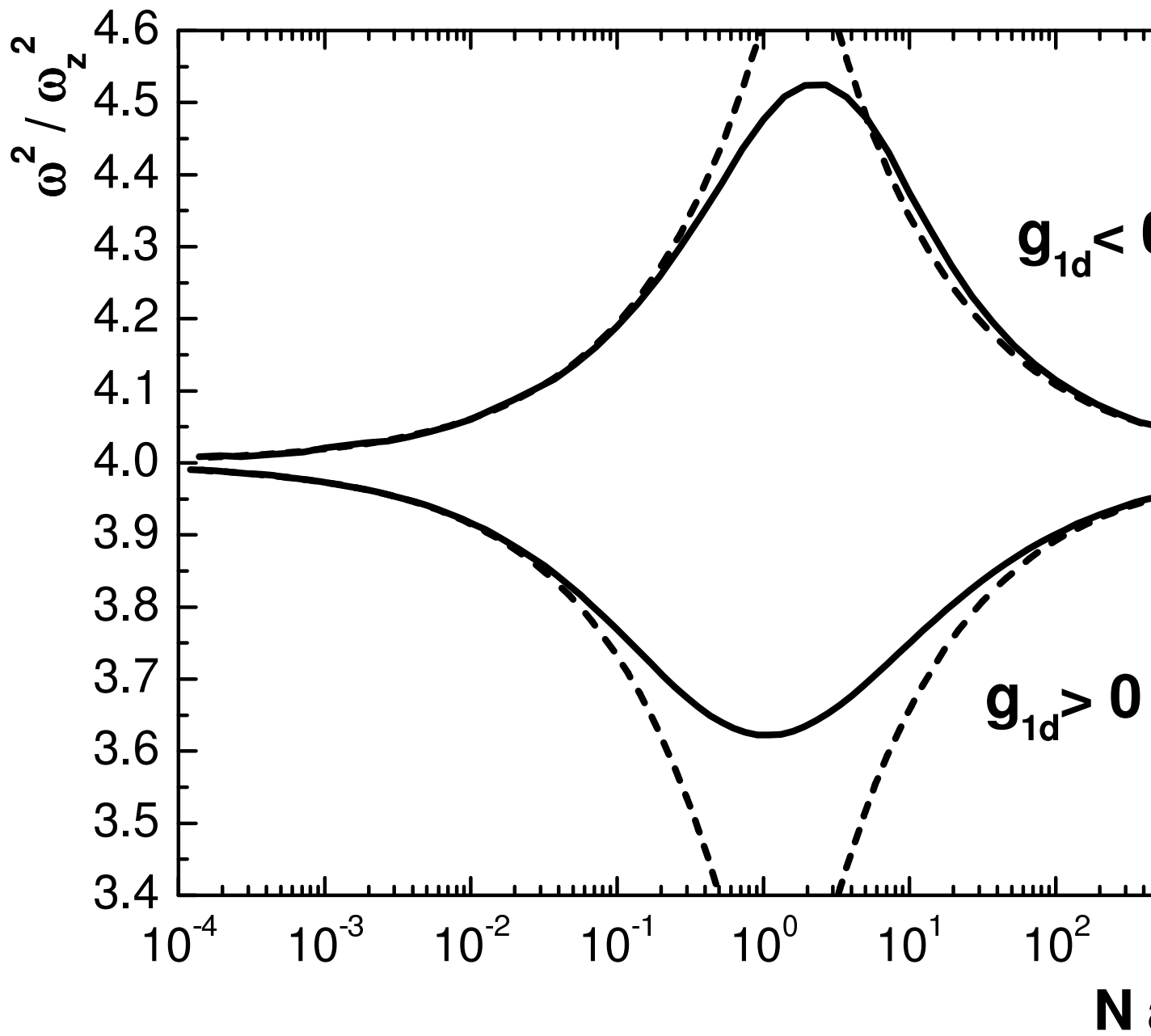


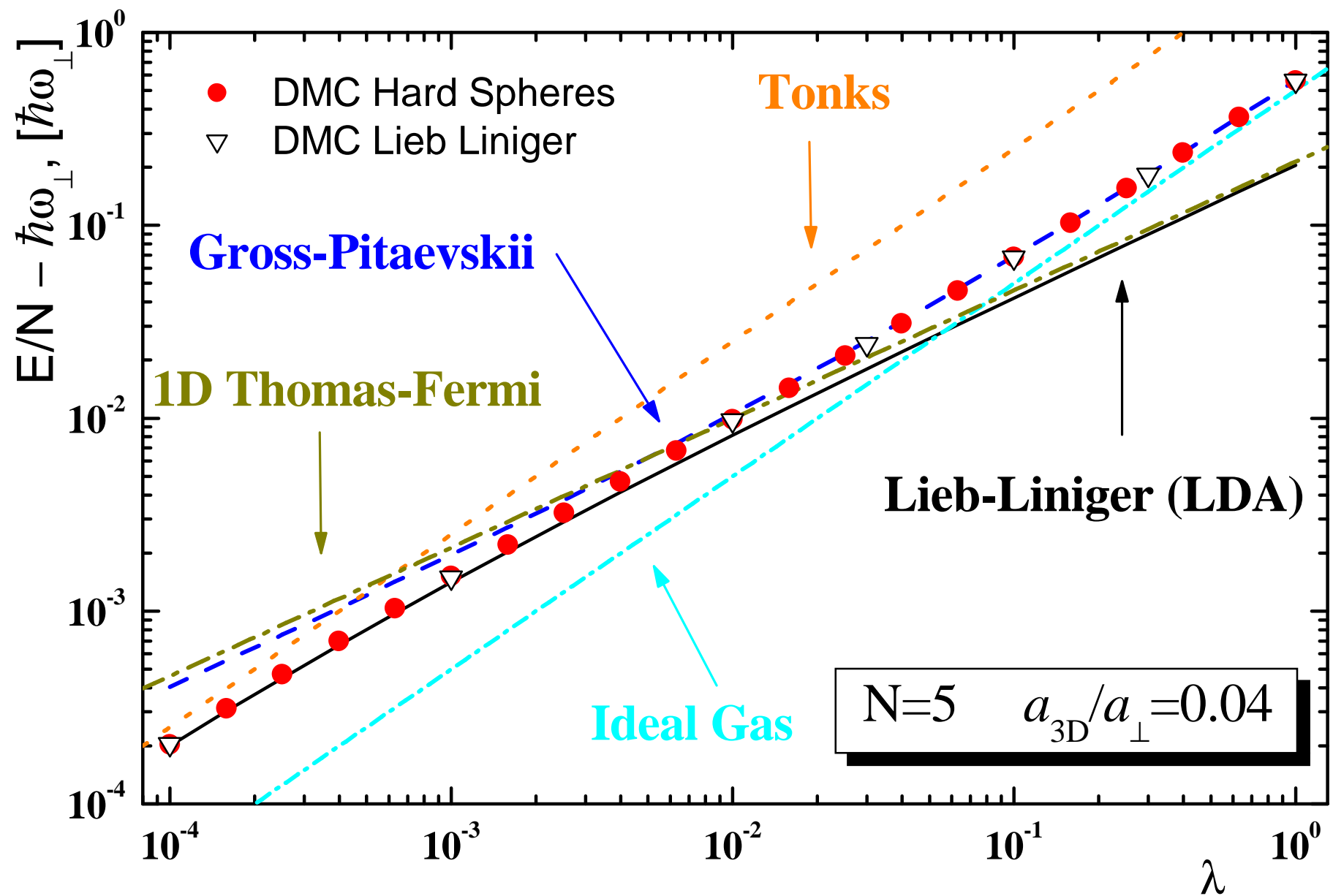


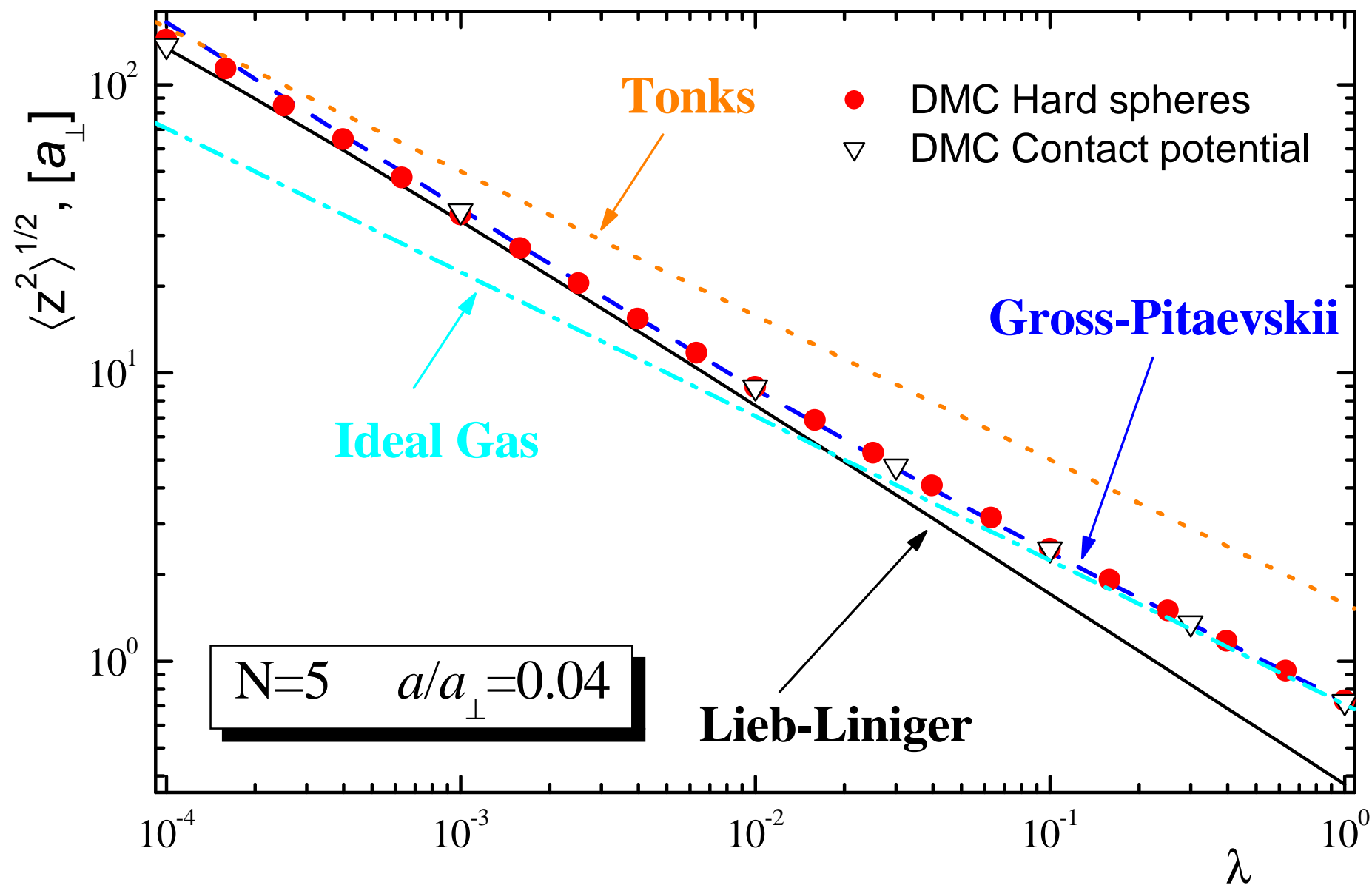




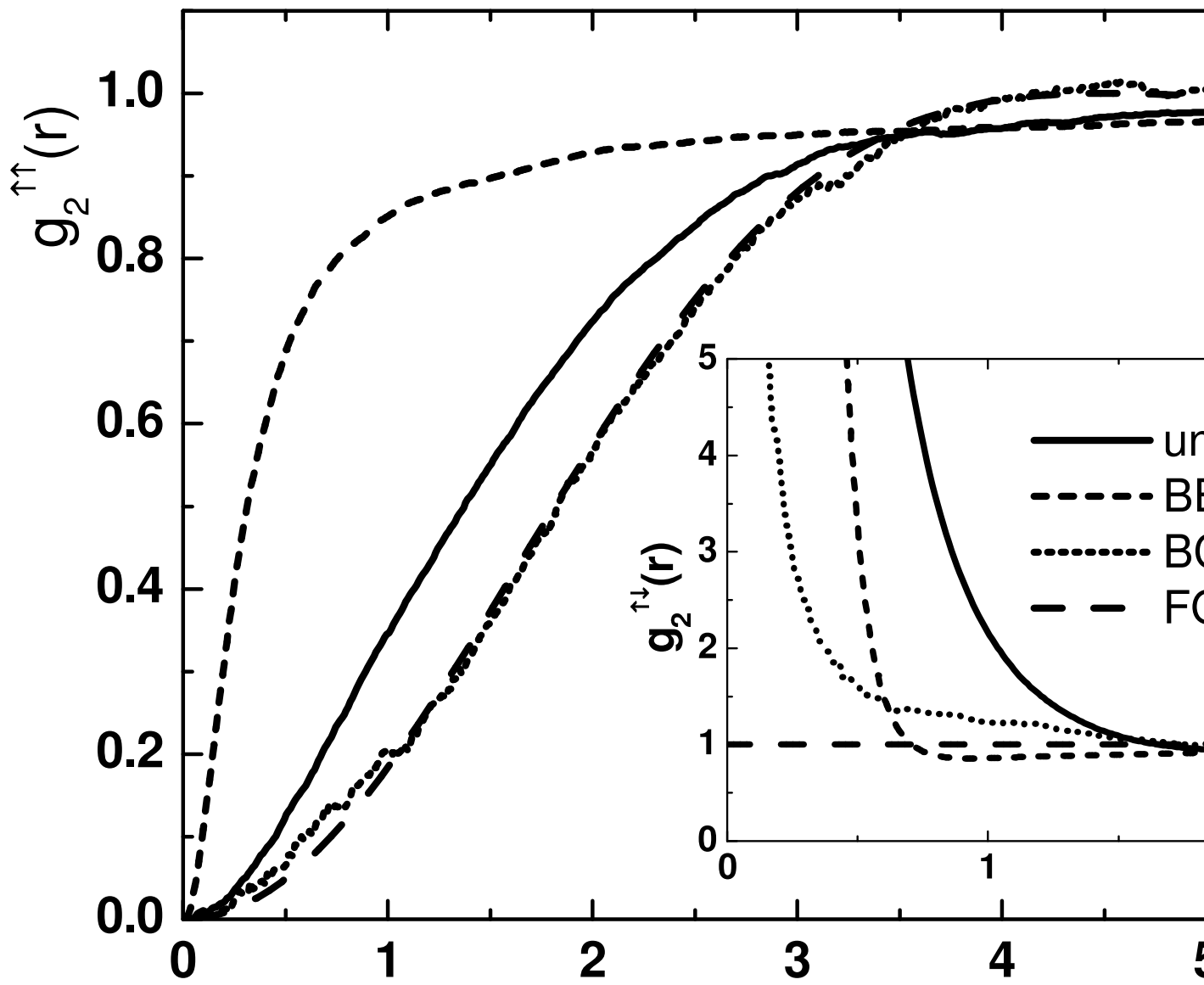


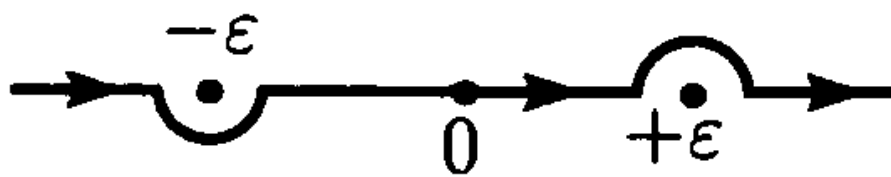












*Im*

*Re*

$\Gamma_1$

L

$\Gamma_2$

